

**Comparison of hepatoma cell lines and primary human
hepatocytes as models to study the development of
hepatic steatosis**

Zoë Huggett BSc MRes

Thesis submitted to the University of Nottingham for the degree of
Doctor of Philosophy

November 2019

Division of Food, Nutrition and Dietetics

School of Biosciences

University of Nottingham

Sutton Bonington Campus

Leicestershire

Abstract

Non-alcoholic fatty liver disease (NAFLD) is a worldwide health burden. The first stage is the accumulation of fat within hepatocytes (hepatic steatosis). Dietary and genetic factors determine steatosis, with particular emphasis on dietary fat, dietary sugars, and patatin-like phospholipase domain containing 3 (PNPLA3) genotype. Primary human hepatocytes (PHH) are currently the gold standard *in vitro* human model of steatosis but hepatoma cell lines are often used. This thesis aimed to compare the lipid accumulation and metabolism of PHH and hepatoma cell lines, and to develop a system to study the PNPLA3 genotype in relation to nutritional stimuli.

Lipid accumulation in response to 48 hours treatment with fatty acids (0 μ M or 200 μ M of palmitic, oleic and linoleic acids in the ratio 2:2:1), glucose (5mM or 11mM) and fructose (0mM, 2mM or 8mM) was measured in HepG2, Huh7, McA-RH7777 and PHH using a Nile Red staining assay normalised to DNA. Insulin sensitivity across the cell lines, and lipid accumulation in response to insulin treatment in HepG2 and PHH, were also measured. RT-qPCR and microarray analysis was used to compare the gene expression profiles of HepG2 and PHH. Human DNA was used to produce lentiviruses to overexpress wild-type or polymorphic PNPLA3.

All cell types accumulated lipid in response to fatty acid treatment ($P < 0.001$), with HepG2 cells and Huh7 cells reaching very similar maximum fold changes of 4.717 and 4.560 respectively. McA-RH7777 cells reached a higher fold change maximum of 7.707, whereas the PHH ranged between 1.403 and 4.822 depending on the liver. Only PHH showed an increase in lipid accumulation in response to fructose ($P < 0.001$) overall but this was not consistent across livers. Both McA-RH7777 cells and PHH accumulated lipid with 11mM glucose treatment when fatty acids were present, but again this was not consistent across livers. HepG2 and Huh7 cells were found to be insulin resistant

compared to the insulin sensitive McA-RH7777 cells, but both HepG2 and PHH accumulated lipid in response to insulin treatment. Gene expression patterns varied between HepG2 and PHH, for example lipogenic gene expression was decreased by fatty acids in HepG2 cells but not PHH. Microarray comparisons showed different baseline levels of gene expression reflecting different phenotypes. PNPLA3 lentiviruses were successfully produced but protein overexpression could not be measured by the commercial antibodies tested. The human cell lines were confirmed to be homozygous for the polymorphic variant of PNPLA3 but all of the livers used for PHH isolation were either homozygous wild type or heterozygous.

The data from this thesis suggests that HepG2 cells are not a suitable model to replace PHH. Further work on the interactions between genotype and dietary factors in different individuals is required.

Contents

Abstract.....	1
Contents.....	3
List of Figures	10
List of Tables	17
Acknowledgements	24
Abbreviations.....	25
Chapter 1: Introduction to non-alcoholic fatty liver disease (NAFLD) and hepatic steatosis.	29
1.1 The Liver.....	29
1.2 Hepatic steatosis.....	30
1.3 NAFLD – definition, diagnosis and epidemiology	33
1.4 NAFLD pathophysiology.....	34
1.5 NAFLD treatment	37
1.6 NAFLD and insulin resistance.....	38
1.7 Dietary factors	39
1.7.1 Macronutrients or calories	39
1.7.2 Sugars.....	39
1.7.3 Fatty acids	42
1.8 Genetic factors.....	43
1.9 Animal models	44
1.10 Towards a physiologically relevant <i>in vitro</i> human model	45

1.11 Aims and objectives	46
Chapter 2: General Methods	48
2.1 Cell culture	48
2.1.1 Cell line culture	48
2.1.2 Primary human hepatocyte culture – liver perfusion.....	48
2.1.3 Solution preparation.....	50
2.1.3.1 Preparation of 24% (w/v) BSA solution	50
2.1.3.2 Preparation of 10mM fatty acid stocks	50
2.1.3.3 Preparation of sugar solutions.....	51
2.1.3.4 Collagen preparation	51
2.1.3.5 Collagen coating plates.....	51
2.1.3.6 Preparation of media and media supplements	52
2.2 Protein analysis.....	52
2.2.1 Harvesting cells for protein analysis.....	52
2.2.2 2D Quant protein assay (GE Healthcare)	53
2.2.3 General western blotting protocol	53
2.3 Statistical analysis	54
Chapter 3: A comparison of lipid accumulation in response to nutritional stimuli in hepatoma cell lines and primary human hepatocytes	55
3.1 Introduction	55
3.1.1 Hepatoma cell lines.....	55
3.1.2 Primary human hepatocytes (PHH)	56
3.1.3 Selecting fatty acid, monosaccharide and insulin concentrations	57
3.1.4 Experimental aims	59
3.2 Methods.....	60

3.2.1 Nile Red staining assay.....	60
3.2.2 DNA assay	60
3.2.3 Experimental protocol – establishing an appropriate fatty acid concentration	61
3.2.4 Experimental protocol – effects of glucose, fructose and fatty acids	62
3.2.5 Experimental protocol – effects of glucose, insulin and fatty acids	63
3.2.6 Experimental protocol – insulin responses of hepatoma cell lines	64
3.2.7 Phospho-AKT and total AKT western blot.....	64
3.3 Results.....	66
3.3.1 Establishing an appropriate fatty acid concentration to induce lipid accumulation	66
3.3.2 The effects of fatty acid, glucose and fructose treatment on lipid accumulation in HepG2, Huh7 and McA-RH7777 cells and primary human hepatocytes: a comparison.....	69
3.3.3 Lipid accumulation in response to fatty acid, glucose and insulin treatment in HepG2 cells and PHH	83
3.3.4 Comparison of insulin sensitivity across hepatoma cell lines.....	87
3.4 Discussion	89
3.4.1 Summary of results	89
3.4.2 Culture conditions for inducing lipid accumulation <i>in vitro</i>	89
3.4.3 Lipid accumulation in response to glucose, fructose and fatty acids	91
3.4.4 Insulin sensitivity and lipid accumulation in response to insulin	96
3.4.5 Concluding remarks	97

Chapter 4: Comparison of gene expression in HepG2 cells and primary human hepatocytes	99
4.1. Introduction	99
4.1.1 Mechanisms of lipid accumulation	99
4.1.2 Experimental aims	104
4.2 Methods.....	105
4.2.1 Experimental protocol	105
4.2.2 RNA extraction from HepG2 cells	105
4.2.3 RNA extraction from primary human hepatocytes	106
4.2.4 RNA quality checks.....	107
4.2.5 cDNA Synthesis	107
4.2.6 Primer design	108
4.2.7 RT-qPCR.....	110
4.2.8 Determination of total cDNA using OliGreen	111
4.2.9 Statistical analysis of RT-qPCR data	111
4.2.10 Microarray Analysis	111
4.3 Results.....	113
4.3.1 Targeted gene expression analyses by RT-qPCR.....	113
4.3.1.1 Total cDNA (OliGreen fluorescence)	113
4.3.1.2 Overview of results	114
4.3.1.3 Lipogenic genes – ACC1, SCD, FASN, SREBP1	115
4.3.1.4 Lipid metabolism related genes – PNPLA3, DGAT1, CPT1 α , ApoB, PPARGC1 α	121
4.3.1.5 Carbohydrate metabolism related genes – ChREBP, LPK, GLUT2, HK2 ..	128
4.3.1.6 Comparative expression levels	131

4.3.1.7 Correlations.....	135
4.3.2 Non-targeted gene expression analysis by microarray	137
4.3.2.1 Comparisons between HepG2 and PHH	137
4.3.2.2 FA vs CON (200µM fatty acid+5mM glucose+0mM fructose vs 0µM fatty acid+5mM glucose+0mM fructose)	146
4.3.2.3 FA+G vs FA (200µM fatty acid+11mM glucose+0mM fructose vs 200µM fatty acid+5mM glucose+0mM fructose)	150
4.3.2.4 FA+F vs FA (200µM fatty acid+5mM glucose+8mM fructose vs 200µM fatty acid+5mM glucose+0mM fructose)	151
4.3.2.5 FA+G+F vs FA+G (200µM fatty acid+11mM glucose+8mM fructose vs 200µM fatty acid+11mM glucose+0mM fructose)	151
4.3.2.6 FA+G+F vs FA+F (200µM fatty acid+11mM glucose+8mM fructose vs 200µM fatty acid+5mM glucose+8mM fructose)	152
4.4 Discussion	154
4.4.1 Summary of results	154
4.4.2 RT-qPCR data	155
4.4.3 Comparing gene expression levels between the cell types.....	157
4.4.4 Points of interest from the microarray data.....	158
4.4.4.1 Fatty acid effects.....	158
4.4.4.2 Glucose effects.....	159
4.4.4.3 Fructose effects	160
4.4.5 Concluding remarks	162
 Chapter 5: Patatin-like phospholipase domain containing 3 (PNPLA3): the study and manipulation of the I148M genotype for NAFLD research	 164
5.1. Introduction	164
5.1.1 PNPLA3 function	164
5.1.2 I148M polymorphism.....	164
5.1.3 PNPLA3 in hepatic stellate cells	168
5.1.4 Experimental aims	168

5.2. Methods.....	170
5.2.1 Genotyping of cell lines and liver samples.....	170
5.2.1.1 Genomic DNA Extraction from HepG2 and Huh7 cells	170
5.2.1.2 Genomic DNA extraction from liver tissue	171
5.2.1.3 PCR and gel purification of a product for sequencing	172
5.2.1.4 SNP TaqMan genotyping assay	173
5.2.2 Cloning of human PNPLA3 cDNA	174
5.2.2.1 cDNA synthesis.....	174
5.2.2.2 Polymerase Chain Reaction (PCR).....	175
5.2.2.3 Agarose gel electrophoresis.....	176
5.2.2.4 PCR product purification.....	176
5.2.2.5 Determining DNA concentration	177
5.2.2.6 BP recombination reaction	177
5.2.2.7 Preparation of agar plates and antibiotic stocks	179
5.2.2.8 Transforming Competent Cells	179
5.2.3 MidiPrep	180
5.2.4 Sequencing and identification of I148M variant	181
5.2.5 Mutagenesis.....	182
5.2.6 GeneJET Plasmid MiniPrep (ThermoFisher).....	184
5.2.7 Envelope and packaging plasmid preparation.....	185
5.2.8 pInducer20 plasmid prep.....	185
5.2.9 LR recombination reaction	187
5.2.10 Stbl3 cell transformation	187
5.2.11 Lentivirus production.....	188
5.2.12 QuickTiter Lentivirus Titer Kit (Cell Biolabs)	189
5.2.13 Transfection test on COS7 and HepG2 cells	192
5.2.14 Lentivirus tests in MCF7 and HepG2 cells.....	193

5.2.15 PNPLA3 antibody optimisation	194
5.3. Results.....	199
5.3.1 Genotyping of HepG2 cells, Huh7 cells and donor livers.....	199
5.3.2 Lentiviral transfection of MCF7 and HepG2 cells	202
5.4. Discussion	204
5.4.1 Summary of results	204
5.4.2 Genotyping.....	204
5.4.3 Technologies for detecting PNPLA3 overexpression	205
5.4.4 Lentivirus optimisation	206
5.4.5 PNPLA3, lipid accumulation and diet.....	207
5.4.6 Concluding remarks	209
Chapter 6: General discussion	211
Bibliography	217
Appendix – Supplementary Tables	228

List of Figures

Figure 1.1: The liver sinusoid, showing the location of the main liver cell types. Re-drawn from Sorensen et al. (2015) and Li et al. (2017).	30
Figure 1.2: Mechanisms of triacylglycerol (TAG) accumulation and secretion/breakdown. TAG stored in hepatocytes can result from <i>de novo</i> lipogenesis from dietary sugars and TAG synthesis from dietary fatty acids or NEFA released from adipose tissue by lipoprotein lipase activity. Stored TAG can be oxidised or secreted in VLDL. For detailed hepatic pathways see Chapter 4, Figure 4.1. NEFA: non-esterified fatty acids, VLDL: very low density lipoprotein, FA: fatty acids, LPL: lipoprotein lipase.....	31
Figure 1.3: Basic overview of hepatic very low density lipoprotein (VLDL) assembly and secretion. MTTP: microsomal triglyceride transfer protein. Drawn using information from Tiwari and Siddiqi (2012) and Choi and Ginsberg (2011).....	32
Figure 1.4: Mitochondrial β -oxidation of fatty acids, providing substrate for ATP production and ketogenesis in the fasted state. ATP: adenosine triphosphate	33
Figure 1.5: Histological sections of livers at difference disease states. Collagen stained blue with Masson's trichrome stain. PT: portal triad (hepatic artery, portal vein, and bile duct), CV: central vein. From Cohen et al. (2011).....	36
Figure 1.6: The molecular structure of A: glucose and B: fructose	40
Figure 3.1: Example of a standard curve produced for the DNA assay.	61
Figure 3.2: Lipid accumulation measured by Nile Red fluorescence in HepG2 cells treated with 0 μ M to 1000 μ M of fatty acids (palmitic, oleic and linoleic acids in the ratio 2:2:1) over 96 hours. Means \pm SEM, <i>n</i> =5	67
Figure 3.3: DNA per well (μ g) in HepG2 cells treated with 0 μ M to 1000 μ M of fatty acids (palmitic, oleic and linoleic acids in the ratio 2:2:1) over 96 hours. Means \pm SEM, <i>n</i> =4 or 5	67

Figure 3.4: Linear regression of DNA assay data from 48, 72 and 96 hours of treatment. 48 hours $P=0.019$, 72 hours $P<0.001$, 96 hours $P<0.001$. Means \pm SEM, $n=4$ or 5..... 68

Figure 3.5: Effects of fatty acids, glucose and fructose on lipid accumulation in HepG2 cells visualised by Nile Red viewed under green fluorescence 70

Figure 3.6: Effects of fatty acids, glucose and fructose on lipid accumulation in Huh7 cells visualised by Nile Red viewed under green fluorescence 71

Figure 3.7: Effects of fatty acids, glucose and fructose on lipid accumulation in McA-RH7777 cells visualised by Nile Red viewed under green fluorescence 72

Figure 3.8: Effects of fatty acids, glucose and fructose on lipid accumulation in PHH (L312) cells visualised by Nile Red viewed under green fluorescence 73

Figure 3.9: Effects of fatty acids, glucose and fructose on DNA content per well in HepG2, Huh7, McA-RH7777 cells and PHH (combined data from five donor livers). HepG2, Huh7 and McA-RH7777: 6 plates combined ($n=30$). PHH: 5 livers with 2 plates each combined ($n=50$). Means \pm SEM 76

Figure 3.10: Effects of fatty acids, glucose and fructose on lipid accumulation in A: HepG2, B: Huh7, and C: McA-RH7777 cells. D: Bonferroni multiple comparisons of the fatty acid \times glucose interaction in McA-RH7777 cells. Lipid accumulation was measured by Nile Red staining and normalised to DNA content, then converted to fold change relative to the control. Six plates combined for each cell type ($n=30$). Means \pm SEM..... 78

Figure 3.11: Effects of fatty acids, glucose and fructose on lipid accumulation in A: PHH combined data from five donor livers. B: Bonferroni multiple comparisons of the fructose effect. C: Bonferroni multiple comparisons of the fatty acid \times glucose interaction. Lipid accumulation was measured by Nile Red staining and normalised to DNA content, then converted to fold change relative to the control. $n=50$ (each liver $n=10$ split across two cell culture plates). Means \pm SEM 79

Figure 3.12: Effects of fatty acids, glucose and fructose on lipid accumulation in PHH from each of the five donor livers. Lipid accumulation was measured by Nile Red staining and normalised to DNA content, then converted to fold change relative to the control. Each liver $n=10$ split across two cell culture plates. Means \pm SEM..... 81

Figure 3.13: Effects of fatty acids, glucose and insulin on DNA content per well in HepG2 cells and PHH (combined data from three donor livers). HepG2: 4 plates combined ($n=20$). PHH: 3 livers with 2 plates each combined ($n=30$). Means \pm SEM..... 83

Figure 3.14: Effects of fatty acids, glucose and insulin on lipid accumulation in A: HepG2 cells. B: Bonferroni multiple comparisons of the insulin effect. Lipid accumulation was measured by Nile Red staining and normalised to DNA content, then converted to fold change relative to the control. 4 plates combined ($n=20$). Means \pm SEM 84

Figure 3.15: Effects of fatty acids, glucose and insulin on lipid accumulation in A: PHH combined data from three donor livers. B: Bonferroni multiple comparisons of the insulin effect. Lipid accumulation was measured by Nile Red staining and normalised to DNA content, then converted to fold change relative to the control. $n=30$ (each liver $n=10$ split across two cell culture plates). Means \pm SEM 85

Figure 3.16: Effects of fatty acids, glucose and insulin on lipid accumulation in PHH from three individual donor livers. Lipid accumulation was measured by Nile Red staining and normalised to DNA content, then converted to fold change relative to the control. Each liver $n=10$ split across two cell culture plates. Means \pm SEM..... 86

Figure 3.17: Phosphorylated AKT (pAKT) to total AKT ratio in three cell lines treated with 100nM insulin compared with untreated cells. Treatment \times cell line $P<0.001$, $n=3$. Means \pm SEM 87

Figure 4.1: Pathways within hepatocytes that result in triacylglycerol (TAG) production. P: phosphate, GCK: glucokinase, PFK: phosphofructokinase, ACC: acetyl-coA carboxylase, FASN: fatty acid synthase, SCD: stearoyl-coA desaturase, LPK: liver pyruvate kinase, PDH:

pyruvate dehydrogenase, DGAT: diacylglycerol transferase, ALDO: aldolase, GPAT: glycerol-3-phosphate acyltransferase, ACL: ATP citrate lyase, KHK: ketohexokinase, PAP: phosphaditic acid phosphorylase, AGPAT: acylglycerophosphate acyltransferase , GPDH: glycerol-3-phosphate dehydrogenase, ELOVL6: fatty acid elongase, PGK: phosphoglycerokinase. GAPDH: glyceraldehyde-3-phosphate dehydrogenase, ACS: acyl-coA synthetase..... 101

Figure 4.2: The SREBP1 isoforms produced from the SREBF gene. Alternative splicing of exons is shown, and the arrows represent transcription start sites. Modified from Felder et al. (2005)..... 103

Figure 4.3: Total cDNA measured by OliGreen fluorescence in all 1 in 8 dilutions of cDNA. Means±SEM, HepG2 *n*=5, PHH *n*=3 114

Figure 4.4: Effects of glucose, fructose and fatty acids on mRNA expression of acetyl-coA carboxylase (ACC1), fatty acid synthase (FASN) and stearyl-coA desaturase (SCD) in HepG2 cells and PHH. Means±SEM, normalised to total cDNA (OliGreen). HepG2 *n*=5, PHH *n*=3 116

Figure 4.5: Effects of glucose, fructose and fatty acids on mRNA expression of sterol regulatory element binding protein 1a (SREBP1a) and SREBP1c in HepG2 cells and PHH. Means±SEM, normalised to total cDNA (OliGreen). HepG2 *n*=5, PHH *n*=3..... 119

Figure 4.6: Effects of glucose, fructose and fatty acids on mRNA expression of patatin-like phospholipase domain-containing protein 3 (PNPLA3), diacylglycerol acyltransferase 1 (DGAT1) and carnitine palmitoyltransferase 1a (CPT1α) in HepG2 cells and PHH. Means±SEM, normalised to total cDNA (OliGreen). HepG2 *n*=5, PHH *n*=3..... 123

Figure 4.7: Effects of glucose, fructose and fatty acids on mRNA expression of apolipoprotein B (ApoB) and peroxisome proliferator-activated receptor gamma coactivator 1-alpha (PPARGC1α) in HepG2 cells and PHH. Means±SEM, normalised to total cDNA (OliGreen). HepG2 *n*=5, PHH *n*=3 126

Figure 4.8: Effects of glucose, fructose and fatty acids on mRNA expression of carbohydrate response element binding protein (ChREBP), liver pyruvate kinase (LPK) and glucose transporter 2 (GLUT2) in HepG2 cells and PHH. Means±SEM, normalised to total cDNA (OliGreen). HepG2 <i>n</i> =5, PHH <i>n</i> =3	129
Figure 4.9: Effects of glucose, fructose and fatty acids on mRNA expression of hexokinase 2 (HK2) in HepG2 cells. Means±SEM, normalised to total cDNA (OliGreen). <i>n</i> =5	131
Figure 4.10: Standard curves from a serial dilution of cDNA pools from HepG2 cells and primary human hepatocytes (L329). Using cDNA pools means that these values are averages of all treatments. Slopes and intercepts compared using linear regression...	133
Figure 4.11: Standard curves from a serial dilution of cDNA pools from HepG2 cells and primary human hepatocytes (L329). Using cDNA pools means that these values are averages of all treatments. Slopes and intercepts compared using linear regression...	134
Figure 4.12: Principle component analysis (PCA) plot of gene expression data from HepG2 (red) and PHH (liver – blue) controls (0µM fatty acids+5mM glucose+0mM fructose). See text for explanation of PCA.....	138
Figure 4.13: Principle component analysis (PCA) plot of gene expression data from HepG2 (red) and PHH (liver – blue) samples treated with 200µM fatty acids+5mM glucose+0mM fructose. See text for explanation of PCA.	139
Figure 4.14: The 40 most different gene expressions in control HepG2 vs PHH (control: 0µM fatty acids+5mM glucose+0mM fructose)	141
Figure 4.15: Top up- and down-regulated KEGG pathways in control PHH compared to control HepG2 (control: 0µM fatty acids+5mM glucose+0mM fructose)	143
Figure 4.16: Top up- and down-regulated KEGG pathways in fatty acid (FA) treated PHH compared to FA treated HepG2 (fatty acid treated: 200µM fatty acids+5mM glucose+0mM fructose)	144

Figure 4.17: Principle component analysis (PCA) plot of gene expression data from all HepG2 treatments. See section 4.3.2.1 for explanation of PCA. Control: CON, Treatment 4: FA, Treatment 6: FA+G, Treatment 10: FA+F, Treatment 12: FA+G+F (See Table 4.5). Ellipses removed due to poor clustering.	148
Figure 4.18: Principle component analysis (PCA) plot of gene expression data from all PHH treatments. See section 4.3.2.1 for explanation of PCA. Control: CON, Treatment 4: FA, Treatment 6: FA+G, Treatment 10: FA+F, Treatment 12: FA+G+F (See Table 4.5). Ellipses removed due to poor clustering.	149
Figure 5.1: Domain structure of human PNPLA3 (1-acylglycerol-3-phosphate O-acyltransferase). CDD: coding domain. The rs738490 single nucleotide polymorphism (SNP) site is highlighted. Compiled using the NCBI website. NCBI Reference Sequence: NP_079501.2.....	166
Figure 5.2: Detailed breakdown of the pDONR221 vector used in the BP recombination reaction. (From the Invitrogen technical booklet)	178
Figure 5.3: A map of the pInducer20 vector used as the destination vector (from www.addgene.org)	186
Figure 5.4: Standard curve for the lentivirus ELISA drawn using hyperbolic fit	191
Figure 5.5: GFP fluorescence in HepG2 cells transfected with a GFP lentivirus with MOI=2.5 TU/cell for 48 hours	193
Figure 5.6: Western blots of HepG2 protein (5µg, 10µg and 20µg protein per lane) using the Abcam PNPLA3 antibody and three different blocking agents; 5% milk, 5% BSA and 2% ECL Select blocking agent. Red line indicates expected band size.	196
Figure 5.7: Western blotting conditions attempted to optimise the Sigma PNPLA3 antibody: varying the blocking agent and antibody concentrations. Percentages are (w/v). Red lines indicate expected band size.	197

Figure 5.8: Further Western blotting conditions attempted to optimise the Sigma
PNPLA3 antibody: increasing the Tween percentage in the wash steps. Percentages for
blocking agent are (w/v) and for Tween are (v/v). Red lines indicate expected band size.
..... 198

Figure 5.9: Endpoint fluorescence scatter plot from the SNP TaqMan genotyping assay.
Green = GG, red = CG, blue = CC..... 199

List of Tables

Table 1.1: Stages of NAFLD and their pathophysiology. Modified from Glen et al. (2016)	36
Table 2.1: Gender and age of the patients from which the liver tissue was donated.....	49
Table 2.2: Supplements added to glucose free Williams Medium E	52
Table 3.1: Treatments prepared for the experiment. Vehicle controls were BSA NaCl solution for fatty acids and water for the sugar solutions	62
Table 3.2: Seeding densities for the different cell types	62
Table 3.3: Treatments prepared for the experiment. Vehicle controls were BSA NaCl solution for fatty acids and water for the glucose and insulin solutions.....	63
Table 3.4: Mean Nile Red fluorescence values minus background for the control group (0 μ M fatty acid, 5mM glucose, 0mM fructose) on each plate. SB: Sutton Bonington, QMC: Queens Medical Centre	74
Table 3.5: Cell line \times insulin interaction after treatment with 100nM insulin for 15 minutes: Bonferroni comparisons	88
Table 4.1: Treatments prepared for the experiment. Vehicle controls were BSA NaCl solution for fatty acids and water for the sugar solutions	105
Table 4.2: Primers used for RT-qPCR analysis, all obtained from Sigma. Orange – lipogenesis, blue – fatty acid metabolism, green – carbohydrate metabolism, yellow – housekeeper	109
Table 4.3: Cycling conditions for SYBR Green RT-qPCR carried out on a Roche LightCycler 480	110
Table 4.4: Conditions for OliGreen analysis carried out on a Roche LightCycler 480	111
Table 4.5: Treatments submitted for microanalysis for both HepG2 and PHH	112
Table 4.6: Effects of glucose, fructose and fatty acids on lipogenic enzyme mRNA expression in HepG2 cells. Mean \pm SEM. Data analysed by three-way ANOVA with	

blocking for plate. <i>n</i> =5 wells per treatment. FA: fatty acid, G: glucose, F: fructose. † <i>P</i> <0.1, * <i>P</i> <0.05, ** <i>P</i> <0.01, *** <i>P</i> <0.001	117
Table 4.7: Effects of glucose, fructose and fatty acids on lipogenic enzyme mRNA expression in primary human hepatocytes. Mean±SEM. Data analysed by three-way ANOVA with blocking for plate. <i>n</i> =3 wells per treatment. FA: fatty acid, G: glucose, F: fructose. † <i>P</i> <0.1, * <i>P</i> <0.05, ** <i>P</i> <0.01, *** <i>P</i> <0.001	117
Table 4.8: Effects of glucose, fructose and fatty acids on SREBP1 mRNA expression in HepG2 cells. Mean±SEM. Data analysed by three-way ANOVA with blocking for plate. <i>n</i> =5 wells per treatment. FA: fatty acid, G: glucose, F: fructose. † <i>P</i> <0.1, * <i>P</i> <0.05, ** <i>P</i> <0.01, *** <i>P</i> <0.001	120
Table 4.9: Effects of glucose, fructose and fatty acids on SREBP1 mRNA expression in primary human hepatocytes. Mean±SEM. Data analysed by three-way ANOVA with blocking for plate. <i>n</i> =3 wells per treatment. FA: fatty acid, G: glucose, F: fructose. † <i>P</i> <0.1, * <i>P</i> <0.05, ** <i>P</i> <0.01, *** <i>P</i> <0.001	120
Table 4.10: Fructose effect on SREBP1a mRNA expression in primary human hepatocytes: Bonferroni multiple comparisons	121
Table 4.11: Fructose effect on SREBP1c mRNA expression in primary human hepatocytes: Bonferroni multiple comparisons	121
Table 4.12: Effects of glucose, fructose and fatty acids on PNPLA3, DGAT1 and CPT1α mRNA expression in HepG2 cells. Mean±SEM. Data analysed by three-way ANOVA with blocking for plate. <i>n</i> =5 wells per treatment. FA: fatty acid, G: glucose, F: fructose. † <i>P</i> <0.1, * <i>P</i> <0.05, ** <i>P</i> <0.01, *** <i>P</i> <0.001	124
Table 4.13: Effects of glucose, fructose and fatty acids on PNPLA3, DGAT1 and CPT1α mRNA expression in primary human hepatocytes. Mean±SEM. Data analysed by three-way ANOVA with blocking for plate. <i>n</i> =3 wells per treatment. FA: fatty acid, G: glucose, F: fructose. † <i>P</i> <0.1, * <i>P</i> <0.05, ** <i>P</i> <0.01, *** <i>P</i> <0.001	124

Table 4.14: Effects of glucose, fructose and fatty acids on PPARGC1 α and ApoB mRNA expression in HepG2 cells. Mean \pm SEM. Data analysed by three-way ANOVA with blocking for plate. $n=5$ wells per treatment. FA: fatty acid, G: glucose, F: fructose. $\dagger P<0.1$, $*P<0.05$, $**P<0.01$, $***P<0.001$	127
Table 4.15: Effects of glucose, fructose and fatty acids on PPARGC1 α and ApoB mRNA expression in primary human hepatocytes. Mean \pm SEM. Data analysed by three-way ANOVA with blocking for plate. $n=3$ wells per treatment. FA: fatty acid, G: glucose, F: fructose. $\dagger P<0.1$, $*P<0.05$, $**P<0.01$, $***P<0.001$	127
Table 4.16: Effects of glucose, fructose and fatty acids on carbohydrate metabolism related mRNA expression in HepG2 cells. Mean \pm SEM. Data analysed by three-way ANOVA with blocking for plate. $n=5$ wells per treatment. FA: fatty acid, G: glucose, F: fructose. $\dagger P<0.1$, $*P<0.05$, $**P<0.01$, $***P<0.001$	130
Table 4.17: Effects of glucose, fructose and fatty acids on carbohydrate metabolism related mRNA expression in primary human hepatocytes. Mean \pm SEM. Data analysed by three-way ANOVA with blocking for plate. $n=3$ wells per treatment. FA: fatty acid, G: glucose, F: fructose. $\dagger P<0.1$, $*P<0.05$, $**P<0.01$, $***P<0.001$	130
Table 4.18: Correlation matrix of mRNA expressions in HepG2 cells (bottom left) and PHH (top right). R values from Pearson's correlation tests. Green $P<0.05$, Orange $P<0.1$. HK2 not measured in PHH. NS: not significant	136
Table 4.19: Differences in gene expression in PHH compared to HepG2 cells determined by microarray pairwise comparison, and the quantitative reverse transcription PCR (RT-qPCR) standard curves analysed using linear regression to compare intercepts.....	145
Table 5.1: PCR primers for confirming HepG2 and Huh7 cell PNPLA3 genotype	172
Table 5.2: Thermocycling conditions for PCR amplification of the PNPLA3 coding sequence from HepG2 and Huh7 genomic DNA. The denaturation, annealing and extension steps were cycled 30 times	172

Table 5.3: Sequencing primers for confirming HepG2 and Huh7 cell PNPLA3 genotype	173
Table 5.4: Cycling conditions for the SNP genotyping assay carried out on a Roche LightCycler 480 II.....	174
Table 5.5: Cloning primers for PNPLA3 incorporating the attB sites for Gateway cloning	175
Table 5.6: Thermocycling conditions for PCR amplification of the PNPLA3 coding sequence. The denaturation, annealing and extension steps were cycled 34 times	176
Table 5.7: Reaction components for the BP recombination reaction before adding the enzyme.....	178
Table 5.8: Antibiotics used in agar plates for culturing each bacterial cell type	180
Table 5.9: Sequencing primers designed to flank the single nucleotide polymorphisms of interest	182
Table 5.10: Mutagenesis primers	183
Table 5.11: Thermocycling conditions for mutagenesis PCR. The denaturation, annealing and extension steps were cycled 18 times	183
Table 5.12: Components of the LR recombination reaction.....	187
Table 5.13: Combinations of antibodies and detection methods tested to optimise the Abcam PNPLA3 antibody	195
Table: 5.14: Raw data and allele calls from the SNP TaqMan genotyping assay. Allele X: C, Allele Y: G.....	200
Table 5.15: Summary of the genotypes and responses of the cell lines and livers to nutritional stimuli. All cells accumulated lipid in response to fatty acid treatment. McA- RH7777 cells not included as they could not be genotyped using the human assay. (See section 3.4.3 for full lipid accumulation data)	201

Table 5.16: PNPLA3 expression in MCF7 cells transfected with lentiviruses, measured by CP value	202
Table 5.17: PNPLA3 expression in HepG2 cells transfected with lentiviruses, measured by CP value.....	203
Table 6.1: Summary table of results presented in this thesis, comparing three hepatoma cell lines and primary human hepatocytes.....	213
Table S1: Effects of fatty acids, glucose and fructose on lipid accumulation in HepG2 cells. Data was measured as Nile Red fluorescence per μg DNA then converted to fold change relative to $0\mu\text{M}$ fatty acid + 5mM glucose + 0mM fructose. Values are expressed as mean \pm SEM. Data analysed by three-way ANOVA with blocking for plate. $n=5$ wells per treatment per plate. FA: fatty acid, G: glucose, F: fructose. $\dagger P<0.1$, $*P<0.05$, $**P<0.01$, $***P<0.001$	228
Table S2: Effects of fatty acids, glucose and fructose on lipid accumulation in Huh7 cells. Data was measured as Nile Red fluorescence per μg DNA then converted to fold change relative to $0\mu\text{M}$ fatty acid + 5mM glucose + 0mM fructose. Values are expressed as mean \pm SEM. Data analysed by three-way ANOVA with blocking for plate. $n=5$ wells per treatment per plate. FA: fatty acid, G: glucose, F: fructose. $\dagger P<0.1$, $*P<0.05$, $**P<0.01$, $***P<0.001$	229
Table S3: Effects of fatty acids, glucose and fructose on lipid accumulation in McA-RH7777 cells. Data was measured as Nile Red fluorescence per μg DNA then converted to fold change relative to $0\mu\text{M}$ fatty acid + 5mM glucose + 0mM fructose. Values are expressed as mean \pm SEM. Data analysed by three-way ANOVA with blocking for plate. $n=5$ wells per treatment per plate. FA: fatty acid, G: glucose, F: fructose. $\dagger P<0.1$, $*P<0.05$, $**P<0.01$, $***P<0.001$	230
Table S4: Effects of fatty acids, glucose and fructose on lipid accumulation in primary human hepatocytes. Data was measured as Nile Red fluorescence per μg DNA then	

converted to fold change relative to 0 μ M fatty acid + 5mM glucose + 0mM fructose.

Values are expressed as mean \pm SEM. Data analysed by three-way ANOVA with blocking for plate. $n=5$ wells per treatment per plate. FA: fatty acid, G: glucose, F: fructose.

$\dagger P<0.1$, $*P<0.05$, $**P<0.01$, $***P<0.001$	231
Table S5: L312 fatty acid \times glucose interaction: Bonferroni multiple comparisons	232
Table S6: L326 fatty acid \times glucose interaction: Bonferroni multiple comparisons	232
Table S7: L321 fatty acid \times glucose interaction: Bonferroni multiple comparisons	232
Table S8: L312 fatty acid \times fructose interaction: Bonferroni multiple comparisons	232
Table S9: L317 fatty acid \times fructose interaction: Bonferroni multiple comparisons	233
Table S10: L329 fatty acid \times fructose interaction: Bonferroni multiple comparisons	233
Table S11: L317 glucose \times fructose interaction: Bonferroni multiple comparisons	233
Table S12: Effects of fatty acids, glucose and insulin on lipid accumulation in HepG2 cells. Data was measured as Nile Red fluorescence per μ g DNA then converted to fold change relative to 0 μ M fatty acid + 5mM glucose + 0nM insulin. Values are expressed as mean \pm SEM. Data analysed by three-way ANOVA with blocking for plate. $n=5$ wells per treatment per plate. FA: fatty acid, G: glucose, I: insulin. $\dagger P<0.1$, $*P<0.05$, $**P<0.01$, $***P<0.001$	234
Table S13: Effects of fatty acids, glucose and insulin on lipid accumulation in primary human hepatocytes. Data was measured as Nile Red fluorescence per μ g DNA then converted to fold change relative to 0 μ M fatty acid + 5mM glucose + 0nM insulin. Values are expressed as mean \pm SEM. Data analysed by three-way ANOVA with blocking for plate. $n=5$ wells per treatment per plate. FA: fatty acid, G: glucose, I: insulin. $\dagger P<0.1$, $*P<0.05$, $**P<0.01$, $***P<0.001$	235
Table S14: L317 fatty acid \times glucose interaction: Bonferroni multiple comparisons	236
Table S15: L317 fatty acid \times insulin interaction: Bonferroni multiple comparisons	236
Table S16: L319 fatty acid \times glucose interaction: Bonferroni multiple comparisons	236

Table S17: L321 fatty acid × glucose interaction: Bonferroni multiple comparisons	236
Table S18: L321 fatty acid × insulin interaction: Bonferroni multiple comparisons.....	237
Table S19: Fatty acid × fructose interaction effect on fatty acid synthase (FASN) mRNA expression in primary human hepatocytes: Bonferroni multiple comparisons	237
Table S20: Glucose × fructose interaction effect on fatty acid synthase (FASN) mRNA expression in primary human hepatocytes: Bonferroni multiple comparisons	237
Table S21: Glucose × fructose interaction effect on stearyl-coA desaturase (SCD) mRNA expression in primary human hepatocytes: Bonferroni multiple comparisons	238
Table S22: Glucose × fructose interaction effect on ApoB mRNA expression in HepG2 cells: Bonferroni multiple comparisons	238
Table S23: Glucose × fructose interaction effect on ApoB mRNA expression in primary human hepatocytes: Bonferroni multiple comparisons.....	238
Table S24: Glucose × fructose interaction effect on ChREBP mRNA expression in primary human hepatocytes: Bonferroni multiple comparisons.....	239
Table S25: Fructose effect on LPK mRNA expression in primary human hepatocytes: Bonferroni multiple comparisons	239
Table S26: Fructose effect on GLUT2 mRNA expression in primary human hepatocytes: Bonferroni multiple comparisons	239

Acknowledgements

Prof Andrew Salter, Prof John Brameld and Dr Andrew Bennett for their continued support over the last 3 years, and for the ideas and knowledge contributed.

My parents for always supporting me and being patient good eggs through all the ups and downs. I love you both.

The technicians at Sutton Bonington (Cathy Wells, Kirsty Jewell and Zoe Daniel) for putting up with years of (often) silly questions and always providing help with a smile. You have all become good friends.

The technicians in the FRAME lab (Monika Owen and Nikki De Vivo) for always providing friendly help and for preparing all the primary hepatocytes, often well into the evening.

All of Nutritional Sciences, particularly the coffee time crew, for endless silliness and cake. Especially Maddy, who has been on my right all the way through (very nearly).

Other staff and students who have helped with my work: Wichitra Asanprakit, Amer Imraish, Marcos Castellanos Uribe, Iqbal Khan, and Richard Emes.

The University of Nottingham, The Rank Prize Funds, and FRAME for funding and resources.

Everyone at Sutton Bonington Baptist Church for being a second family, feeding me and praying for me. Especially my house group for listening to the latest instalments in the PhD story each meeting.

To God for guiding me, sustaining me, and for being a source of inner peace.

To sum up the last few years: *“All I know is that I still don’t know a lot” – Switchfoot*

Abbreviations

ACC	Acetyl-coA carboxylase
ACS	Acyl-coA synthetase
ACSL	Acyl-CoA synthetase long-chain family member 1
AKT	Protein kinase B
AMP	Adenosine monophosphate
ApoB	Apolipoprotein B
ATP	Adenosine triphosphate
BCP	1-bromo-3-chloropropane
BMI	Body mass index
BSA	Bovine serum albumin
cDNA	Complementary DNA
CERS5	Ceramide synthase 5
ChoRE	Carbohydrate response element
ChREBP	Carbohydrate response element binding protein
CON	Control
CP	Crossing point
CPT1 α	Carnitine palmitoyltransferase-1a
CRP	C-reactive protein
CVD	Cardiovascular disease
CYP	Cytochrome P450
CYP1A2	cytochrome P450 family 1 subfamily A polypeptide 2
DAG	Diacylglycerol
DGAT	Diacylglycerol transferase
DMEM	Dulbecco's Modified Eagle Medium
DNA	Deoxyribonucleic acid
DNL	<i>De novo</i> lipogenesis
DTT	Dithiothreitol
ECL	Enhanced chemiluminescence
ECM	Extracellular matrix
EGTA	Ethylene glycol tetraacetic acid
EMEM	Minimum Essential Medium Eagle
ER	Endoplasmic reticulum

FA	Fatty acid
FASN	Fatty acid synthase
FATP	Fatty acid transport protein
FBS	Foetal bovine serum
FC	Fold change
FDR	False discovery rate
FFA	Free fatty acids
FOXO1	Forkhead box protein O1
GCK	Glucokinase
GCKR	Glucokinase regulatory protein
GFP	Green fluorescent protein
GGT	Gamma-glutamyl-transferase
GI	Gastrointestinal
GLUT	Glucose transporter
HBSS	Hank's buffered saline solution
HFCS	High fructose corn syrup
HK2	Hexokinase 2
HSCs	Hepatic stellate cells
HSL	Hormone sensitive lipase
IGF1	Insulin-like growth factor 1
IL6	Interleukin 6
iPLA2-ε	Calcium independent phospholipase A2 epsilon
JAK2	Janus kinase 2
KHK	Ketohexokinase
LB	Lysogeny broth
LDL	Low density lipoprotein
LP	Lentivirus particles
LPAAT	Lysophosphatidic acid acyltransferase
LPK	Liver pyruvate kinase
MAG	Monoacylglycerol
MBOAT7	Membrane bound O-acyltransferase domain-containing 7
MOI	Multiplicity of infection
MRI	Magnetic resonance imaging
mRNA	Messenger RNA

mTORC1	Mammalian target of rapamycin complex 1
MTTP	Microsomal triglyceride transfer protein
MUFA	Monounsaturated fatty acids
MUT	Polymorphic
NAFLD	Non-alcoholic fatty liver disease
NASH	Non-alcoholic steatohepatitis
NC	Negative control
NEFA	Non-esterified fatty acids
NT	Non-transfected
OD	Optical density
pAKT	Phosphorylated AKT
PBS	Phosphate-buffered saline
PC	phosphatidylcholines
PCA	Principal component analysis
PCK1	Phosphoenolpyruvate Carboxykinase 1
PCR	Polymerase chain reaction
PEP	phosphoenolpyruvate
PHH	Primary human hepatocytes
PKC	protein kinase C
PLIN2	Perilipin 2
PNPLA3	Patatin-like phospholipase domain containing 3
PP2A	Protein phosphatase 2A
PPARGC1 α	Peroxisome proliferator-activated receptor gamma coactivator 1-alpha
PUFA	Polyunsaturated fatty acids
RBP4	Retinol binding protein 4
RNA	Ribonucleic acid
RT-qPCR	Quantitative reverse transcription PCR
SCD	Stearoyl-coA desaturase
SDS	Sodium dodecyl sulphate
SFA	Saturated fatty acids
SGMS2	Sphingomyelin Synthase 2
SNP	Single nucleotide polymorphism
SOC	Super optimal broth with catabolite repression
SREBP	Sterol regulatory element-binding protein

STAT	Signal transducer and activator of transcription
TAG	Triacylglycerol
TBST	Tris-buffered saline with 0.1% Tween
TCA	Tricarboxylic acid
TNE	Tris-HCl NaCl EDTA
TNF α	Tumour necrosis factor alpha
VLDL	Very low density lipoprotein
WT	Wild-type

Chapter 1: Introduction to non-alcoholic fatty liver disease (NAFLD) and hepatic steatosis.

1.1 The Liver

The liver is the largest organ in the body and has a central role in maintaining energy homeostasis. It is composed of parenchymal cells (hepatocytes) and non-parenchymal cells (mainly hepatic stellate cells, Kupffer cells and sinusoidal endothelial cells) (Qin and Crawford, 2018). The main functions of hepatocytes are to secrete bile, to metabolise drugs and toxins, to maintain glucose homeostasis, and to uptake and secrete plasma proteins and lipoprotein particles (Qin and Crawford, 2018). Hepatocytes metabolise nutrients delivered from the gastrointestinal (GI) tract via the hepatic portal vein, which provides about 80% of the liver's blood supply (Qin and Crawford, 2018), or transported from other tissues. Sinusoidal endothelial cells provide a fenestrated cell barrier between the sinusoidal blood and the space of Disse (Figure 1.1) (Sorensen et al., 2015). Hepatocytes extend into the space of Disse and absorb nutrients. Hepatic stellate cells (HSCs) have a key role in vitamin A homeostasis by storing vitamin A. They also produce extracellular matrix (ECM) and have immunoregulatory function (Qin and Crawford, 2018). Kupffer cells are phagocytic macrophages, removing dead hepatocytes and gut derived toxins. They have immune function and release cytokines (Qin and Crawford, 2018).

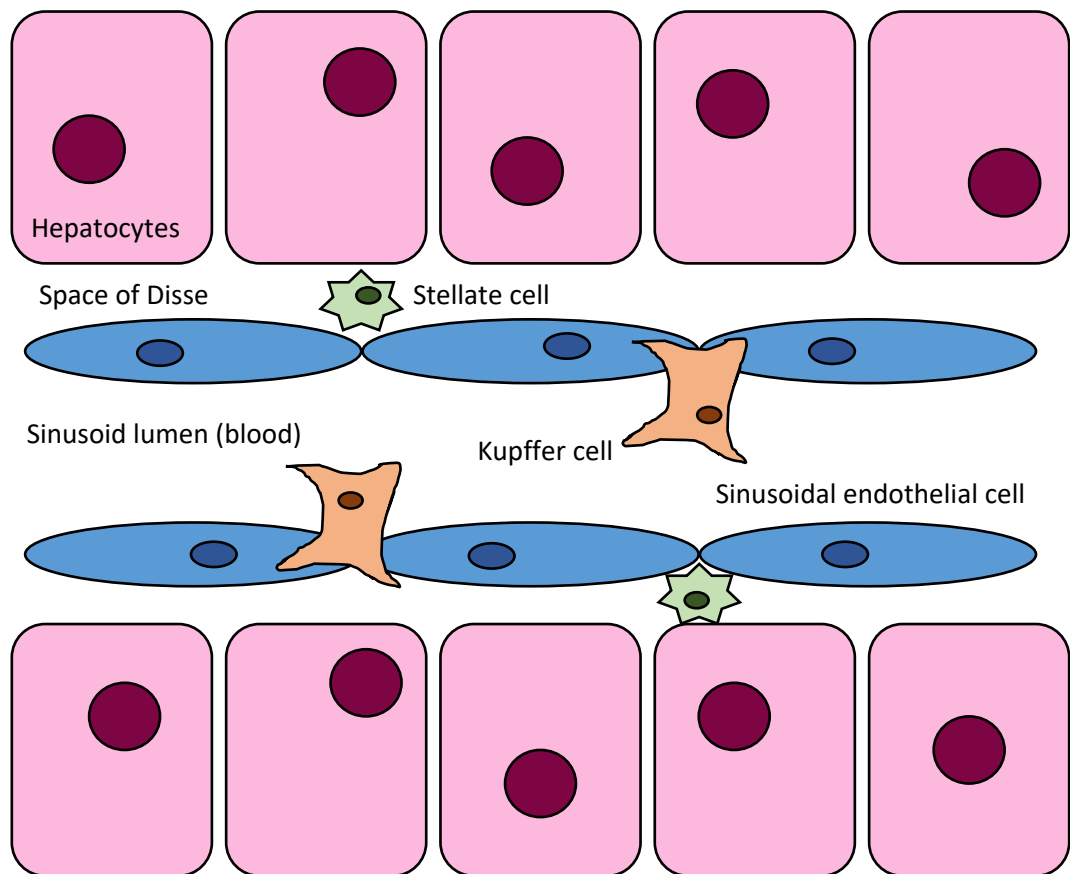


Figure 1.1: The liver sinusoid, showing the location of the main liver cell types. Re-drawn from Sorensen et al. (2015) and Li et al. (2017).

1.2 Hepatic steatosis

Hepatocytes have the capacity to store excess energy as glycogen and triacylglycerol (TAG). The accumulation of TAG as lipid droplets within hepatocytes is termed hepatic steatosis. As there is no clear definition of hepatic steatosis *in vitro*, this will be referred to as lipid accumulation throughout the thesis. Intracellular TAG can originate from re-esterification of plasma non-esterified fatty acids (NEFA) from adipose tissue or dietary sources, or from *de novo* lipogenesis (DNL) from acetate derived from carbohydrates (Figure 1.2). The pathways involved in lipogenesis and TAG synthesis are discussed in more detail in Chapter 4. In non-alcoholic fatty liver disease (NAFLD) patients, on

average 59% of TAG palmitate is from NEFA, 26.1% is from DNL and 14.9% is from dietary fat (Donnelly et al., 2005).

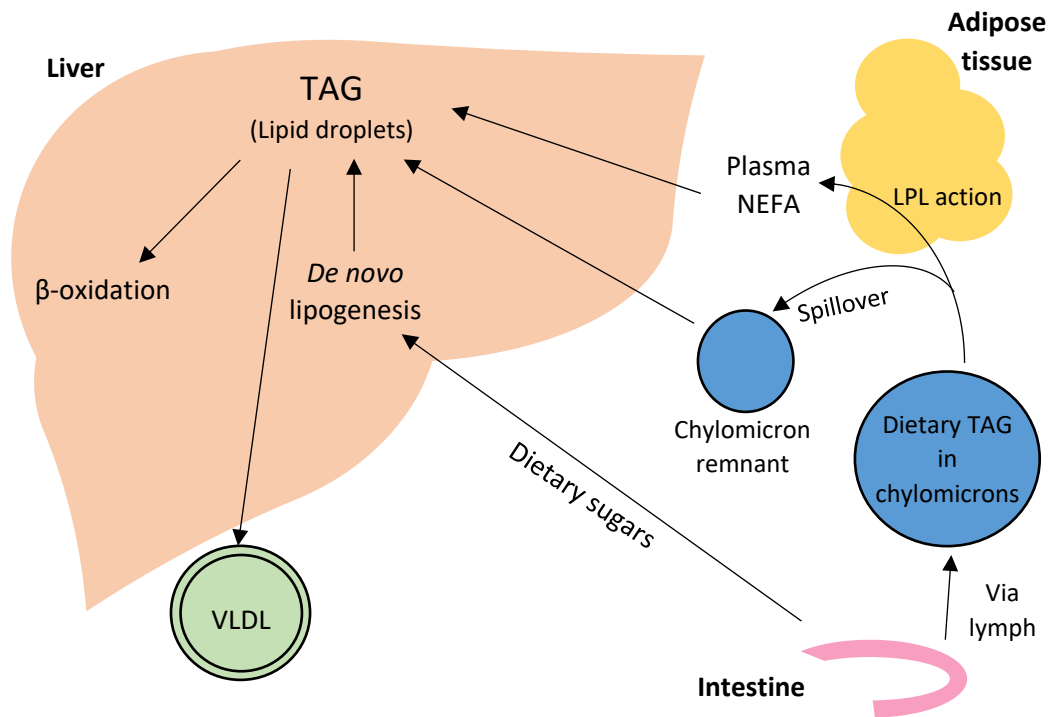


Figure 1.2: Mechanisms of triacylglycerol (TAG) accumulation and secretion/breakdown. TAG stored in hepatocytes can result from *de novo* lipogenesis from dietary sugars and TAG synthesis from dietary fatty acids or NEFA released from adipose tissue by lipoprotein lipase activity. Stored TAG can be oxidised or secreted in VLDL. For detailed hepatic pathways see Chapter 4, Figure 4.1. NEFA: non-esterified fatty acids, VLDL: very low density lipoprotein, FA: fatty acids, LPL: lipoprotein lipase

Simple steatosis can be reversed if the TAG is released from the lipid droplets either secreted in very low density lipoproteins (VLDL), or used as an energy source within the liver via β-oxidation (Figure 1.2). VLDL assembly has two main steps; firstly, apolipoprotein B100 (ApoB) is translocated to the endoplasmic reticulum (ER) which is dependent on initial lipidation by insulin-regulated microsomal triglyceride transfer protein (MTTP) (Choi and Ginsberg, 2011). Secondly, lipids are added to the ApoB protein at the ER to create precursor VLDL particles which are then transported to the

Golgi apparatus for maturation and secretion into the circulation (Figure 1.3) (Tiwari and Siddiqi, 2012).

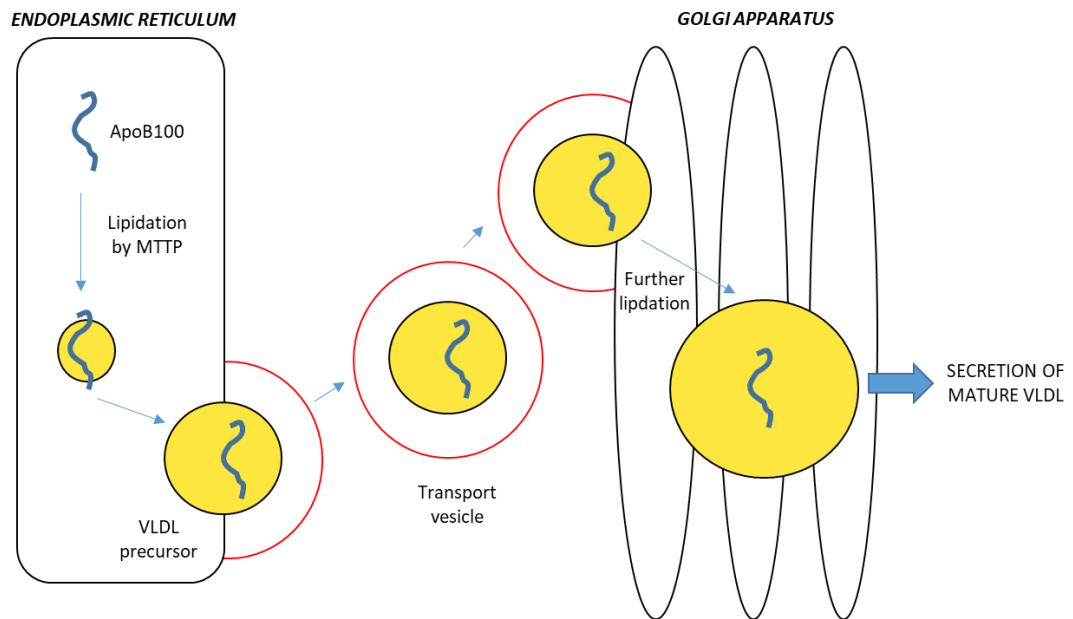


Figure 1.3: Basic overview of hepatic very low density lipoprotein (VLDL) assembly and secretion. MTP: microsomal triglyceride transfer protein. Drawn using information from Tiwari and Siddiqi (2012) and Choi and Ginsberg (2011)

B-oxidation of fatty acids, which occurs in the mitochondria and is elevated in the fasting and starved states, produces ketone bodies to fuel extrahepatic tissues and adenosine triphosphate (ATP) for gluconeogenesis and other pathways (Figure 1.4) (Rui, 2014). Fatty acid derived acyl-coA is initially transported into the mitochondria by carnitine palmitoyltransferase 1 (CPT1), which is introduced in more detail in Chapter 4.

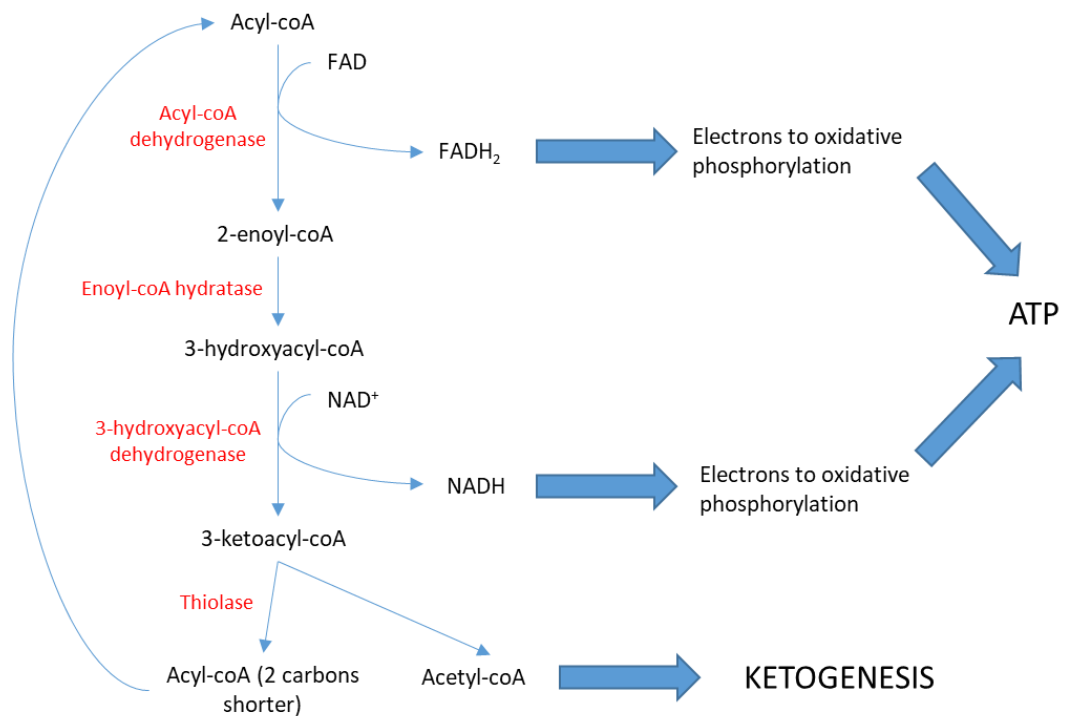


Figure 1.4: Mitochondrial β -oxidation of fatty acids, providing substrate for ATP production and ketogenesis in the fasted state. ATP: adenosine triphosphate

1.3 NAFLD – definition, diagnosis and epidemiology

Non-alcoholic fatty liver disease (NAFLD) is defined as the presence of steatosis in greater than 5% of hepatocytes in the absence of secondary causes, such as excessive alcohol consumption of >30g/day for men or >20g/day for women (EASL–EASD–EASO, 2016, Marchisello et al., 2019). Diagnosis is challenging due to the inaccessibility of the liver and the variability in current methodology. Liver biopsy is considered the most reliable approach and the ‘gold standard’ diagnosis tool, but this comes with risk to the patient and is costly (Chalasani et al., 2012, Marchisello et al., 2019). Non-invasive diagnostic tools include a range of imaging techniques, including ultrasonography and magnetic resonance imaging (MRI), and blood tests for elevated liver enzymes and TAG (Marchisello et al., 2019, EASL–EASD–EASO, 2016). Tools have been developed to predict NAFLD using known risk factors. For example, the Fatty Liver Index combines

body mass index (BMI), waist circumference, fasting blood TAG and gamma-glutamyl-transferase (GGT) into an algorithm to predict fatty liver (Bedogni et al., 2006).

However, blood tests tend to underestimate NAFLD prevalence in comparison with imaging (Younossi et al., 2016b). Of importance, non-alcoholic steatohepatitis (NASH), the more severe progression of NAFLD (see section 1.4), can only be accurately distinguished from NAFLD by liver biopsy to observe lobular inflammation and hepatocyte ballooning (EASL–EASD–EASO, 2016).

A recent meta-analysis (Younossi et al., 2016b), including over 8.5 million people from 22 countries, estimated that 25% of the world adult population has NAFLD, with the highest prevalence rates in the Middle East (32%) and South America (31%). Identified metabolic comorbidities included the metabolic syndrome, obesity, hyperlipidaemia, hypertension and type 2 diabetes (Younossi et al., 2016b). This is consistent with the commonly used statement that NAFLD is the hepatic manifestation of the metabolic syndrome (Buzzetti et al., 2016, Hodson, 2019, Hannah and Harrison, 2016). NAFLD presents a huge economic as well as clinical burden on the world population. One conservative model predicted that in the USA alone, 64 million individuals have NAFLD and the associated annual economic burden is \$103 billion, excluding indirect costs such as work productivity loss due to ill health (Younossi et al., 2016a). Prevention strategies are key to cutting down these figures and preventing them rising further.

1.4 NAFLD pathophysiology

Genetic, environmental and metabolic factors are all instrumental in the development of NAFLD and NASH. The most recent hypothesis is that of the ‘multiple-hit’ pathogenesis described by Buzzetti et al. (2016) and by (Fang et al., 2018). In brief, dietary and environmental factors are thought to lead to adipose tissue dysfunction,

insulin resistance, elevated serum TAG and cholesterol, and a disrupted intestinal microbiome. Insulin resistance increases hepatic DNL and adipose tissue lipolysis, and the increased hepatic fatty acid flux could result in TAG accumulation in hepatocytes. However, it is important to note that elevated plasma NEFA can exist without insulin resistance, and that insulin resistance can exist without raised NEFA (Karpe et al., 2011), suggesting a more complex relationship requiring further research; section 1.6 introduces thoughts on the cycle of NAFLD and insulin resistance. Metabolic stress from lipotoxicity leads to inflammation, further contributing to insulin resistance (Buzzetti et al., 2016). A disrupted microbiome increases small bowel permeability and production of short chain fatty acids (mainly acetate, butyrate and propionate) in the bowel, resulting in further fatty acid absorption and inflammatory pathway activation. Genetic factors affecting the amount of fat stored in the liver can play into these pathways to create a state of chronic inflammation (Buzzetti et al., 2016).

Once established, NAFLD can progress into more severe disease states (Table 1.1, Figure 1.5). The first progression is into non-alcoholic steatohepatitis (NASH), which is characterised by inflammation. The prevalence of NASH amongst NAFLD patients is estimated to be between 7% and 30% (Younossi et al., 2016b). NASH patients diagnosed by biopsy have higher incidence of obesity, hypertriglyceridemia, type 2 diabetes and hypertension (Younossi et al., 2016b). Pro-inflammatory cytokines and chemokines secreted by injured and apoptotic hepatocytes can contribute to inflammation, in addition to activation of pro-inflammatory Kupffer cells and infiltration of other inflammatory cells such as macrophages (Liu et al., 2016a).

Table 1.1: Stages of NAFLD and their pathophysiology. Modified from Glen et al. (2016)	
Stage	Pathophysiology
Non-alcoholic fatty liver (NAFL, hepatic steatosis)	Accumulation of fat in the liver without excessive alcohol consumption.
Non-alcoholic steatohepatitis (NASH)	Fatty liver is combined with inflammation and cell damage.
Fibrosis	Liver scarring and an inflamed liver.
Cirrhosis	Late stage of chronic liver disease. Nodules of damaged cells surrounded by scarring.

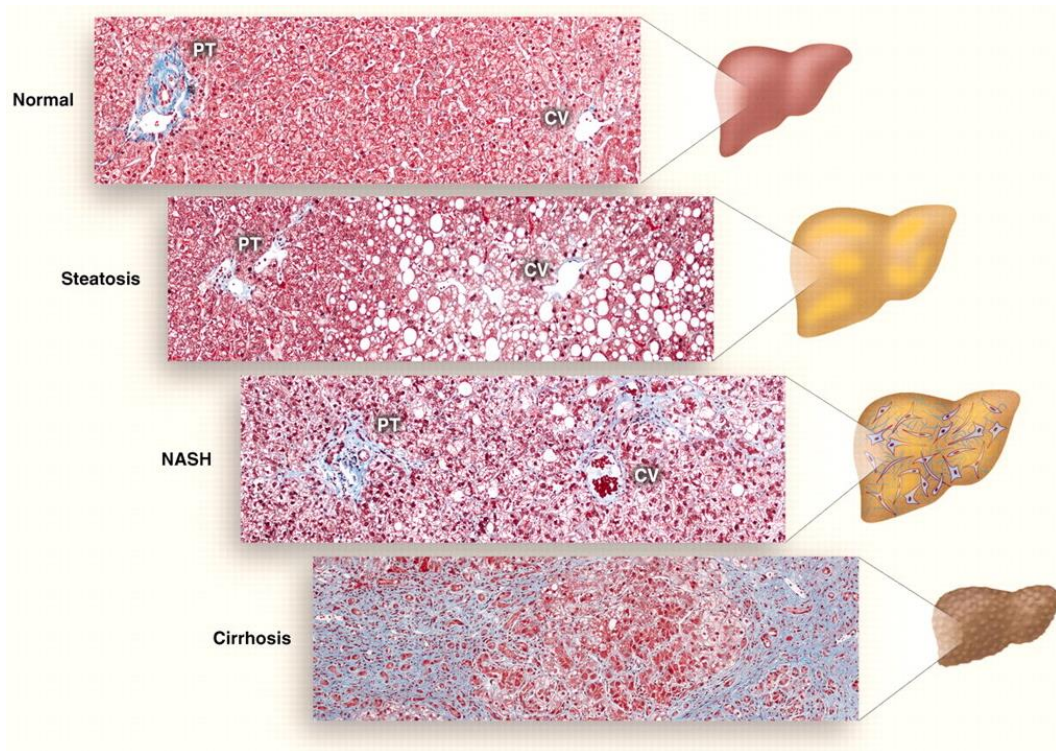


Figure 1.5: Histological sections of livers at different disease states. Collagen stained blue with Masson's trichrome stain. PT: portal triad (hepatic artery, portal vein, and bile duct), CV: central vein. From Cohen et al. (2011)

Fibrosis can progress from NASH, with deposition of ECM (including collagen) forming scar tissue. HSCs are the main cell type in producing ECM; they become activated in liver injury and shift to a myofibroblast-like phenotype (Liu et al., 2016a).

Cirrhosis is the final stage of NAFLD, where the liver is irreversibly damaged and scarred (Figure 1.5). About 20% of NASH patients will progress to cirrhosis (Rinella, 2015).

Complications of cirrhosis include portal hypertension and hepatocellular carcinoma (Calzadilla Bertot and Adams, 2016), and it is one of the leading causes of liver transplant (Marchisello et al., 2019).

Despite this progression, liver related death is not the primary cause of death in NAFLD patients, with cardiovascular disease (CVD) representing the leading cause (Adams et al., 2017). NAFLD is associated with increased risk of CVD events (Targher et al., 2016) and subclinical atherosclerosis (Zheng et al., 2018). Although NAFLD and CVD often share comorbidities such as the metabolic syndrome and obesity, there is evidence that NAFLD is an independent risk factor for hypertension, type 2 diabetes and CVD (Lonardo et al., 2018). The mechanisms behind this are still incompletely understood, but a more pro-atherogenic plasma lipoprotein and triglyceride profile and the release of inflammatory molecules from the liver are thought to be factors (Francque et al., 2016).

1.5 NAFLD treatment

There is currently no “cure” for NAFLD. Dietary and lifestyle changes are recommended, such as calorie restriction, increased physical activity, and following a Mediterranean-style diet (EASL–EASD–EASO, 2016). For adults with NASH, pharmacological treatments such as vitamin E can be used to reduce NASH severity, and in obese patients bariatric surgery is effective to induce weight loss and consequently reduce liver fat and NASH progression (EASL–EASD–EASO, 2016).

1.6 NAFLD and insulin resistance

The relationship between NAFLD and insulin resistance is complex and not fully understood, and it is widely debated which is the first to manifest. On the one hand, insulin resistance inhibits the action of insulin on hormone-sensitive lipase (HSL) in adipose tissue, increasing the release of NEFA into the circulation. These fatty acids may then be incorporated into TAG and deposited in various organs, including the liver. In NAFLD patients about 60% of the TAG palmitate in the liver is derived from NEFA released from adipose tissue (Donnelly et al., 2005). Insulin also plays a role in stimulating DNL in the liver. Consequently it would be expected that insulin resistance decreases DNL, but this does not appear to be the case, suggesting 'selective insulin resistance'. This is the phenomenon where the hepatic insulin signalling pathways involved in inhibiting glycogenolysis and gluconeogenesis, *via* forkhead box protein O1 (FOXO1), are disrupted, but the ability of insulin to stimulate lipogenesis via the mammalian target of rapamycin complex 1 (mTORC1) pathway is retained (although other signalling molecules and pathways may also interact) (Leavens and Birnbaum, 2011). Combined, this results in the liver producing both TAG and glucose. The subsequent hyperglycaemia, hypertriglyceridemia and hyperinsulinemia are all associated with the development of type 2 diabetes.

The converse argument is that hepatic insulin resistance is induced by lipids that have accumulated in the liver. One hypothesis is that diacylglycerol (DAG) accumulation in fat loaded cells activates protein kinase C epsilon (PKC ϵ) which inhibits insulin signalling pathways (Petersen and Shulman, 2017). Another hypothesis is the action of ceramides, which activate PKC ζ , impairing the action of protein kinase B (AKT) in insulin signalling (Petersen and Shulman, 2017). Furthermore, ceramide activation of protein phosphatase 2A (PP2A) leads to de-phosphorylation and consequent deactivation of AKT (Petersen and Shulman, 2017), meaning that insulin signalling is impaired and

glucose and lipid homeostasis are disrupted as above. These pathways require further research.

In reality, all these pathways are likely to interact in forming a vicious circle of insulin resistance and hepatic lipid accumulation.

1.7 Dietary factors

1.7.1 Macronutrients or calories

While diet plays an important role in the development of NAFLD, it is still debated whether it is the macronutrient composition that increases risk or simply the amount of energy consumed. The type of studies carried out makes this question difficult to answer, as human feeding studies are usually short term and use proportions of fat or sugar which would not be found in a normal diet (Sharp et al., 2018). The fact that features of the metabolic syndrome such as increased BMI, waist circumference, and fasting glucose are associated with NAFLD suggests that energy balance is at least in part responsible. However, there is a lot of interest in the specific effects of fatty acids, glucose and fructose. All these nutrients can provide substrate for TAG synthesis and DNL, as well as influencing gene expression, a topic which is discussed in detail in Chapter 4. This section introduces the current thinking derived from human studies. A review by Parry and Hodson (2017) is very informative in this area.

1.7.2 Sugars

Glucose and fructose are two dietary monosaccharides that have the same chemical formula but are structurally different (Figure 1.6). Fructose consumption has increased dramatically over the last century and is the main sugar to be implicated in NAFLD

(Softic et al., 2016, Ter Horst and Serlie, 2017). It has recently been proposed that low doses of fructose are metabolised in the small intestinal enterocytes to glucose and organic acids, but that high doses can exceed the capacity of the enterocytes and there is spill-over into the portal circulation where it is taken up by the liver (Jang et al., 2018). Glucose, on the other hand, is the primary energy source for most cells. It is rarely studied in isolation but is often used as a comparison to fructose in feeding studies. Glucose and fructose are normally ingested together as sucrose or high fructose corn syrup (HFCS, 55% fructose), but feeding studies mostly use fructose or glucose as a single component.

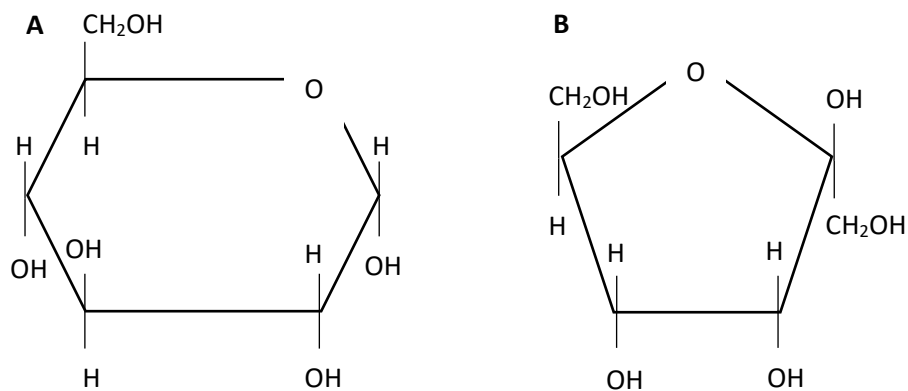


Figure 1.6: The molecular structure of A: glucose and B: fructose

Studies are inconsistent as to whether the steatotic effects of fructose are due to the sugar itself or the weight gain caused by a high fructose diet (Ter Horst and Serlie, 2017). Isocaloric human feeding studies are valuable for determining whether fructose is a risk factor independently of excess energy. One short term study using eight healthy men fed a high fructose (25% of energy) diet under neutral energy balance, which was isocaloric to a diet with the same macronutrient composition but with complex carbohydrates instead of fructose (Schwarz et al., 2015). Whilst weight remained stable, high fructose resulted in increased liver fat and DNL. Another study looked at fructose reduction in Hispanic-American adolescents with steatosis (Jin et al., 2014). Replacing

fructose-containing beverages with calorie matched glucose-only beverages for 4 weeks did not affect hepatic fat but did improve insulin sensitivity and inflammation (Jin et al., 2014). Johnston et al. (2013) fed overweight men glucose or fructose solutions as 25% of their energy intake. In a two week period of consuming the sugars as part of an isocaloric diet, liver fat was not significantly altered in either group, but when consumed as part of a hypercaloric diet both increased liver fat. In another study, Stanhope et al. (2009) showed that fructose at 25% of energy requirement for 10 weeks increased plasma oxidised low density lipoprotein (LDL) and postprandial hepatic DNL but the same amount of glucose did not. One meta-analysis, including studies using isocaloric exchange under conditions of both positive and neutral energy balance, concluded that exchanging fructose for other carbohydrates in an isocaloric context did not affect liver fat (Chiu et al., 2014). Hypercaloric studies, where the fructose was provided as excess energy on top of a control diet, did show an increase in liver fat (Chiu et al., 2014). The analysis also concludes that studies are too short and with too narrow demographics to be of use to real-life situations (Chiu et al., 2014).

One valuable study fed sucrose or HFCS to 64 overweight individuals for 10 weeks at levels found within normal US consumption patterns: 8, 18 or 30% of total energy intake, and found there were no differences in liver fat content (Bravo et al., 2013). In contrast, another study which fed sucrose-sweetened drinks (cola) for 6 months showed significantly increased liver fat compared to subjects drinking milk, diet cola or water (Maersk et al., 2012).

In conclusion, the results from human feeding studies using glucose and fructose are not consistent. There are many confounding factors that could influence the results, such as patient demographics, study duration, the vehicle which is used to ingest the sugar, and whether dietary intake is accurately recorded. *In vitro* models offer the advantage of being able to carefully control the environment and nutrient availability to observe

specific hepatocyte effects, avoiding confounding factors from other tissues such as changes in adipose tissue distribution.

1.7.3 Fatty acids

Dietary fatty acids can be categorised into saturated fatty acids (SFA), monounsaturated fatty acids (MUFA) and polyunsaturated fatty acids (PUFA). Both the amount of fat and the composition of fatty acids in the diet are of interest in NAFLD development. There has been a recent comprehensive review of human feeding trials using dietary fat, which concludes that energy intake is a more important factor than dietary fat percentage (Hodson et al., 2019). Again, results of human studies are difficult to interpret due to different durations, demographics, and the change in dietary carbohydrate content that normally comes alongside altering fat. The review also concludes that high SFA may result in increased liver fat, while supplementation with omega 3 PUFA may reduce liver fat (Hodson et al., 2019).

SFA have come under particular scrutiny for their lipotoxic effects. Incorporation of SFA into the phospholipid membrane of the ER causes ER stress, stimulates apoptotic signalling pathways, and disrupts mitochondrial function (Leamy et al., 2013). ER stress occurs when the ER is no longer able to deal with accumulating misfolded proteins, for example due to changes in membrane fluidity and functionality due to incorporation of SFA phospholipids, and consequently the unfolded protein response is activated which can lead to stimulation of apoptotic pathways (Zhou and Liu, 2014, Leamy et al., 2013). One recent double-blind randomised trial has looked at feeding sunflower oil (high in PUFA, linoleic acid, C18:2n-6) or palm oil (high in SFA, palmitic acid, C16:0) to overweight participants for 8 weeks under conditions of controlled weight gain (Rosqvist et al., 2019). Despite similar weight gain, liver fat increased by over 50% in the

SFA group but decreased by 2% in the PUFA group. Markers of liver injury (plasma ceramides and liver enzymes) were only increased in the SFA group, and PUFA decreased ceramides (Rosqvist et al., 2019). This is convincing evidence that fatty acid composition plays a role in NAFLD. Indeed, Luukkonen et al. (2018) showed that overfeeding SFA increased liver fat more than overfeeding simple sugars or unsaturated fats. Interestingly, SFA also increased adipose tissue lipolysis and plasma ceramides, whereas unsaturated fat decreased lipolysis and did not affect ceramides (Luukkonen et al., 2018), and overfeeding simple sugars resulted in increased DNL.

Overall, composition of dietary fatty acids is an important area for further research and must be taken into account when manipulating fatty acids *in vitro*.

1.8 Genetic factors

In addition to dietary and environmental factors, genetic predisposition plays an important role in the susceptibility of an individual to NAFLD. The genetic variant with the strongest association is a single nucleotide polymorphism (SNP) in the patatin-like phospholipase domain containing 3 (PNPLA3) gene (Kozlitina et al., 2014, Romeo et al., 2008); the rs738409 C/G (I148M) variant is associated with higher liver fat and more severe disease progression (Sookoian and Pirola, 2011). This polymorphism is the focus of Chapter 5 and is discussed in detail within that chapter.

Another SNP associated with liver fat is the transmembrane 6 superfamily member 2 (TM6SF2) rs58542926 C/T (E167K) variant. After PNPLA3, it is the strongest genetic association with liver fat (Kozlitina et al., 2014). The TM6SF2 protein is predominantly localised to the ER, and Huh7 cells expressing the SNP have reduced TM6SF2 protein (Kozlitina et al., 2014). While the exact function of this protein is not yet known, a possible mechanism of this SNP is that carriers have impaired incorporation of PUFA

into TAG, cholesterol esters, and phosphatidylcholines (PC), consequently resulting in increased PUFA free fatty acids (FFA) (Luukkonen et al., 2017). PC deficiency and increased PUFA FFA could reduce lipidation of VLDL particles meaning more lipid is retained in the liver (Luukkonen et al., 2018, Smagris et al., 2016). Other genetic variants that have been implicated in NAFLD include glucokinase regulatory protein (GCKR) and membrane bound O-acyltransferase domain-containing 7 (MBOAT7) (Taliento et al., 2019). GCKR is involved in regulating glucose influx into hepatocytes and the presence of a missense variant impairs activity of the protein, meaning GCKR does not inhibit glucokinase (GCK). Consequently, glucose uptake is constantly active and acetyl-coA production through glycolysis is increased (Taliento et al., 2019). MBOAT7 incorporates unsaturated fatty acids, particularly arachidonic acid, into phosphatidylinositol, and a SNP in this gene results in decreased expression and disrupted phosphatidylinositol remodelling in the liver (Mancina et al., 2016).

1.9 Animal models

Animal models are commonly used in steatosis research, particularly rodent models. They allow for tighter experimental control and longer term studies relative to the lifetime of the animal than is possible in humans. Hyperphagic animal models, for example *ob/ob* and *db/db* mice (both with genetic disruption to leptin signalling), are frequently used but they often need an additional intervention to progress to steatohepatitis (Kanuri and Bergheim, 2013). Dietary rodent models are also common, for example feeding a high fat, high fructose, or methionine and choline deficient diet (Kanuri and Bergheim, 2013). Often these diets are not representative of a typical human diet, for example feeding a diet that is 60% fructose to rats (Ackerman et al., 2005). There are also species differences in metabolism in humans and rodents (see

section 3.1.1); for example, when studying the PNPLA3 polymorphism, Dubuquoy et al. (2011) found that the PNPLA3 gene was regulated by the carbohydrate response element binding protein (ChREBP) in mouse hepatocytes but not in HepG2 cells or immortalised human hepatocytes.

Other non-rodent animal models are less commonly used but have potential. For example, five-week old female Ossabaw pigs fed a Western-style diet high in fat, fructose and cholesterol for 16 or 36 weeks developed NASH and fibrosis (Panasevich et al., 2018). Similarly, five- to ten-month old male and female Ossabaw pigs fed an atherogenic (high fat) diet with high fructose for 24 weeks developed metabolic syndrome and steatosis, but not fibrosis in this instance (Lee et al., 2009). Interestingly, pigs fed high fructose without high fat did not show hepatic steatosis. Non-human primate models also have potential; these species can develop NAFLD and NASH, and are more similar to humans in their physiology, behaviour and genetics (Cox et al., 2017). However, there would be more logistical and ethical issues surrounding the widespread use of non-human primates.

1.10 Towards a physiologically relevant *in vitro* human model

With these points in mind, and the emphasis on the 3Rs (replacement, reduction, refinement) to reduce the number of animals sacrificed to scientific research, the development of human models is desirable. *In vivo* human liver research is challenging due to reasons already mentioned and the invasive procedures required to access the liver. Similar to diagnosing NAFLD, *in vivo* human studies often rely on indirect measurements from the circulation or on stable isotope work (Green et al., 2018) meaning information is often inferred. Therefore the development of relevant human *in vitro* models is an important area; the use of hepatoma cell lines and primary human

hepatocytes (PHH) is discussed in Chapter 3. In addition, recently, co-culture and 3D models of the liver have been developed. For example, Pingitore et al. (2019) used HepG2 cells (a hepatoma cell line) and LX2 cells (a hepatic stellate cell line) to create 3D spheroids of hepatocytes and hepatic stellate cells where lipid accumulation could be induced by fatty acids. Kostrzewski et al. (2017) developed another 3D model using PHH seeded onto a scaffold where media could flow through the system. Creating more physiologically relevant *in vitro* models of NAFLD would be valuable for the research area.

1.11 Aims and objectives

The aims of this thesis were firstly to examine different cell types used as *in vitro* models of lipid accumulation (HepG2, Huh7, McA-RH7777 and primary human hepatocytes) and whether they are consistent in their lipid accumulation in response to nutritional stimuli (Chapter 3). This would be achieved using a fluorescence based system for detecting intracellular lipid droplets in cultured cells. The second aim, if differences in lipid accumulation occur, was to investigate what changes at the messenger RNA (mRNA) level could determine the discrepancies (Chapter 4). The objective here was to use targeted and non-targeted gene expression analyses. Thirdly, we aimed to develop a way to study the influence of the PNPLA3 genotype in *in vitro* models and how genotype could interact with dietary factors (Chapter 5). The objective was use an inducible lentivirus system to overexpress each variant and to detect the PNPLA3 protein.

The overall aim was to further the understanding of *in vitro* NAFLD models, particularly HepG2 cells and PHH, and how they compare in their lipid accumulation phenotype. It was hypothesised that hepatoma cell lines would not store glucose, and possibly fructose, as lipid, due to their cancerous and proliferative phenotype and therefore may

not represent PHH. It was expected that expression of key genes would be affected differently by nutritional stimuli in HepG2 cells versus PHH to reflect differences in lipid accumulation, and that non-targeted gene expression analysis by microarray would show differences in gene expression related to phenotype. It was also hypothesised that PNPLA3 genotype would affect lipid accumulation in both cell lines and PHH, with the presence of the polymorphic variant showing higher lipid content.

Chapter 2: General Methods

2.1 Cell culture

2.1.1 Cell line culture

HepG2, Huh7 and McA-RH7777 cell culture

All three cell lines were maintained in T75 flasks in high glucose (25mM) Dulbecco's Modified Eagle Medium (DMEM, Sigma D6546) containing 10% (v/v) foetal bovine serum (FBS), 100U/ml penicillin, 100µg/ml streptomycin and 2mM L-glutamine. Cells were passaged by trypsinisation every 3–7 days. Incubators were set at 37°C and 5% CO₂.

2.1.2 Primary human hepatocyte culture – liver perfusion

The human liver tissue perfusion was carried out by Monika Owen and Nicola De Vivo. Tissue was obtained from patients undergoing liver resection for secondary liver cancer. Patients gave full consent and were anonymised by the Nottingham Health Sciences Biobank (study number ACP 94). The study was approved by the Research Ethics Committee (reference 04/Q2403/70). The tissue was collected by the Nottingham Health Sciences Biobank staff directly from the operating theatre in cold Soltran buffer. When it reached the lab it was flushed through blood vessels using cold Soltran buffer and a syringe. The liver piece was cannulated and perfused with perfusion buffer and ethylene glycol tetraacetic acid (EGTA) until the whole lobe was blanched uniformly. Total perfusion time was around 15–20 minutes. Another 5–6 minutes of perfusion using EGTA-free perfusion buffer was carried out before changing to perfusion buffer with collagenase for about 20 minutes until tissue marbling was observed and the lobe became soft. After perfusion was finished, the soft lobe was placed into perfusion buffer

and mashed with blunt scissors, then filtered through a 250µm nylon mesh followed by 100µm nylon mesh. The cells were divided into 50ml tubes and pelleted by centrifugation at 60×g for 4 minutes at room temperature. The supernatant containing non-parenchymal cells was removed and the hepatocyte pellets were re-suspended in plating medium. Plating medium is as described in section 2.1.3.6 (serum-containing low glucose Williams Medium E). The hepatocytes were re-spun at 60×g for 3 minutes at room temperature. The supernatant was removed and the pellets re-suspended in plating medium and filtered through a 100µm nylon mesh. After a final spin at 60×g for 3 minutes at room temperature, the cells were re-suspended in plating medium. In a 50ml tube, 35ml of cell suspension was combined with 15ml neutralised Percoll. The tubes were spun for 10 minutes at 100×g at room temperature to pellet viable hepatocytes. A wash with plating medium was carried out by re-suspending the pellet in plating medium and centrifuging at 60×g for 4 minutes at room temperature. The cells were finally re-suspended in 50–100ml of plating medium and counted using trypan blue before seeding into the desired plates.

The gender and age of each patient that donated liver tissue for perfusion are presented in Table 2.1.

Table 2.1: Gender and age of the patients from which the liver tissue was donated		
Liver Number	Gender	Age
L312	F	67
L317	M	63
L319	M	71
L326	F	72
L329	F	25

2.1.3 Solution preparation

2.1.3.1 Preparation of 24% (w/v) BSA solution

Six grams of fatty acid free bovine serum albumin (BSA, Sigma) was added to 17.5ml 150mM NaCl at room temperature and allowed to dissolve. The pH was adjusted to 7.4 using 5M NaOH. The total volume was made up to 25ml using 150mM NaCl and the solution sterilised using a 0.2µm syringe filter.

A vehicle control solution was prepared by diluting 24% (w/v) BSA 1:1 with 150mM NaCl to mimic the solution that the fatty acids were dissolved in.

2.1.3.2 Preparation of 10mM fatty acid stocks

40µl linoleic acid (Sigma) and 39.6mg sodium oleate (Sigma) were weighed into separate flasks and 7ml 150mM NaCl added to each. These were allowed to stir on a gently heated magnetic stirrer for 5 minutes. After this, 7ml 24% (w/v) BSA and 48µl 5M NaOH were added to each. The solutions continued to stir until dissolved.

Palmitic acid preparation required extra steps. 36mg palmitic acid (Sigma) was dissolved in 1ml 100% ethanol by vortexing well. 48µl 5M NaOH was added and mixed. The ethanol was evaporated under nitrogen gas. The remaining crystals were transferred to a bottle containing 7ml 150mM NaCl which was stirred for a few minutes. 7ml 24% (w/v) BSA was added and the bottle left stirring on a heated magnetic stirrer for about a day until an emulsion was formed. Mixed stocks were prepared by mixing the 10mM palmitate, 10mM oleate and 10mM linoleate solutions in the ratio 2:2:1 (see section 3.1.3).

2.1.3.3 Preparation of sugar solutions

1M glucose and 1M fructose solutions were prepared by dissolving 18.016g of glucose or fructose into 100ml water. The solutions were sterile filtered and stored at 4°C.

2.1.3.4 Collagen preparation

Collagen type 1 (Sigma C9791) was diluted to 1mg/ml in 0.1M acetic acid and left to stir for 1–3 hours until dissolved. An amount of chloroform equalling 10% of the collagen volume was layered at the bottom of the glass bottle and this was left at 4°C overnight to sterilise the solution (this is the method specified by the manufacturer, Sigma). The next day, the collagen solution was removed from on top of the chloroform and stored at 2–8°C. A working concentration was made by diluting the collagen 1:10 with cell culture grade water.

2.1.3.5 Collagen coating plates

Cell culture plates were coated with collagen by adding an appropriate amount of working collagen solution to each well to achieve 10–11 $\mu\text{g}/\text{cm}^2$. The plates were left in the safety cabinet overnight with the UV light turned on to sterilise them. Any remaining liquid was removed. The wells were washed once with cold phosphate-buffered saline (PBS) and once with cold sterile cell culture grade water. If the plates were not being used immediately, they were left to air dry in the safety cabinet then sealed with parafilm and stored at 2–8°C until use.

2.1.3.6 Preparation of media and media supplements

The base media for experiments across all cell types was glucose free Williams medium E (US Biological) with the supplements in Table 2.2. This allowed for manipulation of glucose concentration and for the type of medium to be controlled across the cell lines and primary cells. Plating medium contained 10% FBS in addition to the supplements in Table 2.2 and contained 4–5mM glucose.

Supplement	Final concentration, or volume added to 500ml media
Nicotinamide	5mM
Zinc sulphate	1.3mM
Copper sulphate	0.6mM
Dexamethasone	12uM
Sodium selenite	15uM
Transferrin (Sigma T1428)	5µg/ml
Insulin (Sigma I9278)	10nM (unless specified otherwise)
7.5% sodium bicarbonate solution	To pH 7.4
L-Carnitine	1mM
Gentamicin	50µg/ml
7.5% (w/v) BSA Solution	6.5ml

2.2 Protein analysis

2.2.1 Harvesting cells for protein analysis

2x sodium dodecyl sulphate (SDS) solution was prepared with 2ml 90% (v/v) glycerol, 1.25ml 1M Tris-HCl (pH6.8), 4ml 10% (w/v) SDS, 1ml dithiothreitol (DTT), a few grains of bromophenol blue and 1.75ml double distilled water. Concentrated protease and phosphatase inhibitor stock solution was made by dissolving one PhosSTOP tablet

(Roche) and one cOmplete Protease Inhibitor tablet (Roche) in 1ml water. 1×SDS was made by using 1.5ml 2×SDS, 0.3ml 10×inhibitor stock and 1.2ml water. Cells from a 12-well plate were scraped using a pipette tip into 200µl 1×SDS and stored at –20°C.

2.2.2 2D Quant protein assay (GE Healthcare)

This assay was used to determine the protein concentration in each cell lysate. Six standards ranging from 0µg to 50µg protein were prepared using the 2mg/ml BSA standard solution. The cell lysates in 1×SDS mix were heated to 90°C and a small aliquot of each sample (20µl to 30µl) transferred to a new 1.5ml tube. 500µl precipitant was added to each tube including the standards. They were vortexed and incubated at room temperature for 2 minutes. Following this, 500µl co-precipitant was added to each tube and vortexed. The tubes were centrifuged at 15000×g for 15 minutes at 4°C. The supernatant was carefully removed. 100µl copper solution and 400µl water were added, quickly followed by 1ml of working colour reagent (1 part colour reagent B to 100 parts colour reagent A). They were incubated at room temperature for about 20 minutes before reading on a spectrophotometer at 480nm. Protein concentrations of the samples were calculated from the standard curve.

2.2.3 General western blotting protocol

Western blotting was carried out based on the original procedure by Towbin et al. (1979). The cell lysate samples were boiled at 90–100°C for 5 minutes, then centrifuged for 3 minutes at 15000×g at room temperature. A gel tank was prepared with a pre-cast gel (BioRad 4–15% Criterion TGX) and running buffer, and the samples loaded into the wells. The BioRad All Blue protein ladder was used as a marker. The gel was run at 200V until the markers reached the bottom of the gel. A transfer cassette was prepared by

layering a nitrocellulose membrane (wet with water) between two sheets of filter paper on each side, and finally enclosed within two sponges. This was soaked in transfer buffer for at least 5 minutes. The gel was also soaked in transfer buffer then carefully placed on top of the membrane and air bubbles rolled out with a glass rod. The closed cassette was loaded into a transfer tank containing transfer buffer and an ice reservoir. The transfer was run at 0.2A (small cassette) or 0.5A (large cassette) for two hours on a magnetic stirrer. Ponceau S stain was used to confirm the transfer was successful, which was then removed by washing in TBST (tris-buffered saline with 0.1% (v/v) Tween). The membrane was blocked with the appropriate blocking agent dissolved in TBST with gentle rocking for one hour. The primary antibody was diluted to an appropriate concentration in the blocking agent and left on the membrane rocking gently overnight at 4°C. The next morning, the membrane was washed 5 times for 5 minutes each. The secondary antibody was diluted to the required concentration in the blocking agent and left on the membrane for one hour at room temperature with gentle rocking. After five more washes with TBST, the membrane was detected using either enhanced chemiluminescence (ECL) or ECL Select (Amersham) according to the manufacturer's protocol. The chemiluminescence was imaged using a ChemiDoc MP (BioRad) or photographic film.

2.3 Statistical analysis

Graphs were produced using GraphPad Prism 7. Statistical analyses were carried out using Genstat 19th Edition. Statistical significance was set at $P \leq 0.05$ unless otherwise stated.

Chapter 3: A comparison of lipid accumulation in response to nutritional stimuli in hepatoma cell lines and primary human hepatocytes

3.1 Introduction

3.1.1 Hepatoma cell lines

Hepatoma cell lines are commonly used as experimental models of hepatic metabolism. They offer the working advantages of easy cryopreservation and continuous proliferation, making them an accessible *in vitro* option. HepG2 cells are the most commonly used human cell line in NAFLD research. They were originally isolated from a liver tumour from a 15-year-old Caucasian male. Huh7 cells are a second human cell line that were isolated from a liver tumour from a 57-year-old Japanese male (Green et al., 2015b). The advantages and disadvantages of these cell types as models of NAFLD have been recently reviewed (Green et al., 2018). Of note, key disadvantages are that both cell types have a foetal phenotype, secrete mainly LDL rather than VLDL (Thrift et al., 1986), and have low fatty acid oxidation capacity (Green et al., 2018). HepG2 cells have a high capacity for TAG synthesis from oleic acid, of which little is secreted as lipoprotein (Gibbons et al., 1994), allowing for TAG accumulation. Huh7 cells have also been shown to accumulate lipid with oleic acid treatment (Ricchi et al., 2009).

McA-RH7777 cells are a male rat derived cell line (Green et al., 2015b) which are not commonly used in NAFLD research, possibly because there are some fundamental differences between rat and human lipid metabolism. For example, rats secrete both apoB-48 and apoB-100 whereas humans just secrete apoB-100. McA-RH7777 cells secrete apoB-100 associated with VLDL particles, and apoB-48 on VLDL and HDL

particles (Boren et al., 1994). Lipid accumulation studies using McA-RH7777 cells are limited, but they have been shown to accumulate TAG in response to 1mM oleic acid treatment over 48 hours (Ota et al., 2008), demonstrating that they can become steatotic with similar treatment to HepG2 and Huh7 cells.

All cell lines have a cancerous phenotype. For example, Huh7 cells show up-regulation of genes typically up-regulated in tumours (Nwosu et al., 2018). Consequently, there are key differences in energy metabolism that must be taken into account. For example, in non-cancerous cells, ATP is more efficiently produced through oxidative phosphorylation in the mitochondria whereas cancer cells have an increased rate of aerobic glycolysis (Zheng, 2012). This was first described by Otto Warburg, hence named the Warburg effect (Koppenol et al., 2011, Warburg, 1925), and it has been demonstrated in HepG2 cells (Maier et al., 2010). The gene expression patterns of cell lines versus primary cells will be explored further in Chapter 4.

3.1.2 Primary human hepatocytes (PHH)

Primary human hepatocytes (PHH) are currently considered the gold standard *in vitro* human model of NAFLD (Green et al., 2018, Boeckmans et al., 2018, Zeilinger et al., 2016). However, obtaining and maintaining the cells comes with challenges and ethical considerations; logistics are one of the key factors preventing their wider use (Zeilinger et al., 2016). Genetic and inter-individual variability are other key factors to consider when using primary cells from different donors. In addition, long term culture of freshly isolated human hepatocytes is not possible for a variety of reasons. Firstly, PHH are differentiated and therefore do not proliferate, and they have been shown to exhibit de-differentiation when kept in 2D culture (Rowe et al., 2013). Secondly, they undergo a 50% decrease in viability over 3 days in culture, and gradually decrease their ability to

secrete albumin and VLDL over the same time frame (Ling et al., 2013). However, their ability to secrete VLDL and their non-cancerous and non-proliferative phenotype makes them a closer representation of the *in vivo* liver. They have also been shown to display a level of lipid accumulation similar to steatotic livers (Gomez-Lechon et al., 2007). With PHH as the current gold standard, it is important to know whether cell line models are representative of their metabolism.

3.1.3 Selecting fatty acid, monosaccharide and insulin concentrations

Fasting (overnight) plasma non-esterified fatty acid (NEFA) concentrations typically range from about 300-600 μ M, but can be higher or lower, and vary little with body fat mass (Karpe et al., 2011). Periods of prolonged starvation can increase concentrations up to about 1.5mM but this would be unusual in Western culture. Of course the liver does not only receive blood from the hepatic artery but also the hepatic portal vein. Unfortunately, due to the inaccessibility of the human liver, portal vein measurements are not routinely taken but this information would be valuable. The first aim of this chapter was to establish a fatty acid concentration that would induce lipid accumulation *in vitro*. The fatty acid composition of plasma NEFA, the primary source of exogenous fatty acid delivery to the liver *in vivo* in NAFLD patients (Donnelly et al., 2005), has been shown to be in approximately a 45:38:17% SFA:MUFA:PUFA ratio (Hodson et al., 2008). Based on this, we selected a 40:40:20% palmitic:oleic:linoleic acid ratio to induce lipid accumulation in this chapter to be physiologically relevant. Other studies have already used a similar ratio; Green et al. (2015a) used a palmitic:oleic:linoleic acid ratio of 45:30:25% which was replicated by Nikolaou et al. (2016).

5mM and 11mM glucose were chosen to represent a normal fasting blood glucose concentration and a level which could be seen postprandially in diabetic patients (Yu et

al., 2014). Reported serum fructose concentrations vary depending on the study and analytical method. In one study, fasting fructose was thought to be around 2mM in healthy individuals measured by both an enzymatic assay and GC-MS (Hui et al., 2009). After an oral glucose and fructose challenge following a fast, serum fructose rose as high as 16.3mM, reducing to around 8mM after 120 minutes (Hui et al., 2009). In an individual regularly consuming fructose rich food and drinks, serum fructose may remain closer to this level if these measurements are accurate. In contrast, Teff et al. (2009) found that after consumption of a high fructose drink, plasma fructose rose to only 500 μ M in obese subjects. In another study, fructose concentrations at 180 minutes after consumption of a fructose and glucose containing meal were found to be only 231 μ M on average in healthy patients (Theytaz et al., 2014). However, there is a dramatic gradient in fructose concentrations entering and leaving the liver as the liver metabolises the majority of fructose spilled over from the small intestinal enterocytes (Jang et al., 2018); therefore portal vein fructose concentrations would be significantly higher than those found systemically. For example, in sucrose fed (directly into the stomach) rats, portal fructose reached about 1mM whereas peripherally it only reached about 150 μ M (Sugimoto et al., 2010). More accurate measurements from the human portal vein would be valuable but difficult to achieve. For our experiment, 2mM and 8mM fructose were chosen, which would hopefully represent a concentration physiologically found in the portal vein (2mM), and possibly postprandially (8mM). Depending on the accuracy of the measurements by Hui et al. (2009), 8mM could be supraphysiological. Fructose was not tested in the absence of glucose as this situation would never occur under normal feeding conditions.

Fasting portal insulin concentrations are approximately 1.13ng/ml (equivalent to about 0.2nM) which rise to a peak of 25.13ng/ml (4.3nM) 90 seconds after intravenous infusion of 25g glucose in healthy patients (Horwitz et al., 1975). The 10nM used as

standard culture conditions in our experiments is therefore supraphysiological but it is a concentration often used to culture primary hepatocytes (Gomez-Lechon et al., 2007, Zamule et al., 2008, Olsavsky et al., 2007).

3.1.4 Experimental aims

The aims and objectives of this chapter were as follows:

- To establish a fatty acid treatment concentration that induces lipid accumulation *in vitro* by testing a range of fatty acid concentrations over a range of time periods.
- To compare how HepG2, Huh7, McA-RH7777 cells and PHH accumulate lipid in response to fatty acid treatment and how this is modulated by glucose and fructose by using a consistent Nile Red fluorescence based assay across cell types.
- To compare insulin sensitivity across the cell lines using Western blotting, and to observe the effects of insulin on lipid accumulation in HepG2 cells versus PHH using the Nile Red assay.

It was hypothesised that the hepatoma cell lines would not store monosaccharides as lipid, but that the non-proliferating PHH would show some lipid accumulation in response to glucose and fructose treatment. It was expected that all cell types would accumulate lipid with fatty acid treatment.

3.2 Methods

3.2.1 Nile Red staining assay

Nile Red is a fluorescent stain used to detect intracellular lipid droplets, with better specificity at yellow gold fluorescence than red fluorescence (Greenspan et al., 1985). A stock solution of 1mM Nile Red was prepared by dissolving 15.8mg Nile Red (Sigma) and 500mg Pluronic F-127 (Sigma) in 50ml dimethyl sulfoxide (DMSO). The stock solution was aliquoted and stored at -20°C .

1mM Nile Red was diluted in Hank's buffered saline solution (HBSS, Sigma) to $30\mu\text{M}$ immediately before use and protected from light using foil. The cells were washed twice with HBSS before adding an appropriate volume of Nile Red to each well ($100\mu\text{l}$ for a 96-well plate). The plate was left to incubate in the dark for 15 minutes. After this time, the waste liquid was removed and the cells washed with HBSS. The cells were covered with HBSS for measuring fluorescence on a FLUOstar Optima or FLUOstar Omega microplate reader (BMG Labtech). Wavelengths were for yellow gold fluorescence (excitation 485nm , emission 590nm). Orbital scanning was used at a diameter of 3mm to take an average of ten points around the well. If images were taken, they were taken at this point using a Leica DM IL fluorescence microscope. If a DNA assay was to be performed subsequently, the HBSS was removed and $100\mu\text{l}$ water added in its place before freezing the plate at -20°C to lyse the cells.

3.2.2 DNA assay

DNA was quantified using a Bisbenzimidazole dye (Hoechst 33258 dye, Labarca and Paigen (1980)) method. Frozen 96-well cell culture plates containing cells stored in water were thawed. A standard curve was produced using a serial dilution of calf thymus DNA (Sigma, 1mg/ml initially diluted to $40\mu\text{g/ml}$ working stock). An example of a standard

curve is shown in Figure 3.1; the serial dilution means that the assay is more sensitive at the lower end of the standard curve. A working dye solution was prepared by diluting 1mg/ml Bisbenzimidazole (Sigma) to 2µg/ml in 2×Tris-HCl NaCl EDTA (TNE) buffer. 100µl of the diluted dye was added to each well and the plate read on a FLUOstar Optima or FLUOstar Omega microplate reader (excitation 355nm, emission 460nm).

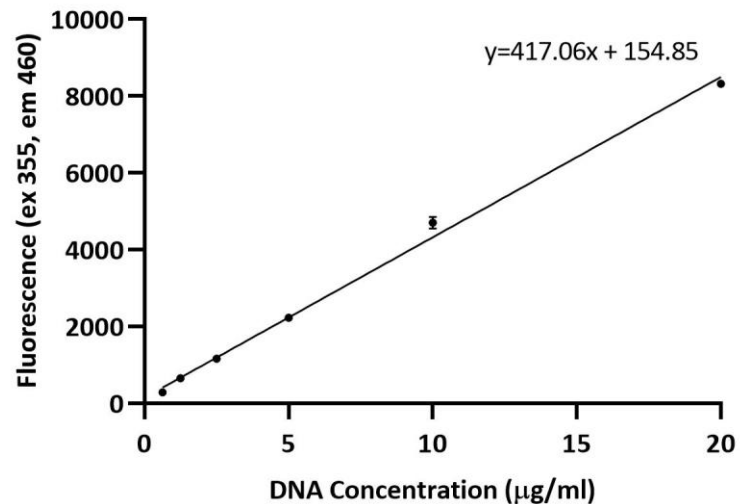


Figure 3.1: Example of a standard curve produced for the DNA assay.

3.2.3 Experimental protocol – establishing an appropriate fatty acid concentration

HepG2 cells were seeded into five 96-well plates at a density of 1×10^4 cells per well in plating medium (see section 2.1.3.6). The next day the cells were treated with increasing concentrations (0, 100, 200, 300, 400, 500 or 1000µM) of fatty acid mix (see section 2.1.3.2). There were 5 replicates of each treatment per plate. One plate was stained with Nile Red at 0 hours (before treatment), then another plate every 24 hours of treatment up to 96 hours. Media was refreshed every 24 hours. After Nile Red staining, DNA assays were performed on all plates. The data were analysed by 2-way ANOVA (fatty acid × time).

3.2.4 Experimental protocol – effects of glucose, fructose and fatty acids

This experiment was performed on HepG2, Huh7 and McA-RH7777 cells and PHH.

Treatment media were prepared in order to allow for the treatments in Table 3.1.

Table 3.1: Treatments prepared for the experiment. Vehicle controls were BSA NaCl solution for fatty acids and water for the sugar solutions		
	0µM fatty acid	200µM fatty acid
5mM glucose	0mM fructose	0mM fructose
	2mM fructose	2mM fructose
	8mM fructose	8mM fructose
11mM glucose	0mM fructose	0mM fructose
	2mM fructose	2mM fructose
	8mM fructose	8mM fructose

Cells were seeded onto collagen coated 96-well plates in a volume of 200µl plating medium per well the afternoon before the treatments were to be added. The seeding densities for the three cell lines were selected to allow a confluent monolayer by the end of the treatment period (Table 3.2).

Table 3.2: Seeding densities for the different cell types	
Cell Type	Cells per well (96-well)
HepG2	1.25×10 ⁴
Huh7	1.5×10 ⁴
McA-RH7777	2×10 ⁴
PHH	4.5×10 ⁴

For the three cell lines, the cells were washed with PBS the next morning before adding the different treatment media. For PHH, they were first given 4 hours in low glucose (4mM) FBS-free medium to acclimatise. After this period, the treatment media were

added. All treatment media were FBS-free to prevent interference from lipoproteins or hormones present in the serum. After 24 hours of treatment, the media was refreshed on all wells. At 48 hours, Nile Red assays were performed to measure lipid accumulation. The plates were then frozen for DNA assays. The experiment was performed successfully on five cultures of primary hepatocytes from five different livers with two plates per liver. It was performed multiple times on each of the cell lines for a total of six plates of each. Each plate had $n=5$ wells per treatment with two rows left empty to allow room for a DNA standard curve. The raw fluorescence data were normalised by expressing the fluorescence values per μg DNA. Then, to allow for correction across machines, plates, and cells, fold change values were calculated by dividing each value by the average of the control values. The data were analysed using three-way ANOVA (glucose \times fructose \times fatty acids) with blocking for plate.

3.2.5 Experimental protocol – effects of glucose, insulin and fatty acids

This experiment was performed on HepG2 cells and PHH. Treatment media were prepared in order to allow for the treatments in Table 3.3.

Table 3.3: Treatments prepared for the experiment. Vehicle controls were BSA NaCl solution for fatty acids and water for the glucose and insulin solutions		
	0μM fatty acid	200μM fatty acid
5mM glucose	0nM insulin	0nM insulin
	5nM insulin	5nM insulin
	10nM insulin	10nM insulin
11mM glucose	0nM insulin	0nM insulin
	5nM insulin	5nM insulin
	10nM insulin	10nM insulin

The same protocol and seeding densities described in section 3.2.4 were used. The data were analysed using three-way ANOVA (glucose × insulin × fatty acids) with blocking for plate.

3.2.6 Experimental protocol – insulin responses of hepatoma cell lines

This experiment was performed on HepG2, Huh7 and McA-RH7777 cells. Cells were seeded in the afternoon onto collagen coated 12-well plates all at a density of 3×10^5 cells per well using standard plating medium. The next morning, the cells were starved of insulin for 5 hours. Then half the cells were stimulated with 100nM insulin for 15 minutes to replicate treatment by Ricchi et al. (2009), and the other half had the insulin-free media refreshed. The cells were harvested into 1×SDS (see section 2.2.1). There was $n=3$ for each treatment of each cell type which were split across three gels for Western blot analysis (see section 3.2.7). The data were analysed using two-way ANOVA (cell type × insulin) with blocking for gel.

3.2.7 Phospho-AKT and total AKT western blot

This Western blot determined the phosphorylated AKT (pAKT) to total AKT ratio in the cells harvested from the experiment in section 3.2.6, as a measure of insulin response.

The protocol in section 2.2.3 was followed using the following consumables. Rabbit anti-phospho-AKT (Ser473, #9271), rabbit anti-AKT (#9272) anti-rabbit IgG HRP-linked antibody (#7074) were all purchased from Cell Signalling Technologies. 10-well gels with 50µl capacity were used, and the blocking agent was 5% (w/v) milk powder. Detection was by ECL visualised on a ChemiDoc MP. Samples were split over three gels with one replicate of each treatment and cell line on each gel.

Anti-pAKT was the first antibody to be used. The membranes were then stripped as follows before probing with anti-total-AKT; the membranes were submerged in stripping buffer and rocked for 15 minutes in a fume hood. They were then washed 5 times for 5 minutes with TBST before probing with the secondary antibody to check there was no remaining anti-pAKT antibody bound to the protein. It should be noted that Ponceau staining showed that there was some protein loss during the stripping process.

3.3 Results

3.3.1 Establishing an appropriate fatty acid concentration to induce lipid accumulation

Lipid accumulation was measured over 96 hours in HepG2 cells incubated with fatty acid concentrations up to 1mM to determine a concentration and treatment duration that would induce lipid accumulation without significant cell loss through death or detachment.

For both lipid accumulation (Nile Red fluorescence, Figure 3.2) and DNA content (Figure 3.3), there was a significant time × fatty acid interaction ($P < 0.001$). There were two clear outlier wells (one close to the blank measurement and one over two standard deviations higher than others in the group) in the 96 hour DNA data that were removed, meaning two groups had $n=4$ compared to all others with $n=5$.

There was a dose response to fatty acids from 24 hours onwards in the lipid accumulation data (Figure 3.2). With increasing cell number, fluorescence increased for the control throughout the experiment. Fluorescence began to plateau, and decreased, in the higher fatty acid concentrations at 96 hours due to cell loss, as confirmed by the DNA assay (Figure 3.3). There appeared to be a reduction in DNA across all treatments at 24 hours (Figure 3.3), possibly because this plate was seeded less densely or alternatively because each plate was analysed separately, meaning the DNA standard curves are different on each plate and the dye could have been left for a slightly different length of time before reading the plate. Due to the nature of the assays, it was not possible to measure the lipid accumulation or DNA content in the same wells over 96 hours. By 48 hours, there was a significant downward trend in DNA content with increasing fatty acid concentration, which was much more pronounced at 72 and 96 hours (Figure 3.4).

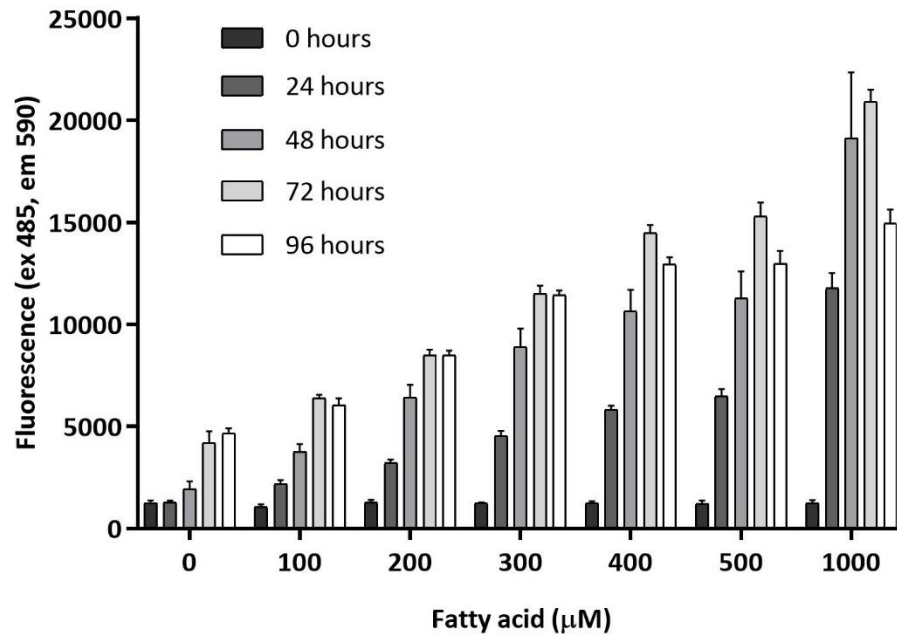


Figure 3.2: Lipid accumulation measured by Nile Red fluorescence in HepG2 cells treated with 0μM to 1000μM of fatty acids (palmitic, oleic and linoleic acids in the ratio 2:2:1) over 96 hours. Means±SEM, n=5

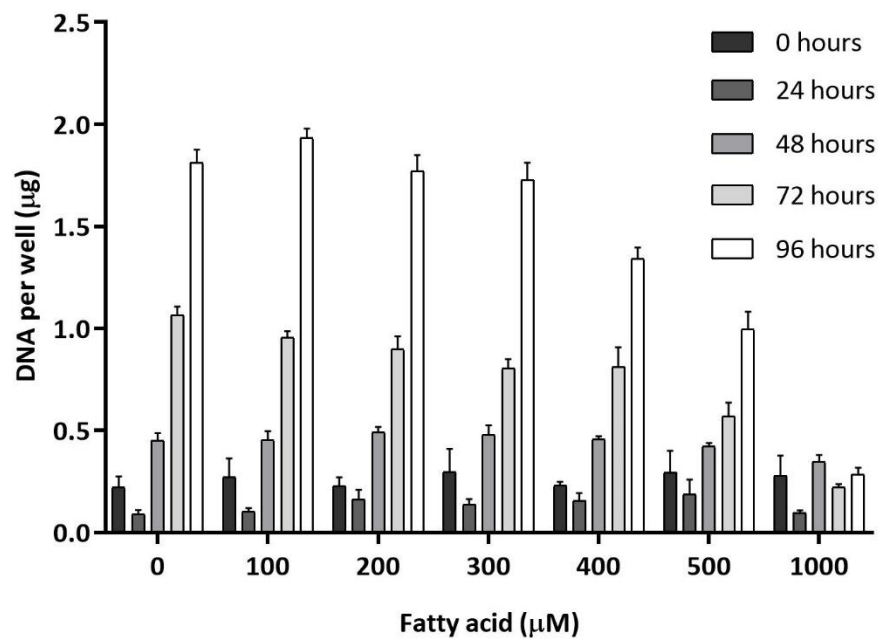


Figure 3.3: DNA per well (μg) in HepG2 cells treated with 0μM to 1000μM of fatty acids (palmitic, oleic and linoleic acids in the ratio 2:2:1) over 96 hours. Means±SEM, n=4 or 5

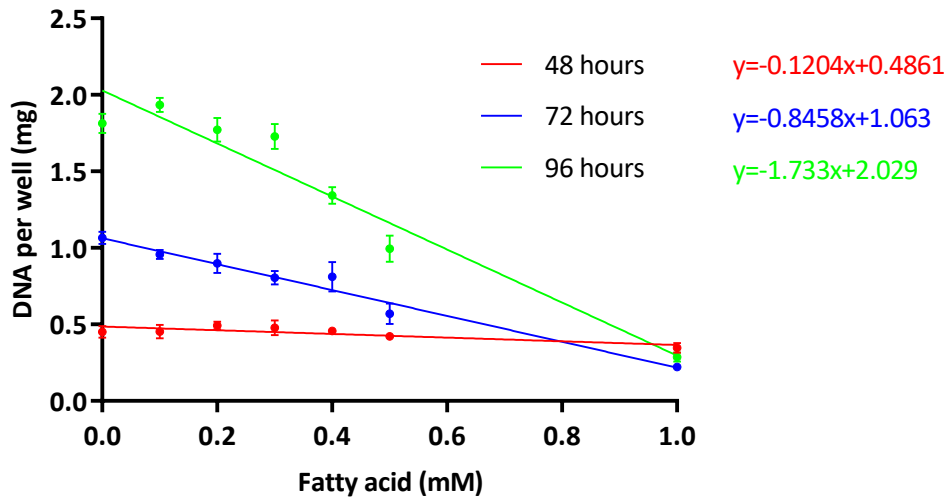


Figure 3.4: Linear regression of DNA assay data from 48, 72 and 96 hours of treatment. 48 hours $P=0.019$, 72 hours $P<0.001$, 96 hours $P<0.001$. Means \pm SEM, $n=4$ or 5

Based on the results of this experiment, it was decided to use a fatty acid concentration of 200 μ M for 48 hours in future experiments, which represented the maximum accumulation of lipid without resulting in cytotoxicity. Under these conditions, HepG2 cells showed an average of a 3.33 \pm 0.32 fold increase in lipid accumulation with no reduction in DNA content suggesting no cell loss.

3.3.2 The effects of fatty acid, glucose and fructose treatment on lipid

accumulation in HepG2, Huh7 and McA-RH7777 cells and primary human

hepatocytes: a comparison

Fluorescence microscopy aimed to confirm the Nile Red data with visualisation of the lipid droplets. The representative images for HepG2 (Figure 3.5), Huh7 (Figure 3.6) and McA-RH7777 (Figure 3.7) cells clearly showed an increase in fluorescence with fatty acid treatment but there were no clear changes with glucose or fructose treatment. PHH images from L312 also showed a visual increase in lipid droplets with fatty acid treatment (Figure 3.8) but this was less pronounced than the cells lines, partially due to visibly higher lipid content in the control cells. Changes with glucose and fructose were more difficult to discern visually, demonstrating the need for fluorimeter measurements. When comparing the control images (0 μ M fatty acid, 5mM glucose, 0mM fructose), McA-RH7777 cells appear to have the lowest lipid content at baseline. This was confirmed by the raw fluorescence readings of the control wells; however these values cannot be used to draw conclusions over all the data as different fluorimeters and settings have been used over the duration of data collection (Table 3.4). Nonetheless, they are useful for comparing baseline fluorescence between the livers. L321 had a much higher fluorescence in the control wells (Table 3.4) which may explain the lower fold change in this liver with treatment (Figure 3.12).

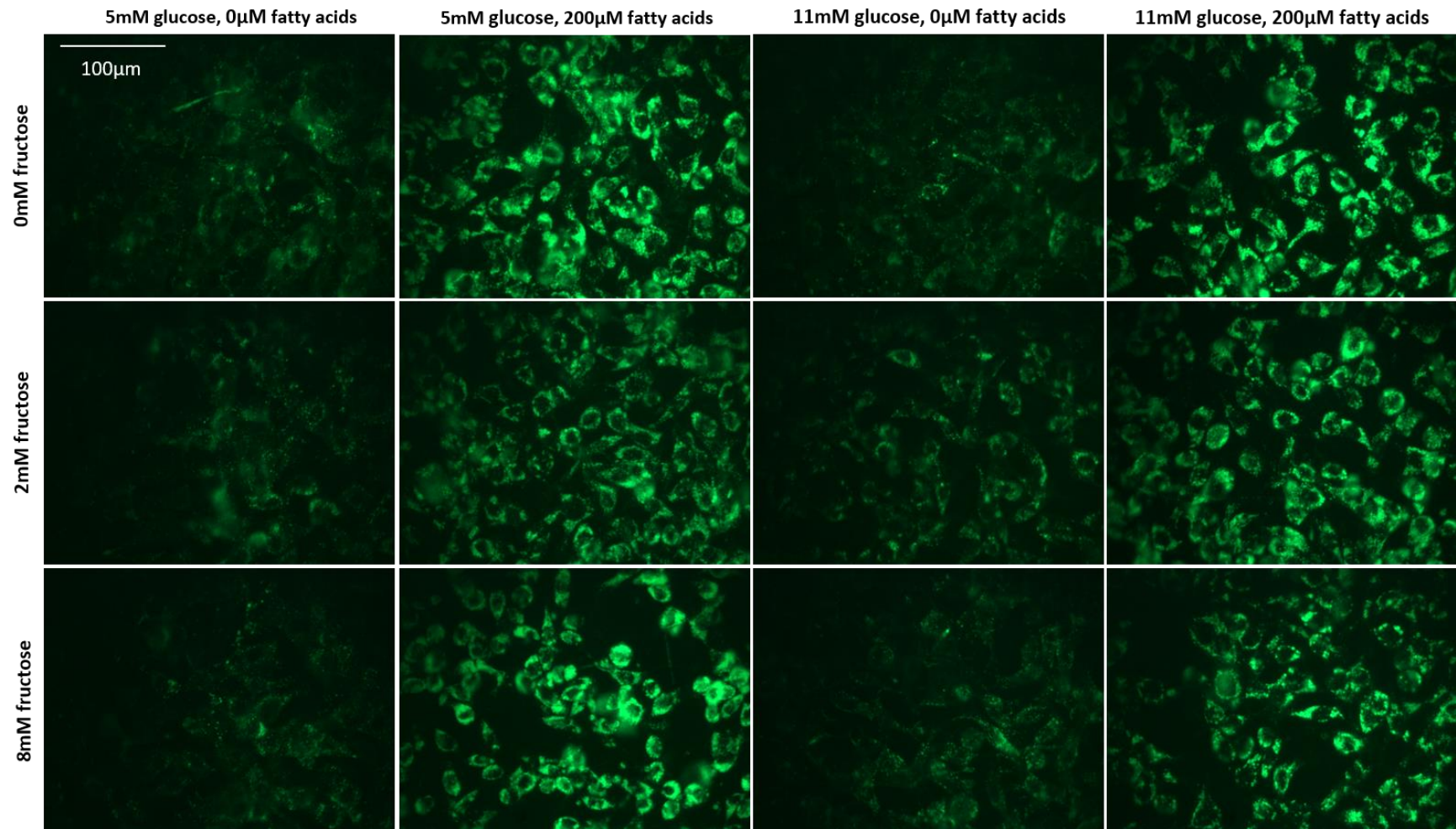


Figure 3.5: Effects of fatty acids, glucose and fructose on lipid accumulation in HepG2 cells visualised by Nile Red viewed under green fluorescence

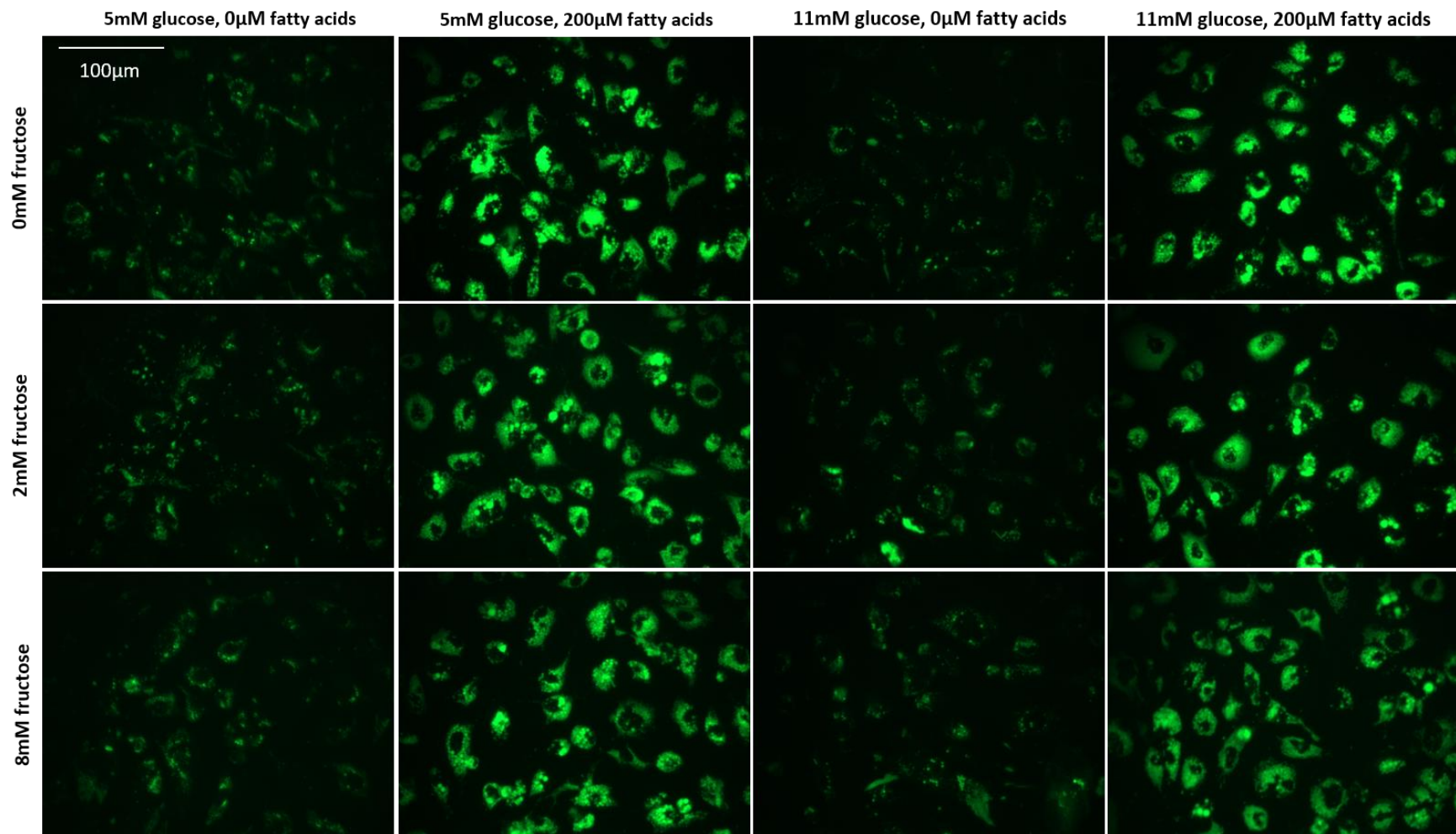


Figure 3.6: Effects of fatty acids, glucose and fructose on lipid accumulation in Huh7 cells visualised by Nile Red viewed under green fluorescence

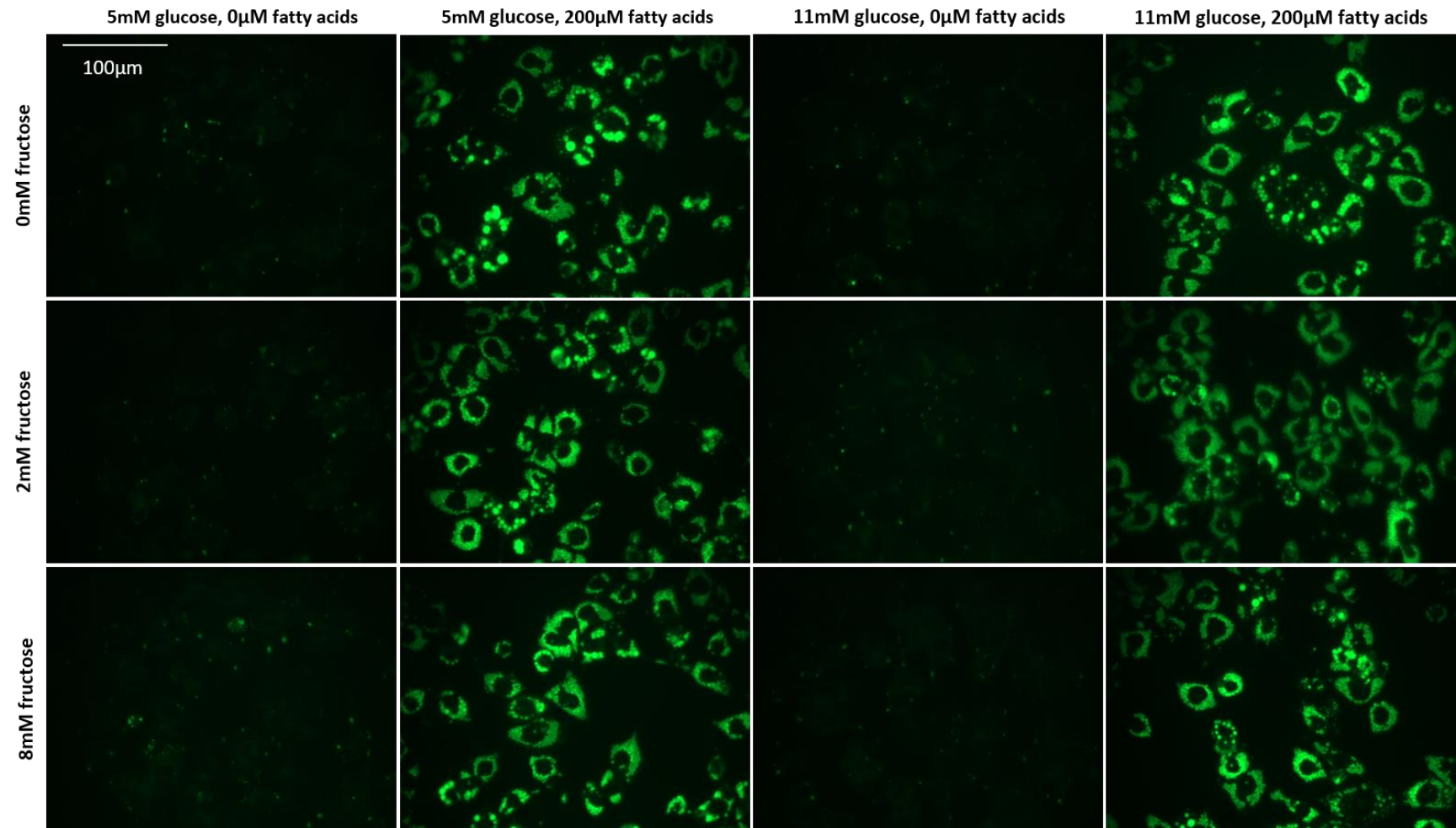


Figure 3.7: Effects of fatty acids, glucose and fructose on lipid accumulation in McA-RH7777 cells visualised by Nile Red viewed under green fluorescence

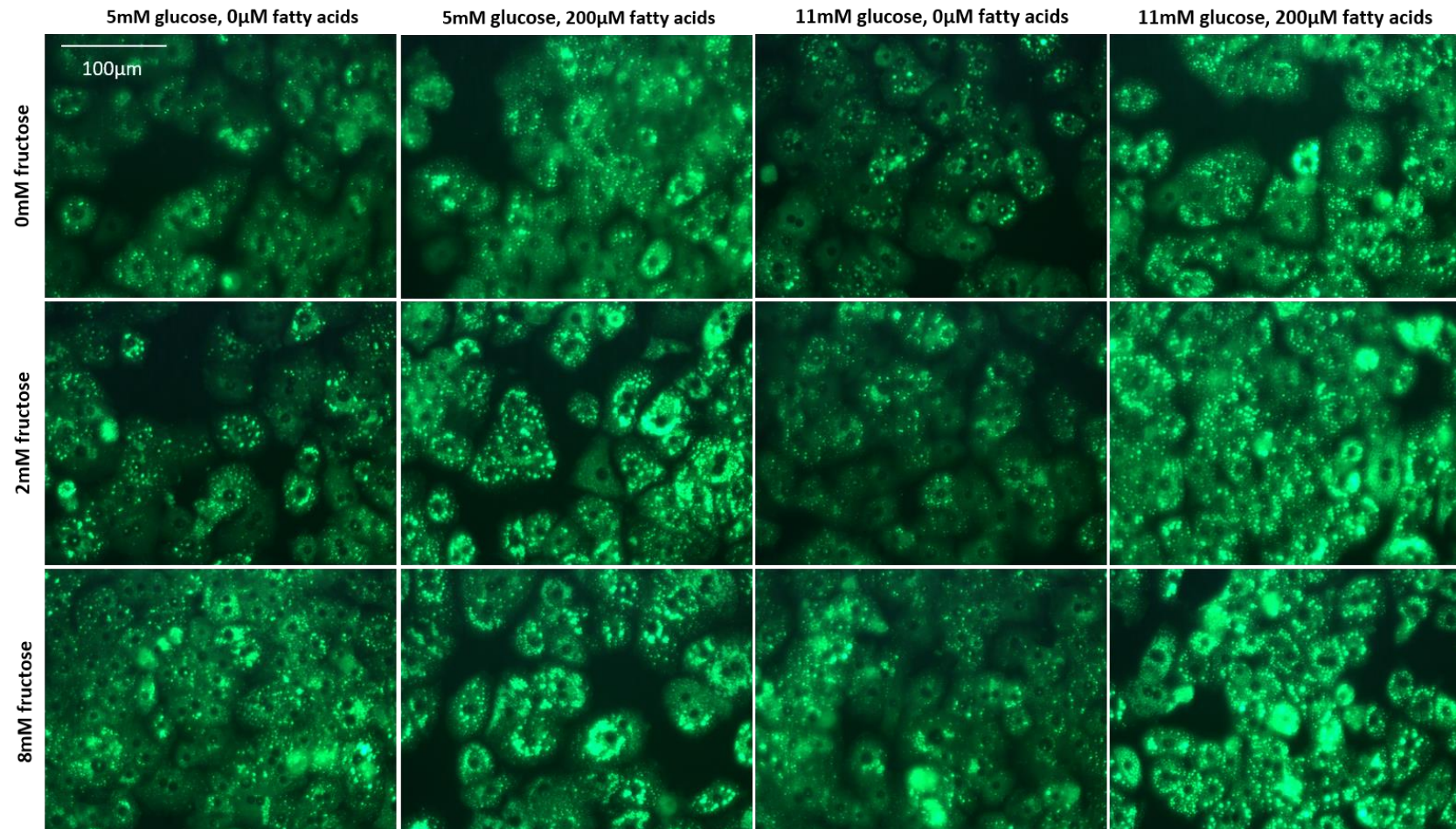


Figure 3.8: Effects of fatty acids, glucose and fructose on lipid accumulation in PHH (L312) cells visualised by Nile Red viewed under green fluorescence

Table 3.4: Mean Nile Red fluorescence values minus background for the control group (0 μ M fatty acid, 5mM glucose, 0mM fructose) on each plate. SB: Sutton Bonington, QMC: Queens Medical Centre

Cell Type	Plate	Location	Machine	Gain	Mean Control Fluorescence
HepG2	1	SB	FLUOstar Optima	2000	2704
HepG2	2	SB	FLUOstar Optima	2000	3084
HepG2	3	SB	FLUOstar Optima	2000	2555
HepG2	4	SB	FLUOstar Optima	2000	3517
HepG2	5	SB	FLUOstar Omega	1250	15240
HepG2	6	SB	FLUOstar Omega	1250	14552
McA-RH7777	1	SB	FLUOstar Omega	1250	10664
McA-RH7777	2	SB	FLUOstar Omega	1250	11717
McA-RH7777	3	SB	FLUOstar Omega	1250	8564
McA-RH7777	4	SB	FLUOstar Omega	1250	7916
McA-RH7777	5	SB	FLUOstar Omega	1250	6195
McA-RH7777	6	SB	FLUOstar Omega	1250	6186
Huh7	1	SB	FLUOstar Omega	1250	10397
Huh7	2	SB	FLUOstar Omega	1250	12532
Huh7	3	SB	FLUOstar Omega	1250	11434
Huh7	4	SB	FLUOstar Omega	1250	22005
Huh7	5	SB	FLUOstar Omega	1250	21083
Huh7	6	SB	FLUOstar Omega	1250	18494
PHH	L312 1	QMC	FLUOstar Omega	1500	10110
PHH	L312 2	QMC	FLUOstar Omega	1500	10518
PHH	L317 1	QMC	FLUOstar Omega	1500	11249
PHH	L317 2	QMC	FLUOstar Omega	1500	11895
PHH	L321 1	QMC	FLUOstar Omega	1500	39686
PHH	L321 2	QMC	FLUOstar Omega	1500	35705
PHH	L326 1	QMC	FLUOstar Omega	1500	15884
PHH	L326 2	QMC	FLUOstar Omega	1500	13047
PHH	L329 1	QMC	FLUOstar Omega	1500	9244
PHH	L329 2	QMC	FLUOstar Omega	1500	10667

The amount of DNA per well (Figure 3.9) was reduced by fatty acids in PHH ($P=0.045$) and there was a trend towards an increase in DNA with high glucose ($P=0.053$). In HepG2 cells, DNA per well was reduced by fatty acids ($P<0.001$) and there was a trend towards a three-way interaction ($P=0.099$). This was similar in Huh7 cells (fatty acids $P<0.001$, three-way interaction $P=0.085$) but there was also a fatty acid \times glucose interaction ($P=0.049$). In McA-RH7777 cells, there was a fatty acid \times glucose interaction ($P=0.007$). These changes in DNA demonstrate that normalisation was a necessary step to ensure cell number was corrected for in the fluorescence readings.

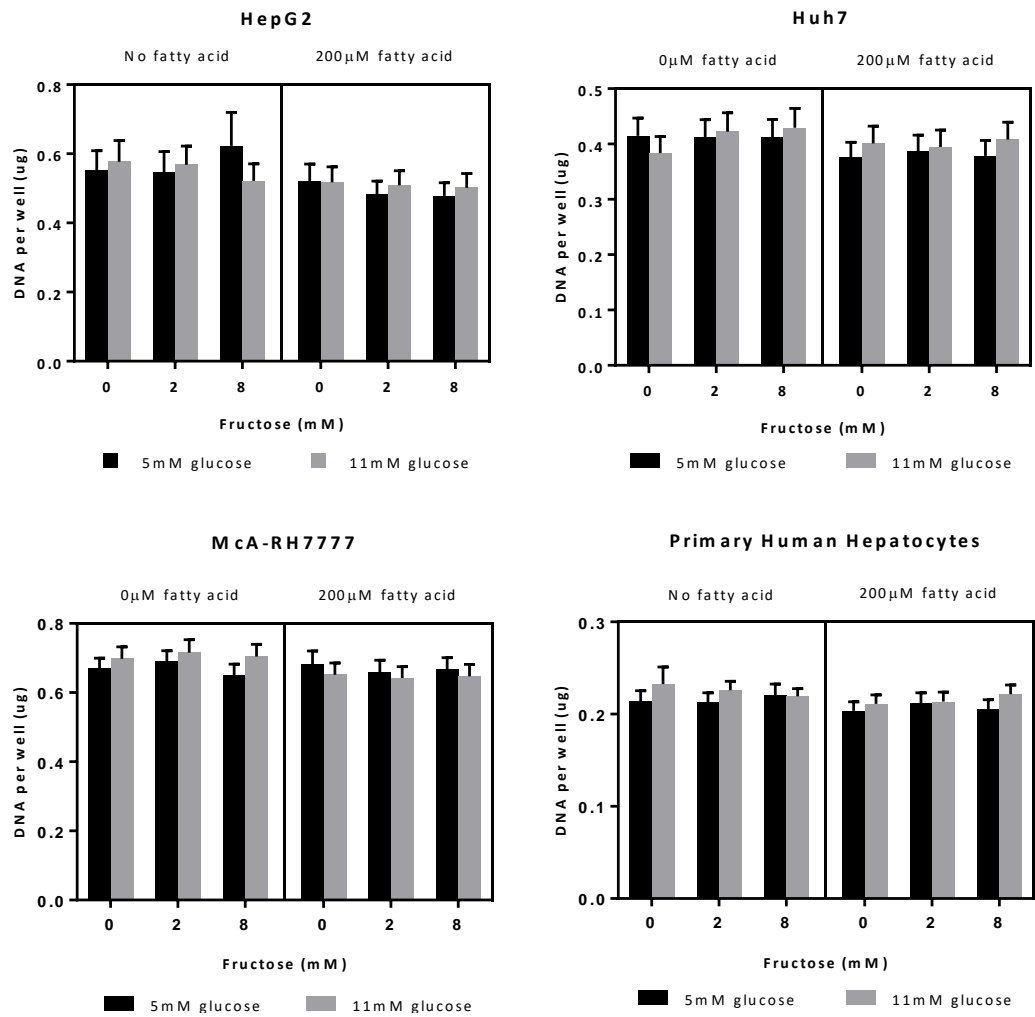


Figure 3.9: Effects of fatty acids, glucose and fructose on DNA content per well in HepG2, Huh7, McA-RH7777 cells and PHH (combined data from five donor livers). HepG2, Huh7 and McA-RH7777: 6 plates combined ($n=30$). PHH: 5 livers with 2 plates each combined ($n=50$). Means \pm SEM

Overall, HepG2 cells accumulated lipid over the 48 hours in response to fatty acid treatment ($P < 0.001$) but did not show any response to glucose or fructose treatment ($P = 0.953$ and $P = 0.752$ respectively) (Figure 3.10, Table S1). Huh7 cells showed a similar pattern (Figure 3.10, Table S2), accumulating lipid in response to fatty acid treatment ($P < 0.001$), but no effects of glucose ($P = 0.315$) or fructose ($P = 0.676$). McA-RH7777 cells showed consistent lipid accumulation with fatty acid treatment ($P < 0.001$) (Figure 3.10, Table S3), but there was also a significant fatty acid \times glucose interaction ($P = 0.002$) overall. Bonferroni multiple comparisons of the interaction showed that there was no significant difference between 5mM and 11mM glucose in the absence of fatty acids, but when fatty acids were present 11mM glucose resulted in significantly higher lipid accumulation than 5mM glucose (Figure 3.10).

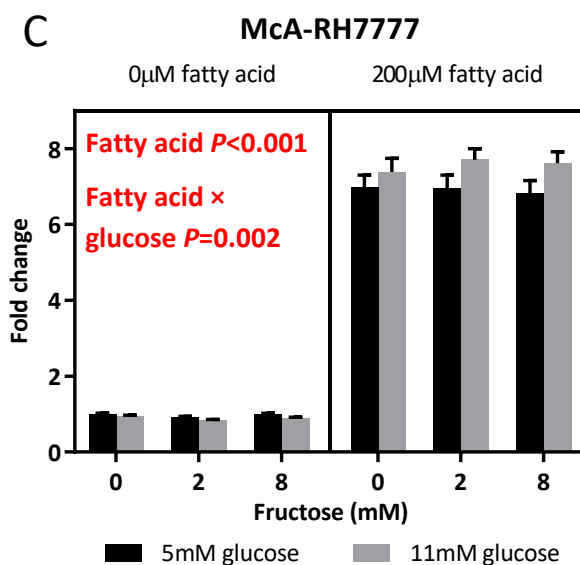
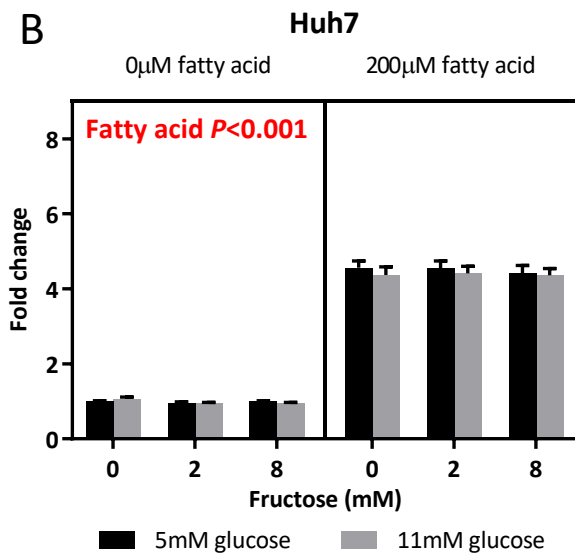
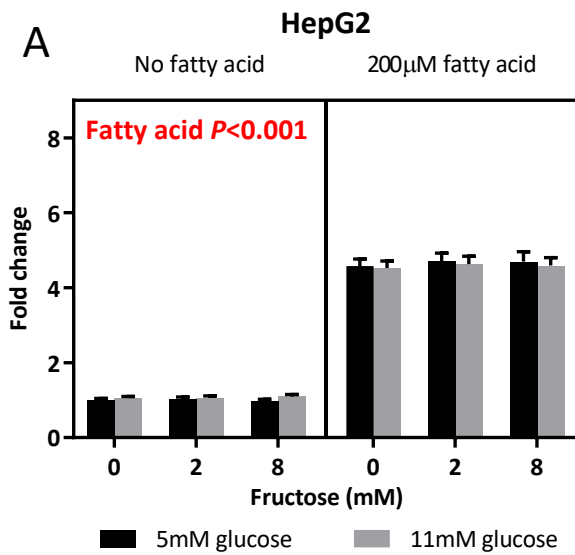


Figure 3.10: Effects of fatty acids, glucose and fructose on lipid accumulation in A: HepG2, B: Huh7, and C: McA-RH7777 cells. D: Bonferroni multiple comparisons of the fatty acid × glucose interaction in McA-RH7777 cells. Lipid accumulation was measured by Nile Red staining and normalised to DNA content, then converted to fold change relative to the control. Six plates combined for each cell type ($n=30$). Means±SEM

D

Fatty acid (µM)	Glucose (mM)	Mean
0	5	0.971 a
0	11	0.882 a
200	5	6.920 b
200	11	7.568 c
(s.e.d = 0.1709)		

When data from all five livers were combined into one analysis there was a significant fatty acid × glucose interaction ($P=0.004$) for lipid accumulation in PHH (Figure 3.11, Table S4) as well as a significant effect of fructose ($P<0.001$). Bonferroni comparisons showed that the interaction followed the same pattern as in the McA-RH7777 cells; no difference between 5mM and 11mM glucose in the absence of fatty acids but a significant increase between 5mM and 11mM glucose with fatty acids (Figure 3.11). The fatty acid × fructose interaction was not significant ($P=0.121$). For the overall fructose effect, there was a significant increase between 0mM and 2mM fructose but no further increase between 2mM and 8mM fructose (Figure 3.11).

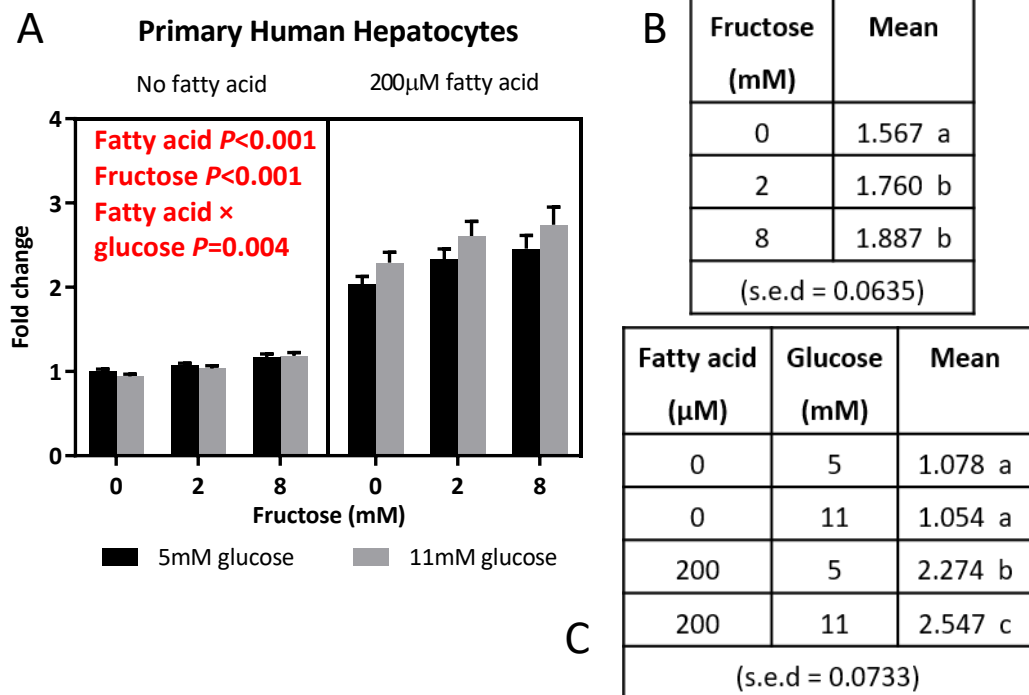


Figure 3.11: Effects of fatty acids, glucose and fructose on lipid accumulation in A: PHH combined data from five donor livers. B: Bonferroni multiple comparisons of the fructose effect. C: Bonferroni multiple comparisons of the fatty acid × glucose interaction. Lipid accumulation was measured by Nile Red staining and normalised to DNA content, then converted to fold change relative to the control. $n=50$ (each liver $n=10$ split across two cell culture plates). Means \pm SEM

When the PHH isolated from different livers (Table 2.1) were analysed individually, the only consistent effect was the increase in lipid with fatty acid treatment ($P < 0.001$ for all) (Figure 3.11, Table S4). The responses to glucose and fructose were variable. L312 and L326 were the two livers to show a significant fatty acid \times glucose interaction ($P = 0.013$ and $P = 0.031$) which post-hoc tests confirmed were the same pattern as the interaction found in the combined data (Tables S5 and S6). L321 also showed a fatty acid \times glucose interaction ($P < 0.001$). However, post-hoc tests from L321 showed that the interaction was slightly different; in the absence of fatty acids, there was a significant decrease in lipid accumulation between 5mM and 11mM glucose (Table S7). A fatty acid \times fructose interaction was found in L312 ($P = 0.007$), L317 ($P = 0.006$) and L329 ($P = 0.049$). In L312, there was no difference between the fructose concentrations in the absence of fatty acids, but there was an increase between 0mM and 8mM fructose when fatty acids were present (Table S8). 2mM fructose was not statistically different from either of the other concentrations but numerically the mean was almost exactly in the middle (Table S8). The fatty acid \times fructose interaction in L317 was of a different nature; all the values were different from each other and increased from 0mM to 8mM fructose both with and without fatty acids (Table S9). In L329, Bonferroni comparisons did not elucidate further on the nature of the interaction (Table S10). The only liver to demonstrate a glucose \times fructose interaction was L317 ($P = 0.045$) (Table S11). Bonferroni comparisons showed that at 5mM glucose, there was no significant increase between 2mM and 8mM fructose but there was at 11mM glucose (Table S11).

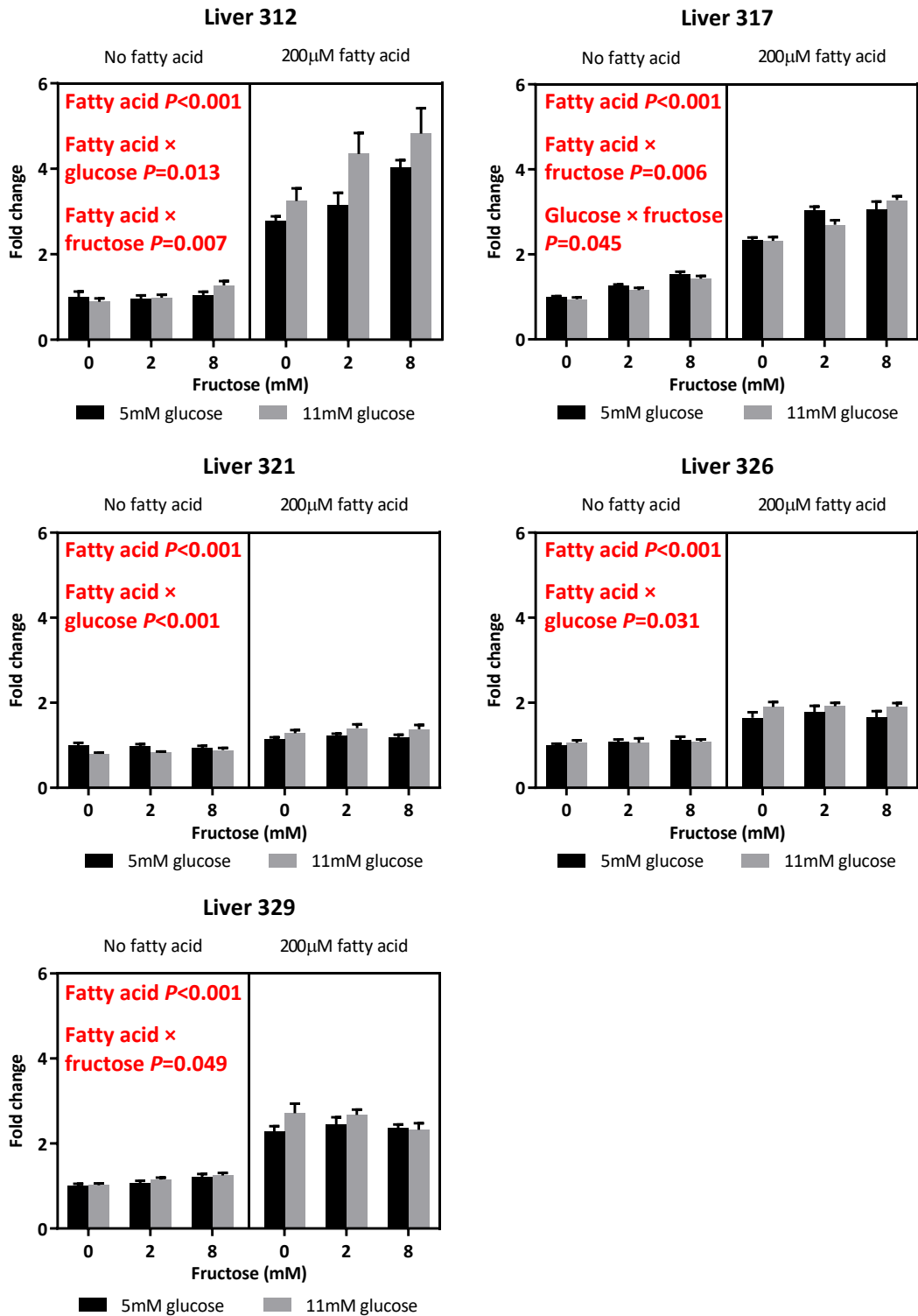


Figure 3.12: Effects of fatty acids, glucose and fructose on lipid accumulation in PHH from each of the five donor livers. Lipid accumulation was measured by Nile Red staining and normalised to DNA content, then converted to fold change relative to the control. Each liver $n=10$ split across two cell culture plates. Means \pm SEM

In terms of fold change (using fluorescence per μg DNA), HepG2 cells reached a maximum of 4.717 ± 0.205 in the $200\mu\text{M}$ fatty acid+ 5mM glucose+ 2mM fructose treatment. Huh7 cells reached a very similar maximum of 4.560 ± 0.181 in the $200\mu\text{M}$ fatty acid+ 5mM glucose+ 0mM fructose treatment. McA-RH7777 stretched to a higher fold change of 7.707 ± 0.295 in the $200\mu\text{M}$ fatty acid+ 11mM glucose+ 2mM fructose treatment. Overall, PHH reached a lower fold change of 2.741 ± 0.212 ($200\mu\text{M}$ fatty acid+ 11mM glucose+ 8mM fructose) but this was highly variable between livers. For example, L321 only reached a maximum of 1.403 ± 0.091 ($200\mu\text{M}$ fatty acid, 11mM glucose, 2mM fructose) whereas L312 reached a maximum of 4.822 ± 0.594 ($200\mu\text{M}$ fatty acid+ 11mM glucose+ 8mM fructose) (Figure 3.12).

3.3.3 Lipid accumulation in response to fatty acid, glucose and insulin treatment in HepG2 cells and PHH

In HepG2 cells, DNA content was significantly higher with high glucose treatment ($P<0.001$) (Figure 3.13). This is in contrast to section 3.3.2 where DNA was affected by fatty acids but not glucose. In PHH (Figure 3.13), DNA was significantly elevated with glucose ($P<0.001$) and insulin ($P<0.001$) treatment. Again, normalisation corrected for any fluorescence changes due to these differences in cell number.

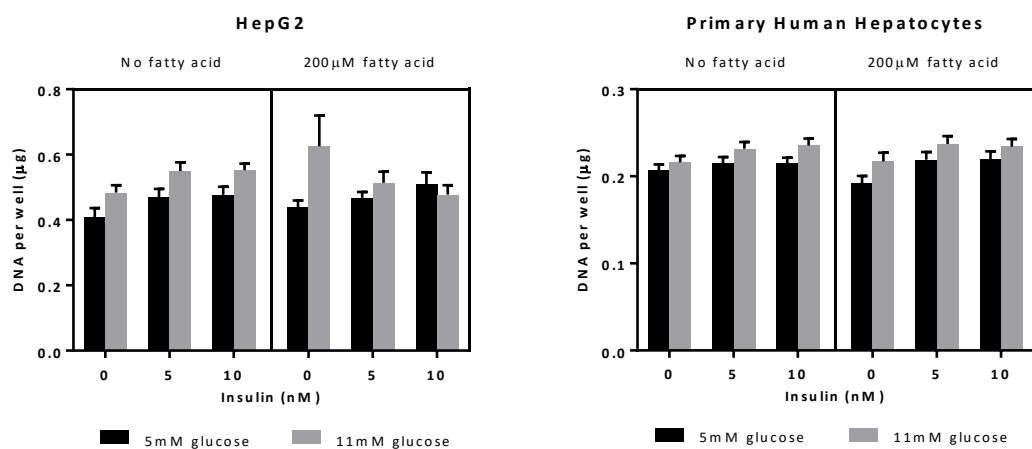


Figure 3.13: Effects of fatty acids, glucose and insulin on DNA content per well in HepG2 cells and PHH (combined data from three donor livers). HepG2: 4 plates combined ($n=20$). PHH: 3 livers with 2 plates each combined ($n=30$). Means \pm SEM

HepG2 cells accumulated lipid with fatty acid treatment ($P<0.001$) similar to the previous experiments. There was no response to glucose, again in line with the results in section 3.3.2, but they did increase lipid accumulation in response to insulin ($P=0.043$) (Figure 3.14, Table S12). Post-hoc tests did not elucidate the effect of insulin further (Figure 3.14). Although not significant, there was a trend towards a fatty acid \times insulin interaction ($P=0.101$).

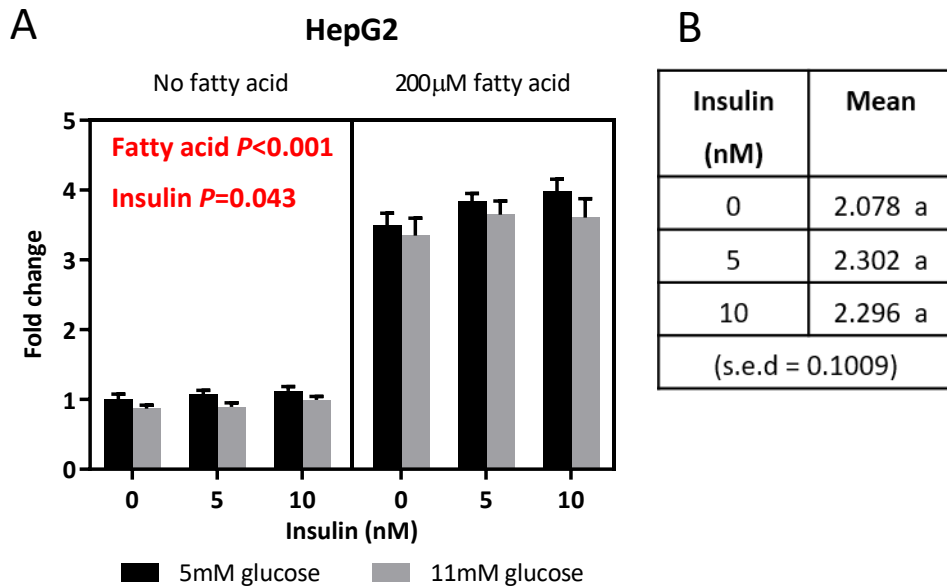


Figure 3.14: Effects of fatty acids, glucose and insulin on lipid accumulation in A: HepG2 cells. B: Bonferroni multiple comparisons of the insulin effect. Lipid accumulation was measured by Nile Red staining and normalised to DNA content, then converted to fold change relative to the control. 4 plates combined ($n=20$). Means \pm SEM

In the combined PHH data (Figure 3.15, Table S13), lipid accumulation was increased by fatty acids ($P<0.001$) and insulin ($P=0.003$), and there was a trend towards a fatty acid \times glucose interaction ($P=0.089$). Post-hoc tests showed that there was a significant increase between 0nM and 5nM insulin but no further increase to 10nM insulin (Figure 3.15). In this experiment only three livers were used; other livers used in the previous experiments were either not set up for this experiment early in the experimental planning, or were excluded due to errors or extreme outlier values in the DNA assays.

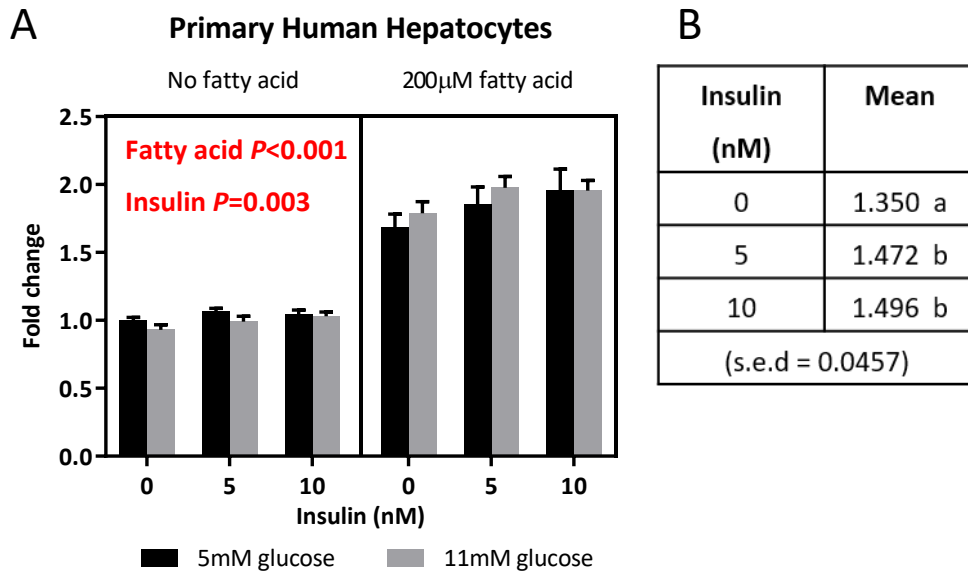


Figure 3.15: Effects of fatty acids, glucose and insulin on lipid accumulation in A: PHH combined data from three donor livers. B: Bonferroni multiple comparisons of the insulin effect. Lipid accumulation was measured by Nile Red staining and normalised to DNA content, then converted to fold change relative to the control. $n=30$ (each liver $n=10$ split across two cell culture plates). Means \pm SEM

As with the previous experiment, the PHH isolated from three different donor livers did not show the same responses (Figure 3.16, Table S13). L317 showed significant interactions between fatty acid \times glucose ($P<0.001$) and fatty acid \times insulin ($P=0.003$). The fatty acid \times glucose interaction (Table S14) showed an increase between 5mM and 11mM glucose only when fatty acids were present. This significant interaction was not seen in this liver in section 3.3.2. Post-hoc tests of the fatty acid \times insulin interaction showed an increase between 0nM insulin and 5nM insulin only in the presence of fatty acids, with no further increase to 10nM insulin (Table S15). In L317, there was also a trend towards a glucose \times insulin interaction ($P=0.054$) and a three way interaction ($P=0.087$). L319 showed a fatty acid \times glucose interaction ($P<0.001$) but this liver did not respond to increasing insulin concentrations. The fatty acid \times glucose interaction again

showed an increase between 5mM and 11mM glucose only when fatty acids were present (Table S16). L321 showed fatty acid \times glucose ($P<0.001$) and glucose \times insulin ($P=0.036$) interactions. Bonferroni comparisons showed that the fatty acid \times glucose interaction was of the same nature as found in this liver in section 3.3.2 (Table S17). The glucose \times insulin interaction was less clear upon post-hoc testing, but there was no significant increase between 5nM and 10nM insulin at either glucose concentration (Table S18).

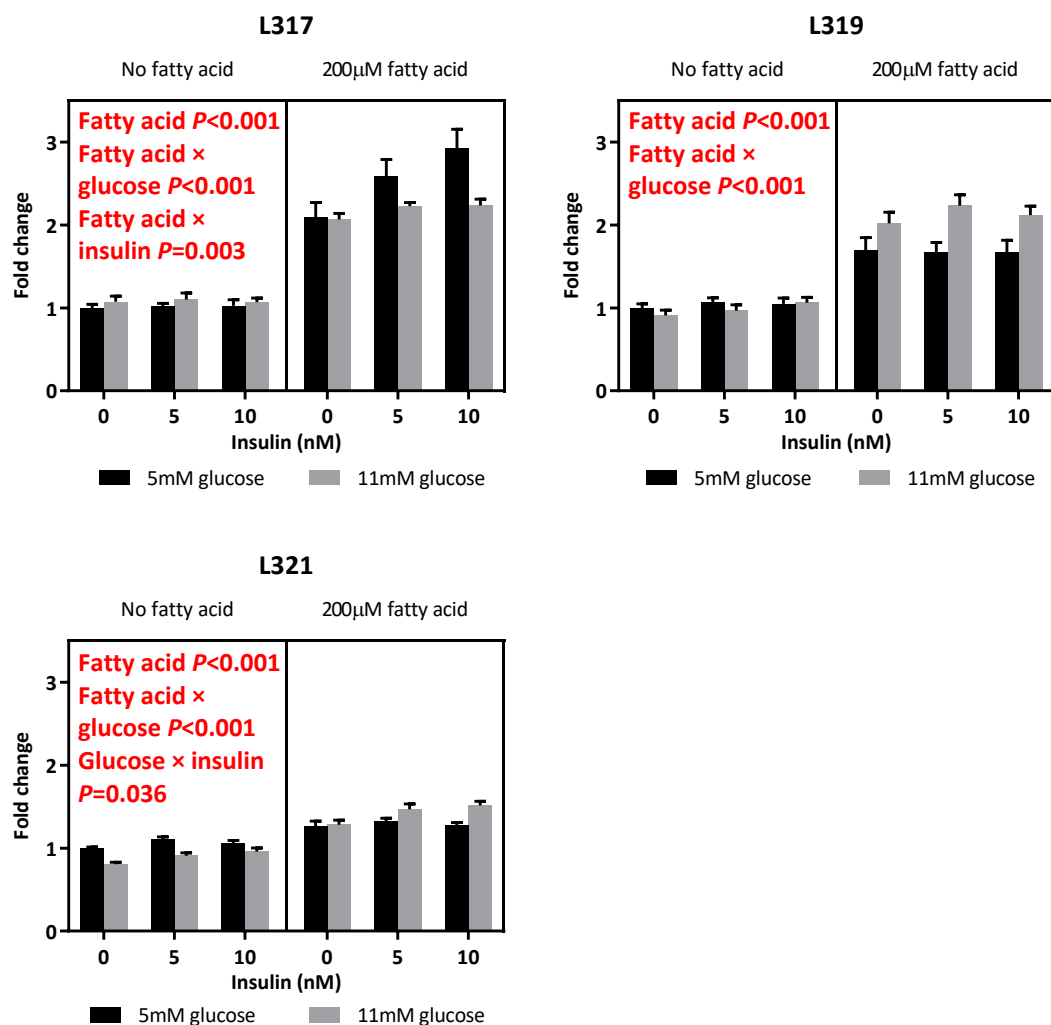


Figure 3.16: Effects of fatty acids, glucose and insulin on lipid accumulation in PHH from three individual donor livers. Lipid accumulation was measured by Nile Red staining and normalised to DNA content, then converted to fold change relative to the control. Each liver $n=10$ split across two cell culture plates. Means \pm SEM

3.3.4 Comparison of insulin sensitivity across hepatoma cell lines

Phosphorylated AKT (pAKT) and total AKT protein were measured by Western blot to determine which cell line was the most insulin sensitive.

Overall there was a significant insulin \times cell line interaction effect ($P < 0.001$). Post-hoc Bonferroni multiple comparisons of this interaction showed that the only significant increase in pAKT to total AKT ratio was in insulin treated McA-RH7777 cells; therefore McA-RH7777 cells were the only cell type to show sensitivity to stimulation with 100nM insulin for 15 minutes (Figure 3.17, Table 3.5). HepG2 and Huh7 cells showed a much smaller non-significant increase (Figure 3.17).

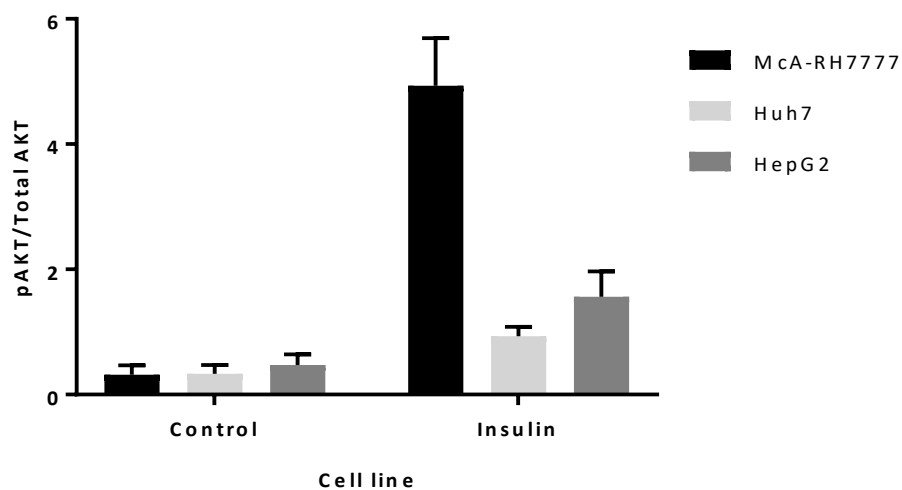


Figure 3.17: Phosphorylated AKT (pAKT) to total AKT ratio in three cell lines treated with 100nM insulin compared with untreated cells. Treatment \times cell line $P < 0.001$, $n=3$. Means \pm SEM

Table 3.5: Cell line × insulin interaction after treatment with 100nM insulin for 15 minutes: Bonferroni comparisons

Cell Line	Treatment	Mean	Bonferroni	s.e.d
McA-RH7777	Control	0.318	a	0.464
Huh7	Control	0.332	a	
HepG2	Control	0.474	a	
Huh7	Insulin	0.931	a	
HepG2	Insulin	1.561	a	
McA-RH7777	Insulin	4.935	b	

3.4 Discussion

3.4.1 Summary of results

The main findings of this chapter are as follows:

- All cell types accumulated lipid in response to incubation with exogenous fatty acids.
- Lipid content of HepG2 and Huh7 cells was not affected by exogenous glucose or fructose at the concentrations used.
- Glucose, but not fructose, increased lipid content of McA-RH7777 cells in combination with fatty acids.
- The responses of PHH to glucose and fructose treatment varied considerably between individual livers; for example treatment with 11mM glucose, 8mM fructose and 200 μ M fatty acids gave a fold change ranging from 1.38 to 4.82. This can also be seen in the statistically significant effects when analysing each liver individually. However, overall, they were the only cell type to show any increased lipid accumulation in response to fructose.
- HepG2 and Huh7 cells are insulin resistant in comparison to McA-RH7777 cells.

3.4.2 Culture conditions for inducing lipid accumulation *in vitro*

It was established that 200 μ M fatty acid treatment for 48 hours would be suitable to induce lipid accumulation in HepG2 cells without significant cell loss. It should be noted that 200 μ M is quite a modest concentration in terms of what may be found in human plasma. As stated in section 3.1.3, fasting NEFA concentrations typically range from about 300-600 μ M (Karpe et al., 2011). If unsaturated fatty acids alone were used to induce lipid accumulation, the concentration could be higher without inducing

apoptosis. For example, Ricchi et al. (2009) found that treatment with 1.32mM oleic acid for 24 hours did not induce apoptosis in HepG2 or Huh7 cells, whereas treatment with 0.66mM palmitic acid alone induced apoptosis in both lines. Similarly, Gomez-Lechon et al. (2007) found that treating HepG2 cells and primary hepatocytes with 1mM oleic acid for 24 hours did not induce cytotoxicity, but treatment with 1mM palmitic acid for 24 hours reduced cell viability significantly. However, it would be unphysiological to have a SFA free environment. Therefore it is common to induce lipid accumulation using a combination of oleic and palmitic acids (Gomez-Lechon et al., 2007, Ricchi et al., 2009, Breher-Esch et al., 2018). It is less common, but more physiologically relevant, to include PUFA in the treatment mix. Our 40:40:20% palmitic:oleic:linoleic acid ratio is closer to the actual ratio found in the blood (Hodson et al., 2008). Although our modest fatty acid treatment concentration would be unlikely to induce maximal lipid accumulation, this left the potential for glucose and fructose to have an additional effect to the fatty acids. Both Ricchi et al. (2009) and Gomez-Lechon et al. (2007) concluded that 24 hours was sufficient to induce maximal lipid accumulation in HepG2 cells treated with fatty acids and that treatment for longer periods would be of no benefit. Again, as we were also treating with sugars, an extra 24 hours with a media refresh allowed observation of the effects of continued exposure rather than sudden changes.

Often in lipid accumulation experiments using cell lines, insulin is not included in the culture conditions. However, the routine use of FBS would mean that there is a variable amount of insulin present. The removal of serum from our treatments removed any interference of insulin present in FBS, allowing for consistent and accurate insulin concentrations. The fact that FBS is rich in insulin is thought to be a possible cause of insulin resistance in cell lines; using human serum improves insulin sensitivity (Gunn et al., 2017). Insulin sensitivity will be discussed further in section 3.4.4.

3.4.3 Lipid accumulation in response to glucose, fructose and fatty acids

All four cell types accumulated lipid consistently and reproducibly with 48 hours of treatment with 200 μ M fatty acids. The ability to induce lipid accumulation in hepatoma cell lines and primary hepatocytes with fatty acids is well characterised (Breher-Esch et al., 2018, Ricchi et al., 2009, Alkhatatbeh et al., 2016, Ling et al., 2013). There was also a reduction in DNA content of the wells with fatty acid treatment across all cell types. Palmitic acid treatment and the induction of lipid accumulation itself can cause apoptosis (Ricchi et al., 2009, Gomez-Lechon et al., 2007). However, additional cell viability assays would need to be carried out to determine whether fatty acid treatment truly decreased cell viability or whether they caused a reduction in proliferation rate. On the other hand, PHH do not proliferate, so apoptosis is more likely.

The results showed that 11mM glucose does not induce lipid accumulation in HepG2 cells or Huh7 cells. Contrary to our findings, studies from other authors using supra-physiological concentrations have shown that HepG2 cells do accumulate intracellular lipid with glucose treatment. For example, Green et al. (2015a) found that HepG2 cells increased lipid accumulation with 22.5mM glucose treatment. Similarly, Hao et al. (2014) found increased lipid accumulation and mRNA expression of both SREBP1c and ChREBP with high (25mM) versus low (5.5mM) glucose. One study using Huh7 cells (Windemuller et al., 2016) treated them for 24 hours with unusually low concentrations of glucose (0.65, 0.68 and 0.72mM) and found that glucose did not increase cellular TAG. We also found no increase in lipid accumulation with glucose treatment in Huh7 cells, but at more physiological concentrations. PHH and McA-RH7777 cells both showed a fatty acid \times glucose interaction where there was an increase in lipid accumulation between 5mM and 11mM glucose only when fatty acids were present, although it is important to remember that this effect was not consistent across all livers. There are a number of possible reasons for fatty acid and sugar interaction effects. Fatty

acids would provide a higher excess of energy substrate so less carbohydrates might be used to produce energy and are instead stored as TAG. PHH do not proliferate and therefore have a lower energy demand; as such, excess carbohydrate may be more readily stored as TAG. Alternatively, glucose and fructose could provide a ready source of glycerol-3-phosphate which is a necessary component for TAG formation. Fatty acids may have limited storage as TAG unless there is enough available glycerol-3-phosphate, meaning that increased glucose and fructose could increase TAG storage when fatty acids are present, as was the case in some livers. Accumulation of TAG in lipid droplets itself is not necessarily detrimental and may represent a relatively inert and safe storage form of potentially toxic fatty acids. Preventing TAG formation in mice by injecting them with a DGAT2 antisense oligonucleotide reduced steatosis, but the mice had increased tumour necrosis factor alpha (TNF α) expression suggesting inflammation (Yamaguchi et al., 2007). In this case, carbohydrates in combination with high fat might be protective; this has been suggested in a study by Softic et al. (2017) who fed mice with either chow or a high fat diet (HFD) supplemented with tap water, 30% fructose solution or 30% glucose solution, enabling the interactions between dietary fat and sugars to be observed. Fructose increased fasting blood glucose only when in combination with a HFD, but supplementation of a HFD with glucose brought fasting glucose down to a comparable level to those on a standard chow diet. Similarly, HFD+fructose or HFD became insulin resistant but HFD+glucose did not, indicating a potential protective effect of glucose. Glucose or fructose supplementation of a chow diet resulted in mild steatosis and TAG accumulation and HFD alone resulted in moderate steatosis. However, glucose and fructose supplementation of a HFD resulted in severe steatosis. It is also possible that fatty acids and sugars interact to regulate gene expression which will be discussed in Chapter 4.

There has been a comprehensive study comparing fatty acid and glucose metabolism between McA-RH7777 cells and primary rat hepatocytes. Hansson et al. (2004) treated both cell types with 50 μ M or 500 μ M palmitate in combination with 5.6mM or 20mM glucose, all with or without the addition of 175nM insulin. They found that McA-RH7777 cells have twice the capacity for palmitate uptake and conversion to TAG. In contrast, the primary rat hepatocytes had higher glucose uptake, higher capacity for glycogen storage, and higher glucose oxidation capacity. More glucose was channelled into fatty acid synthesis from glucose in McA-RH7777 cells which, combined with the fact that McA-RH7777 cells have lower fatty acid oxidation capacity, could be because McA-RH7777 cells are proliferating and need to preferentially use fatty acids for cell membrane synthesis (Hansson et al., 2004). This is a consideration for all proliferating cell lines.

The results showed that fructose had no effect on lipid accumulation in any of the three cell lines. The effect of fructose on NAFLD is still a controversial topic (Ter Horst and Serlie, 2017). *In silico* predictions, which were confirmed in HepG2 cells, show no difference between the ability of glucose and fructose to induce lipid accumulation (Maldonado et al., 2018). There was no difference between HepG2 cells treated with 25mM glucose or 25mM fructose compared to control (0mM of both). This study also found no effect of 100nM insulin on lipid accumulation in HepG2 cells (Maldonado et al., 2018). Although our results agree with the negligible effect of glucose and fructose, we did find a small but significant increase in lipid accumulation with increasing insulin from 0nM to 10nM. However, the fact that this seemed more prominent in fatty acid treated cells (fatty acid \times insulin $P=0.101$) could be why Maldonado et al. (2018) did not see an effect as their treatments did not include fatty acids. Zhao et al. (2016) found lipid accumulation with fructose treatment in HepG2 cells; however, there are a number of factors that make this study unreliable. The control was 25mM glucose, a highly

supra-physiological concentration, and the data were analysed by one-way ANOVA which meant that overall effects could not be determined. Supra-physiological concentrations of fructose were also used (up to 25mM) and there were some treatments with fructose without glucose which would not occur *in vivo*. Hoang et al. (2019) also found that both glucose and fructose increased lipid accumulation in HepG2 cells. However, again the concentrations were highly supra-physiological. Windemuller et al. (2016) found that increasing the fructose:glucose ratio resulted in increased lipid accumulation in Huh7 cells but using much lower concentrations. Our results do not support this. To our knowledge, no studies to date have shown effects of fructose on lipid accumulation in McA-RH7777 cells. We found that, similar to HepG2 and Huh7 cells, fructose did not induce lipid accumulation in McA-RH7777 cells. This could be because of their cancerous phenotype, drawing on work by Speicher et al. (2010); aldolase B activity is very low and hexokinase 2 is much more highly expressed in HepG2 and Huh7 cells compared to PHH, although the activity of fructokinase has been shown to be similar (Speicher et al., 2010). Due to this difference in metabolic capacity, ATP depletion caused by fructose was not found in HepG2 or Huh7 cells. The fact that the cell lines express aldolase A rather than aldolase B and have a high hexokinase 2 expression gives them more of a muscle phenotype in terms of fructose metabolism (Speicher et al., 2010). This could be one factor limiting the incorporation of fructose into lipid in these cells; fructose is more readily channelled into glycolysis.

We found that the four cell types had the following order in terms of the greatest fold change of lipid accumulation; McA-RH7777, HepG2, Huh7, (almost identical to HepG2), PHH. However, as noted in section 3.3.2, the livers were variable in terms of their fold change. This could partly be due to the amount of lipid already accumulated when the cells were isolated; for future work, a measurement of baseline TAG content of the liver tissue could be useful. There could also be a number of other factors at play. Although

we have age and gender information (see methods section 2.1.2), the sample size is not large enough to draw any conclusions about whether these factors have influenced the results. PNPLA3 genotype could be another factor that determines the amount of lipid accumulation and will be discussed further in Chapter 5. However, it is important to note at this point that McA-RH7777 cells are different to HepG2 and Huh7 cells in terms of their PNPLA3 genotype; McA-RH7777 cells do not carry the I148M polymorphism (Pirazzi et al., 2012) which could be a reason why the McA-RH7777 cells appear to have lower TAG content at baseline. The fact that HepG2 cells accumulate more lipid than PHH is in contrast to results reported by Gomez-Lechon et al. (2007), who found that PHH accumulated more lipid than HepG2 cells over 24 hours. However, they used higher fatty acid concentrations of 0.5mM to 2mM with varying oleate and palmitate ratios. Inter-individual variability in the amount of lipid accumulated in PHH would also be a factor to consider, therefore it is not possible to conclude that one cell type accumulates more lipid than the other when including PHH, although careful measurement of baseline lipid content of donor livers would be useful. It has been suggested that Huh7 cells are able to store more TAG, and have an increased rate of lipogenesis, compared to HepG2 cells; this was shown in culture conditions with 11mM glucose and no exogenous fatty acid supply except that found in either 10% FBS or 2% human serum for 1 week (Gunn et al., 2017). We found that HepG2 cells and Huh7 cells reached a very similar level of lipid accumulation after 48 hours of fatty acid treatment in serum free conditions. It is thought that culturing in human serum can improve the fatty acid metabolism to be more physiologically relevant with increased TAG secretion, fatty acid oxidation and insulin sensitivity (Gunn et al., 2017). Our cell culture treatment conditions were serum free, removing the effects of any hormones, lipoproteins, or other factors that are present in FBS and would vary between batches. This could be a reason why results differ between studies.

3.4.4 Insulin sensitivity and lipid accumulation in response to insulin

The results looking at AKT phosphorylation suggest that McA-RH7777 cells are more insulin sensitive than HepG2 or Huh7 cells. To our knowledge, this has not been investigated before in McA-RH7777 cells, but similar work with HepG2 and Huh7 cells has been carried out. Ricchi et al. (2009) found that HepG2 cells phosphorylated AKT in response to treatment with 100nM insulin for 15 minutes, however the ratio of pAKT to total AKT was not measured and the data appeared not to be analysed statistically. Another study showed that with 111nM insulin stimulation for 10 minutes, similar to that used here, there was only a small increase in pAKT in Huh7 cells and a slightly larger but still small increase in HepG2 cells (Gunn et al., 2017). This is very similar to our results, but again the results were not analysed statistically. In the same study, culturing with 2% human serum instead of 10% FBS significantly improved the insulin sensitivity of both cell types. In contrast, another study found a highly significant 8-fold increase in pAKT/AKT ratio in HepG2 cells after stimulation with 100nM insulin for 15 minutes (Maldonado et al., 2018). It is not clear from this paper whether the cells had been serum and insulin starved prior to the insulin stimulation.

We did not carry out any insulin sensitivity measurements on PHH, but testing each liver for insulin sensitivity would be a valuable addition to future data. Further information about the patients, such as diabetes status, would also be valuable. Insulin sensitivity is another factor which is likely to be variable between livers and could affect any lipid accumulation results. It would also be interesting to carry out lipid accumulation experiments using insulin in McA-RH7777 cells to determine if their increased insulin sensitivity affects the way they accumulate lipid in response to insulin.

When looking at lipid accumulation in response to insulin, it appears that both HepG2 and PHH accumulate lipid in response to insulin treatment, but again this depended

upon the liver. This would be expected, as insulin can induce lipogenesis through its action on SREBP1c (Dentin et al., 2005). In addition, insulin inhibits the amount of TAG secreted as VLDL (Salter et al., 1998); this may affect PHH more than HepG2 cells as HepG2 cells do not efficiently secrete lipoprotein (Gibbons et al., 1994). As mentioned previously, *in vitro* lipid accumulation experiments are often carried out with highly supra-physiological concentrations of insulin which could be affecting the lipid accumulation of cultured cells. The fact that HepG2 cells did show an increase in lipid content with insulin treatment suggests that they are not completely insulin resistant, however this could be the paradox of 'selective insulin resistance' in the liver found in type 2 diabetes, where pathways involved in glucose metabolism are impaired but the stimulation of lipid metabolism and lipogenesis remains (Leavens and Birnbaum, 2011). This results in an environment of glucose production (raising blood glucose) and lipid accumulation.

3.4.5 Concluding remarks

Overall, the four cell types are quite different in terms of their lipid accumulation in response to nutrient availability, calling into question whether the commonly used hepatoma cell lines accurately model the human liver. The gene expression analysis in Chapter 4 will help to elucidate further differences between hepatoma cell lines and PHH. Inter-individual variability is key to highlight in experiments using PHH, this may relate to a wide range of factors including age, sex and metabolic health of the individuals. Thus, while PHH may represent the best model of human hepatic metabolism *in vivo*, further careful assessment of the impact of the donor characteristics of such cells is required. This is somewhat confounded by the fact that hepatic biopsy poses a significant risk and is unlikely to be performed on 'healthy'

individuals. Considerable data is available relating to lipid metabolism of primary cultures of animal hepatocytes but clear species differences, for example rat versus hamster (Salter et al., 1998), have been identified. There appears to be no advantage of using Huh7 cells over HepG2 cells to study lipid accumulation as they behave very similarly and neither was reflective of PHH. McA-RH7777 cells may offer a more insulin sensitive model with a better lipoprotein secretion profile, but whether a rat cell line can truly offer a better model of human hepatic lipid accumulation than a human cell line requires further work.

Chapter 4: Comparison of gene expression in HepG2 cells and primary human hepatocytes

4.1. Introduction

4.1.1 Mechanisms of lipid accumulation

The intracellular pathways resulting in TAG accumulation link together fatty acid and carbohydrate metabolism (Figure 4.1) and involve a large number of genes that have complex interactions. Glucose, fructose and fatty acids can all act as substrates for TAG synthesis and factors to alter gene expression.

Glucose and fructose enter hepatocytes mainly via the passive glucose transporter 2 (GLUT2) which is insulin-independent (Bechmann et al., 2012). Glucose is phosphorylated to glucose-6-phosphate by glucokinase (GCK), and can then be used in glycogen synthesis or channelled into glycolysis (Figure 4.1) (Rui, 2014). Fructose is phosphorylated to fructose-1-phosphate by ketohexokinase (KHK). This enzyme has a higher phosphorylation rate than GCK and it is not feedback inhibited (Geidl-Flueck and Gerber, 2017). KHK is elevated in livers from obese patients with NASH (Softic et al., 2017). Glucose can provide substrate for TAG accumulation by conversion to acetyl-coA through glycolysis which then feeds into lipogenesis (Figure 4.1). Fructose can enter glycolysis at a lower point by metabolism to glyceraldehyde-3-phosphate, and therefore can also be converted to acetyl-coA. Both glucose and fructose can also provide a source of glycerol-3-phosphate for TAG synthesis (Figure 4.1). The final stage of glycolysis is the conversion of phosphoenolpyruvate into pyruvate by liver pyruvate kinase (LPK). Pyruvate can then enter the mitochondria and be converted to acetyl-coA to be used in the TCA cycle or exported into the cytosol for fatty acid synthesis.

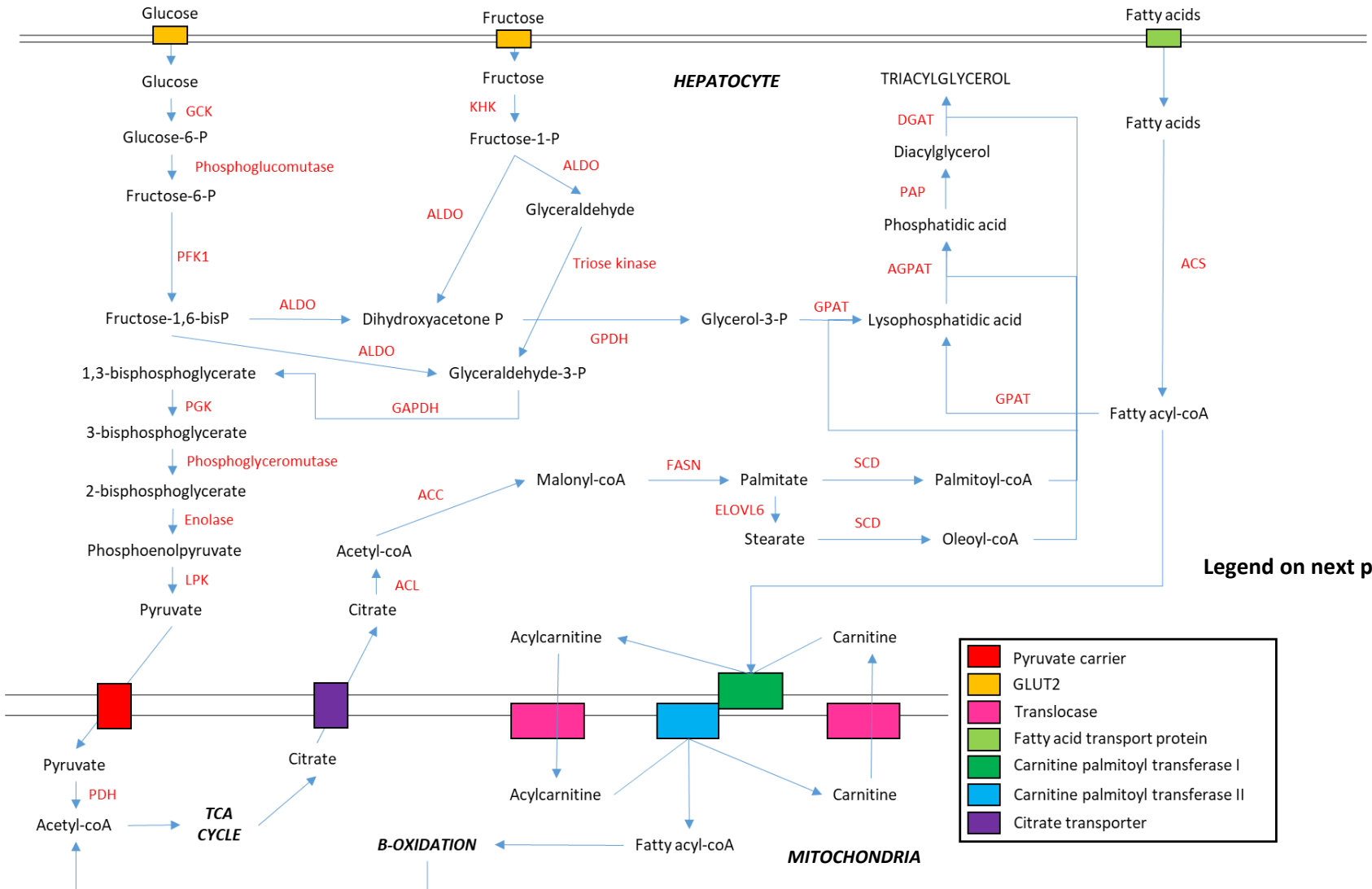


Figure 4.1: Pathways within hepatocytes that result in triacylglycerol (TAG) production. P: phosphate, GCK: glucokinase, PFK: phosphofructokinase, ACC: acetyl-coA carboxylase, FASN: fatty acid synthase, SCD: stearoyl-coA desaturase, LPK: liver pyruvate kinase, PDH: pyruvate dehydrogenase, DGAT: diacylglycerol transferase, ALDO: aldolase, GPAT: glycerol-3-phosphate acyltransferase, ACL: ATP citrate lyase, KHK: ketohexokinase, PAP: phosphaditic acid phosphorylase, AGPAT: acylglycerophosphate acyltransferase, GPDH: glycerol-3-phosphate dehydrogenase, ELOVL6: fatty acid elongase, PGK: phosphoglycerokinase. GAPDH: glyceraldehyde-3-phosphate dehydrogenase, ACS: acyl-coA synthetase

Fatty acids enter the cell through fatty acid transport proteins (FATP). They are activated in the cytosol by acyl-CoA synthetase (ACS) to fatty acyl-CoA, which can then be directly incorporated into TAG or can enter the mitochondria for oxidation. Carnitine palmitoyltransferase-1 α (CPT1 α) transports fatty acyl-CoA across the mitochondrial membrane where they can then be used for aerobic β -oxidation to produce acetyl-coA (Figure 4.1). This can be used in the TCA cycle to produce ATP, and the TCA intermediate oxaloacetate can be used in gluconeogenesis. Therefore, CPT1 α is a key rate-limiting protein in the β -oxidation process.

Lipogenesis converts acetyl-coA to fatty acyl-CoA and this process contributes about a quarter of the TAG palmitate found in the livers of NAFLD patients (Donnelly et al., 2005). Key enzymes in the lipogenic pathway are acetyl-coA carboxylase (ACC), fatty acid synthase (FASN), and stearoyl-CoA desaturase (SCD) (Figure 4.1). TAG synthesis requires glycerol-3-phosphate and fatty acyl-CoA from either extracellular origin (predominantly dietary or released from adipose tissue) or produced by lipogenesis (Figure 4.1). DGAT catalyses the final addition of a fatty acid to DAG to produce TAG which is stored in lipid droplets. Patatin-like phospholipase domain containing 3

(PNPLA3), introduced in detail in Chapter 5, is associated with lipid droplets and acts predominantly as a TAG hydrolase (Pingitore and Romeo, 2019).

Transcription factors play a major role in regulating the expression of genes involved in fatty acid and carbohydrate metabolism. A key lipogenic transcription factor is sterol regulatory element-binding protein 1 (SREBP1) which has three isoforms: SREBP1a (accession number NM_004176.4), SREBP1c (NM_001321096.3), and the less recognised isoform termed SREBP1ac (NM_001005291.3) which contributes very little to the total SREBP1 pool (Felder et al., 2005). These isoforms are products of the same gene (SREBF) originating from different transcription start sites and have alternative exon splicing (Figure 4.2). While both SREBP1a and SREBP1c have been suggested to regulate lipogenesis, SREBP1a is a much more potent transcription factor than SREBP1c. It has long been thought that the 1a isoform is the dominantly expressed isoform in cell lines whereas the 1c isoform is more highly expressed in liver (Shimomura et al., 1997). SREBP1c is responsive to insulin, meaning it mediates, in part, increased expression of lipogenic and glycolytic genes in response to carbohydrate feeding (Dentin et al., 2005). It is also downregulated by PUFA (Georgiadi and Kersten, 2012).

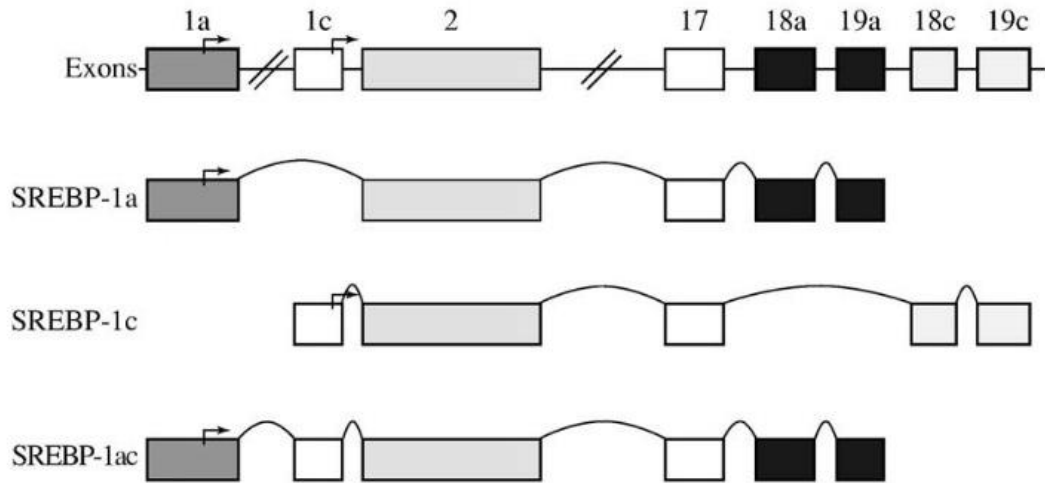


Figure 4.2: The SREBP1 isoforms produced from the SREBF gene. Alternative splicing of exons is shown, and the arrows represent transcription start sites. Modified from Felder et al. (2005)

Another transcription factor mediating the response to carbohydrates is ChREBP. Many glycolytic and lipogenic genes contain a carbohydrate response element (ChoRE) in the promoter which allow binding of ChREBP, which is induced by glucose rather than insulin (Dentin et al., 2005).

Peroxisome proliferator-activated receptor gamma coactivator 1-alpha (PPARGC1 α , also known as PGC-1a), is a transcriptional coactivator involved in the upregulation of gluconeogenic genes, as well as having a role in mitochondrial oxidative metabolism, including β -oxidation (Lin et al., 2005a). SNPs and low expression of this gene are associated with NAFLD (Yoneda et al., 2008).

Once TAG is stored in lipid droplets, it can be incorporated into VLDL and secreted into the circulation. ApoB (in humans ApoB100) is an essential protein in VLDL assembly; ApoB is lipidated in the ER by the microsomal triglyceride transfer protein (MTTP) and

the VLDL particle is eventually transported to the Golgi apparatus from where it is secreted into the circulation via the space of Disse (Sanders and Griffin, 2016).

4.1.2 Experimental aims

In Chapter 3 we found that hepatoma cell lines and PHH accumulate lipid differently in response to glucose, fructose and fatty acid treatment. This chapter aimed to explore possible mechanisms behind those differences at the mRNA level, and how treatments affected gene expression within cell types. We used HepG2 cells, the most commonly used cell line model of NAFLD, and PHH isolated from liver 329 which originated from a 25-year-old female patient (Table 2.1). Two different approaches were taken to comparing the response of PHH and HepG2 cells. Firstly, the response of a range of genes known to be involved in carbohydrate and lipid metabolism was investigated using quantitative reverse transcription polymerase chain reaction (RT-qPCR) to determine steady state concentrations of mRNA. Secondly, a microarray approach was taken that would identify differences in mRNA concentrations for genes in a wide range of metabolic pathways including those that might be expected to occur 'downstream' of lipid accumulation, such as those involved in the inflammatory responses associated with NAFLD.

The aims of this chapter were as follows:

- To carry out targeted gene expression analyses using RT-qPCR to compare the mRNA expression of key genes of lipid and carbohydrate metabolism in HepG2 and PHH treated with glucose, fructose and fatty acids as in Chapter 3.
- To compare mRNA profiles of HepG2 and PHH by microarray, including responses to glucose, fructose and fatty acids.

4.2 Methods

4.2.1 Experimental protocol

The experiment from section 3.2.4 was performed on HepG2 cells and one liver (L329) using 12-well plates in order to harvest cells for RNA extraction. HepG2 cells were seeded at 1.48×10^5 cells per well and PHH at 4.8×10^5 cells per well, in a volume of 1.2ml media. Five 12-well plates were used with each plate including one replicate per treatment group ($n=5$ in total). At 48 hours, after the treatments in section 3.2.4 (shown in Table 4.1), cells were scraped using a cell scraper into 200 μ l RNase free PBS before transferring immediately to ice and freezing at -80°C as soon as possible.

Table 4.1: Treatments prepared for the experiment. Vehicle controls were BSA NaCl solution for fatty acids and water for the sugar solutions

	0μM fatty acid	200μM fatty acid
5mM glucose	0mM fructose	0mM fructose
	2mM fructose	2mM fructose
	8mM fructose	8mM fructose
11mM glucose	0mM fructose	0mM fructose
	2mM fructose	2mM fructose
	8mM fructose	8mM fructose

4.2.2 RNA extraction from HepG2 cells

RNA was extracted from cells frozen in PBS using the Roche High Pure Isolation kit in batches. 400 μ l lysis buffer was added to each sample and the tubes vortexed until the sample was dissolved. The samples were transferred to a spin column and spun at 6000 $\times g$ (Microfuge 22R Centrifuge, Beckman Coulter) for 15 seconds at 4°C . The flow-through was removed and 100 μ l of DNase plus incubation buffer was added to the filter. This was left at room temperature for 15 minutes. 500 μ l wash buffer 1 was added

to the columns which were spun at $6000\times g$ for 15 seconds at 4°C . This step was repeated with wash buffer 2. Finally, $200\mu\text{l}$ wash buffer 2 was added to the filter and spun at $6000\times g$ for 2 minutes at 4°C . The RNA was eluted in $50\mu\text{l}$ elution buffer into 1.5ml tubes.

4.2.3 RNA extraction from primary human hepatocytes

It was intended to use the same RNA extraction method as for HepG2 cells; however, after extracting one replicate of each treatment using this method, the concentrations of nucleic acids were very low. As low starting material could have been the issue, a further six samples were extracted using the Qiagen Micro RNA kit as per the manufacturer's instructions. This yielded worse results than the Roche kit. It was therefore decided to use a phenol chloroform extraction method for the remaining samples; this meant that only $n=3$ replicates per treatment were remaining.

$800\mu\text{l}$ Qiazol was added to each sample and the tubes vortexed well. The homogenate was passed at least six times through a 20-gauge needle and syringe and incubated at room temperature for 5 minutes. $200\mu\text{l}$ chloroform was added to each tube and the lids tightly closed before shaking vigorously. A further 3 minute incubation at room temperature was performed before spinning at $13000\times g$ for 15 minutes at 4°C to separate the phases. The top aqueous phase was carefully transferred to a new tube containing $600\mu\text{l}$ isopropanol. The tubes were mixed by shaking and left to incubate at room temperature for 10 minutes before spinning at $13000\times g$ for 10 minutes at 4°C . The supernatant was removed and two washes performed with 75% (v/v) ethanol. The pellets were air dried then re-suspended in $40\mu\text{l}$ RNase free water. The concentrations were more successful at around $100\text{ng}/\mu\text{l}$. The 260/280 and 260/230 ratios were not as expected, possibly due to the presence of DNA or other contaminants. A phenol

chloroform and DNase clean-up test was trialled on surplus samples, but the ratios were unchanged and when the samples were run on an agarose gel there was no difference between DNase treated and non-DNase treated samples, and they were identical to an RNA sample of known good quality. Therefore, all samples used for complementary DNA (cDNA) synthesis did not undergo clean-up.

4.2.4 RNA quality checks

RNA quantity and quality were assessed by measurement of 1.5 μ l aliquots on a NanoDrop 2000 Spectrophotometer (ThermoScientific) in duplicate. RNA samples were also run on agarose gels and stained with ethidium bromide to check for the typical double bands. After measuring concentration, all RNA samples were diluted to 100ng/ μ l (or as close as possible based on the most dilute sample) using RNase free water and stored at -80°C .

4.2.5 cDNA Synthesis

cDNA synthesis was carried out using the RevertAid RT Reverse Transcription Kit (ThermoFisher). In a 96-well PCR plate, 1 μ l random hexamer primer and enough water to ensure a final reaction volume of 12 μ l were added to each well. Then the RNA (usually 500ng) was added to each well, along with a water control well. The plate was incubated in a thermocycler at 65°C for 5 minutes then immediately transferred to ice. A master mix was made containing the following for each reaction: 4 μ l 5 \times reaction buffer, 1 μ l RiboLock RNase inhibitor, 2 μ l 10mM dNTP mix, 1 μ l RevertAid RT. 8 μ l of the master mix was added to each well directly into the liquid to ensure mixing. The plate was incubated at 25°C for 5 minutes, 42°C for 1 hour, 70°C for 5 minutes then cooled to 4°C

using the GeneAmp PCR System 9700 (Applied Biosystems). 80µl RNase-free water was added to each well and mixed, then the plate was stored at –20°C.

4.2.6 Primer design

Primers were designed using the Primer Express software, apart from the SREBP1a and SREBP1c primers which were taken from Sewter et al. (2002). Where possible, primers were chosen to be over an exon boundary to ensure that any residual genomic DNA was not amplified. All primers are shown in Table 4.2.

Table 4.2: Primers used for RT-qPCR analysis, all obtained from Sigma. Orange – lipogenesis, blue – fatty acid metabolism, green – carbohydrate metabolism, yellow – housekeeper			
Gene	Other Names / Abbreviations	Forward Primer	Reverse Primer
ACACA	ACC1, acetyl-coA carboxylase	TGATGGGCTGCTTCTCTGACT	TCCCTGGGAACCTTATCCTCAT
FASN	Fatty acid synthase	GCTCGCCACCTACGTAAGT	TGCTCCATGTCCGTGAACTG
SCD	Stearoyl-coA desaturase	CACGTGGGTTGGCTGCTT	AGGTTTGTAGTACCTCCTCTGGAACA
SREBP1a	Sterol regulatory element binding protein 1A	TGCTGACCGACATCGAAGAC	CCAGCATAGGGTGGGTCAAA
SREBP1c	Sterol regulatory element binding protein 1C	CCATGGATTGCACTTTCGAA	CCAGCATAGGGTGGGTCAAA
DGAT1	Diacylglycerol acyltransferase 1	ACTGGTGGAACTCCGAGTCTGT	GGCTTGTAGAAGTGTCTGATGCA
CPT1 α	Carnitine palmitoyltransferase 1A	CCATGTTGTACAGCTTCCAGACA	CACCGACTGTAGATACCTGTTTACA
PPARGC1 α	PPARG coactivator 1 alpha, PCG1 α	ACAGCAGCAGAGACAAATGCA	TTGGTTTGGCTTGTAAAGTGTGTTG
APOB	Apolipoprotein B	GTCAGTACACACTGGACGCTAAGAG	TGCTACCATCCCATACTTATTCTTGTAG
PNPLA3	Patatin-like phospholipase domain-containing protein 3	TCAGAGGCGTGCGATATGTG	GGGACACGGTGATGGTTGTT
LPK	Liver pyruvate kinase	GGGTGGACTACCCCAATATTGTC	CCTCTGGGCCGATTTTCTG
GLUT2	SLC2A2, glucose transporter type 2	GCTGCTCAACTAATCACCATGCT	CATGGCTTTGATTCTTCCAAGTG
HK2	Hexokinase 2	CGGCAAGCAGAGGTTCTGA	TGTCTTGAGCCGCTCTGAGA
GCK	Glucokinase, hexokinase 4	TGCTGAGATGCTCTTCGACTACA	GCTTCTTGTGTTTCATCTGATGCT
MLXIPL	Total ChREBP, carbohydrate regulatory element binding protein	ATCTCAGACACTCTTTCACCATGA	TGCCGACGTAGGCATCCT
ACTB	Beta actin, β -actin	CCTGGCACCCAGCACAAAT	GCCGATCCACACGGAGTACT

4.2.7 RT-qPCR

Before measuring gene expression, all cDNA and RNA samples were tested using β -actin primers. A master mix was prepared containing 7.5 μ l SYBR Green (Roche), 0.45 μ l forward primer, 0.45 μ l reverse primer and 1.6 μ l water per reaction. This was the standard master mix for all RT-qPCR. 10 μ l of master mix was added to each required well of a white 384-well plate using a multi-dispensing pipette. 5 μ l of neat cDNA or 1 μ l RNA and 4 μ l water were added to the wells. This was to ensure that the cDNA produced a product and that the RNA either produced no product or completed at a very late crossing point (CP) value. All cDNA samples that were within two standard deviations of one another were used to create a pool of cDNA to use for creating a serial dilution standard curve. Separate pools were used for the HepG2 and PHH cDNA. For gene expression analysis of each sample, a 1 in 8 dilution of the cDNA was made. For the HepG2 cDNA two separate 1 in 8 dilutions were used but all the PHH analyses were from the same dilution. 10 μ l of master mix and 5 μ l of the samples (or standards) were added to each well using a multi-channel multi-dispensing pipette. The plate was sealed with sealing foil then spun down in a plate spinner. The cycling conditions are shown in Table 4.3.

Stage	Target Temp (°C)	Time (mins:secs)	Ramp rate (°C/sec)
Pre-incubation	95	05:00	4.8
Amplification ($\times 45$)	95	00:10	4.8
	60	00:15	2.5
	72	00:15	4.8
Melt Curve	95	00:05	4.8
	65	01:00	2.5
	97	(Continuous)	0.11
Cooling	40	00:10	2

4.2.8 Determination of total cDNA using OliGreen

Total cDNA was measured using OliGreen (Invitrogen) to use for normalisation instead of a housekeeping gene because β -actin expression was not stable. OliGreen was diluted into TE buffer (5 μ l OliGreen per ml TE buffer). 5 μ l of the diluted OliGreen was added to each well of a white 384-well plate. 5 μ l of cDNA (1:8 dilution) was added to each well. A standard curve made from the cDNA pool was also used. The plate was measured on a LightCycler 480 using the conditions in Table 4.4. The data read closest to 80°C was used for analysis. For the HepG2 cell RNA where the data was split over two dilutions, OliGreen analysis was performed on each dilution.

Table 4.4: Conditions for OliGreen analysis carried out on a Roche LightCycler 480			
Stage	Target Temp (°C)	Time (mins:secs)	Ramp rate (°C/sec)
Melt Curve	95	(Continuous)	0.11

4.2.9 Statistical analysis of RT-qPCR data

The normalised data for each gene was analysed by three-way ANOVA (fatty acid \times glucose \times fructose) with blocking for plate. For comparing standard curves of cDNA pools in section 4.3.1.6, linear regression was carried out in GraphPad Prism to test whether the slopes or intercepts of the lines were significantly different. The intercepts could only be tested if the slopes were not significantly different.

4.2.10 Microarray Analysis

RNA from HepG2 cells and primary human hepatocytes (L329) subjected to treatments in Table 4.5 ($n=3$) were submitted for microarray analysis.

Treatment Code	Fatty Acid (μM)	Glucose (mM)	Fructose (mM)
CON	0	5	0
FA	200	5	0
FA+F	200	5	8
FA+G	200	11	0
FA+G+F	200	11	8

The assays (Clariom S human assays, Applied Biosystems) were carried out by the team at The Nottingham Arabidopsis Stock Centre (NASC) who also assisted with the data analysis, using the Partek Genomics Suite software. T-test comparisons were carried out across cell types for CON and FA, and treatments within cell types that were a single nutrient addition: CON vs FA, FA vs FA+G, FA vs FA+F, FA+G vs FA+G+F, FA+F vs FA+G+F. Applying false discovery rate (FDR) correction resulted in no significantly changed genes for the majority of comparisons within the same cell type. Therefore, we used a non-FDR adjusted P -value of $P \leq 0.05$ for these comparisons and a fold change outside -2 and 2 or outside -1.5 and 1.5 depending upon the number of significantly changed genes. Comparisons of CON and FA between the cell types resulted in a large number of significant genes, so the more stringent parameters of an FDR adjusted P -value of $P \leq 0.01$ and a fold change outside -2 and 2 were applied. Pathway analysis was carried out by Prof Richard Emes using the Ingenuity Pathway Analysis (IPA) program. Significantly enriched KEGG pathways were looked at for each comparison.

4.3 Results

4.3.1 Targeted gene expression analyses by RT-qPCR

4.3.1.1 Total cDNA (*OliGreen fluorescence*)

There was no significant effect of treatment on total cDNA in any cDNA dilution (Figure 4.3). There was a trend towards a fatty acid × fructose interaction ($P=0.083$) in the first HepG2 cDNA dilution. However, as β -actin expression was significantly increased by fatty acids in both the PHH cDNA and the second HepG2 cDNA dilution (data not shown), it was decided that total cDNA would be better to use for normalisation. Using this method does not account for the small amount of variability generated by PCR amplification, but it does account for the variation generated during cDNA synthesis. It reflects the amount of total mRNA, rather than assuming that the β -actin mRNA represents the total mRNA.

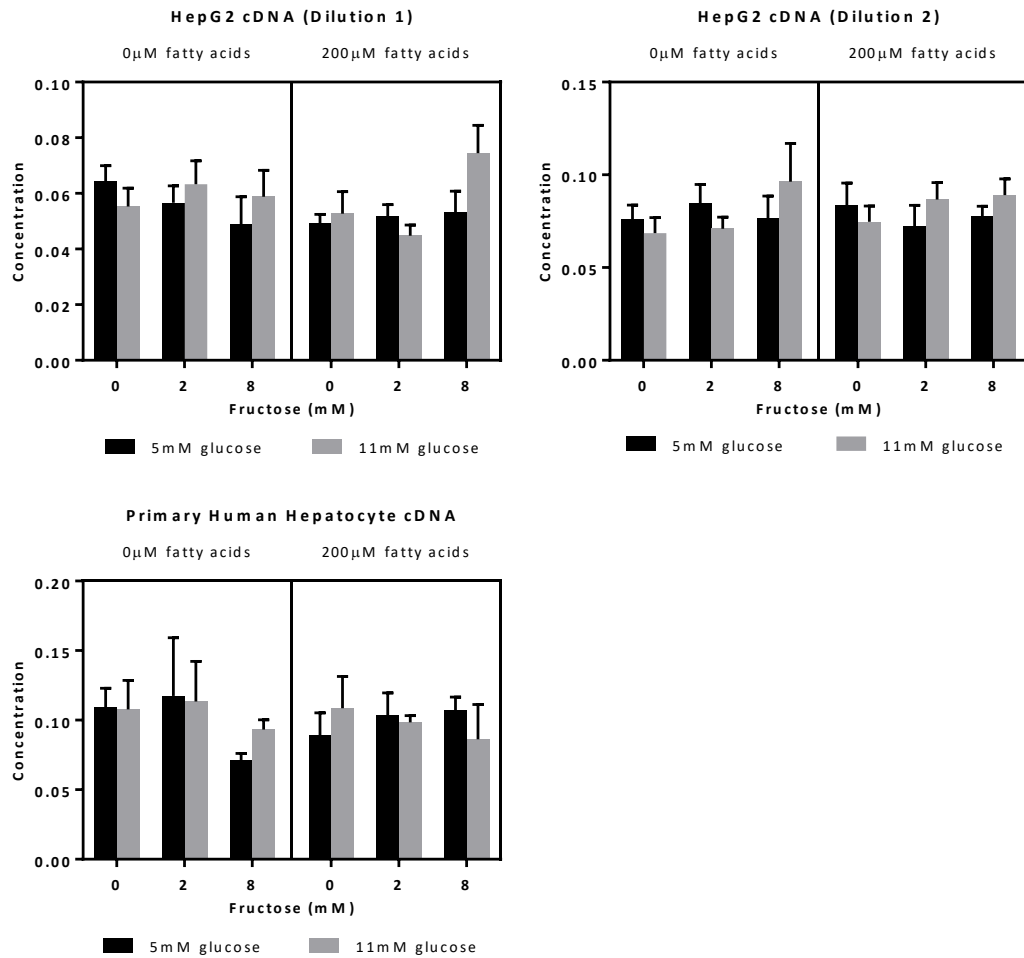


Figure 4.3: Total cDNA measured by OliGreen fluorescence in all 1 in 8 dilutions of cDNA. Means±SEM, HepG2 $n=5$, PHH $n=3$

4.3.1.2 Overview of results

Overall, there were a lot of fatty acid responsive genes in HepG2 cells which did not follow the same pattern in PHH. Glucose and fructose effects were more common in PHH; no genes responded to fructose treatment in HepG2 cells. Many of the effects in PHH were non-significant trends ($P<0.1$) rather than statistically significant effects. This could be because of the small number of replicates ($n=3$) in this cell type, or alternatively because they are not real effects.

It should be noted that lipid accumulation was measured in a plate of HepG2 cells alongside the plates used for mRNA extraction to confirm that the batch of cells displayed the same lipid accumulation pattern as those in Chapter 3. With the PHH from L329, the lipid accumulation plates presented in Chapter 3 were run alongside the plates used for mRNA extraction.

4.3.1.3 Lipogenic genes – *ACC1*, *SCD*, *FASN*, *SREBP1*

In HepG2 cells, *ACC1* expression was suppressed by fatty acid treatment ($P=0.029$) (Figure 4.4, Table 4.6) whereas in PHH, *ACC1* expression was reduced with high glucose ($P=0.021$) (Figure 4.4, Table 4.7).

FASN was also suppressed by fatty acids in HepG2 cells ($P<0.001$) (Figure 4.4, Table 4.6). In PHH, *FASN* showed a significant fatty acid \times fructose ($P=0.017$) interaction (Figure 4.4, Table 4.7), where the only significant difference was a decrease in expression between 0 μ M fatty acid + 8mM fructose and 200 μ M fatty acid + 8mM fructose (Bonferroni $P<0.05$, Table S19). There was also a glucose \times fructose ($P=0.048$) interaction but post-hoc Bonferroni tests were unable to identify the cause of the interaction (Table S20).

SCD was the third lipogenic enzyme to be suppressed by fatty acid treatment in HepG2 cells ($P<0.001$) (Figure 4.4, Table 4.6). In PHH, *SCD* showed a glucose \times fructose interaction ($P=0.037$) (Figure 4.4, Table 4.7) but Bonferroni comparisons did not elucidate any specific significant treatment differences (Table S21).

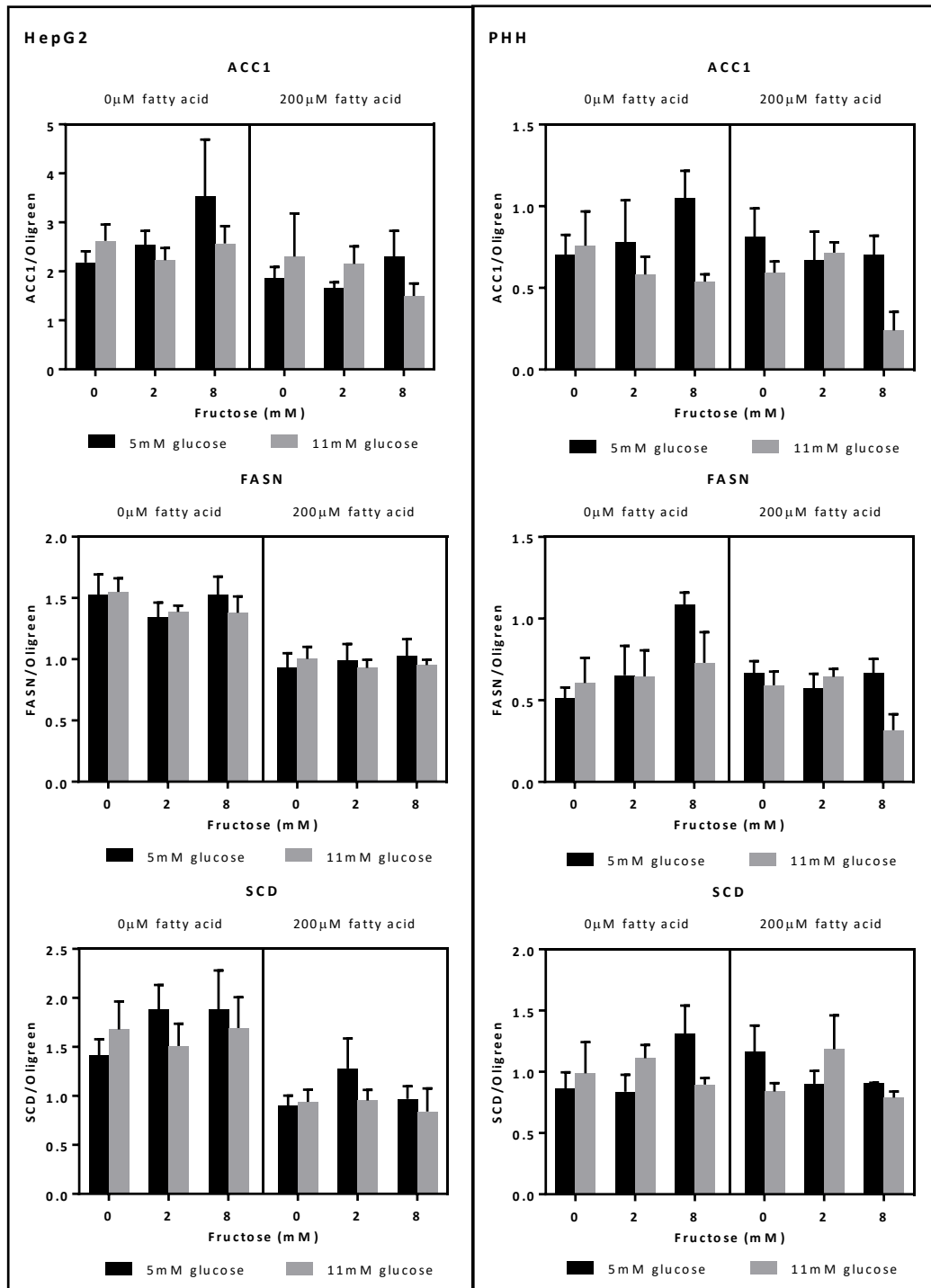


Figure 4.4: Effects of glucose, fructose and fatty acids on mRNA expression of acetyl-coA carboxylase (ACC1), fatty acid synthase (FASN) and stearoyl-coA desaturase (SCD) in HepG2 cells and PHH. Means±SEM, normalised to total cDNA (OliGreen). HepG2 $n=5$, PHH $n=3$

Table 4.6: Effects of glucose, fructose and fatty acids on lipogenic enzyme mRNA expression in HepG2 cells. Mean±SEM. Data analysed by three-way ANOVA with blocking for plate. $n=5$ wells per treatment. FA: fatty acid, G: glucose, F: fructose. $†P<0.1$, $*P<0.05$, $P<0.01$, $***P<0.001$**

HepG2	5mM G, 0 μ M FA			11mM G, 0 μ M FA			5mM G, 200 μ M FA			11mM G, 200 μ M FA			P-values from three-way ANOVA								
F (mM)	0	2	8	0	2	8	0	2	8	0	2	8	FA	G	F	FA \times G	FA \times F	G \times F	FA \times G \times F	PCR Efficiency	Average CP value
ACC1	2.181 ± 0.231	2.538 ± 0.289	3.529 ± 1.160	2.621 ± 0.335	2.226 ± 0.251	2.568 ± 0.354	1.865 ± 0.223	1.665 ± 0.114	2.307 ± 0.522	2.303 ± 0.878	2.154 ± 0.356	1.498 ± 0.254	*							2.213	26.5
FASN	1.524 ± 0.167	1.342 ± 0.121	1.528 ± 0.146	1.549 ± 0.113	1.385 ± 0.053	1.379 ± 0.133	0.927 ± 0.121	0.991 ± 0.133	1.025 ± 0.139	1.003 ± 0.099	0.930 ± 0.066	0.953 ± 0.042	***							1.992	22.2
SCD	1.416 ± 0.162	1.880 ± 0.253	1.881 ± 0.400	1.678 ± 0.286	1.510 ± 0.227	1.693 ± 0.314	0.901 ± 0.101	1.281 ± 0.306	0.970 ± 0.130	0.939 ± 0.124	0.952 ± 0.109	0.842 ± 0.235	***							1.964	22.0

Table 4.7: Effects of glucose, fructose and fatty acids on lipogenic enzyme mRNA expression in primary human hepatocytes. Mean±SEM. Data analysed by three-way ANOVA with blocking for plate. $n=3$ wells per treatment. FA: fatty acid, G: glucose, F: fructose. $†P<0.1$, $*P<0.05$, $P<0.01$, $***P<0.001$**

PHH	5mM G, 0 μ M FA			11mM G, 0 μ M FA			5mM G, 200 μ M FA			11mM G, 200 μ M FA			P-values from three-way ANOVA								
F (mM)	0	2	8	0	2	8	0	2	8	0	2	8	FA	G	F	FA \times G	FA \times F	G \times F	FA \times G \times F	PCR Efficiency	Average CP value
ACC1	0.702 ± 0.122	0.781 ± 0.256	1.050 ± 0.166	0.759 ± 0.210	0.582 ± 0.109	0.538 ± 0.046	0.813 ± 0.173	0.668 ± 0.176	0.702 ± 0.118	0.594 ± 0.068	0.715 ± 0.064	0.239 ± 0.113		*						1.888	31.3
FASN	0.511 ± 0.067	0.653 ± 0.180	1.087 ± 0.072	0.605 ± 0.155	0.646 ± 0.159	0.730 ± 0.187	0.668 ± 0.071	0.572 ± 0.090	0.666 ± 0.087	0.592 ± 0.083	0.643 ± 0.049	0.317 ± 0.097	†				*	*		1.922	26.1
SCD	0.860 ± 0.136	0.838 ± 0.138	1.313 ± 0.228	0.987 ± 0.255	1.110 ± 0.108	0.896 ± 0.054	1.162 ± 0.216	0.902 ± 0.106	0.905 ± 0.007	0.839 ± 0.068	1.184 ± 0.276	0.789 ± 0.051						*		1.804	26.1

In HepG2 cells, SREBP1a and SREBP1c were suppressed by fatty acid treatment ($P<0.001$ for both) (Figure 4.5, Table 4.8). In PHH, there was a reduction in SREBP1a expression only with fatty acid treatment ($P=0.024$) although there was a trend in SREBP1c ($P=0.064$) (Figure 4.5, Table 4.9). Of particular interest, and in contrast to HepG2 cells, there was a highly significant reduction in SREBP1c expression with fructose treatment ($P<0.001$) (Figure 4.5, Table 4.9) but only with 8mM fructose compared to 0mM and 2mM (Bonferroni $P<0.05$, Table 4.11). This effect was also evident in SREBP1a ($P=0.003$) (Figure 4.5, Table 4.9) with the same pattern shown after post-hoc testing (Table 4.10). There was also a glucose effect specific to this isoform, where glucose reduced expression ($P=0.018$) (Figure 4.5, Table 4.9).

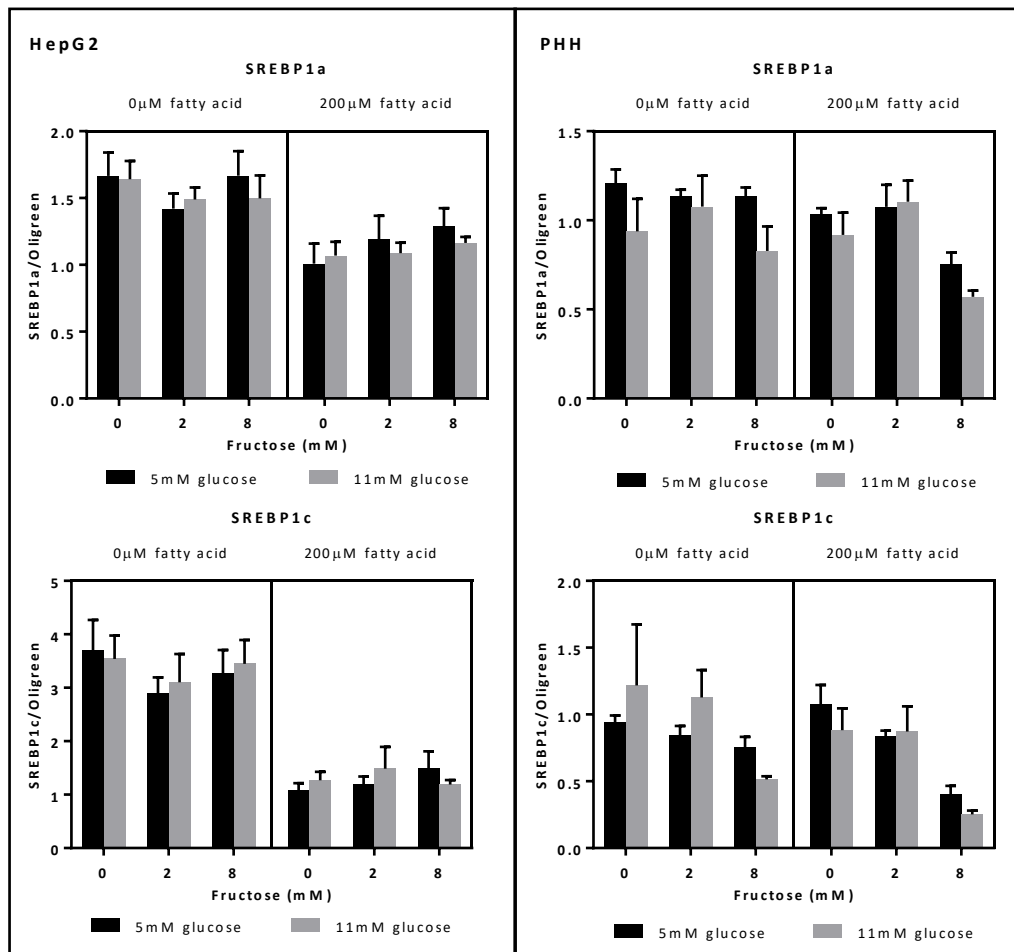


Figure 4.5: Effects of glucose, fructose and fatty acids on mRNA expression of sterol regulatory element binding protein 1a (SREBP1a) and SREBP1c in HepG2 cells and PHH. Means±SEM, normalised to total cDNA (OliGreen). HepG2 $n=5$, PHH $n=3$

Table 4.8: Effects of glucose, fructose and fatty acids on SREBP1 mRNA expression in HepG2 cells. Mean±SEM. Data analysed by three-way ANOVA with blocking for plate. n=5 wells per treatment. FA: fatty acid, G: glucose, F: fructose. †P<0.1, *P<0.05, **P<0.01, *P<0.001**

HepG2	5mM G, 0µM FA			11mM G, 0µM FA			5mM G, 200µM FA			11mM G, 200µM FA			P-values from three-way ANOVA								
F (mM)	0	2	8	0	2	8	0	2	8	0	2	8	FA	G	F	FA × G	FA × F	G × F	FA × G × F	PCR Efficiency	Average CP value
SREBP1a	1.666 ±0.175	1.420 ±0.114	1.667 ±0.183	1.642 ±0.137	1.489 ±0.091	1.498 ±0.172	1.009 ±0.149	1.193 ±0.174	1.291 ±0.133	1.070 ±0.103	1.087 ±0.079	1.164 ±0.046	***							1.998	27.0
SREBP1c	3.695 ±0.572	2.892 ±0.303	3.265 ±0.441	3.540 ±0.437	3.101 ±0.529	3.449 ±0.443	1.076 ±0.138	1.185 ±0.156	1.497 ±0.314	1.270 ±0.158	1.486 ±0.406	1.188 ±0.086	***							2.334	29.0

120

Table 4.9: Effects of glucose, fructose and fatty acids on SREBP1 mRNA expression in primary human hepatocytes. Mean±SEM. Data analysed by three-way ANOVA with blocking for plate. n=3 wells per treatment. FA: fatty acid, G: glucose, F: fructose. †P<0.1, *P<0.05, **P<0.01, *P<0.001**

PHH	5mM G, 0µM FA			11mM G, 0µM FA			5mM G, 200µM FA			11mM G, 200µM FA			P-values from three-way ANOVA								
F (mM)	0	2	8	0	2	8	0	2	8	0	2	8	FA	G	F	FA × G	FA × F	G × F	FA × G × F	PCR Efficiency	Average CP value
SREBP1a	1.210 ±0.075	1.133 ±0.039	1.135 ±0.049	0.938 ±0.183	1.077 ±0.173	0.828 ±0.138	1.036 ±0.032	1.075 ±0.124	0.755 ±0.064	0.919 ±0.124	1.104 ±0.119	0.570 ±0.035	*	*	**					1.949	29.8
SREBP1c	0.941 ±0.052	0.846 ±0.068	0.752 ±0.080	1.218 ±0.457	1.128 ±0.204	0.515 ±0.023	1.077 ±0.145	0.837 ±0.042	0.404 ±0.061	0.882 ±0.164	0.873 ±0.188	0.252 ±0.029	†		***					1.992	31.7

Table 4.10: Fructose effect on SREBP1a mRNA expression in primary human hepatocytes: Bonferroni multiple comparisons			
Fructose (mM)	Mean	Bonferroni	s.e.d
0	1.0257	b	0.0727
2	1.0976	b	
8	0.8223	a	

Table 4.11: Fructose effect on SREBP1c mRNA expression in primary human hepatocytes: Bonferroni multiple comparisons			
Fructose (mM)	Mean	Bonferroni	s.e.d
0	1.0294	b	0.1125
2	0.9208	b	
8	0.4807	a	

4.3.1.4 Lipid metabolism related genes – PNPLA3, DGAT1, CPT1 α , ApoB, PPARGC1 α

PNPLA3 was another enzyme that had decreased mRNA expression with fatty acid treatment in HepG2 cells ($P < 0.001$) (Figure 4.6, Table 4.12), whereas there were no effects of any of the treatments on the expression of this enzyme in PHH (Figure 4.6, Table 4.13).

DGAT1 mRNA expression was unaffected by treatment in HepG2 cells (Figure 4.6, Table 4.12). In PHH there were also no statistically significant effects, although there were trends for effects of fatty acids ($P = 0.057$), glucose \times fructose ($P = 0.055$) and a 3-way interaction ($P = 0.093$) (Figure 4.6, Table 4.13). Although not significant, there was a numerical increase in expression between 5mM and 11mM glucose at 0mM fructose in the absence of fatty acids, but in the presence of fatty acids there was a decrease between these two groups. At 2mM fructose there was always an increase in expression

between 5mM and 11mM glucose, and a reduction at 8mM glucose. Expression was trending higher with fatty acids (Figure 4.6).

CPT1 α mRNA expression was increased with fatty acid treatment in both HepG2 cells and PHH ($P < 0.001$) (Figure 4.6, Tables 4.12 and 4.13). This was one of the only consistent effects across the two cell types. There were also some trends in PHH for an effect of glucose ($P = 0.096$), fructose ($P = 0.071$) and a glucose \times fructose interaction ($P = 0.057$) on CPT1 α expression (Figure 4.6, Table 4.13). Looking at the glucose \times fructose interaction, the data suggested the largest reduction in expression between 5mM glucose + 0mM fructose and 11mM glucose + 8mM fructose (Figure 4.6).

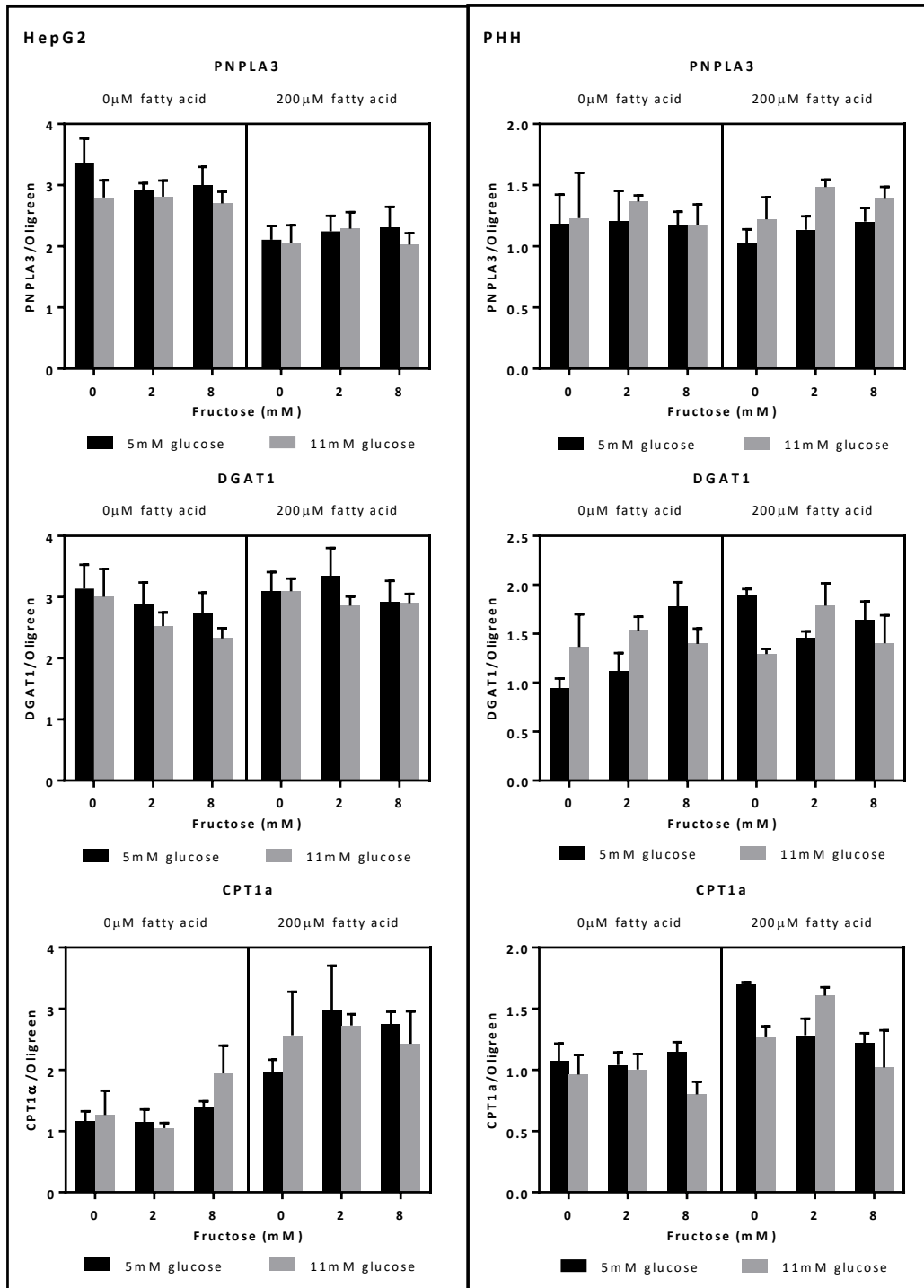


Figure 4.6: Effects of glucose, fructose and fatty acids on mRNA expression of patatin-like phospholipase domain-containing protein 3 (PNPLA3), diacylglycerol acyltransferase 1 (DGAT1) and carnitine palmitoyltransferase 1a (CPT1 α) in HepG2 cells and PHH. Means \pm SEM, normalised to total cDNA (OliGreen). HepG2 $n=5$, PHH $n=3$

Table 4.12: Effects of glucose, fructose and fatty acids on PNPLA3, DGAT1 and CPT1 α mRNA expression in HepG2 cells. Mean \pm SEM. Data analysed by three-way ANOVA with blocking for plate. $n=5$ wells per treatment. FA: fatty acid, G: glucose, F: fructose. $1P<0.1$, $*P<0.05$, $P<0.01$, $***P<0.001$**

HepG2	5mM G, 0 μ M FA			11mM G, 0 μ M FA			5mM G, 200 μ M FA			11mM G, 200 μ M FA			P-values from three-way ANOVA								
F (mM)	0	2	8	0	2	8	0	2	8	0	2	8	FA	G	F	FA \times G	FA \times F	G \times F	FA \times G \times F	PCR Efficiency	Average CP value
PNPLA3	3.365 ± 0.397	2.906 ± 0.125	2.999 ± 0.301	2.799 ± 0.281	2.810 ± 0.265	2.702 ± 0.190	2.108 ± 0.224	2.246 ± 0.253	2.305 ± 0.342	2.054 ± 0.289	2.287 ± 0.272	2.027 ± 0.189	***							2.018	26.4
DGAT1	3.140 ± 0.389	2.886 ± 0.351	2.728 ± 0.345	3.007 ± 0.453	2.526 ± 0.222	2.326 ± 0.165	3.096 ± 0.312	3.345 ± 0.456	2.919 ± 0.347	3.096 ± 0.206	2.859 ± 0.149	2.903 ± 0.148								1.900	25.6
CPT1 α	1.164 ± 0.160	1.149 ± 0.206	1.398 ± 0.091	1.266 ± 0.396	1.051 ± 0.082	1.946 ± 0.453	1.957 ± 0.210	2.984 ± 0.720	2.746 ± 0.207	2.568 ± 0.710	2.729 ± 0.183	2.429 ± 0.530	***							2.004	28.4

Table 4.13: Effects of glucose, fructose and fatty acids on PNPLA3, DGAT1 and CPT1 α mRNA expression in primary human hepatocytes. Mean \pm SEM. Data analysed by three-way ANOVA with blocking for plate. $n=3$ wells per treatment. FA: fatty acid, G: glucose, F: fructose. $1P<0.1$, $*P<0.05$, $P<0.01$, $***P<0.001$**

PHH	5mM G, 0 μ M FA			11mM G, 0 μ M FA			5mM G, 200 μ M FA			11mM G, 200 μ M FA			P-values from three-way ANOVA								
F (mM)	0	2	8	0	2	8	0	2	8	0	2	8	FA	G	F	FA \times G	FA \times F	G \times F	FA \times G \times F	PCR Efficiency	Average CP value
PNPLA3	1.181 ± 0.242	1.207 ± 0.247	1.172 ± 0.111	1.230 ± 0.370	1.365 ± 0.051	1.176 ± 0.166	1.031 ± 0.109	1.136 ± 0.109	1.203 ± 0.109	1.221 ± 0.180	1.483 ± 0.061	1.388 ± 0.097								2.088	28.0
DGAT1	0.945 ± 0.098	1.121 ± 0.183	1.780 ± 0.246	1.365 ± 0.334	1.534 ± 0.140	1.396 ± 0.156	1.899 ± 0.059	1.456 ± 0.069	1.638 ± 0.192	1.292 ± 0.054	1.787 ± 0.229	1.403 ± 0.286	†					†	†	1.856	31.1
CPT1 α	1.074 ± 0.141	1.041 ± 0.103	1.146 ± 0.081	0.963 ± 0.160	1.005 ± 0.126	0.801 ± 0.103	1.705 ± 0.012	1.285 ± 0.134	1.218 ± 0.082	1.273 ± 0.085	1.608 ± 0.067	1.021 ± 0.303	***	†	†			†		1.969	28.2

In HepG2 cells, there was a significant glucose × fructose interaction on the expression of ApoB ($P=0.036$) (Figure 4.7, Table 4.14) but there were no specific treatment differences (Bonferroni $P>0.05$, Table S22). There were trends towards effects of fatty acids ($P=0.085$) and a fatty acid × fructose interaction ($P=0.083$), suggesting an increase in expression with increasing fructose only in the absence of fatty acids (Figure 4.7). In PHH, there was also a glucose × fructose interaction ($P=0.034$) and there was a trend towards an increase in expression with fatty acid treatment ($P=0.059$) (Figure 4.7, Table 4.15). Again, post-hoc tests of the glucose × fructose interaction did not find any significant differences between specific treatments (Bonferroni $P>0.05$, Table S23). PPARGC1 α was unaffected by treatment in both cell types (Figure 4.7, Tables 4.14 and 4.15).

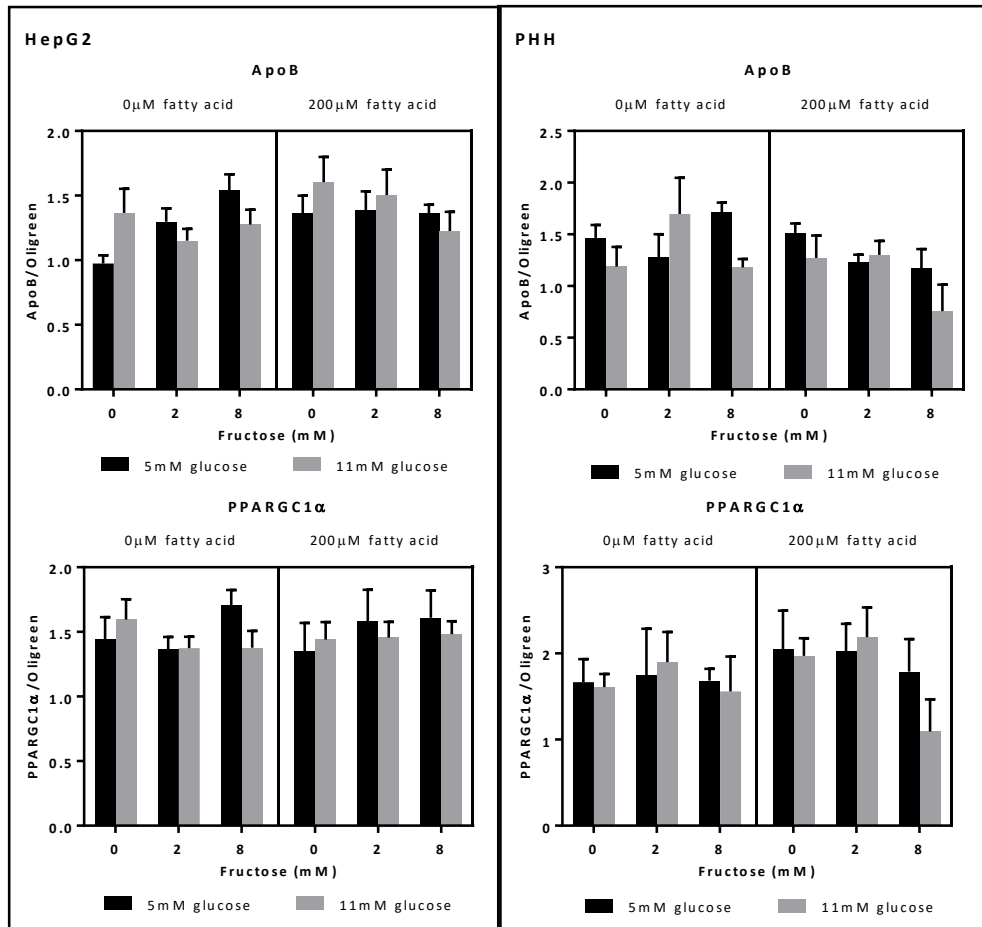


Figure 4.7: Effects of glucose, fructose and fatty acids on mRNA expression of apolipoprotein B (ApoB) and peroxisome proliferator-activated receptor gamma coactivator 1-alpha (PPARGC1α) in HepG2 cells and PHH. Means±SEM, normalised to total cDNA (OliGreen). HepG2 n=5, PHH n=3

Table 4.14: Effects of glucose, fructose and fatty acids on PPARGC1 α and ApoB mRNA expression in HepG2 cells. Mean \pm SEM. Data analysed by three-way ANOVA with blocking for plate. $n=5$ wells per treatment. FA: fatty acid, G: glucose, F: fructose. $\dagger P<0.1$, $*P<0.05$, $P<0.01$, $***P<0.001$**

HepG2	5mM G, 0 μ M FA			11mM G, 0 μ M FA			5mM G, 200 μ M FA			11mM G, 200 μ M FA			P-values from three-way ANOVA								
F (mM)	0	2	8	0	2	8	0	2	8	0	2	8	FA	G	F	FA \times G	FA \times F	G \times F	FA \times G \times F	PCR Efficiency	Average CP value
ApoB	0.974 ± 0.064	1.297 ± 0.104	1.540 ± 0.125	1.367 ± 0.187	1.151 ± 0.092	1.275 ± 0.115	1.364 ± 0.136	1.387 ± 0.145	1.363 ± 0.066	1.605 ± 0.194	1.504 ± 0.196	1.225 ± 0.148	\dagger				\dagger	*		2.069	21.6
PPARGC1 α	1.441 ± 0.173	1.365 ± 0.096	1.708 ± 0.116	1.596 ± 0.157	1.374 ± 0.089	1.378 ± 0.129	1.350 ± 0.220	1.580 ± 0.246	1.608 ± 0.213	1.442 ± 0.134	1.455 ± 0.123	1.482 ± 0.100								2.062	26.7

Table 4.15: Effects of glucose, fructose and fatty acids on PPARGC1 α and ApoB mRNA expression in primary human hepatocytes. Mean \pm SEM. Data analysed by three-way ANOVA with blocking for plate. $n=3$ wells per treatment. FA: fatty acid, G: glucose, F: fructose. $\dagger P<0.1$, $*P<0.05$, $P<0.01$, $***P<0.001$**

PHH	5mM G, 0 μ M FA			11mM G, 0 μ M FA			5mM G, 200 μ M FA			11mM G, 200 μ M FA			P-values from three-way ANOVA								
F (mM)	0	2	8	0	2	8	0	2	8	0	2	8	FA	G	F	FA \times G	FA \times F	G \times F	FA \times G \times F	PCR Efficiency	Average CP value
ApoB	1.465 ± 0.126	1.279 ± 0.221	1.713 ± 0.095	1.188 ± 0.190	1.697 ± 0.349	1.181 ± 0.081	1.514 ± 0.091	1.226 ± 0.076	1.170 ± 0.187	1.272 ± 0.218	1.300 ± 0.136	0.757 ± 0.256	\dagger					*		2.021	25.1
PPARGC1 α	1.667 ± 0.267	1.744 ± 0.543	1.683 ± 0.138	1.609 ± 0.152	1.900 ± 0.349	1.560 ± 0.405	2.051 ± 0.446	2.030 ± 0.315	1.788 ± 0.380	1.971 ± 0.205	2.188 ± 0.345	1.094 ± 0.372								1.971	31.2

4.3.1.5 Carbohydrate metabolism related genes – ChREBP, LPK, GLUT2, HK2

ChREBP mRNA expression was not significantly affected by treatment in HepG2 cells although there were trends towards an effect of glucose ($P=0.080$) and a fatty acid \times fructose interaction ($P=0.099$) (Figure 4.8, Table 4.16). These trends suggested an increase in ChREBP expression with high glucose, and an increase with fructose only in the absence of fatty acids (Figure 4.8). In PHH, there was a significant glucose \times fructose interaction ($P=0.016$) (Figure 4.8, Table 4.17). Post-hoc tests of this interaction showed that the only significant increase was between 0mM and 8mM fructose at 5mM glucose (Table S24).

LPK was not affected by treatment in HepG2 cells (Figure 4.8, Table 4.16) but behaved differently in PHH; expression was increased with fatty acid treatment ($P=0.004$) and affected by fructose treatment ($P=0.040$) (Figure 4.8, Table 4.17). Bonferroni comparisons showed that there was a significant reduction between 2mM and 8mM fructose, but 0mM was not different from either (Table S25). There were trends towards fatty acid \times fructose ($P=0.051$) and glucose \times fructose ($P=0.061$) interactions, suggesting a decrease with fructose only in the presence of fatty acids and larger expression changes with fructose at 11mM glucose (Figure 4.8).

GLUT2 expression was not affected by treatment in HepG2 cells (Figure 4.8, Table 4.16) but was reduced by both glucose ($P=0.039$) and fructose ($P=0.010$) in PHH (Figure 4.8, Table 4.17). Bonferroni comparisons of the fructose effect found that the reduction was only significant between 0mM and 8mM (Table S26).

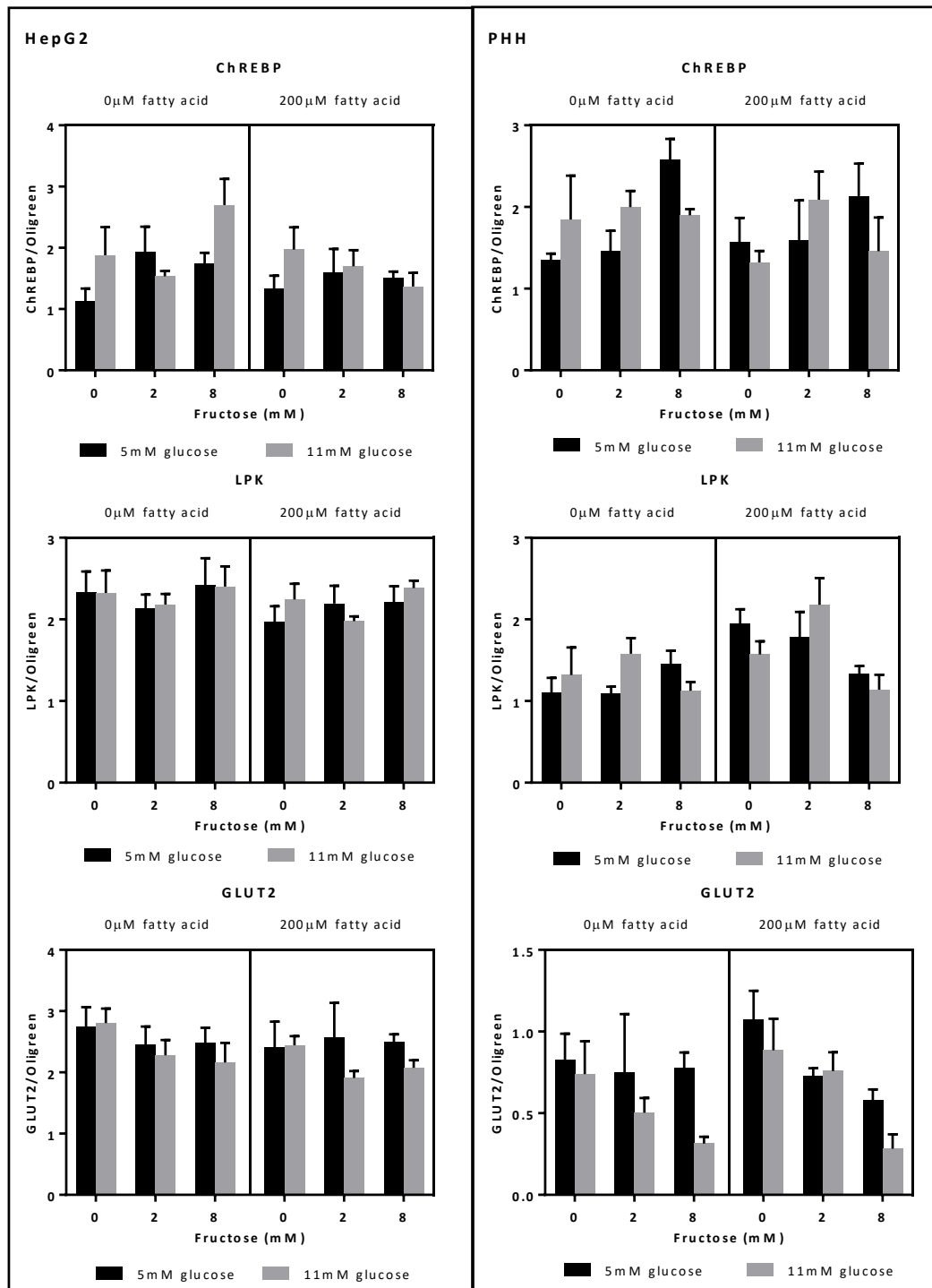


Figure 4.8: Effects of glucose, fructose and fatty acids on mRNA expression of carbohydrate response element binding protein (ChREBP), liver pyruvate kinase (LPK) and glucose transporter 2 (GLUT2) in HepG2 cells and PHH. Means±SEM, normalised to total cDNA (OliGreen). HepG2 $n=5$, PHH $n=3$

Table 4.16: Effects of glucose, fructose and fatty acids on carbohydrate metabolism related mRNA expression in HepG2 cells. Mean±SEM. Data analysed by three-way ANOVA with blocking for plate. $n=5$ wells per treatment. FA: fatty acid, G: glucose, F: fructose. † $P<0.1$, * $P<0.05$, ** $P<0.01$, * $P<0.001$**

HepG2	5mM G, 0 μ M FA			11mM G, 0 μ M FA			5mM G, 200 μ M FA			11mM G, 200 μ M FA			P-values from three-way ANOVA						PCR Efficiency	Average CP value	
F (mM)	0	2	8	0	2	8	0	2	8	0	2	8	FA	G	F	FA \times G	FA \times F	G \times F	FA \times G \times F		
ChREBP	1.132 ±0.201	1.932 ±0.415	1.743 ±0.177	1.879 ±0.458	1.537 ±0.086	2.697 ±0.429	1.327 ±0.218	1.596 ±0.386	1.511 ±0.101	1.973 ±0.364	1.697 ±0.264	1.370 ±0.222		†			†			1.908	28.5
LPK	2.330 ±0.256	2.132 ±0.171	2.417 ±0.332	2.324 ±0.276	2.181 ±0.130	2.401 ±0.249	1.969 ±0.193	2.194 ±0.218	2.211 ±0.194	2.243 ±0.194	1.978 ±0.057	2.383 ±0.092								1.961	27.2
GLUT2	2.748 ±0.317	2.453 ±0.294	2.485 ±0.244	2.806 ±0.234	2.277 ±0.251	2.163 ±0.318	2.408 ±0.420	2.564 ±0.571	2.500 ±0.123	2.441 ±0.151	1.907 ±0.113	2.075 ±0.122								2.007	27.7
HK2	2.341 ±0.127	1.990 ±0.137	2.435 ±0.149	2.686 ±0.527	1.964 ±0.242	2.007 ±0.090	2.088 ±0.292	2.567 ±0.387	2.167 ±0.410	2.030 ±0.261	2.451 ±0.494	2.106 ±0.169					†			1.772	33.7

Table 4.17: Effects of glucose, fructose and fatty acids on carbohydrate metabolism related mRNA expression in primary human hepatocytes. Mean±SEM. Data analysed by three-way ANOVA with blocking for plate. $n=3$ wells per treatment. FA: fatty acid, G: glucose, F: fructose. † $P<0.1$, * $P<0.05$, ** $P<0.01$, * $P<0.001$**

PHH	5mM G, 0 μ M FA			11mM G, 0 μ M FA			5mM G, 200 μ M FA			11mM G, 200 μ M FA			P-values from three-way ANOVA						PCR Efficiency	Average CP value	
F (mM)	0	2	8	0	2	8	0	2	8	0	2	8	FA	G	F	FA \times G	FA \times F	G \times F	FA \times G \times F		
ChREBP	1.353 ±0.076	1.465 ±0.245	2.575 ±0.257	1.845 ±0.539	1.998 ±0.200	1.899 ±0.074	1.571 ±0.296	1.596 ±0.485	2.133 ±0.398	1.320 ±0.140	2.090 ±0.343	1.459 ±0.412			†			*		1.832	31.5
LPK	1.106 ±0.179	1.091 ±0.084	1.455 ±0.163	1.319 ±0.337	1.578 ±0.193	1.127 ±0.107	1.948 ±0.177	1.783 ±0.308	1.333 ±0.096	1.571 ±0.159	2.178 ±0.328	1.138 ±0.182	**		*		†	†		1.990	28.8
GLUT2	0.825 ±0.162	0.750 ±0.357	0.775 ±0.097	0.740 ±0.201	0.503 ±0.090	0.314 ±0.041	1.073 ±0.176	0.729 ±0.047	0.579 ±0.067	0.886 ±0.193	0.758 ±0.114	0.284 ±0.087		*	**					1.996	29.9

HK2 was not affected by treatment in HepG2 cells, although there was a trend towards a fatty acid × fructose interaction ($P=0.070$) (Figure 4.9, Table 4.16). The interaction suggested a decreased in expression between 0mM and 2mM fructose without fatty acids, but an increase between these two groups with fatty acids (Figure 4.9). This gene was not measured in PHH as the expression was too low to be detected.

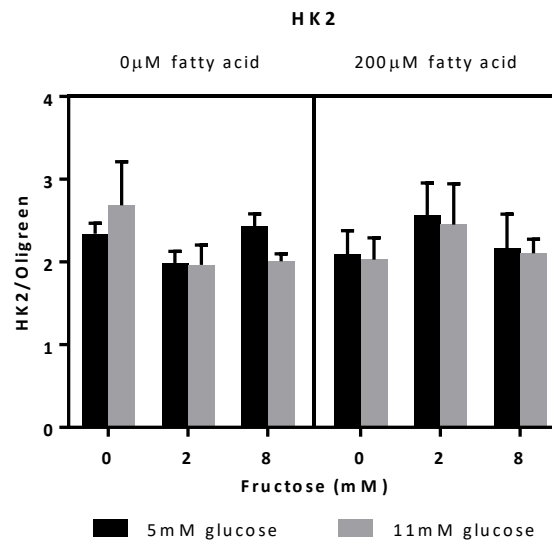


Figure 4.9: Effects of glucose, fructose and fatty acids on mRNA expression of hexokinase 2 (HK2) in HepG2 cells. Means±SEM, normalised to total cDNA (OliGreen). $n=5$

4.3.1.6 Comparative expression levels

A standard curve using cDNA from each cell type was measured on the same RT-qPCR plate in order to determine in which cell type each gene was more highly expressed. The standard curves were produced using serial dilutions of cDNA pools, meaning that they are an average of all treatments for each cell type.

Most of the genes measured were more highly expressed in HepG2 cells (Figures 4.10 and 4.11). The exceptions were β -actin and GLUT2, where the standard curves were not significantly different, and total SREBP1 and LPK where the slopes were too different to

analyse the intercepts (Figure 4.11). In contrast, the average CP values of GLUT2 suggested higher expression in HepG2 cells (Tables 4.16 and 4.17), likely because GLUT2 expression was reduced in some treatments in PHH (Figure 4.8). ApoB and CPT1 α were the only genes to be more highly expressed in PHH when looking at the standard curves (Figures 4.10 and 4.11), but the average CP values for CPT1 α only differed by 0.2 (Tables 4.12 and 4.13).

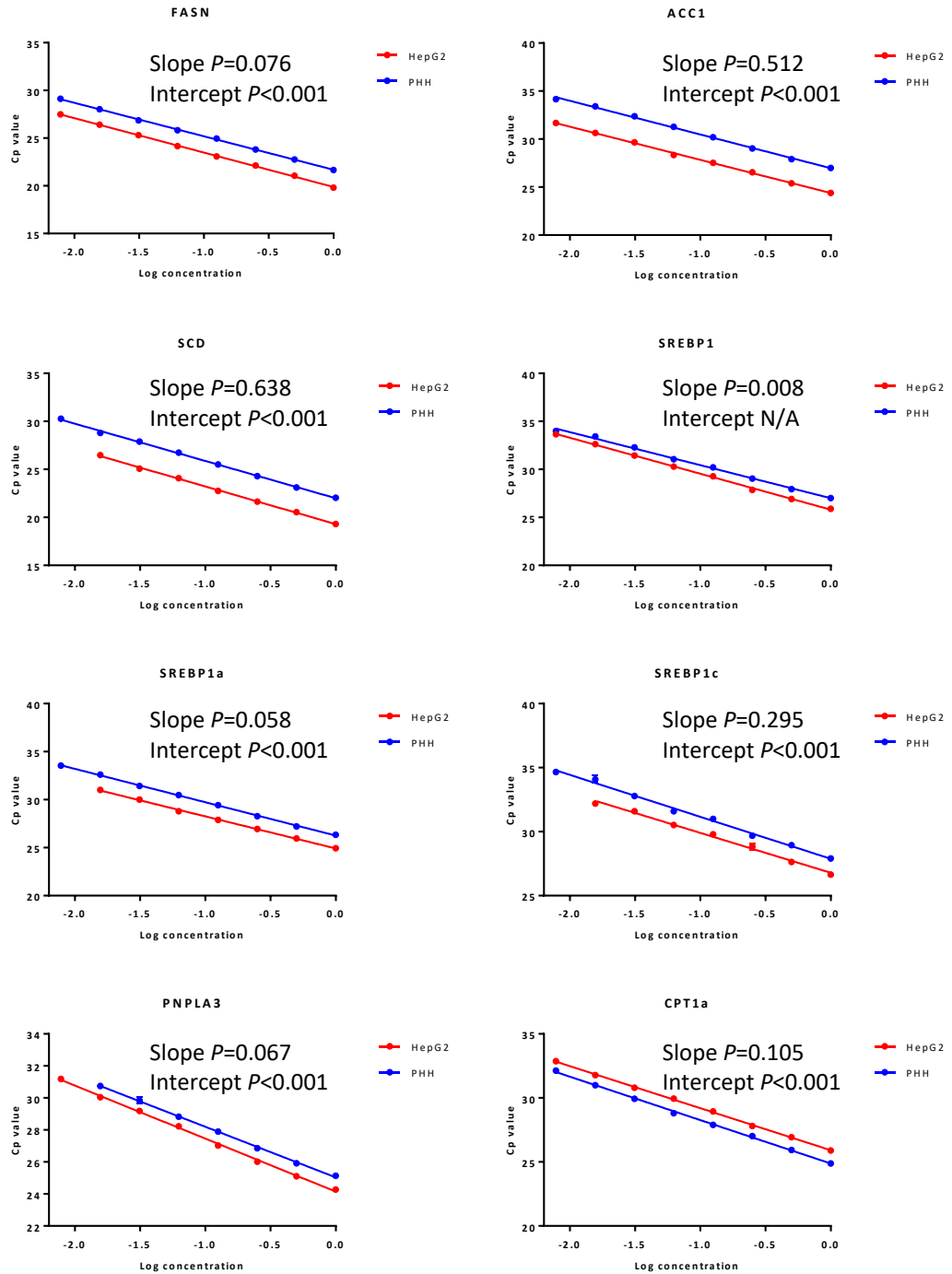


Figure 4.10: Standard curves from a serial dilution of cDNA pools from HepG2 cells and primary human hepatocytes (L329). Using cDNA pools means that these values are averages of all treatments. Slopes and intercepts compared using linear regression.

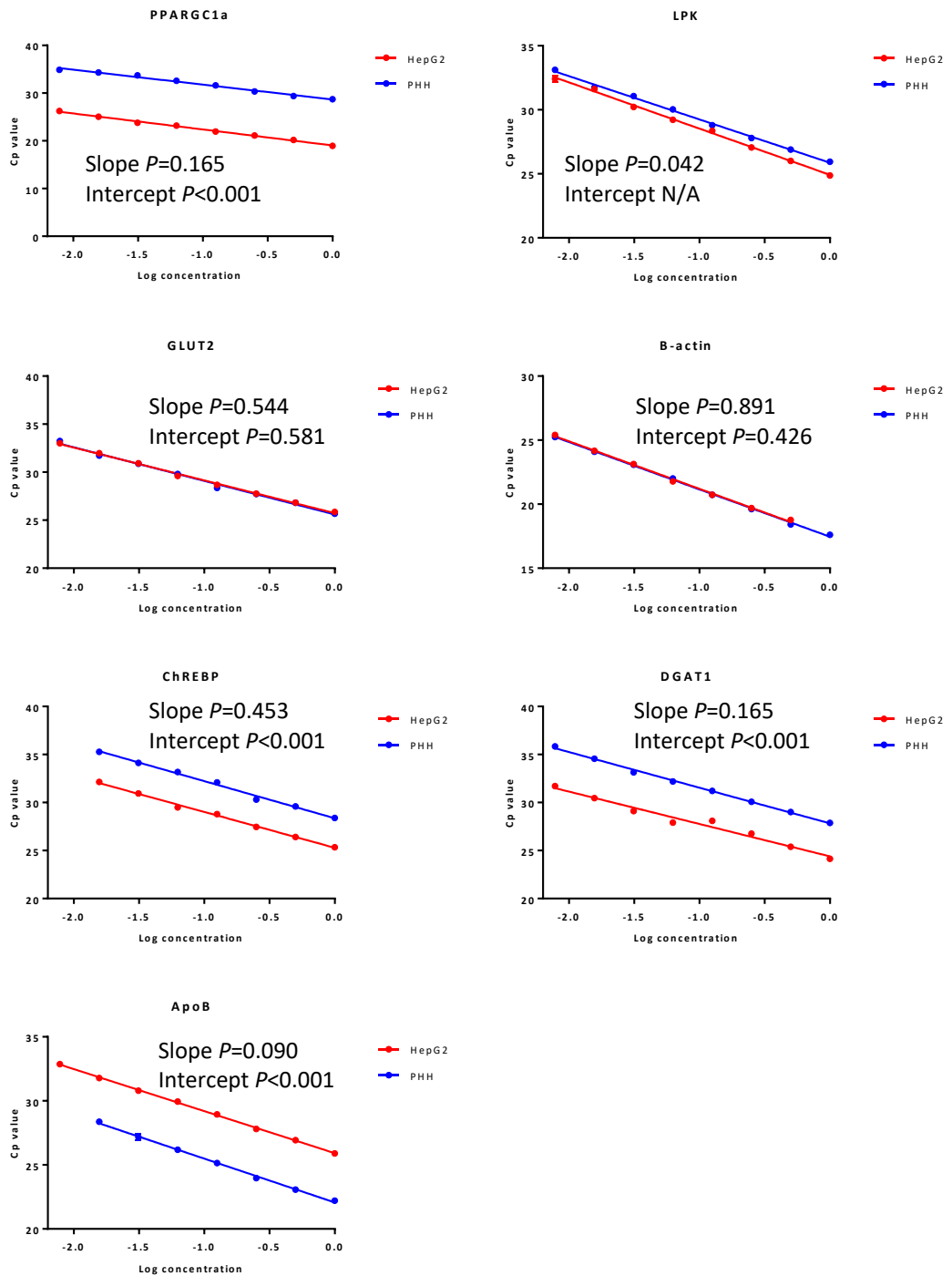


Figure 4.11: Standard curves from a serial dilution of cDNA pools from HepG2 cells and primary human hepatocytes (L329). Using cDNA pools means that these values are averages of all treatments. Slopes and intercepts compared using linear regression.

4.3.1.7 Correlations

Correlation matrices for both cell types were composed to determine where there could be co-regulation and interactions between the genes, and whether these differ between the cell types. Significant correlations are highlighted in Table 4.18. The strongest correlation in HepG2 cells was between SREBP1c and FASN ($R=0.93$) whereas in PHH it was between FASN and ACC1 ($R=0.788$). In general the Pearson's R values were less robust for PHH, possibly due to having a smaller sample size ($n=3$ rather than $n=5$ in HepG2 cells). Of particular interest, there were significant negative correlations between CPT1 α and SREBP1c, as well as FASN and PNPLA3 in HepG2 cells but these negative correlations were not present in PHH. In fact, there were no negative correlations in the PHH data (Table 4.18)

Table 4.18: Correlation matrix of mRNA expressions in HepG2 cells (bottom left) and PHH (top right). R values from Pearson's correlation tests. Green $P < 0.05$, Orange $P < 0.1$. HK2 not measured in PHH. NS: not significant

PHH \ HepG2	SREBP1a	SREBP1c	SCD	ACC1	FASN	PNPLA3	DGAT1	PPARGC1 α	CPT1 α	ApoB	ChREBP	LPK	HK2	GLUT2
SREBP1a		0.678	0.380	0.426	0.289	NS	NS	NS	NS	0.445	0.357	0.473		0.391
SREBP1c	0.731		0.478	0.451	0.306	NS	NS	NS	NS	0.483	NS	0.460		0.510
SCD	0.390	0.463		0.496	0.513	NS	0.658	0.280	0.426	0.346	0.613	0.497		0.416
ACC1	NS	0.225	NS		0.788	NS	0.377	0.592	0.376	0.514	0.288	NS		0.712
FASN	0.930	0.794	0.470	NS		NS	0.355	0.330	NS	0.586	0.517	NS		0.488
PNPLA3	0.761	0.703	0.355	NS	0.700		0.285	0.371	NS	NS	NS	NS		NS
DGAT1	0.448	NS	NS	NS	0.382	NS		0.354	0.597	0.286	0.619	0.693		NS
PPARGC1 α	0.667	0.245	NS	NS	0.553	0.479	0.668		0.485	0.332				0.593
CPT1 α	-0.237	-0.433	NS	NS	-0.310	-0.281	NS	NS		0.326	0.295	0.660		0.554
ApoB	NS	NS	NS	0.238	NS	NS	NS	NS	0.425		0.340	0.300		0.349
ChREBP	NS	NS	0.269	0.399	NS	NS	NS	NS	0.331	0.295		0.462		NS
LPK	0.713	0.299	NS	NS	0.663	0.268	0.664	0.604	NS	NS	NS			NS
HK2	0.318	0.058	NS	NS	0.275	NS	0.335	0.519	NS	NS	NS	0.262		
GLUT2	0.644	0.249	NS	NS	0.536	0.403	0.665	0.676	NS	NS	NS	0.552	0.290	

4.3.2 Non-targeted gene expression analysis by microarray

4.3.2.1 Comparisons between HepG2 and PHH

A total of 21448 genes were measured in the microarrays. Principle component analysis (PCA) plots were produced to visualise the variability in the data set. The principle components are new variables created by a mathematical algorithm which reduces the dimensionality of a data set with a large number of variables (Ringner, 2008). These principle components account for the vast majority of the variability within the original variables, but are themselves independent and uncorrelated (Raychaudhuri et al., 2000). The first principle component, PC #1, accounts for the most variability and so on. Replicates of the same treatment would be expected to cluster together, and different treatments would be expected to cluster apart from one another if there are treatment effects. The PCA plots showed good separation of the data for comparison across cell types (Figures 4.12 and 4.13), suggesting large effects of cell type on gene expression.

Out of all the genes measured, 931 were significantly different ($P < 0.01$ with FDR correction) between the HepG2 and PHH controls (CON, Table 4.5) with a fold change outside -2 and 2 . When comparing FA treated HepG2 and PHH, 653 genes were significantly different. Out of these, 370 were also found in the CON comparison.

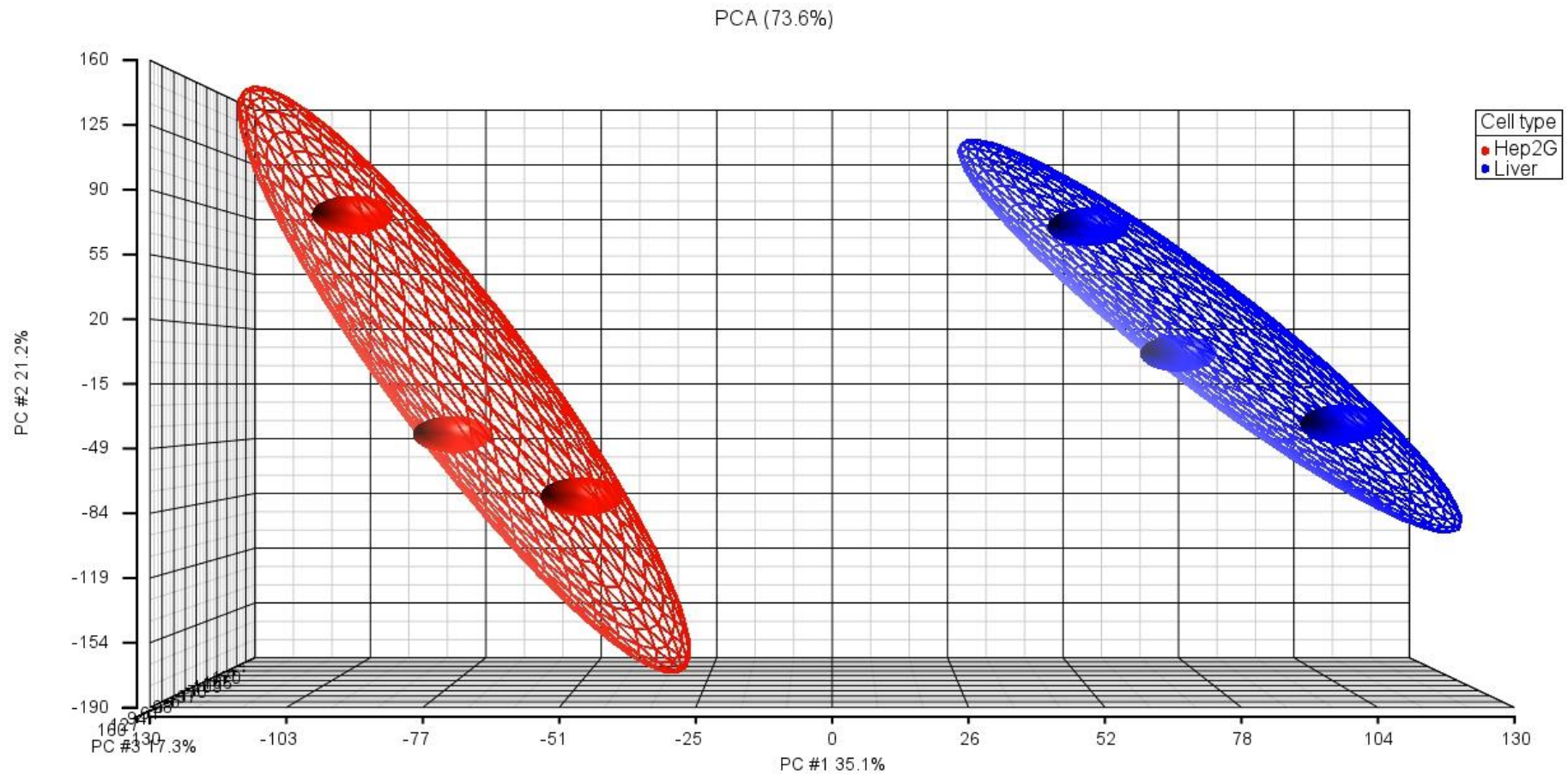


Figure 4.12: Principle component analysis (PCA) plot of gene expression data from HepG2 (red) and PHH (liver – blue) controls (0 μ M fatty acids+5mM glucose+0mM fructose). See text for explanation of PCA.

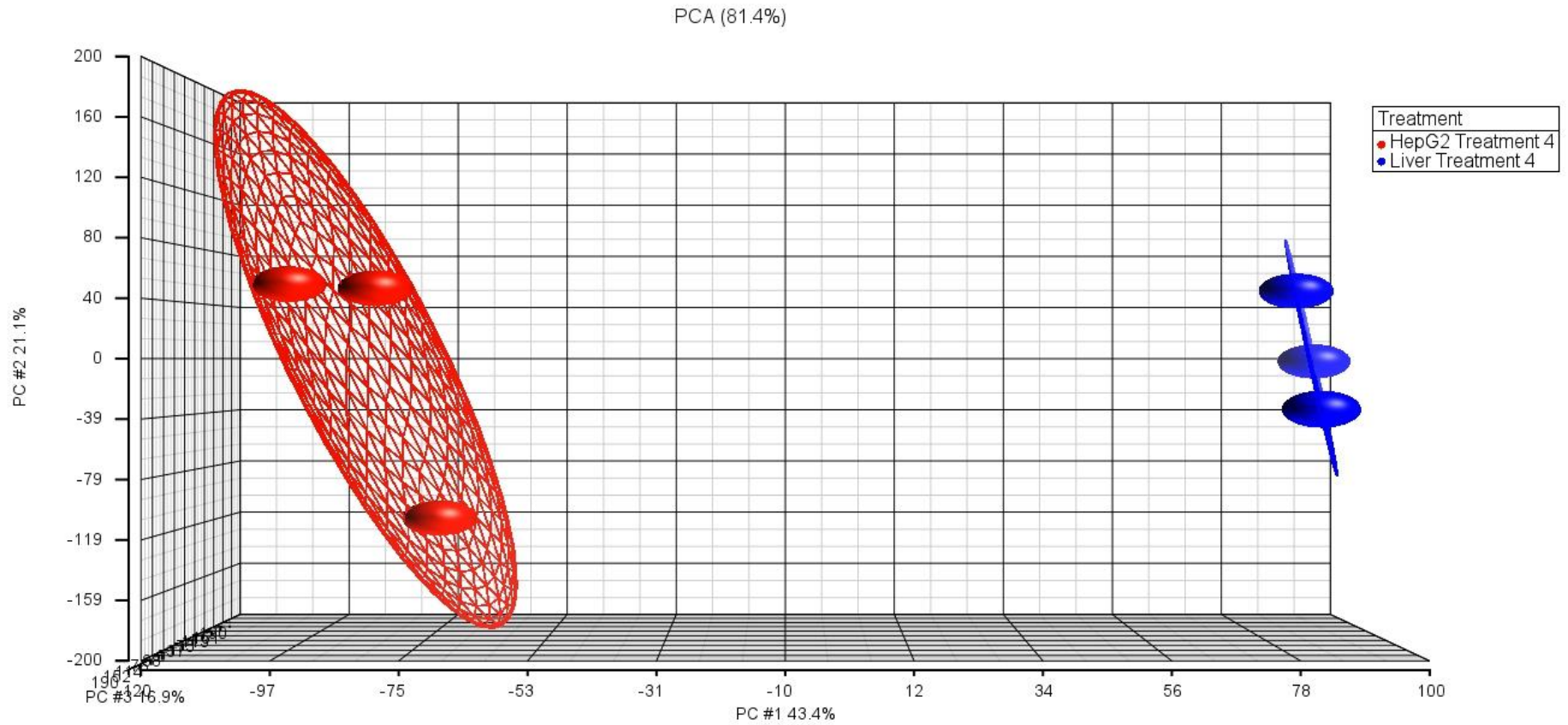


Figure 4.13: Principle component analysis (PCA) plot of gene expression data from HepG2 (red) and PHH (liver – blue) samples treated with 200 μ M fatty acids+5mM glucose+0mM fructose. See text for explanation of PCA.

The largest fold changes in the CON comparison are shown in Figure 4.14. The most decreased gene in PHH was alpha-fetoprotein (AFP, FC=-222.9, $P<0.001$), and the most increased gene in PHH was aldolase B (ALDOB, FC=183.4, $P<0.001$). This would be expected as HepG2 cells have a foetal phenotype and aldolase A is the more dominant isoform in HepG2 cells compared to hepatocytes (Wisniewski et al., 2016).

In the FA comparison, PPARGC1 α was significantly lower in PHH compared to HepG2 (FC=-6.95, $P<0.001$) but not in the CON comparison. Conversely, acyl-CoA synthetase long-chain family member 1 (ACSL) was elevated in PHH compared to HepG2 in the FA comparison but not the CON comparison (FC=2.91, $P<0.001$).

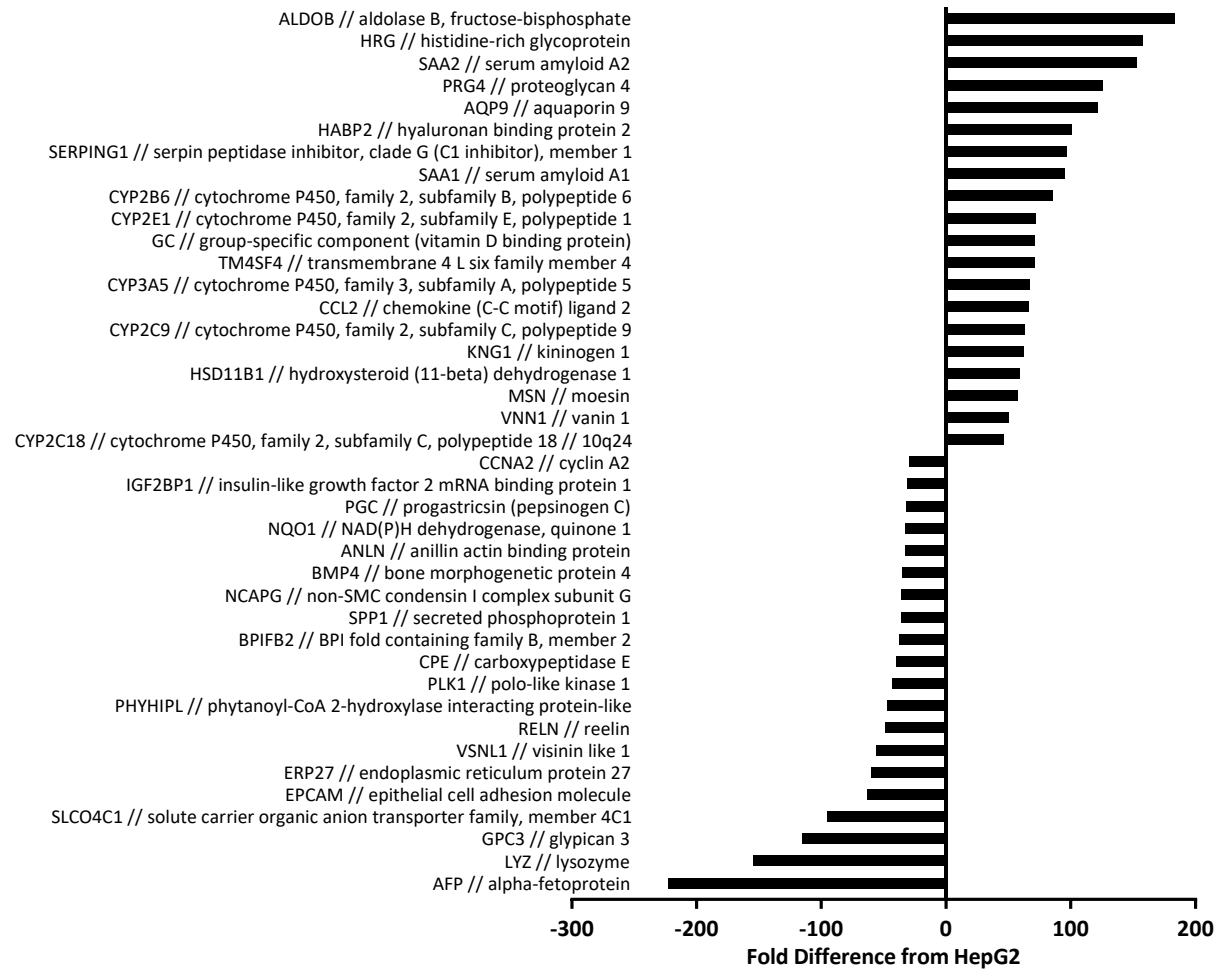


Figure 4.14: The 40 most different gene expressions in control HepG2 vs PHH (control: 0 μ M fatty acids+5mM glucose+0mM fructose)

The top ten most enriched (by number of genes) up- and down-regulated pathways in PHH compared to HepG2 cells are shown in Figures 4.15 (CON) and 4.16 (FA). There was some overlap in up and downregulated pathways; for example hsa05200 pathways in cancer and hsa04151 PI3K-Akt signalling pathway. Metabolism by cytochrome P was consistently higher in PHH; these pathways were also upregulated in the FA treated cells but they were not in the top 10 pathways. Other pathways of interest upregulated in CON PHH compared to CON HepG2 were hsa00071 fatty acid degradation, hsa04932 non-alcoholic fatty liver disease (NAFLD), hsa00051 fructose and mannose metabolism, and hsa04910 insulin signalling pathway. Downregulated pathways included hsa04975 fat digestion and absorption, hsa04110 cell cycle and hsa03030 DNA replication. The cell cycle and DNA replication genes would be expected to be more highly expressed in HepG2 cells as they are proliferating, whereas PHH are terminally differentiated and unable to proliferate.

A total of 151 pathways were upregulated in FA treated PHH compared to FA treated HepG2. The majority of these pathways were also enriched in the control comparison, and there were no additional pathways relating to lipid metabolism. In contrast, downregulated pathways in the FA comparison for PHH and HepG2 not found in the CON comparison included hsa00071 Fatty acid degradation, hsa00062 Fatty acid elongation, hsa00020 Citrate cycle (TCA cycle) and hsa00030 Pentose phosphate pathway.

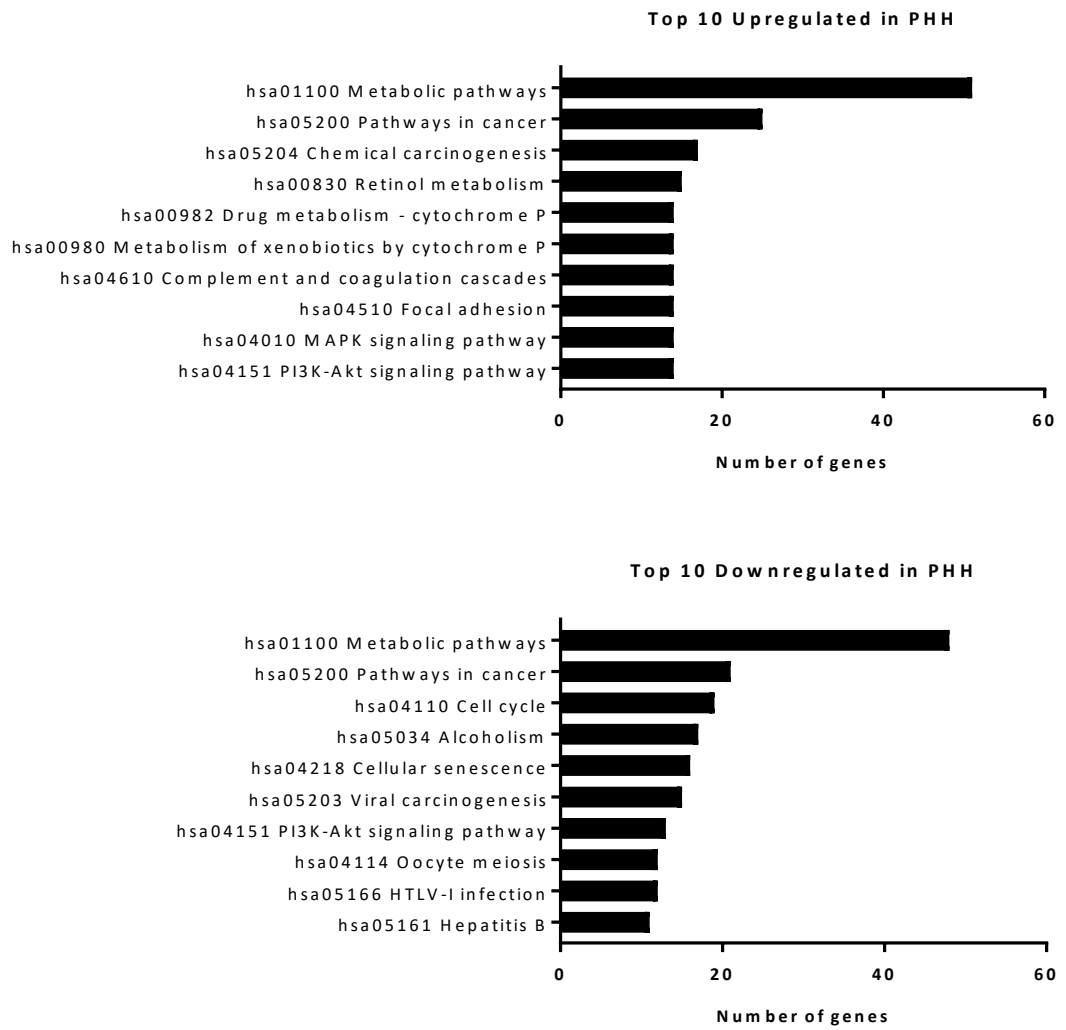


Figure 4.15: Top up- and down-regulated KEGG pathways in control PHH compared to control HepG2 (control: 0µM fatty acids+5mM glucose+0mM fructose)

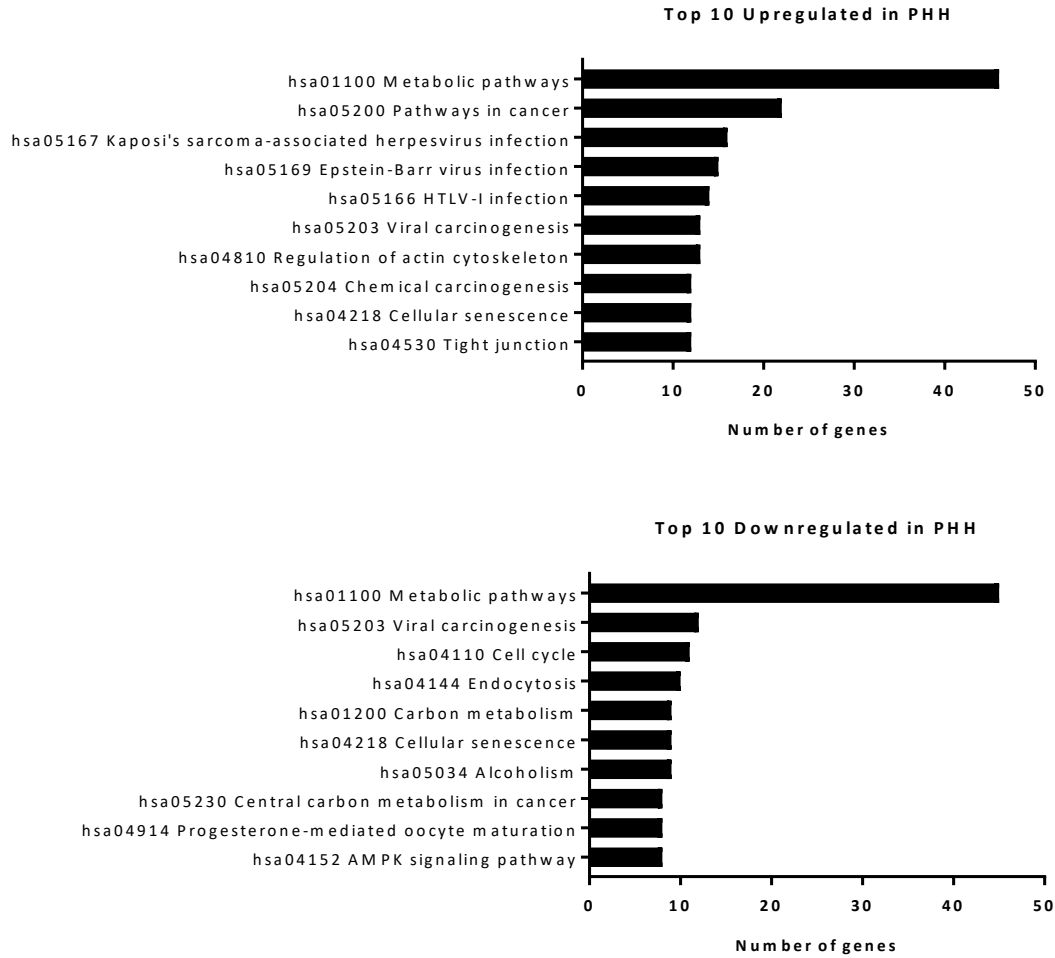


Figure 4.16: Top up- and down-regulated KEGG pathways in fatty acid (FA) treated PHH compared to FA treated HepG2 (fatty acid treated: 200 μ M fatty acids+5mM glucose+0mM fructose)

All the genes measured by RT-qPCR in section 4.3.1 were compared between the two cell types (Table 4.19). These results were not consistent with the RT-qPCR data; for example, the microarray data showed that ApoB was significantly less expressed in PHH (Table 4.19) whereas the RT-qPCR data showed that it was significantly higher in PHH (Figure 4.11, Table 4.19).

Table 4.19: Differences in gene expression in PHH compared to HepG2 cells determined by microarray pairwise comparison, and the quantitative reverse transcription PCR (RT-qPCR) standard curves analysed using linear regression to compare intercepts.

Note: RT-qPCR standard curves were produced using pooled cDNA from all treatments whereas microarray comparisons are control only. *Slopes significantly different. †Not measured in both cell types by RT-qPCR.

			PHH vs HepG2	
Gene	Name	Array Fold Change	Array	RT-qPCR Curves
CPT1A	carnitine palmitoyltransferase 1A (liver)	2.66	PHH ↑ P=0.015	PHH ↑ P<0.001
SLC2A2 (GLUT2)	solute carrier family 2 (facilitated glucose transporter)	2.47	PHH ↑ P=0.006	PHH = P=0.581
SREBF	sterol regulatory element binding transcription factor 1	1.46	PHH ↑ P=0.063	*
PNPLA3	patatin-like phospholipase domain containing 3	1.38	PHH = P=0.130	PHH ↓ P<0.001
PKLR	pyruvate kinase, liver	1.35	PHH = P=0.325	*
GCK	glucokinase (hexokinase 4)	-1.08	PHH = P=0.351	†
MLXIPL (ChREBP)	MLX interacting protein-like	-1.81	PHH ↓ P=0.048	PHH ↓ P<0.001
FASN	fatty acid synthase	-1.90	PHH ↓ P=0.098	PHH ↓ P<0.001
APOB	apolipoprotein B	-1.96	PHH ↓ P<0.001	PHH ↑ P<0.001
SCD	stearoyl-CoA desaturase (delta-9-desaturase)	-2.23	PHH ↓ P=0.002	PHH ↓ P<0.001
ACACA	acetyl-CoA carboxylase alpha	-3.03	PHH ↓ P=0.003	PHH ↓ P<0.001
HK2	hexokinase 2	-3.76	PHH ↓ P=0.012	†
DGAT1	diacylglycerol O-acyltransferase 1	-5.56	PHH ↓ P<0.001	PHH ↓ P<0.001
PPARGC1A	peroxisome proliferator-activated receptor gamma, coactivator	-7.79	PHH ↓ P=0.004	PHH ↓ P<0.001

Although DGAT1 was less expressed in PHH (Table 4.19), DGAT2 was more highly expressed in PHH when measured by microarray (FC=2.57, $P=0.001$). An initial RT-qPCR test with DGAT2 primers showed that DGAT2 was expressed at a low level in HepG2 cells compared to DGAT1 (data not shown).

4.3.2.2 FA vs CON (200 μ M fatty acid+5mM glucose+0mM fructose vs 0 μ M fatty acid+5mM glucose+0mM fructose)

The PCA plots of each treatment within the same cell type showed a lot of overlap of treatments and poor clustering of replicates, particularly in the controls (Figures 4.17 and 4.18). This could be a reason why no significant genes were found using FDR correction.

There was a total of 79 significantly changed genes in FA treated HepG2 cells compared to CON (fold change outside -2 and 2). The most significantly downregulated gene was SREBF1 (SREBP1) ($P<0.001$, fold change -2.26) which fits with the RT-qPCR data in section 4.3.1.3, but no other lipogenic genes were significantly changed. In terms of fold change, the most downregulated gene (with an accession number) was olfactory receptor family 4 subfamily D member 1 (OR4D1, FC= -2.56 , $P=0.016$) and the most upregulated gene was cytochrome P450 family 7 subfamily A polypeptide 1 (CYP7A1, FC= 2.92 , $P=0.010$). There were no fatty acid metabolism related KEGG pathways upregulated, but the most significantly down-regulated pathway was hsa04146 peroxisome (2 out of 83 genes) which could relate to lipid metabolism.

In PHH, 30 genes were changed with FA treatment (fold change outside -2 and 2) but no pathways were significantly changed. A particularly interesting upregulated gene was perilipin 2 (PLIN2, FC= 2.45 , $P<0.001$) which is a lipid droplet structural protein involved in the regulation of fatty acid release and lipolysis (Xu et al., 2018). In contrast to HepG2

cells, SREBF was not significantly down regulated by fatty acids in PHH, which fits with the RT-qPCR data where SREBP1 was less influenced by fatty acids in PHH (Figure 4.5).

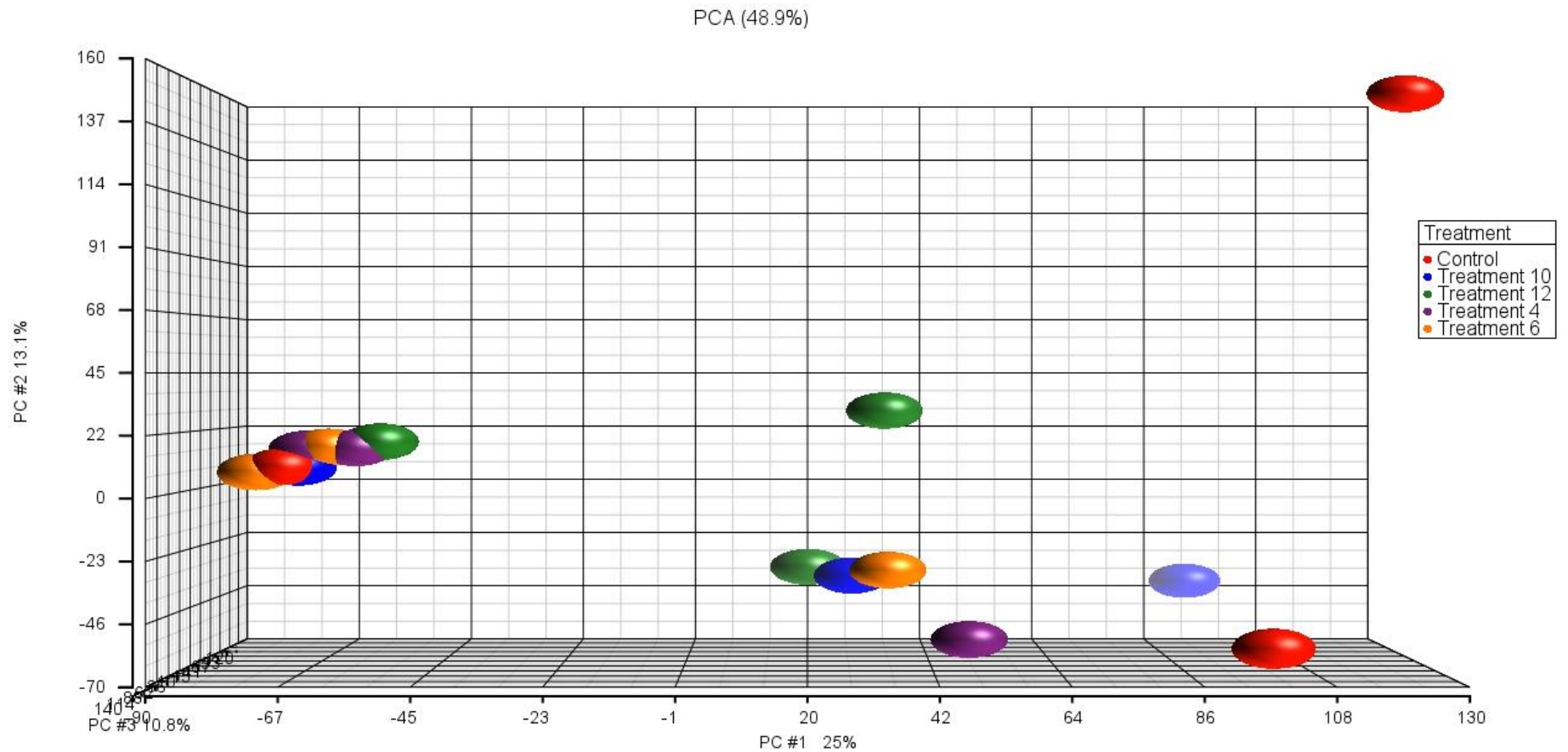


Figure 4.17: Principle component analysis (PCA) plot of gene expression data from all HepG2 treatments. See section 4.3.2.1 for explanation of PCA.

Control: CON, Treatment 4: FA, Treatment 6: FA+G, Treatment 10: FA+F, Treatment 12: FA+G+F (See Table 4.5). Ellipses removed due to poor clustering.

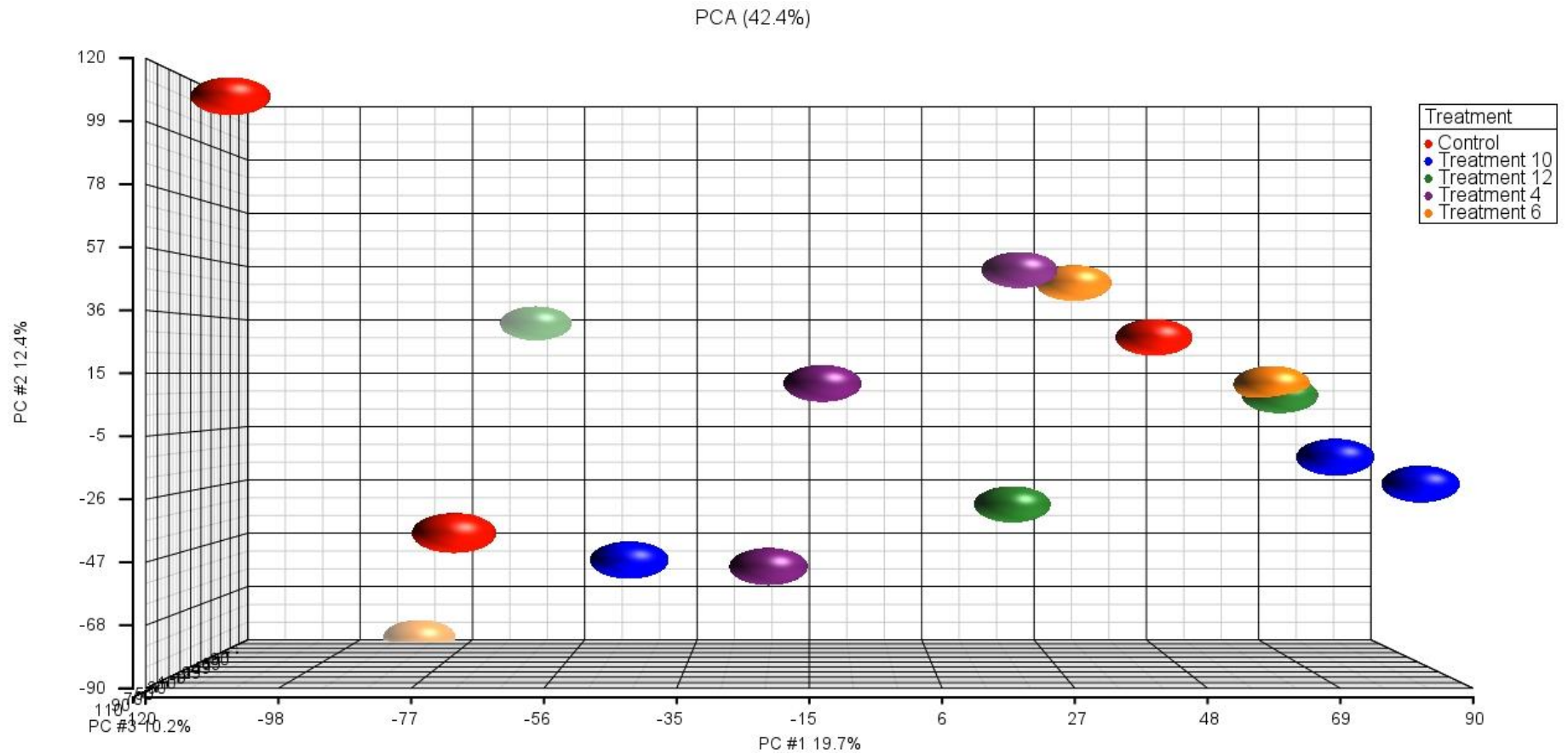


Figure 4.18: Principle component analysis (PCA) plot of gene expression data from all PHH treatments. See section 4.3.2.1 for explanation of PCA.

Control: CON, Treatment 4: FA, Treatment 6: FA+G, Treatment 10: FA+F, Treatment 12: FA+G+F (See Table 4.5). Ellipses removed due to poor clustering.

4.3.2.3 FA+G vs FA (200 μ M fatty acid+11mM glucose+0mM fructose vs 200 μ M fatty acid+5mM glucose+0mM fructose)

There were 45 genes with significantly altered expression in HepG2 cells treated with FA+G compared to FA alone (fold change outside -1.5 and 1.5), suggesting that they are all genes responsive to glucose. The second most highly upregulated gene was the glucose transporter SLC2A6 (GLUT6, FC=1.86, $P=0.023$) behind RAB30 (FC=1.99, $P=0.021$). No other glucose transporters were significantly changed. SREBF1 was also amongst the significantly upregulated genes (FC=1.57, $P=0.023$). One of the most downregulated genes was FOXO1 (FC= -1.82 , $P=0.019$), a transcription factor that promotes gluconeogenesis (Gross et al., 2008). The top most upregulated KEGG pathway was hsa04932 non-alcoholic fatty liver disease, with 2 out of a possible 149 genes being upregulated; SREBF1 and UQCRHL (ubiquinol-cytochrome c reductase hinge protein like).

In PHH, 219 genes had significantly different expression between FA+G and FA alone (fold change outside -1.5 and 1.5). The most significantly down regulated gene, which remained even with FDR correction, was cytochrome P450 family 1 subfamily A polypeptide 2 (CYP1A2, FC= -3.12 , $P<0.001$). In terms of fold changes, the most upregulated gene was ceramide synthase 5 (CERS5, FC=2.65, $P=0.012$). Other upregulated genes of interest were ChREBP (MLXIPL, FC=1.61, $P=0.007$), phosphoenolpyruvate carboxykinase 1 (PCK1, FC=2.21, $P=0.004$), acetyl-coA acetyltransferase 2 (ACAT2, FC=1.53, $P=0.007$) and C-reactive protein (CRP, FC=2.21, $P<0.001$). There were a large number of up and downregulated KEGG pathways. Downregulated pathways included cytochrome P related pathways and glucagon signalling. Upregulated pathways included pyruvate metabolism, insulin signalling and insulin resistance.

4.3.2.4 FA+F vs FA (200µM fatty acid+5mM glucose+8mM fructose vs 200µM fatty acid+5mM glucose+0mM fructose)

A total of 275 genes were changed with the addition of fructose to fatty acid treatment in HepG2 cells (fold change outside -1.5 and 1.5). The two most downregulated genes were oxysterol binding protein like 11 (OSBPL11, FC= -2.44 , $P=0.037$) and protein kinase cAMP-activated catalytic subunit beta (PRKACB, FC= -2.30 , $P=0.019$). Another downregulated gene was insulin-like growth factor 1 (IGF1), contributing to a downregulation of the insulin signalling (3 out a possible 137 genes) and MAPK signalling (6 of out a possible 295 genes) pathways. Upregulated genes of interest were lactate dehydrogenase A Like 6A and 6B (LDHAL6A and LDHAL6B), which contributed to the significant upregulation of propanoate, pyruvate, cysteine and methionine metabolism pathways and the glycolysis/gluconeogenesis pathway. Interestingly, purine metabolism was upregulated (4 out of a possible 130 genes); this is the pathway resulting in uric acid formation.

A total of 28 genes were changed with FA+F compared to FA in PHH (fold change outside -2 and 2). The significantly upregulated genes sphingomyelin synthase 2 (SGMS2, FC= 2.08 , $P=0.011$) and CERS5 (FC= 2.86 , $P=0.008$) meant that there was a significant upregulation of sphingolipid metabolism and sphingolipid signalling pathways. There were no significantly downregulated pathways.

4.3.2.5 FA+G+F vs FA+G (200µM fatty acid+11mM glucose+8mM fructose vs 200µM fatty acid+11mM glucose+0mM fructose)

This comparison also looked at fructose addition, but this time in the presence of high glucose, as well as FA. In HepG2 cells a total of 207 genes were significantly changed (fold change outside -1.5 and 1.5) but only 4 of these (adenylate kinase 7, AK7, cation

transport regulator homolog 2, CHAC2, HLA complex P5 non-protein coding, HCP5 and SET domain bifurcated 2, SETDB2) were also changed when comparing FA and FA+F. The most downregulated gene was phosphatidylinositol glycan anchor biosynthesis class H (PIGH, FC=-2.46, P=0.018) and the most upregulated gene was paraneoplastic Ma antigen family member 5 (PNMA5, FC=2.01, P=0.034). Another of the most downregulated genes was UQCRHL (FC=-2.39, P=0.006); this gene was originally upregulated by glucose when comparing FA and FA+G (section 4.3.2.3). The most significantly upregulated pathway was hsa00730 thiamine metabolism (2 out of 16 genes).

In PHH, 207 genes were also significantly changed (fold change outside -1.5 and 1.5). Similar to FA+F vs FA (section 4.3.2.4), the sphingolipid signalling pathway was upregulated by fructose but due to increased expression of different genes (ACER2, PLCB3 and S1PR1). The only gene common to the list in section 4.3.2.4 was TBC1 domain family member 24 (TBC1D24) which was downregulated in both. Upregulated genes of interest included 3-hydroxybutyrate dehydrogenase type 2 (BDH2, FC=2.01, P=0.001), janus kinase 2 (JAK2 FC=1.60, P=0.028) and acyl-CoA dehydrogenase C-4 to C-12 straight chain (ACADM, FC=1.76, P=0.004). Upregulated pathways included hsa04071 sphingolipid signalling pathway, hsa04630 Jak-STAT signalling pathway, and hsa04932 non-alcoholic fatty liver disease (NAFLD). There were far fewer downregulated pathways, suggesting that the effect of fructose was mainly stimulatory.

4.3.2.6 FA+G+F vs FA+F (200µM fatty acid+11mM glucose+8mM fructose vs 200µM fatty acid+5mM glucose+8mM fructose)

A total of 346 genes were significantly changed in this comparison in HepG2 cells (fold change outside -1.5 and 1.5). The only common gene to FA+G vs FA (section 4.3.2.3)

was G protein-coupled receptor 37 like 1 (GPR37L1). IGF1 was upregulated (FC=1.74, $P=0.044$) which was originally downregulated by fructose in section 4.3.2.4. Another upregulated gene of interest was the fatty acid transporter SLC27A4 (FATP4, FC=1.67, $P=0.032$). Upregulated pathways included hsa04150 mTOR signalling pathway and hsa04010 MAPK signalling pathway, suggesting increased proliferation and anabolic processes such as protein synthesis.

In PHH, a total of 424 genes had significantly changed expression (fold change outside – 1.5 and 1.5). Of these, 25 were common to the genes in section 4.3.2.3, including CYP1A2, PCK1, CRP, alcohol dehydrogenase 6 (ADH6) and cyclic AMP-responsive element-binding protein 3-like protein 3 (CREB3L3). The most downregulated gene, by significance and fold change, was CYP1A2 (FC=-3.22, $P<0.001$). This gene remained significant even with FDR correction, as in section 4.3.2.3. An upregulated gene was PCK1 (FC=1.61, $P=0.049$), and this contributed to the upregulation of hsa04931 insulin resistance, hsa04922 glucagon signalling pathway, hsa04068 FoxO signalling pathway, and hsa04910 insulin signalling pathway. Cytochrome P related pathways were downregulated, consistent with the other glucose comparison in the absence of fructose.

4.4 Discussion

4.4.1 Summary of results

Firstly, it is important to note that there was no biological replication of samples in this experiment, as all of the PHH data was from a single liver sample obtained from a 25-year-old female (L329). HepG2 cells are derived from the liver of a 15-year-old male. Therefore, in comparing the two cell types, some caution should be shown in attributing any differences to the cell type or to the donor characteristics. Also, PHH do not proliferate in culture while HepG2 cells do, therefore differences in expression of genes associated with cell division and replication would be expected. Chapter 3 quite clearly showed that both cell types accumulated lipid in response to exogenous fatty acids while specific differences were seen in response to sugars. The aim of the present experiment was to identify specific similarities and differences in gene expression in response of the two cell types to fatty acid and sugar treatment.

The main findings of this chapter are as follows:

- The RT-qPCR data showed that lipogenic genes were downregulated by exogenous fatty acids in HepG2 cells but not PHH, and that responses to glucose and fructose were more pronounced in PHH.
- Microarray analysis showed that the gene expression profiles of HepG2 cells and PHH are very different, demonstrating the proliferative phenotype of the HepG2 cells and the differentiated phenotype of PHH.
- Microarray comparisons across treatments within the cell types did not show as many significant changes but highlighted some points for further research.

4.4.2 RT-qPCR data

As described in section 4.1.1, hepatocytes have the ability to synthesise fatty acids from carbohydrate precursors using the lipogenic pathway (Figure 4.1). As illustrated, key genes in this pathway are ACC, FAS and SCD, all of which are regulated by SREBP1. Both endogenously synthesised fatty acids and those derived from exogenous sources can then be incorporated into TAG (for which DGAT is a key regulator) and either stored in intracellular lipid droplets, secreted in VLDL with the ApoB100 protein, or transported by CPT1 α into the mitochondria for β -oxidation.

Fatty acids reduced lipogenic gene expression in HepG2 cells, despite the consistent increase in intracellular lipid (Chapter 3). This suggests that the fatty acids are providing substrate for re-esterification and TAG synthesis, and therefore reduce lipogenesis from acetyl-coA because newly synthesised fatty acids are not required. It is known that unsaturated fatty acids decrease SREBP1c expression *in vitro* (Ou et al., 2001, Hannah et al., 2001) and that a diet high in saturated fatty acids increases SREBP1c expression in mice (Lin et al., 2005b). It seems that the fatty acid ratio and concentrations used here (palmitic, oleic and linoleic acids in the ratio 2:2:1 to a total of 200 μ M) are such that the effects of the unsaturated fatty acids outweigh those of palmitic acid. Fatty acids also increased CPT1 α expression, suggesting that mitochondrial β -oxidation may be increased, possibly to break down some of the excess fatty acids.

In PHH, fatty acids had a much more subtle effect on lipogenic genes; the only statistically significant effect was a reduction in SREBP1a expression. Although SREBP1a expression was correlated with ACC and SCD expression, lipogenic enzymes were not significantly suppressed by fatty acids. Interestingly, despite the apparent maintenance of lipogenesis, lipid accumulation in response to fatty acids was less in this cell type

(Chapter 3). However, the suppression of SREBP1a and SREBP1c expression by fructose is interesting as it is contrary to current thinking (see section 4.4.3).

Glucose and fructose enter hepatocytes through GLUT2 and can act as substrate for glycolysis and lipogenesis (section 4.4.1, Figure 4.1). They can also provide a source of glycerol-3-phosphate for TAG synthesis. However, there was little effect of glucose or fructose on gene expression in HepG2 cells. There was a trend for an effect of glucose on ChREBP expression, but not other glucose responsive genes such as LPK. This does fit with the lipid accumulation data, where the sugars had no effect on lipid accumulation in these cells (Chapter 3). HepG2 cells are known to uptake and metabolise glucose and fructose (Hirahatake et al., 2011), and their cancerous phenotype means that they have a high rate of glycolysis (Vander Heiden et al., 2009). Treatment of HepG2 cells with 5mM glucose and 5mM fructose has been shown to increase glucose-6-phosphate and fructose-6-phosphate levels further than 10mM glucose treatment (Meissen et al., 2015). Additionally, the microarray results showed changes in gene expression with glucose and fructose treatment, so it is highly unlikely that the glucose or fructose were not entering the cells. Glucose and fructose assays would help to confirm this. The gene correlations also differed between the cell types; for example, ChREBP correlated with LPK in PHH but not HepG2 cells. Together, the data suggest that there could be some fundamental differences in gene regulation between the two cell types which make them behave differently in response to nutritional stimuli. However, it is important to remember that we only used RNA from PHH isolated from one female liver. As HepG2 cells are male derived, sex differences could account for some of the differences in gene expression. Also, the differences in PHH lipid accumulation between individual livers (Chapter 3) could mean that gene expression patterns are equally as variable between individuals.

4.4.3 Comparing gene expression levels between the cell types

The RT-qPCR and microarray data were not consistent in showing which genes were more highly expressed in each cell type (Table 4.19). This could be in part because the cDNA pools are made up of all treatments whereas the microarray comparisons are one treatment only. There was also variation amongst the controls in the microarray data as seen in the PCA plots (Figures 4.17 and 4.18). Using cDNA pools from both cell types, we found that GSK3 was expressed poorly in both cell types (data not shown), and HK2 was only expressed in HepG2 cells. Low expression of HK2 in PHH was expected, as Hirahatake et al. (2011) found that HK2 was expressed over 14000% more in HepG2 cells than in human liver. It was expected that GSK3 (HK4) would be expressed in its place. In this instance, the microarray data confirmed that there was no significant difference in GSK3 expression between the cell types, and that HK2 expression was lower in PHH (FC=3.76. $P=0.012$).

While it is widely accepted that SREBP1a is expressed more highly than SREBP1c in cell lines and vice versa in liver (Shimomura et al., 1997), we found that SREBP1a was in fact more highly expressed than SREBP1c in both cell types. This is more in line with Bitter et al. (2015) who found that SREBP1a contributed 20-58% of the total SREBP1 pool in PHH and had an important role in inducing lipogenic gene expression. This data suggests that further study of the potential role of SREBP1a on lipid metabolism and NAFLD in human liver is warranted. There was a highly significant decrease in both SREBP1a and SREBP1c expression in HepG2 cells with fatty acid treatment which was backed up by the microarray analysis, although the microarray could not separate the isoforms. However, the decrease in SREBP1 expression with fructose treatment in PHH (determined by RT-qPCR) is unexpected. It is thought that fructose induces both SREBP1c and ChREBP expression (Moore et al., 2014), but this work is often done in rodent models. Further research into the direct effects of fructose on SREBP1a and SREBP1c expression (and

post-translational protein modification such as phosphorylation) in human liver is needed. Our results did not show any effects on SREBP1 downstream target genes, and the fact that the significant decrease was only observed at 8mM fructose may mean that supraphysiological concentrations are required for the effect.

4.4.4 Points of interest from the microarray data

4.4.4.1 Fatty acid effects

PLIN2 was upregulated in FA treated PHH compared to CON. Expression was also increased with FA treatment in HepG2 cells but the increase was not within the set parameters. This lipid droplet protein is thought to reduce TAG hydrolysis, thereby slowing TAG turnover, so is of interest in NAFLD. It has been shown to be a marker of lipid accumulation in HepG2 cells, but only at the protein level (Hoang et al., 2019). Interestingly, PLIN2 appears to reduce the association of PNPLA3 with lipid droplets (Listenberger et al., 2007) so there could possibly be an interaction between the PNPLA3 genotype (Chapter 5) and PLIN2 expression in determining liver fat accumulation.

In HepG2 cells, SREBP1 expression was decreased by FA treatment (confirming the RT-qPCR data) but increased again with the addition of high glucose, which was not shown in the RT-qPCR data. In contrast, SREBP1 was not significantly affected by treatment in PHH. However, changes at the protein level could have occurred, as much of the regulation of SREBP1 is post-translational (Wang et al., 2015). That said, downstream targets of SREBP1 were also not affected in both cell types. This is in contrast to the marked reduction of ACC, FAS and SCD mRNA by fatty acid treatment in the HepG2 RT-qPCR data.

4.4.4.2 Glucose effects

The cytochrome P450 enzyme system is involved in hepatic drug metabolism, an important function of the liver. Cytochrome P450 (CYP) metabolic pathways were consistently upregulated in PHH compared to HepG2 cells; HepG2 cells are known to have a much lower expression of CYP enzymes than human hepatocytes (Wilkening et al., 2003). One particular CYP enzyme of interest is CYP1A2, which was significantly downregulated in response to glucose treatment in PHH but not HepG2 cells.

Interestingly, Donato et al. (2006) found that CYP1A2 expression was reduced in PHH treated with fatty acids, along with the expression of a number of other CYP enzymes. In addition, CYP1A2 protein has been shown to decrease with NAFLD progression in humans (Fisher et al., 2009). In contrast, Kostrzewski et al. (2017) did not find a decrease in CYP1A2 expression in fatty acid treated human hepatocytes but other CYP enzymes were affected. Our results suggest that CYP1A2 reduction could be a marker of high blood sugar or possibly glucose induced lipid accumulation, as there were no effects of fatty acids. Both mRNA and protein levels of CYP1A2 are very low or undetectable in HepG2 cells (Wilkening et al., 2003, Olsavsky et al., 2007, Wisniewski et al., 2016) and Huh7 cells (Olsavsky et al., 2007). We found a 40-fold higher expression in control PHH compared to HepG2 cells. Along with drug metabolism, a key function of CYP1A2 is to be almost solely responsible for caffeine metabolism, and variations in CYP1A2 activity are related to an individual's ability to metabolise caffeine (Nehlig, 2018). If CYP1A2 expression is reduced in steatosis or with exposure to high blood sugar, these individuals could have a lower capacity for drug and caffeine metabolism.

PCK1, also known as PEPCCK-C, converts oxaloacetate (a TCA cycle intermediate) to phosphoenolpyruvate (PEP), a key step in hepatic gluconeogenesis. PCK1 mRNA in PHH was upregulated with high glucose in both comparisons involving a change from 5mM to 11mM glucose (FA+G vs FA and FA+G+F vs FA+F), suggesting an increase in

gluconeogenesis. This is surprising as gluconeogenesis would be expected to decrease with high glucose availability, therefore if this translates to the *in vivo* liver it has implications for insulin resistance and type 2 diabetes. Importantly, patients with increased liver fat have increased gluconeogenesis as well as increased mitochondrial fat metabolism and TCA cycle activity (Sunny et al., 2011). We did not see any effects on PCK1 in HepG2 cells, although the gluconeogenic transcription factor FOXO1 was downregulated in HepG2 cells treated with FA+G compared to FA. This could be another area where HepG2 cells and PHH differ in their metabolism.

GLUT6 was upregulated in HepG2 cells with high glucose plus FA treatment compared to FA alone. However, this gene cannot encode a functional protein (Kayano et al., 1990) so it is unlikely to affect the ability of HepG2 cells to uptake glucose. The fact that PHH have a greater expression of GLUT2 mRNA might suggest that they have higher capacity for glucose and fructose uptake, but the other glucose transporters must also be taken into account. GLUT1 is thought to be more highly expressed than GLUT2 in HepG2 cells (Takanaga et al., 2008) and the microarray results confirmed this with PHH having 10.40 fold less GLUT1 expression than HepG2 cells ($P < 0.001$). GLUT9 and GLUT3 were also significantly higher in HepG2 cells, so overall the capacity for glucose uptake may be considerably greater in HepG2 cells.

Glucose treatment upregulated the insulin signalling pathway in PHH but not HepG2 cells, confirming the results in Chapter 3 suggesting that HepG2 cells are insulin resistant.

4.4.4.3 Fructose effects

IGF1 was downregulated by FA+F in HepG2 cells compared to FA alone, but expression was raised again when 11mM glucose was included (FA+G+F). IGF1 has an anti-

inflammatory effect; when HepG2 cells are incubated with 10nM or 100nM IGF1 in addition to interleukin 6 (IL6), CRP and fibrinogen expression are reduced compared to IL6 alone (Hribal et al., 2013). Additionally, a reduction in IGF1 expression is associated with NAFLD development and progression (Adamek and Kasprzak, 2018, Hribal et al., 2013). Our results suggest that in HepG2 cells fructose is detrimental to IGF1 expression, but in combination with high glucose expression can be restored. However, this did not translate to PHH so the physiological relevance requires further research.

JAK2 was upregulated in PHH treated with FA+G+F compared to FA+G, and consequently the JAK-STAT signalling pathway was upregulated. This pathway has been implicated in the development of NAFLD, however it is ablation of this pathway that has been shown to be associated with NAFLD (Riordan and Nadeau, 2014). In this instance, fructose appears to not be detrimental to this pathway. Interestingly, this links to IGF1; binding of IGF1 to its receptor activates the JAK-STAT pathway (Himpe and Kooijman, 2009). We did not see any effects on IGF1 in PHH but further research into these pathways is warranted.

The production of uric acid is thought to be one of the mechanisms by which fructose exerts its toxic effects. The phosphorylation of fructose by KHK is rapid which depletes cellular ATP levels and raises adenosine monophosphate (AMP) and uric acid levels (Ter Horst and Serlie, 2017). The conversion of AMP to uric acid is part of the purine metabolism pathway, which was significantly upregulated when comparing FA+F and FA alone in HepG2 cells, but not in PHH. In contrast, sphingolipid metabolism and signalling were upregulated in PHH with FA+F compared to FA; the upregulated genes in these pathways were CERS5 and SGMS2. The production of ceramides is another mechanism thought to be responsible for the detrimental effects of fructose in the liver (see section 1.6). CERS5 expression was upregulated by both glucose (FA+G vs FA) and fructose (FA+F

vs FA) in PHH. These results together support the idea that fructose has detrimental effects on hepatic metabolism beyond providing additional substrate, but the effects were not consistent between the two cell types.

Another fructose effect not consistent between the two cell types was the upregulation of lactate dehydrogenases in HepG2 cells but not PHH. This suggests that fructose increases lactate production in HepG2 cells but not PHH. Possibly, this indicates that fructose is more channelled into glycolysis in HepG2 cells. As HepG2 cells are cancerous, they are continuously proliferating and they require energy for this process which they derive from glycolysis (Vander Heiden et al., 2009). There is also evidence that fructose treated HepG2 cells have increased glycine, serine, and threonine pools (Meissen et al., 2015), suggesting that fructose could also be directed into amino acid synthesis.

Measuring lactate in the media would help to confirm any differences in lactate production between the two cell types or between treatments. Visually, there was no clear differences in media colour between the cell types; all wells in both cell types turned more yellow after 24 hours, indicating lower pH.

4.4.5 Concluding remarks

The RT-qPCR data showed that the two cell types respond differently to fatty acid, glucose and fructose treatment at the mRNA level. Further work should aim to confirm these effects, for example the unexpected decrease in SREBP1 with fructose treatment in PHH, and whether these changes are seen at the protein level. Post-translational modifications must not be overlooked, particularly for transcription factors.

The variation within treatments, particularly the controls, made it difficult to analyse the microarray data, meaning that the stringency of the parameters had to be reduced for comparisons between treatments. However, the data has highlighted some interesting

points for further research; for example, the differences in SREBP1 expression between the two cell types, the highly significant reduction of CYP1A2 expression with 11mM glucose in the presence of fatty acids (with or without fructose), and the potential increase in the gluconeogenic gene PCK1 with high glucose in the presence of fatty acids (with or without fructose).

Overall, it is clear that HepG2 cells and PHH are extremely different in their metabolism and responses to nutrients, calling into question whether HepG2 cells really represent a useful *in vitro* model of NAFLD in humans.

Chapter 5: Patatin-like phospholipase domain containing 3 (PNPLA3): the study and manipulation of the I148M genotype for NAFLD research

5.1. Introduction

5.1.1 PNPLA3 function

Patatin-like phospholipase domain containing 3 (PNPLA3), also known as calcium independent phospholipase A2 epsilon (iPLA2- ϵ) or adiponutrin, is a protein in the patatin-like phospholipase family which is associated with membranes and lipid droplets (He et al., 2010). It has been shown to be a major genetic determinant for NAFLD (see section 5.1.2). Modelling of the enzymes tertiary structure indicates that there are no membrane-spanning domains (He et al., 2010), despite its localisation to membranes. The physiological role of PNPLA3 is yet to be fully elucidated. *In vitro*, human PNPLA3 has been shown to hydrolyse TAG, but overexpressing human PNPLA3 in mice did not affect liver TAG content (He et al., 2010). A recent review (Pingitore and Romeo, 2019) catalogues the development in the understanding of the enzymatic role of PNPLA3, and concludes that its role in hepatocytes is predominantly as a TAG hydrolase with a small amount of acyltransferase activity, with a higher affinity for MUFA and PUFA. Further work is still needed to clarify the role of wild-type PNPLA3.

5.1.2 I148M polymorphism

A single nucleotide polymorphism (SNP) at codon 148 substitutes isoleucine for methionine (I148M) in the PNPLA3 protein (Figure 5.1) due to a cytosine (C) to guanine

(G) substitution in the gene. This SNP (rs738490) is highly associated with hepatic fat content irrespective of BMI, alcohol consumption, ancestry and diabetes status (Romeo et al., 2008). The highest frequency of this SNP is in Hispanics (Romeo et al., 2008). A recent meta-analysis (Dai et al., 2019) has shown that the GG and CG genotypes are not only associated with NAFLD, but NAFLD patients with the GG or CG genotype are more likely to develop NASH. In addition, the GG genotype is associated with higher serum ALT levels, an established marker of liver damage.

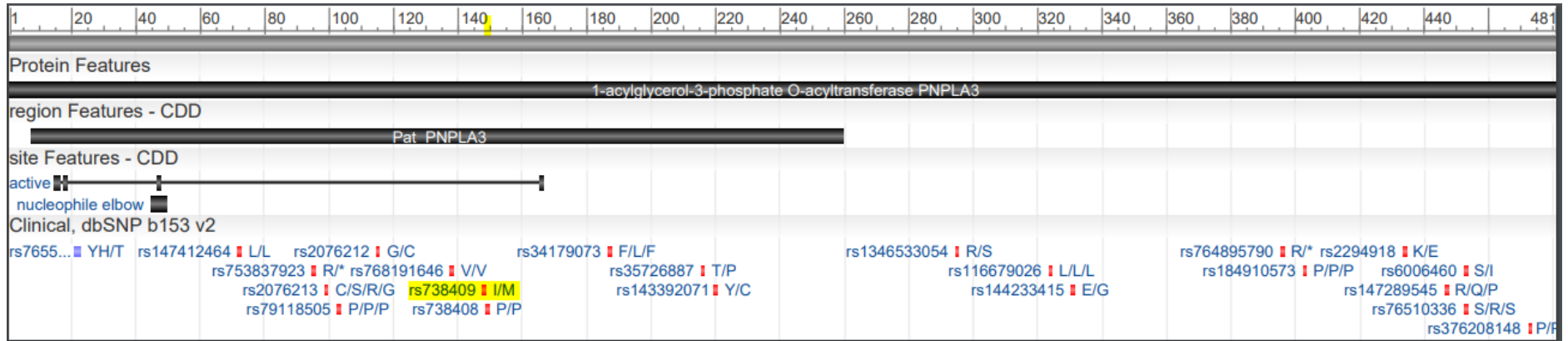


Figure 5.1: Domain structure of human PNPLA3 (1-acylglycerol-3-phosphate O-acyltransferase). CDD: coding domain. The rs738490 single nucleotide polymorphism (SNP) site is highlighted. Compiled using the NCBI website. NCBI Reference Sequence: NP_079501.2

Due to the current uncertainty about the physiological function of PNPLA3, it is also uncertain how I148M results in increased liver fat. Initial work showed that overexpressing the mutated protein in mice increased liver TAG, suggesting the fat accumulating effects of the SNP are due to the mutant protein itself and not the absence of the wild-type protein (He et al., 2010). One theory is that the mutation blocks catalytic function due to the methionine residue blocking access to the substrate (He et al., 2010). Other work has shown that purified human PNPLA3 protein has TAG hydrolase activity and a lower rate of lysophosphatidic acid acyltransferase (LPAAT) activity; the I148M mutation reduces both of these effects (Pingitore et al., 2014). Huang et al. (2011) also showed that the isolated PNPLA3 protein has hydrolase activity for TAG, DAG and monoacylglycerol (MAG), and that the I148M mutation dramatically reduced this activity but did not completely eliminate it. More recent work found that differences in post-translational modification could be a factor; the wild-type protein was ubiquitinated by E3 ligase and turned over by proteasomal degradation, but the I148M variant avoided this process by an unknown mechanism and accumulated on lipid droplets in mice (BasuRay et al., 2017). This idea was confirmed in a later study in mice where expression of a synthetic ubiquitination-resistant PNPLA3 resulted in PNPLA3 accumulation and steatosis (BasuRay et al., 2019). Again, further study is needed to confirm the mechanism behind the effects of the SNP.

Another SNP in the PNPLA3 gene, substituting isoleucine in place of serine at codon 453 (S453I, rs6006460), is prevalent in African Americans. This is associated with decreased liver fat and is independent of the I148M mutation (Romeo et al., 2008). These two mutations account for a large amount of the genetic influence on liver fat.

5.1.3 PNPLA3 in hepatic stellate cells

The PNPLA3 protein is not only found in hepatocytes, but also has an important role in hepatic stellate cells (HSCs) where it is more highly expressed than in hepatocytes in humans (Pirazzi et al., 2014). Here it acts as a retinyl-palmitate lipase, releasing retinol and palmitic acid from retinyl-palmitate. The I148M mutation reduces retinyl-palmitate lipase activity (Pirazzi et al., 2014). Under normal conditions, PNPLA3 expression is increased with retinol deficiency to increase retinol release into the circulation where it circulates bound to retinol binding protein 4 (RBP4). Subjects with the I148M mutation have less circulating RBP4 as the retinol is retained within HSCs (Pirazzi et al., 2014). This has been confirmed in NAFLD patients with the I148M mutation who have lower fasting retinol and RBP4 levels (Mondul et al., 2015). Although the current work does not involve HSCs, it is important to recognise that its role in these cells may contribute to its involvement in NAFLD/NASH.

5.1.4 Experimental aims

The overall aim of the work described in this chapter was to develop cell model systems that would help to elucidate the role of PNPLA3 in the development of NAFLD. We also aimed to genotype the human cell lines and all livers used. The hypotheses were that the human cell lines would carry the polymorphism, and the livers would display the ratio of genotypes described in the population.

The specific aims and objectives were as follows:

- To develop a way to measure PNPLA3 expression by identifying an antibody capable of detecting the PNPLA3 protein.
- To confirm the HepG2 and Huh7 cell genotype and genotype each of the livers used in Chapters 3 and 4 by using a SNP assay.

- To develop a system that could be used in overexpressing the PNPLA3 variants in cell culture models by producing lentiviruses for the wild-type and polymorphic variants.

5.2. Methods

5.2.1 Genotyping of cell lines and liver samples

5.2.1.1 Genomic DNA Extraction from HepG2 and Huh7 cells

Genomic DNA was extracted from HepG2 and Huh7 cells using the Qiagen DNeasy Blood and Tissue Kit. Samples of cells were spun down, washed with PBS then re-suspended in 200µl PBS. 20µl proteinase K was added to each sample followed by 4µl of RNase A (Qiagen 4mg/ml). The tubes were vortexed and incubated at room temperature for 2 minutes. 200µl buffer AL was added, the samples vortexed then incubated in a hot block set to 56°C for 10 minutes. After removing from the hot block, 200µl 100% ethanol was added and the tubes vortexed before the solution was transferred to a spin column. They were spun at 6000×g for one minute at room temperature and the flowthrough was discarded. 500µl buffer AW1 was added to the column and spun in the same way. 500µl buffer AW2 was added and the columns spun at 18000×g for 3 minutes at room temperature. The filter was transferred to a clean 1.5ml tube. 200µl buffer AE was added directly to the filter, and after a short incubation at room temperature they were spun at 6000×g for 1 minute at room temperature to elute the DNA.

The concentration and purity were checked on the NanoDrop. For some samples, the concentrations were very low and the purity was bad. To clean up and concentrate the DNA, ethanol precipitations of the samples were carried out. 20µl 3M sodium acetate and 600µl 100% ethanol were added to each tube and they were frozen at –80°C at least overnight. When they were removed from the freezer, they were spun at 15000×g for 15 minutes at 4°C to pellet the DNA. The supernatant was removed then 1ml cold 70% ethanol added to wash the pellet. After briefly vortexing, the tubes were spun again at 15000×g for 10 minutes at 4°C. The ethanol was carefully removed and the pellet left to

air dry for a few minutes before re-suspending in 30µl buffer AE. This procedure successfully cleaned up and concentrated the DNA.

5.2.1.2 Genomic DNA extraction from liver tissue

At time of perfusion, a piece of liver tissue was homogenised into 2ml Trizol by Monika Owen and Nicola De Vivo. The samples were stored at -40°C . Genomic DNA was extracted from each homogenised sample as follows. Each sample was split into two 1ml aliquots in 1.5ml tubes. 200µl 1-bromo-3-chloropropane (BCP) was added to each tube and mixed by vigorous shaking. The tubes were spun at $10000\times g$ for 15 minutes at 4°C to separate the phases. The upper phase was removed and the lower phase used for DNA extraction. 300µl ethanol was added to each tube and mixed by inversion. The tubes were left to stand for 3 minutes at room temperature, then spun at $2000\times g$ for 5 minutes at 4°C . The supernatant was removed. The DNA pellet was washed three times in 0.1M trisodium citrate 10% (v/v) ethanol solution. For each wash, 1ml of the solution was added to the tubes which were then left to stand with occasional mixing for half an hour before spinning at $2000\times g$ for 5 minutes at 4°C , and finally removing the wash solution. After three washes, the pellets were re-suspended in 1.5ml 75% ethanol and left to stand at room temperature for about 15 minutes. The samples were stored at 4°C . When required, the DNA was precipitated by adding 35µl 3M sodium acetate to each tube and leaving overnight at -20°C . The next day the tubes were spun at $15000\times g$ for 15 minutes at 4°C . The pellets were washed once with 70% (v/v) ethanol, air dried, and re-suspending in 300µl 8mM NaOH. Finally, the tubes were spun at $12000\times g$ for 10 minutes at room temperature and the liquid transferred to clean tubes to leave behind any unwanted residue.

5.2.1.3 PCR and gel purification of a product for sequencing

HepG2 and Huh7 genomic DNA was used for PCR and gel extraction in order to send the PNPLA3 SNP site for sequencing to confirm genotype. PCR was carried out using the Q5 High Fidelity DNA Polymerase enzyme (New England Biolabs). A master mix containing the following components per reaction was made: 10 μ l 5 \times Q5 reaction buffer, 1 μ l 10mM dNTP mix, 2.5 μ l 10 μ M forward primer, 2.5 μ l 10 μ M reverse primer, 0.5 μ l Q5 polymerase, and made up to 50 μ l with water. A volume of DNA to allow 500ng per reaction was used. The primers are detailed in Table 5.1 and the thermocycling conditions are shown in Table 5.2.

Primer Name	Sequence
hPNPLA3_gen_SNP_fw	CATGGATTAACCTACTCTGTGC
hPNPLA3_gen_SNP_rv	ATGGGACAGACCCTGAGGT

Step	Temperature (°C)	Time (mins:secs)
Initial Denaturation	98	1:00
Denaturation	98	0:10
Annealing	64	0:20
Extension	72	0:10
Final Extension	72	2:00
Cooling	4	∞

The reactions were run on a 1.5% (w/v) agarose gel to confirm the correct band size. The samples were mixed with loading buffer and 1 μ l 100 \times SYBR green dye to allow

visualisation under UV light. The bands were extracted and purified using the QIAquick Gel Extraction Kit (Qiagen). Using a scalpel blade, the bands were cut from the gel using the aid of a UV light block. The agarose sections were transferred to 1.5ml tubes and weighed. Three volumes of buffer QG were added and the tubes incubated at 50°C for 10 minutes with periodic vortexing to dissolve the gel. One volume (original gel weight) of isopropanol was added and mixed. The solution was transferred to a spin column and spun at 15000×g for 1 minute at room temperature. Next, 750µl of buffer PE was added to the column and left to stand for a few minutes before spinning at 15000×g for 1 minute at room temperature. The flowthrough was removed and a further minute spin carried out to remove residual buffer. Finally, the DNA was eluted using 50µl water into a 1.5ml tube. DNA concentration was measured using a NanoDrop. DNA was sent to Source Bioscience for sequencing with primers flanking the SNP region (Table 5.3). Both cell types were confirmed to have the polymorphic ATG codon.

Table 5.3: Sequencing primers for confirming HepG2 and Huh7 cell PNPLA3 genotype	
Primer Name	Sequence
hPNPLA3_SNPseq_fw	TTGCCCTGCTCACTTGGAGA
hPNPLA3_SNPseq_rv	TGTGAGCACACTTCAGAGGC

5.2.1.4 SNP TaqMan genotyping assay

A predesigned and validated TaqMan SNP Genotyping assay was obtained from Applied Biosystems which was specific for the I148M SNP. The 40×assay solution was diluted to 20×working stock in TE buffer and frozen in aliquots protected from light. One reaction in a white 384-well plate contained 0.25µl 20×assay stock, 2.5µl probes master mix (Roche) and 2.25µl DNA diluted to 8.8ng/µl to ensure the addition of 20ng DNA to each well. Negative control reactions contained water instead. The plate was read on a

LightCycler 480 II using the Dual Colour Hydrolysis Probe setting for FAM (465–510nm) and VIC/HEX (533–580nm). Cycling conditions are in Table 5.4.

Stage	Target Temp (°C)	Time (mins:secs)	Ramp rate (°C/sec)
Pre-incubation	95	10:00	4.8
Amplification (×40)	95	00:15	4.8
	60	01:00	2.5
	72	00:01	4.8
Cooling	40	00:30	2.5

5.2.2 Cloning of human PNPLA3 cDNA

5.2.2.1 cDNA synthesis

cDNA was synthesised using the AffinityScript Multi-temperature cDNA synthesis kit (Agilent Technologies). Human liver RNA and the kit components were defrosted on ice. The following were added to a 0.5ml tube: 5µl RNA (approximately 100ng/µl), 6µl RNase free water and 3µl random primers (0.1µg/µl). This mix was incubated using a Biometra Trio Thermoblock at 65°C for 5 minutes then at room temperature for 10 minutes to allow the primers to anneal to the RNA. The following components were added to the tube via a master mix: 2µl 10×AffinityScript RT buffer, 2µl DTT (100mM), 0.5µl dNTP mix, 0.5µl RNase block ribonuclease inhibitor (40U/µl) and 1µl AffinityScript reverse transcriptase. The reactions were gently mixed and spun down before incubating at 25°C for 10 minutes followed by 50°C for 1 hour and finally terminated at 70°C for 15 minutes. The cDNA was stored at –20°C until use.

5.2.2.2 Polymerase Chain Reaction (PCR)

Primers were designed to incorporate *attB* sites as detailed in the Gateway® Technology with Clonase® II protocol booklet (Table 5.5). The primers flanked the coding sequence of the PNPLA3 mRNA sequence (NCBI Reference Sequence: NM_025225.2) which is between 174–1619 base pairs.

Table 5.5: Cloning primers for PNPLA3 incorporating the attB sites for Gateway cloning	
Primer Name	Sequence
Clohu_PNPLA3_fw	GGGACAAGTTTGTACAAAAAAGCAGGCTTCGCCACCAGGGTAGA GAGCGCTTGCGGGC
Clohu_PNPLA3_rv	GGGACCACCTTTGTACAAGAAAGCTGGGTTAGTGCTGGACCGCTG CACAGGC

PCR was carried out using the Phusion High-Fidelity DNA Polymerase Kit (New England Biolabs). The synthesised human cDNA and the kit components were thawed on ice. Primers were diluted to 10µM in sterile water. The cDNA was diluted 1 in 4 so that there was less than 250ng in the reaction. The following components were added to a 0.2ml PCR tube by means of a master mix: 10µl 5×HF buffer, 1µl 10mM dNTP, 2.5µl 10µM forward primer, 2.5µl 10µM reverse primer, 1.5µl DMSO and 0.5µl DNA polymerase. 2µl diluted cDNA was added and the volume made up to 50µl with RNase free water. The reactions were transferred to a thermocycler preheated to 98°C. After trial and error, the thermocycling conditions were optimised to those in Table 5.6. The reactions were stored at 4°C until use.

Table 5.6: Thermocycling conditions for PCR amplification of the PNPLA3 coding sequence. The denaturation, annealing and extension steps were cycled 34 times

Step	Temperature (°C)	Time (mins:secs)
Initial Denaturation	98	0:30
Denaturation	98	0:10
Annealing	71	0:30
Extension	72	1:35
Final Extension	72	5:00
Cooling	4	∞

5.2.2.3 Agarose gel electrophoresis

A 1% (w/v) agarose gel was prepared using 1×TAE buffer as follows. The gel was heated in a microwave until clear and left to cool slightly. 10mg/ml ethidium bromide was added to a final concentration of 1µg/ml and swirled to mix before pouring into a gel tray. The gel was left to set for an hour before transferring to an electrophoresis gel tank and covering with 1×TAE buffer. 10µl of the PCR samples were mixed with 2µl purple loading dye and loaded into the wells. A 1kb DNA ladder was also loaded. The gel was left to run for approximately 45 minutes at 80V. The bands were visualised under UV light to check the band was the correct size.

5.2.2.4 PCR product purification

The *attB*-flanked PCR product was purified using the protocol in the Gateway® Technology with Clonase® II (Invitrogen) booklet with some amendments. 25µl of the PCR reaction was taken into a fresh 0.5ml tube and 75µl TE buffer added. 50µl of PEG 8000 / 30mM MgCl₂ (supplied with Gateway kit) was added. The mix was vortexed then immediately centrifuged at 11000×g for 20 minutes at room temperature. This is longer and faster than the manual specified, but a product was not detected by agarose gel

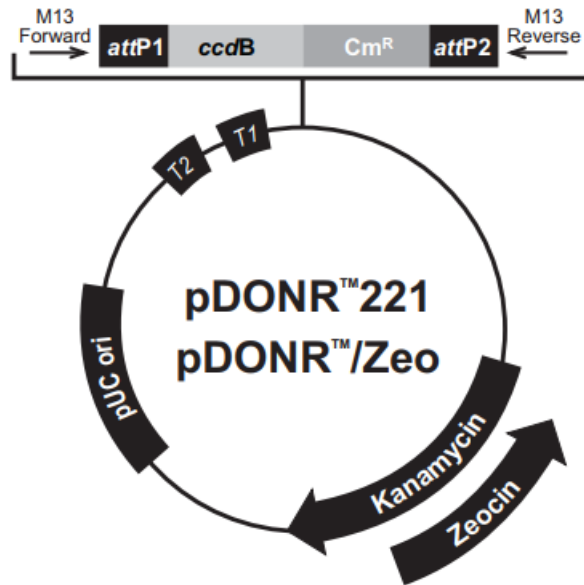
electrophoresis until the speed and time were increased. The supernatant was removed and the pellet re-suspended in 25µl TE buffer by vortexing in pulses. The product was confirmed by running an agarose gel as specified in the above protocol.

5.2.2.5 Determining DNA concentration

The purified product was quantified using an LVis plate (BMG LABTECH) in a FLUOStar OMEGA plate reader; 2µl of DNA was loaded into each well of the LVis plate for absorbance measurements.

5.2.2.6 BP recombination reaction

The pDONRTM221 vector detailed in Figure 5.2 was used to perform the BP recombination reaction with the *attB*-flanked PCR product. The components in Table 5.7 were added to 1.5ml tubes.



Comments for:	pDONR™221 4761 nucleotides	pDONR™/Zeo 4291 nucleotides
<i>rmb</i> T2 transcription termination sequence (c):	268-295	268-295
<i>rmb</i> T1 transcription termination sequence (c):	427-470	427-470
M13 Forward (-20) priming site:	537-552	537-552
<i>attP1</i> :	570-801	570-801
<i>ccdB</i> gene (c):	1197-1502	1197-1502
Chloramphenicol resistance gene (c):	1825-2505	1847-2506
<i>attP2</i> (c):	2753-2984	2754-2985
M13 Reverse priming site:	3026-3042	3027-3043
Kanamycin resistance gene:	3155-3964	---
EM7 promoter (c):	---	3486-3552
Zeocin resistance gene (c):	---	3111-3485
pUC origin:	4085-4758	3615-4288

(c) = complementary strand

Figure 5.2: Detailed breakdown of the pDONR221 vector used in the BP recombination reaction. (From the Invitrogen technical booklet)

Component	Sample Reaction	pEXP7-tet positive control
PCR product	3.6 μ l (to achieve 50fmol)	
pDONR™221 vector	1 μ l	1 μ l
pEXP7-tet		2 μ l
TE buffer	3.4 μ l	5 μ l

The Gateway® Clonase® II enzyme mix was thawed on ice for 2 minutes and vortexed twice for 2 seconds. 2µl of the enzyme mix was added to each reaction and they were vortexed twice for 2 seconds. The reactions were incubated at 25°C for 1 hour before adding 1µl proteinase K. Finally, the reactions were incubated at 37°C for 10 minutes before storing at –20°C for a few days.

5.2.2.7 Preparation of agar plates and antibiotic stocks

50mg/ml solutions of kanamycin and tetracycline were prepared by dissolving 250mg antibiotic powder in 5ml sterile water. The solutions were sterile filtered, aliquoted and stored at –20°C.

Agar plates were prepared by melting lysogeny broth (LB) agar in a microwave, waiting for it to cool slightly, dispensing the appropriate amount and adding the required amount of antibiotic solution for the desired concentration. Approximately 20ml was poured into each plate and left to set at room temperature before storing at 4°C until use.

5.2.2.8 Transforming Competent Cells

One vial of OmniMax 2-T1 (Invitrogen) cells and two vials of DH10β (New England Biolabs) cells were thawed on ice. For the OmniMax cells, 1µl of the BP recombination was added. To one vial of DH10β cells, 1µl of the positive control BP recombination reaction was added, and to the other 1µl of pUC19 positive control DNA. The vials were mixed gently by tapping and incubated on ice for 30 minutes. After this, the vials were heat shocked at 42°C for 30 seconds before returning to ice for 2 minutes. 250µl of room temperature super optimal broth with catabolite repression (SOC medium, pre-prepared in another lab) was added to each vial, then they were shaken horizontally at 370rpm

and 37°C for 1 hour in a shaking heat block. The whole of each sample were spread onto agar plates containing the antibiotics in Table 5.8.

Reaction	Antibiotic
OmniMax 2-T1 with sample plasmid	50µg/ml kanamycin
DH10β with pEXP7-tet	20µg/ml tetracycline
DH10β with pUC19	50µg/ml kanamycin*
*this should have been ampicillin so the pUC19 control was not successful	

The plates were incubated at 37°C overnight. In the morning, a single colony was selected and scraped into 5ml LB medium containing 50µg/ml kanamycin. This was left in a shaking incubator at 225rpm and 37°C for 8 hours. 250µl of this starter culture was taken and diluted 1:1000 in pre-warmed LB medium containing 50µg/ml kanamycin. This was left shaking in the same conditions overnight in a 1L conical flask.

5.2.3 MidiPrep

The entry vector plasmid was isolated from the overnight culture using the NucleoBond Xtra kit (Machery-Nagel). The optical density (OD) of the overnight culture was determined at 600nm. A reference value was taken using LB medium. A 1:10 dilution of the overnight culture was loaded, and the OD was this value multiplied by 10. The volume of culture to use for the MidiPrep was calculated using 400/OD.

50ml of the culture was transferred to a 50ml tube and centrifuged at 6000×g for 10 minutes at 4°C. The supernatant was discarded and another 50ml of the culture added to the tube. This was repeated until the calculated volume had all been spun down in one tube to form a bacterial pellet. The plasmid was isolated from the bacterial pellet

using the NucleoBond Xtra kit (Machery-Nagel) as follows. The pellet was re-suspended in 8ml RES buffer containing RNase by vortexing until all clumps were dissolved. 8ml LYS buffer was added and the tube inverted 5 times, then left at room temperature for 5 minutes. During this time, the column filter was equilibrated by adding 12ml EQU buffer around the rim of the filter. 8ml of NEU buffer was added to the tube and mixed by gently inverting until the blue colour had disappeared. The mix was centrifuged at $7500\times g$ for 10 minutes at 4°C to remove the precipitate. The supernatant was poured into the column filter and allowed to run through. When it had finished dripping, the filter was washed with 5ml EQU buffer applied around the rim. After this had run through, the filter was discarded. The column was washed with 8ml WASH buffer. After this, 15ml tubes were placed under the columns to collect subsequent flow-through. 5ml ELU buffer was added to the column, collected in the tube, then the column discarded. 3.5ml isopropanol was added to the tube and vortexed well. This was spun at $10648\times g$ for 30 minutes at 4°C . The supernatant was carefully aspirated, then 1ml 70% ethanol added to the tube. This was carefully transferred to a 1.5ml tube, being careful to transfer the visible white pellet. This was centrifuged at $15000\times g$ for 5 minutes at room temperature. The supernatant was removed and another 1ml 70% ethanol added for a second wash. After the second spin, as much ethanol as possible was removed by aspiration, then the pellet was left to air dry for about 10 minutes. The pellet was dissolved in $200\mu\text{l}$ sterile water.

5.2.4 Sequencing and identification of I148M variant

Sequencing of the vector was carried out externally by Source Bioscience. Firstly, the vector was sequenced using M13 primers but the results came back with many unidentified bases. Also, the base after the codon of interest was called as a G whereas

in the sequence it is a C. However, the peaks were ambiguous for this base, suggesting it could be a G or C. Secondly, the cloning primers described in Table 5.5 were used but this also came back with many unidentified bases and the ambiguous base adjacent to the base of interest. To try and obtain clearer sequencing, the glycerol stock was streaked onto an agar plate containing kanamycin and left overnight. In the morning, a single colony was isolated and cultured and the plasmid purified by a MidiPrep as previously described.

To better isolate the regions of interest, primers closer to the SNP sites were designed for sequencing use and obtained from Sigma (Table 5.9). Using these primers, clear sequencing was returned. Both SNP sites were wild-type.

Table 5.9: Sequencing primers designed to flank the single nucleotide polymorphisms of interest	
Primer Name	Primer Sequence
huPNPLA3_I148M_fw	TAGGCATCTCTTTACCAGAGTG
huPNPLA3_I148M_rv	ACGTTGTCACTCACTCCTCC
huPNPLA3_S453I_fw	ATGCACACCTGAGCAGGA
huPNPLA3_S453I_rv	TCAAGTGA CT CACAGACTCTTCT

5.2.5 Mutagenesis

The I148M site was mutated from ATC to ATG (causing an isoleucine to methionine amino acid substitution in the protein) using the QuikChange XL Mutagenesis kit (Agilent) in order to have a wild-type (WT) and polymorphic (MUT) entry vector. Primers were designed using the manufacturer's online tool (Table 5.10).

Table 5.10: Mutagenesis primers	
Forward:	5'-GGTATGTTCTGCTTCATGCCCTTCTACAGTGG-3'
Reverse:	5'-CCACTGTAGAAGGGCATGAAGCAGGAACATACC-3'

The following components were added to a 200µl thin-walled tube: 5µl 10×reaction buffer, 10ng of dsDNA template (PNPLA3 entry vector), 125ng forward mutagenesis primer, 125ng reverse mutagenesis primer, 1µl dNTP mix, 3µl QuikSolution, and RNase free water to a total volume of 50µl. A control reaction was also prepared using control primers and pWhitescript DNA according to the kit instructions. 1µl of Pfu DNA polymerase was added to each reaction and they were thermocycled using the conditions in Table 5.11.

Table 5.11: Thermocycling conditions for mutagenesis PCR. The denaturation, annealing and extension steps were cycled 18 times		
Step	Temperature (°C)	Time (mins:secs)
Initial Denaturation	95	1:00
Denaturation	95	0:50
Annealing	60	0:50
Extension	68	6:15
Final Extension	68	7:00
Cooling	4	∞

After cooling to 4°C, 1µl of Dpn restriction enzyme was added to the reaction and transferred to a 0.5ml tube. The reaction was mixed by pipetting up and down and incubated at 37°C for one hour.

XL-10 Gold ultra-competent cells were used for transformation. A 45µl aliquot of cells (thawed on ice) was transferred to a 14ml round bottomed falcon tube which had been pre-chilled. 2µl of β-mercaptoethanol was added to the cells and incubated on ice for 10

minutes, swirling every 2 minutes. Then 2µl of the Dpn treated DNA was added to the cells and gently swirled. The tube was incubated on ice for 30 minutes. After this time, the tube was heat shocked at 42°C for 30 seconds then transferred back to ice for 2 minutes. 500µl of pre-warmed SOC medium was added to the tube and it was placed in a shaking incubator for 1 hour at 225rpm and 37°C. Two LB agar plates with kanamycin were warmed to 37°C and 250µl of the transformation spread onto each. The plates were incubated overnight at 37°C. The following day, six single colonies were selected and inoculated in 5ml LB medium containing kanamycin. These were shaken overnight at 37°C and 225rpm. All six cultures grew successfully. 2ml of each culture was used for a MiniPrep to identify which colonies had been successfully mutated.

5.2.6 GeneJET Plasmid MiniPrep (ThermoFisher)

1ml of bacterial culture was transferred to a 1.5ml tube and centrifuged at 6800×g for 2 minutes at room temperature. The supernatant was discarded and another 1ml of culture added to the tube and spun as above. 250µl resuspension buffer was added to the bacterial pellet and vortexed. 250µl lysis solution was added and the tube inverted 6 times. 350µl neutralisation buffer was added and the tube inverted another six times. The tube was spun for 5 minutes at 13000×g at room temperature to pellet the debris. The supernatant was transferred to a spin column and spun for 1 minute at 13000×g at room temperature. The flowthrough was removed. 500µl wash solution was added to the column and spun for 1 minute at 13000×g at room temperature and the flow through removed. This wash step was repeated then the column spun for an extra minute. The column was transferred to a fresh 1.5ml tube and 50µl water added to the filter. This was left to incubate for 2 minutes before spinning for 2 minutes to collect the plasmid DNA.

All six samples were sequenced and 80% contained the desired C to G mutation. Two of the glycerol stocks of the successful preps were streaked onto agar plates, cultured and taken through a MidiPrep before sending for full sequencing.

5.2.7 Envelope and packaging plasmid preparation

Glycerol stocks of the pMD2.G (Addgene plasmid 12260) and psPAX2 (Addgene plasmid 12259) plasmids had been previously prepared by another member of the research group. These were streaked onto agar plates containing 100µg/ml ampicillin. Colonies were taken through a MidiPrep and stored at -20°C.

5.2.8 pInducer20 plasmid prep

A pre-prepared glycerol stock of the pInducer20 vector (Figure 5.3) was streaked onto agar plates containing 50µg/ml ampicillin and 30µg/ml chloramphenicol. These were left to incubate at 30°C instead of 37°C. Colonies were taken through a MidiPrep to purify the empty vector.

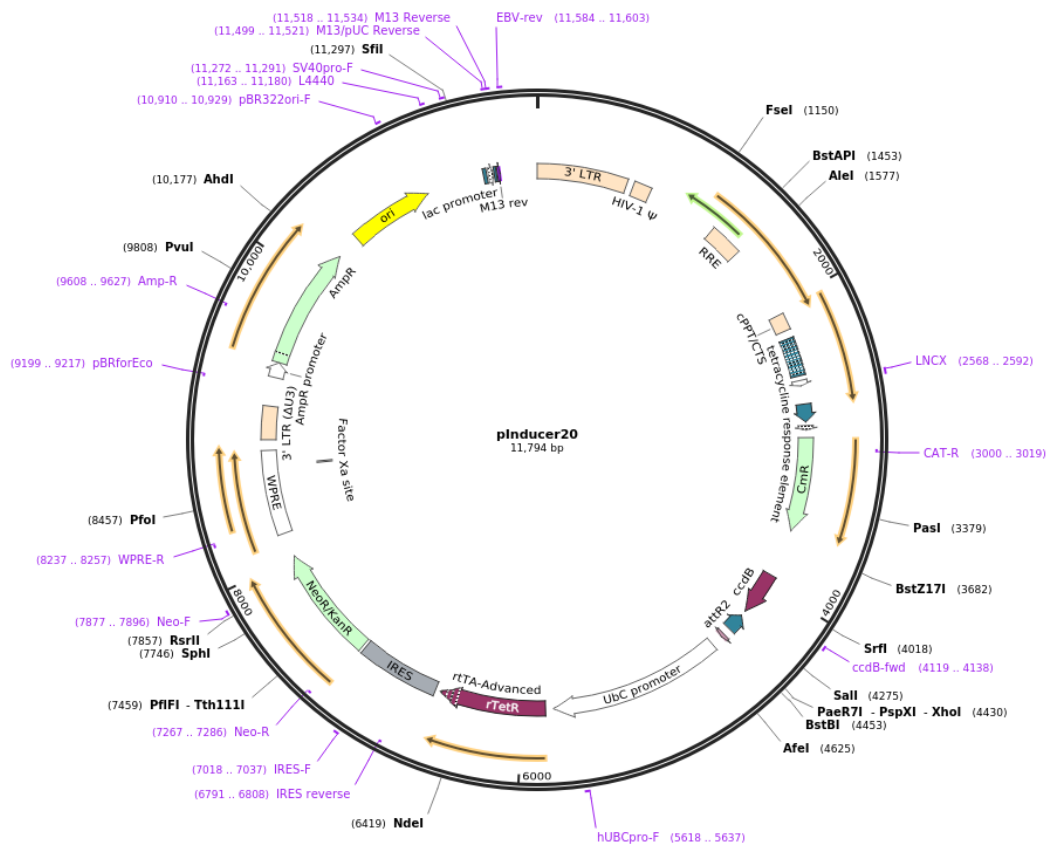


Figure 5.3: A map of the pInducer20 vector used as the destination vector (from www.addgene.org)

5.2.9 LR recombination reaction

The pInducer20 vector was used to perform the LR recombination reaction with the entry vectors. The components in Table 5.12 were added to 1.5ml tubes.

Component	Sample Reaction (WT)	Sample Reaction (MUT)	Positive control	Negative control
Entry vector (WT)	1.24 μ l*			
Entry vector (MUT)		1 μ l*		1 μ l*
pENTR-gus			2 μ l	
pInducer20 (150ng/ μ l)	1 μ l	1 μ l	1 μ l	1 μ l
TE buffer	5.76 μ l	6 μ l	5 μ l	8 μ l
*The volumes of plasmid used are to ensure that 50–150ng is used for the reaction				

The Gateway® LR Clonase® II enzyme mix was thawed on ice for 2 minutes and vortexed twice for 2 seconds. 2 μ l of the enzyme mix was added to each reaction except the negative control and they were vortexed twice for 2 seconds. The reactions were incubated at 25°C overnight. In the morning, 1 μ l proteinase K was added to each reaction and they were incubated at 37°C for 10 minutes before storing at –20°C for a few days.

5.2.10 Stbl3 cell transformation

Five vials of Stbl3 cells were thawed on ice. 2 μ l of each LR recombination, and 2 μ l of a green fluorescent protein (GFP)-pInducer20 plasmid prepared by another student, were added to the vials (one reaction per vial). They were gently mixed by swirling and tapping, and incubated on ice for 30 minutes. Following this, the vials were heat shocked at 42°C for 45 seconds then returned quickly to ice for 2 minutes. 250 μ l of pre-

warmed SOC medium was added to each vial and they were shaken at 225rpm at 30°C for 1 hour. The transformations were spread onto agar plates containing the appropriate antibiotics and incubated at 30°C overnight.

In the morning, the positive control plate had many colonies but none of the pInducer20 based vectors had grown any colonies. Troubleshooting revealed that once the pInducer20 vector is used for cloning it loses its resistance to chloramphenicol. However, this does not explain why the empty vector did not produce colonies. Further transformations (including the pUC19 positive control) eventually yielded colonies for all required vectors. The pUC19 transformation efficiency was low, but using the pMD2.G to test the transformation protocol resulted in a lawn of colonies. Further troubleshooting would be useful in this area. However, successful MidiPreps of each plasmid were obtained and the presence of the PNPLA3 sequence in the pInducer20 vector confirmed by sequencing from Source Bioscience using the LNCX forward primer and the pInducer20 reverse primer.

5.2.11 Lentivirus production

HEK 298FT cells were seeded at a density of 1.2×10^6 cells per dish in 10cm cell culture dishes. The medium used was Minimum Essential Medium Eagle (Sigma M4526) supplemented with 10% FBS but no antibiotic. After 24 hours, the cells were transfected as follows. A transfection complex was prepared for each lentivirus in a 2ml tube. This consisted of 600µl Opti-MEM media, 2µg of the pInducer20 plasmid containing the sequence of interest (or the empty vector), 2µg of the pMD2.G envelope plasmid, 2µg of the psPAX2 packaging plasmid, and 18µl of X-tremeGENE HP transfection reagent (Roche). The 3:1 ratio of reagent (µl) to DNA (µg) is important to maintain. The complex was left to incubate at room temperature for 30 minutes.

The MEM was removed from the dish and replaced with 7ml of Opti-MEM. 600µl of transfection complex was added dropwise around the dish, and the dish swirled gently to mix. The dishes were returned to the incubator for 6 hours. After this time, the media was removed and replaced with 10ml MEM supplemented with 10% (v/v) FBS and 2mM L-glutamine. The cells were left in the incubator for 48 hours to produce the lentiviruses. After the incubation, the media was collected into a syringe, passed through a 0.45µm filter and stored at 4°C.

To prepare for ultracentrifugation, 1ml 10% (w/v) sucrose solution was layered at the bottom of an ultracentrifuge tube. The supernatant was carefully layered on top by running it slowly down the side of the tube using a plastic pipette. The tubes were spun at 100,000×g for 2 hours at 4°C to pellet the virus. The supernatant was poured away and the tubes inverted on paper towel to ensure all liquid had been removed. 300µl PBS was added to the pellet and it was left to dissolve at 4°C overnight.

The next morning, the PBS was pipetted up and down to mix. Two 25µl aliquots of the neat virus were made. One was stored at –80°C and the other at 4°C. To the rest of the virus in PBS, 50% (v/v) glycerol was added in the ratio 1:1 and 50µl aliquots made. One was stored at 4°C and the rest at –80°C.

5.2.12 QuickTiter Lentivirus Titer Kit (Cell Biolabs)

This enzyme immunoassay measures the lentivirus associated HIV-1 p24 core protein which allows for the calculation of virus titer.

For each virus, four samples were measured: one with glycerol stored at 4°C, one without glycerol stored at 4°C, one with glycerol stored at –80°C, and one without

glycerol stored at -80°C . This enabled us to determine if freezing reduced virus titer or if the additional of glycerol for storage also affected virus titer.

The frozen samples were thawed on ice. To each samples, $10\mu\text{l}$ of ViraBind Lentivirus reagent A was added and mixed by tapping, followed by $10\mu\text{l}$ of ViraBind Lentivirus reagent B which was also mixed in by tapping. All samples were incubated at 37°C for 30 minutes.

A serial dilution of the HIV-1 p24 antigen was made using sample diluent from 100ng/ml ($10\mu\text{l}$ of the neat standard with $990\mu\text{l}$ sample diluent) down to $1.5625\text{ng}/\mu\text{l}$. A blank tube contained $500\mu\text{l}$ sample diluent alone. These were incubated at 37°C for 30 minutes.

Once the samples had finished their incubation, they were centrifuged at $13000\times g$ for 5 minutes at room temperature to pellet the virus. The supernatant was carefully removed with a pipette, then $250\mu\text{l}$ sample diluent added to each tube. They were vortexed then incubated for a further 30 minutes at 37°C . All samples and standards were loaded onto the plate in duplicate, $100\mu\text{l}$ in each well. The plate was covered with a plate cover and left to incubate overnight at 4°C . In the morning the wells were emptied by aspiration. The $10\times$ wash buffer was diluted 1:9 with sterile water to create $1\times$ wash buffer. This was used to wash the wells three times ($250\mu\text{l}$ each time). After the last wash, the plate was tapped onto paper towel to remove any remaining liquid. The FITC-conjugated anti-p24 monoclonal antibody was diluted 1:1000 with assay diluent, then $100\mu\text{l}$ added to each well. The plate was incubated at room temperature on an orbital shaker for 1 hour. Then three more washes were performed. The second antibody, HRP-conjugated anti-FITC monoclonal antibody, was diluted 1:1000 with assay diluent and $100\mu\text{l}$ added to each well. Again, the plate was incubated at room temperature on an orbital shaker for 1 hour. After three more washes, $100\mu\text{l}$ substrate

solution was added to each well. The colour changed rapidly so the plate was only left for about 5 minutes before 100 μ l of the stop solution was added. The absorbance was read at 450nm.

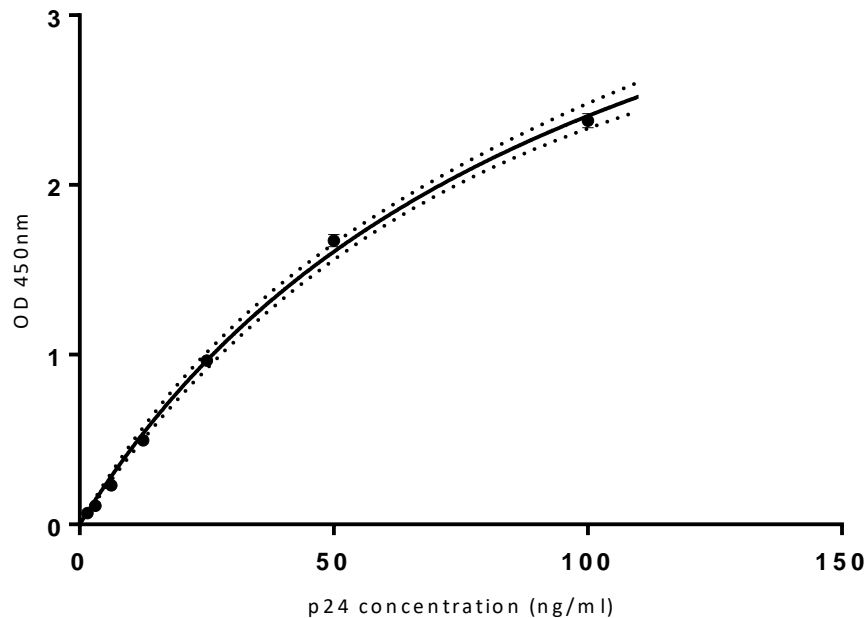


Figure 5.4: Standard curve for the lentivirus ELISA drawn using hyperbolic fit

The lentivirus sample ODs fell above the range of the standard curve (Figure 5.4). It was not possible to repeat the ELISA with a diluted samples, so p24 concentrations were estimated using GraphPad Prism to extrapolate from the standard curve (using a hyperbolic fit as the curve was not linear, see Figure 5.4). From these values, the number of lentivirus particles per ml (LP/ml) was estimated. TU/ml is estimated to be between 100 and 1000 fold lower than LP/ml so the value 500 times lower was used for further calculations.

5.2.13 Transfection test on COS7 and HepG2 cells

HepG2 cells were cultured in DMEM (Sigma D6546) with 10% (v/v) FBS, 100U/ml penicillin, 100µg/ml streptomycin and 2mM L-glutamine. COS7 cells were cultured in DMEM (Sigma D5796) with 10% (v/v) FBS, 100U/ml penicillin, 100µg/ml streptomycin and 2mM L-glutamine.

In order to estimate the cell number at time of infection, cells were seeded in a 12-well plate at 1.48×10^5 (HepG2) or 2×10^4 (COS7) cells per well. The next morning the cells were trypsinised and counted using a haemocytometer. From knowing the cell densities and the viral titer it was possible to calculate how much virus would be needed per well to achieve a multiplicity of infection (MOI) of 5 TU/cell.

To test the virus transfection, COS7 and HepG2 cells were seeded in 12-well plates at the densities above. The next day, aliquots of media were prepared containing 5µg/ml polybrene and the appropriate volume of each virus (WT, MUT, GFP, NC) to achieve MOI=0.5 TU/cell. The viruses were thawed on ice and kept on ice. The media was changed to the virus containing media. Some wells were left non-transfected and the media was simply changed to media containing polybrene only. After 4 hours of transfection, the media was changed to media containing 1µg/ml doxycycline in order to induce lentiviral gene expression. One plate of each cell type was not induced and was viewed under a fluorescence microscope. There was no fluorescence visible in the GFP transfected wells at this time as expected. At 24 hours one plate of each cell type was viewed under the fluorescence microscope and there was still no fluorescence and this was the same at 48 hours. At each time point the wells were harvested into 1×SDS mix with protease inhibitors and stored at -20°C .

As the transfections appeared not to be infective at this MOI, a range of MOIs were tried using the GFP virus on HepG2 cells on a 96-well plate (seeded at 5×10^3 cells per well).

Using the same protocol and time scale as above, MOIs of 0, 0.5, 1, 1.5, 2 and 2.5 TU/cell were tested. At 24 hours there was a very small amount of fluorescence observed in one MOI=1.5 TU/cell well, one MOI=2 TU/cell well and all MOI=2.5 TU/cell wells. At 48 hours, this had increased and was apparent in more wells. However, the transfection was not consistent or efficient. The best result was in one well with MOI=2.5 shown in Figure 5.5. It is possible that at higher MOIs there would have been higher transfection efficiency.

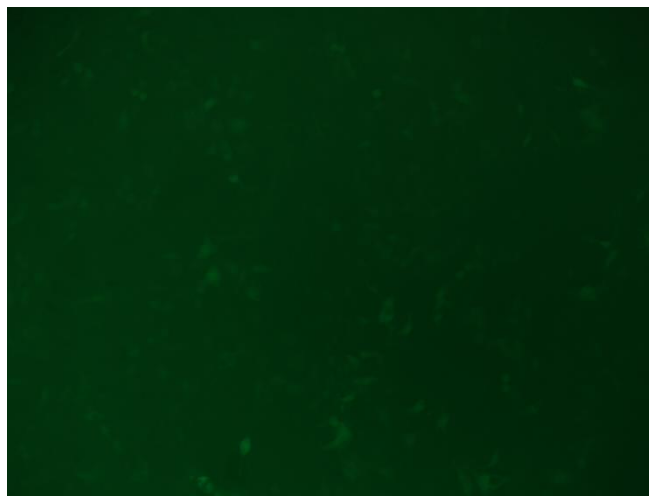


Figure 5.5: GFP fluorescence in HepG2 cells transfected with a GFP lentivirus with MOI=2.5 TU/cell for 48 hours

5.2.14 Lentivirus tests in MCF7 and HepG2 cells

The WT, MUT and negative control lentiviruses were tested on MCF7 cells (a breast cancer cell line) by Wichitra Asanprakit, using a whole aliquot of virus per well. MCF7 cells were seeded onto a 12-well plate at a density of 2×10^5 cells per well in 1ml of EMEM (Minimum Essential Medium Eagle, Sigma M2279) supplemented with 10% (v/v) FBS, 2mM L-glutamine, 1mM sodium pyruvate, 1% (v/v) MEM non-essential amino acids, and 10 μ g/ml insulin. They were incubated for 24 hours. The media was then replaced with EMEM containing 10 μ g/ml polybrene. The lentiviruses were thawed on

ice and one 50 μ l aliquot added dropwise over one well (estimated MOI 5 TU/cell). The plate was gently shaken to ensure even distribution, then incubated for 4 hours. One well was left as a non-transfected control. After the 4 hours, the media was replaced to contain 1 μ g/ml doxycycline and incubated for 48 hours. Samples were harvested for RNA and protein extraction. RNA and protein were extracted by Wichitra Asanprakit. cDNA was synthesised from the RNA using the RevertAid RT Reverse Transcription Kit as previously described. RT-qPCR using SYBR Green and PNPLA3 primers (Table 4.2) was carried out as previously described undiluted cDNA to determine if there was higher expression in the WT and MUT lentivirus treated samples. Samples were measured in triplicate. CP values were compared using one-way ANOVA with post-hoc Bonferroni multiple comparisons.

The above protocol was repeated with HepG2 cells but also including the GFP lentivirus and using standard HepG2 growth media (see section 2.1.1). Cells were only harvested for RNA analysis and were extracted using the phenol chloroform method (see section 4.2.3) apart from the cells were harvested straight into 1ml Qiazol).

5.2.15 PNPLA3 antibody optimisation

In order to measure any resulting increase in PNPLA3 protein levels from lentiviral transfection, it was necessary to identify an antibody that could detect it. The predicted molecular weight of the PNPLA3 protein was 53kDa.

The first antibody attempted was from Abcam. Samples from the first attempted HepG2 transfection (section 5.2.13) that had been induced for 48 hours were used. The protein concentration was measured by 2D Quant Assay as previously described and the samples diluted to 1 μ g/ μ l. 10 μ g protein was loaded into each well of a 10-well gel. The standard Western blot protocol previously described (section 2.2.3) was used, with 5%

(w/v) milk powder as the blocking agent. The primary PNPLA3 antibody was diluted 1:1000 and the secondary antibody (anti-rabbit IgG HRP-linked antibody, #7074 Cell Signalling Technologies) was diluted 1:5000. ECL was used as the detection method. No bands were seen in any lanes.

Total HepG2 protein from non-transfected cells was harvested and the concentration determined to be approximately 1µg/µl by 2D Quant assay. This total protein, containing all endogenous HepG2 proteins, was used for future antibody optimisation to try and detect the endogenous PNPLA3 protein.

An 18-well gel was loaded with varying volumes of protein from 5µl to 20µl. The membrane was cut into four strips in order to test the combinations in Table 5.13.

Membrane	Primary antibody	Secondary antibody	Detection method
A	PNPLA3 1:5000	1:20000	ECL Select
B	PNPLA3 1:5000	1:40000	ECL Select
C	PNPLA3 1:1000	1:2500 Plex Cy5	Fluorescence
D	Total AKT 1:1000	1:5000	ECL

Strong bands were detected on membranes A and B at about 80kDa but this is not the correct size. The fluorescent secondary antibody was unsuccessful. The total AKT antibody showed bands of the correct size, demonstrating that the protocol itself was working.

On advice from the manufacturer, different blocking agents were attempted. A new membrane was cut into three strips, each with a lane of approximately 5µg, 10µg and 20µg HepG2 protein. The blocking agents tried were 5% (w/v) milk powder, 5% (w/v)

BSA and 2% (w/v) ECL select blocking agent. The primary PNPLA3 antibody was used at 1:5000 for all membranes and the secondary at 1:40000. ECL Select was used for detection. The bands were still the wrong size and multiple bands were detected (Figure 5.6).

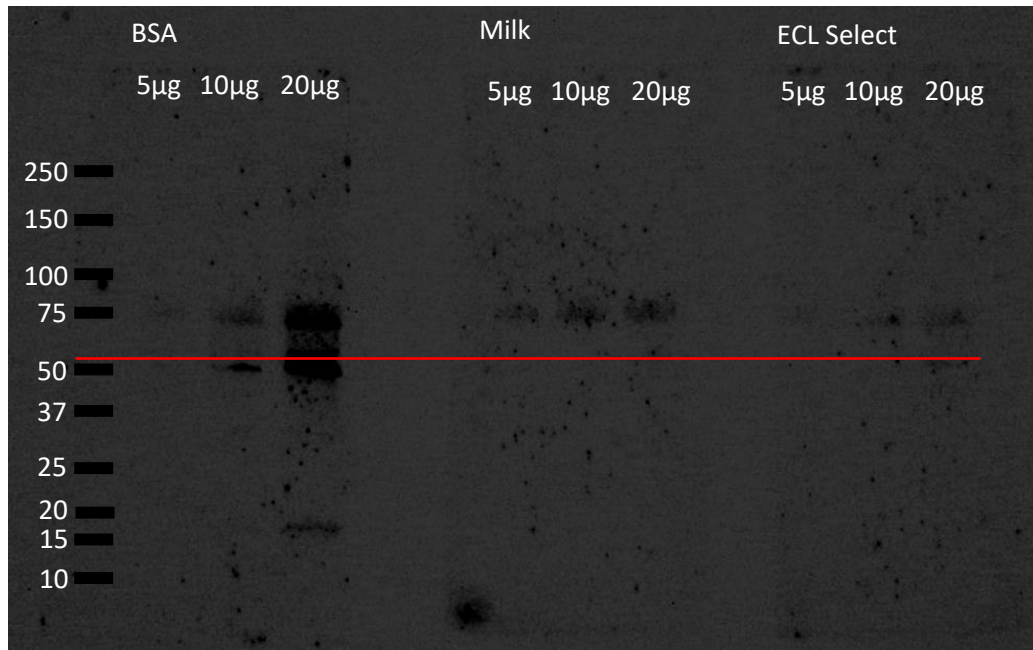


Figure 5.6: Western blots of HepG2 protein (5µg, 10µg and 20µg protein per lane) using the Abcam PNPLA3 antibody and three different blocking agents; 5% milk, 5% BSA and 2% ECL Select blocking agent. Red line indicates expected band size.

A new primary antibody was purchased from Sigma. More HepG2 cell protein was run on a gel with either 5µl, 10µl or 20µl per lane (approximately equating to 5µg, 10µg and 20µg protein). Various conditions were attempted (Figure 5.7). Blocking with 5% (w/v) BSA caused complete non-specific binding whereas blocking with 5% (w/v) milk powder resulted in no bands (blots not shown). Using 2% (w/v) ECL Select block proved most effective, but the strongest band was not the correct size (Figure 5.7) and there was still a lot of non-specific binding.

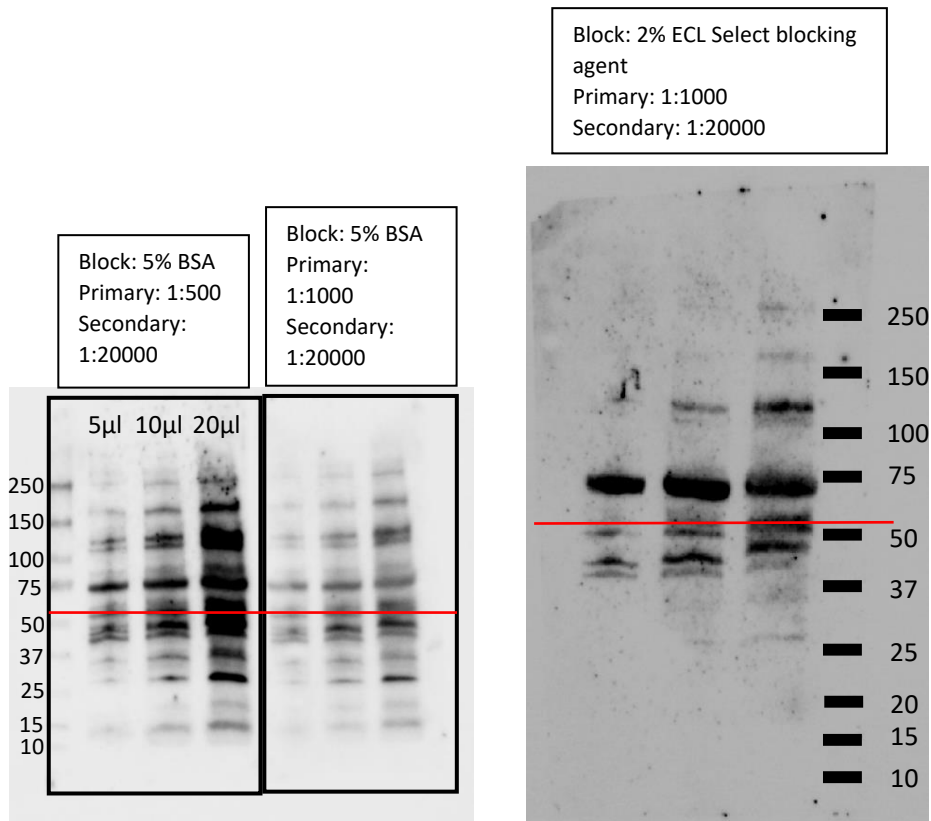


Figure 5.7: Western blotting conditions attempted to optimise the Sigma PNPLA3 antibody: varying the blocking agent and antibody concentrations. Percentages are (w/v). Red lines indicate expected band size.

On advice from the manufacturer, another gel was attempted but with increased Tween concentration in TBST from 0.1% (v/v) to 0.3% (v/v) for all washes. This did not stop non-specific binding in BSA blocked membranes and prevented any binding in the membrane using 2% (w/v) ECL Select blocking agent (Figure 5.8).

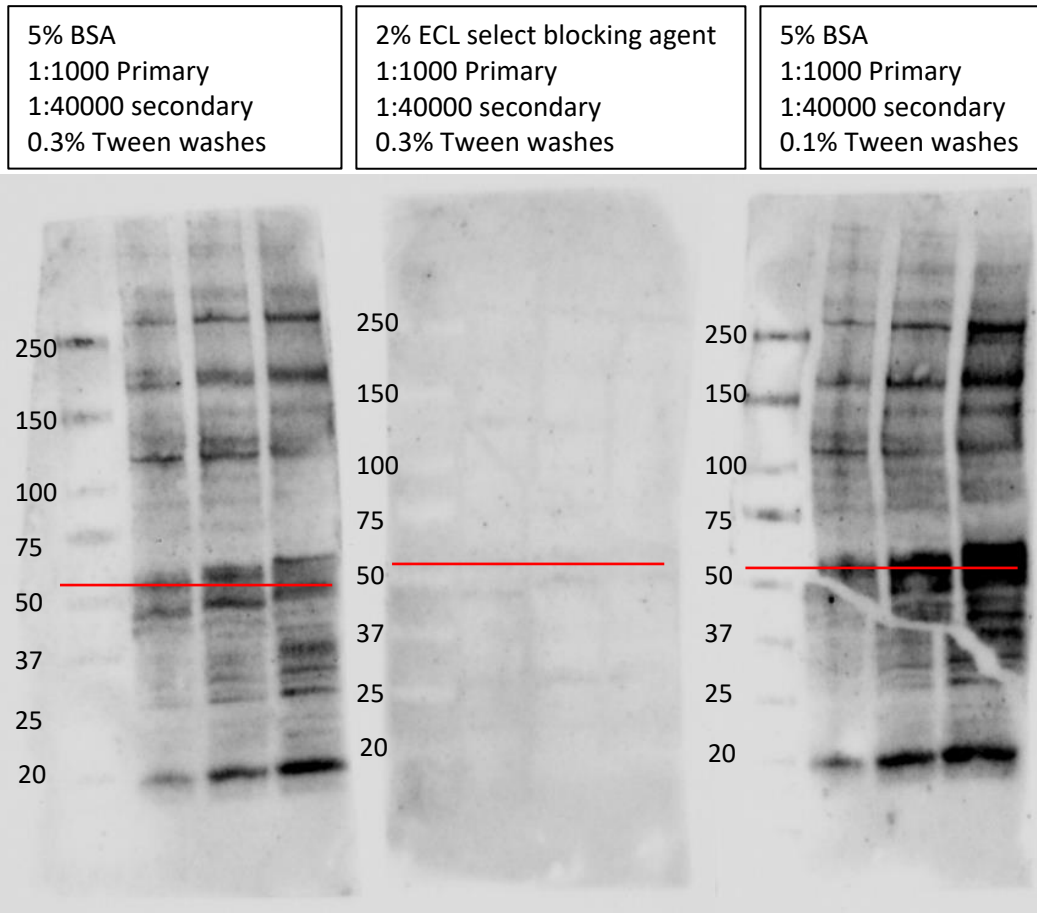


Figure 5.8: Further Western blotting conditions attempted to optimise the Sigma PNPLA3 antibody: increasing the Tween percentage in the wash steps. Percentages for blocking agent are (w/v) and for Tween are (v/v). Red lines indicate expected band size.

Time constraints prevented further optimisation of these antibodies.

5.3. Results

5.3.1 Genotyping of HepG2 cells, Huh7 cells and donor livers

HepG2 and Huh7 cells were confirmed by sequencing to be homozygous for the polymorphism as previously reported (Green et al., 2015a, Min et al., 2014). We were then able to use these cells to confirm the results of the SNP TaqMan genotyping assay. Both HepG2 and Huh7 cells were identified as GG using the assay, as was expected (Table 5.14). Out of the six livers, L312 and L319 were heterozygous, whereas L317, L321, L326 and L329 were homozygous wild-type CC (Table 5.14). The endpoint scatter plot (allelic discrimination plot) is shown in Figure 5.9. A summary of the genotypes and the responses to nutritional stimuli from section 3.4.3 are shown in Table 5.15.

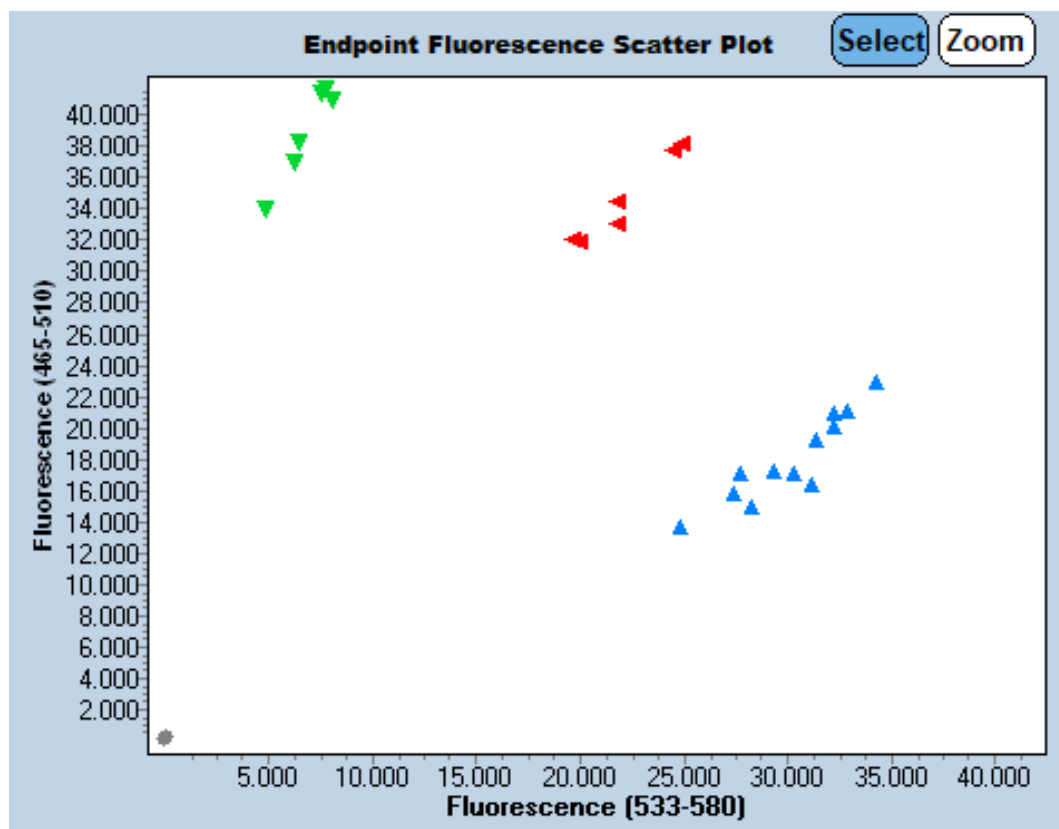


Figure 5.9: Endpoint fluorescence scatter plot from the SNP TaqMan genotyping assay. Green = GG, red = CG, blue = CC

Table: 5.14: Raw data and allele calls from the SNP TaqMan genotyping assay. Allele X: C, Allele Y: G

DNA	Endpoint Fluorescence		Call	Score	Genotype
	533-580 (VIC)	465-510 (FAM)			
HepG2	4.932	33.856	Allele Y	0.94	GG
	6.267	36.82	Allele Y	1	
	6.474	38.225	Allele Y	1	
Huh7	7.784	41.568	Allele Y	0.95	GG
	7.574	41.273	Allele Y	0.96	
	8.103	40.909	Allele Y	0.92	
L312	20.066	31.879	Both Alleles	0.98	CG
	19.719	32.06	Both Alleles	0.95	
	24.554	37.734	Both Alleles	0.98	
L317	24.872	13.697	Allele X	0.92	CC
	27.402	15.907	Allele X	0.97	
	27.755	17.146	Allele X	0.97	
L319	21.845	33.06	Both Alleles	0.96	CG
	21.874	34.449	Both Alleles	0.99	
	24.92	38.137	Both Alleles	0.97	
L321	31.421	19.296	Allele X	0.98	CC
	32.858	21.041	Allele X	0.93	
	32.269	20.917	Allele X	0.92	
L326	29.324	17.295	Allele X	0.98	CC
	32.266	20.071	Allele X	0.96	
	34.226	22.914	Allele X	0.88	
L329	28.29	15.059	Allele X	0.89	CC
	31.129	16.415	Allele X	0.89	
	30.295	17.096	Allele X	0.94	

Table 5.15: Summary of the genotypes and responses of the cell lines and livers to nutritional stimuli. All cells accumulated lipid in response to fatty acid treatment. McA-RH7777 cells not included as they could not be genotyped using the human assay. (See section 3.4.3 for full lipid accumulation data)

Cell Line / Liver	Genotype	Maximum Fold Change	Effects of glucose or fructose on lipid accumulation
HepG2	GG	4.717	<ul style="list-style-type: none"> • None
Huh7	GG	4.560	<ul style="list-style-type: none"> • None
L312	CG	4.822	<ul style="list-style-type: none"> • Increase between 5mM and 11mM glucose with fatty acids present • Increase between 0mM and 8mM fructose with fatty acids present
L317	CC	3.278	<ul style="list-style-type: none"> • Greater increase with 2mM or 8mM fructose treatment with fatty acids present
L321	CC	1.403	<ul style="list-style-type: none"> • Increase between 5mM and 11mM glucose with fatty acids present • Decrease between 5mM and 11mM glucose without fatty acids present
L326	CC	1.916	<ul style="list-style-type: none"> • Increase between 5mM and 11mM glucose with fatty acids present
L329	CC	2.715	<ul style="list-style-type: none"> • Fatty acid × fructose interaction of unclear direction (see Table S10)
Note: L319 was not used for the fatty acid × glucose × fructose experiment			

5.3.2 Lentiviral transfection of MCF7 and HepG2 cells

In MCF7 cells, there was an effect of transfection on PNPLA3 expression ($P < 0.001$). The CP values for the non-transfected cells and the negative control transfected cells were not significantly different (Table 5.16). These values should be endogenous expression only. Both the WT and MUT virus transfected cells showed an increase in PNPLA3 expression but the WT virus gave a significantly lower CP value of about 22.5 compared to the MUT virus at 26.5, suggesting that the WT virus resulted in higher PNPLA3 expression (Table 5.16).

Table 5.16: PNPLA3 expression in MCF7 cells transfected with lentiviruses, measured by CP value			
Sample	CP value (mean±SD)	Bonferroni	s.e.d
WT virus transfected	22.52±0.11	a	0.1234
MUT virus transfected	26.52±0.05	b	
Non transfected	29.72±0.24	c	
Negative control virus transfected	30.11±0.14	c	

In HepG2 cells, the differences between the CP values were much smaller but there was still an overall effect of transfection ($P < 0.001$), and both WT and MUT virus transfection resulted in significantly higher CP values than negative control virus transfection (Table 5.17). The highest expression was seen in the WT virus transfected cells (Table 5.17). There was a significant difference in PNPLA3 expression between two non-transfected samples (Table 5.17) suggesting there may have been contamination of non-transfected sample 1. The CP values suggested higher baseline expression of PNPLA3 in HepG2 cells.

Table 5.17: PNPLA3 expression in HepG2 cells transfected with lentiviruses, measured by CP value

Sample	CP value (mean±SD)	Bonferroni	s.e.d
WT virus transfected	22.29±0.13	a	0.0893
MUT virus transfected	22.72±0.13	b	
Non transfected sample 1	22.92±0.12	bc	
GFP virus transfected	23.05±0.08	c	
Non transfected sample 2	23.56±0.08	d	
Negative control virus transfected	23.53±0.10	d	

5.4. Discussion

5.4.1 Summary of results

The main findings of this chapter are as follows:

- HepG2 and Huh7 cells were confirmed to be the GG genotype. All donor livers used for PHH preparation were either CC or CG.
- The WT and MUT viruses resulted in PNPLA3 mRNA overexpression in MCF7 cells, but WT resulted in much higher expression than MUT.
- HepG2 cells appeared to be successfully transfected but expression was markedly reduced compared to MCF7 cells.
- The Sigma and Abcam PNPLA3 antibodies were not successful at detecting the PNPLA3 protein under the conditions tested.

5.4.2 Genotyping

Of all the livers used for this thesis, four were homozygous wild-type (CC) and two were heterozygous (CG). In two studies using European participants, polymorphic homozygotes (GG) made up 7% of the sample (Pirazzi et al., 2012, Romeo et al., 2010) so, as individuals were not selected on the basis of displaying NAFLD, it is not surprising that we did not come across any GG livers. In the same studies, the proportions of heterozygotes were 36% and 38% which is consistent with a third of our small sample being heterozygous. Using our method in Chapter 3 to look at the effect of PNPLA3 genotype on lipid accumulation in response to nutritional stimuli would require specifically selecting patients with the GG genotype. This would be dependent on whether such patients were undergoing elective surgery requiring liver biopsy or resection, which could take an extended period of time to generate the number of samples required to show statistically validated results. This demonstrates the need for

other technologies, such as lentiviruses, in order to study this polymorphism. Gene editing technologies offer the advantage of the ability to change just one gene in an otherwise genetically identical batch of PHH.

HepG2 and Huh7 cells were found to be homozygous for the polymorphism, confirming results found by others (Green et al., 2015a, Min et al., 2014, Dutta, 2015). As the SNP TaqMan genotyping assay was for human samples it was not possible to run the rat derived McA-RH7777 cells with this assay, but others have reported that this cell line is homozygous wild-type (Pirazzi et al., 2012). Lentiviruses would offer the opportunity to produce stably transfected cell lines, for example HepG2 and Huh7 cells expressing the wild-type variant, to see if changing their genotype aligns them more closely to PHH in their lipid accumulation phenotype. It has been suggested that Huh7 cells do not express PNPLA3 at the protein level as it was undetectable at the endogenous level, and the cells accumulated a similar amount of lipid to those overexpressing the wild-type variant (Ruhanen et al., 2014). A direct comparison between HepG2 and Huh7 cells would be useful to clarify this further, and to determine whether the endogenous protein levels within the cell types could affect their behaviour. However, we found that HepG2 and Huh7 cells were very similar in their lipid accumulation pattern (Chapter 3).

5.4.3 Technologies for detecting PNPLA3 overexpression

We did not find an antibody that would successfully detect the endogenous PNPLA3 protein in HepG2 cells despite following the instructions and advice of the manufacturers. Therefore, we used RT-qPCR to measure overexpression. This method could potentially amplify any unincorporated lentiviral vector in the sample, so it is not an ideal method for accurate determination of expression. However, it gives some indication of whether the lentiviruses are effective. In MCF7 cells, the WT and MUT

viruses did result in increased PNPLA3 expression but the WT virus was more effective at inducing overexpression. If this is because of differences in virus transduction efficiency, or inducibility between these two viruses, then optimisation would be required to achieve a comparable level of overexpression to prevent false conclusions being drawn. The advantage in using the pInducer20 vector is that expression can be turned up or down using doxycycline (Meerbrey et al., 2011). It would be interesting to see if the WT virus also results a higher protein expression within the cells.

5.4.4 Lentivirus optimisation

At an MOI of 2.5 TU/cell there was a small amount of fluorescence in HepG2 cells transfected with a GFP lentivirus. In contrast, in the experiment using 50µl virus per well (estimated MOI between 6 and 7 TU/cell) there was no GFP fluorescence or overexpression as measured by RT-qPCR. An MOI of 5 TU/cell has been shown to effectively induce GFP expression in Huh7 and HepG2 cells, with Huh7 cells being more efficiently transduced than HepG2 (Zamule et al., 2008). It could be that the lentiviruses had been in storage for too long by this point and had a reduced titer. Preparation of a fresh virus and repeating the experiment would help to determine if this is the case.

Lentiviruses have the ability to transduce non-dividing cells, making them ideal for work with primary cells. Lentiviral transfection of PHH at an MOI of 10 TU/cell does not alter levels of various nuclear receptors, does not inhibit albumin secretion, and does not interfere with CYP3A4 induction, suggesting that their differentiation status is not affected (Zamule et al., 2008). However, as PHH are only viable for a short time in culture, careful planning would be necessary. The lentiviral transfection and induction process takes over 3 days using the method in section 5.2.14, and it is possible that PHH may de-differentiate by the time they are transfected and ready for experimentation.

5.4.5 PNPLA3, lipid accumulation and diet

The genotypes and responses of the livers have been summarised in Table 5.15. However, with only five livers in the experiment observing the effects of glucose, fructose and fatty acids, it is not possible to draw clear conclusions as to whether the PNPLA3 genotype was a factor in the differences in lipid accumulation between livers. Of interest, the heterozygote L312 did show one of the most dramatic changes in lipid accumulation due to glucose and fructose treatment in the presence of fatty acids (Figure 3.12), and reached the highest fold change of all the livers, even surpassing the human cell lines (Table 5.15). However, it was not the only liver to display lipid accumulation in response to fructose treatment so it is unlikely that genotype is the only factor mediating this response. In the experiment observing the effects of glucose, insulin and fatty acids, the heterozygote L319 also showed a large increase in lipid accumulation in response to glucose when fatty acids were present (Figure 3.16). Further work could help determine if PNPLA3 genotype influences lipid accumulation in response to glucose and fructose. It has been hypothesised that PNPLA3 genotype could determine response to fructose restriction (McGeoch et al., 2018) but a study is yet to be done.

There have been a number of studies demonstrating that PNPLA3 genotype may influence an individual's hepatic response to dietary factors. For example, the presence of the GG allele may influence the liver's response to dietary omega 6 to omega 3 ratio; in a study of children and adolescents, there was only an association between n-6 to n-3 ratio and liver fat in subjects with the GG genotype rather than CG or CC (Santoro et al., 2012). Another study using children found that the response to treatment of NAFLD with DHA was reduced in patients homozygous for the I148M mutation (Nobili et al., 2013). In addition, in a study of Hispanic children, hepatic fat content was positively correlated to dietary carbohydrate, total sugar and added sugar intake independently of total

energy intake only in subjects homozygous for the I148M mutation (Davis et al., 2010).

This is compelling evidence that PNPLA3 genotype could influence an individual's hepatic response to diet, although the associations do not prove cause and effect.

Animal studies have shown a responsiveness of PNPLA3 to dietary carbohydrate. Mice fed a high carbohydrate diet had a 7-fold increase in PNPLA3 mRNA which correlated to liver fat (Hao et al., 2014). Addition of a lipid supplement (mainly MUFA and PUFA) to the diet prevented the increase in PNPLA3 mRNA in a dose-dependent manner (Hao et al., 2014). Although a high fat diet also resulted in increased liver fat, PNPLA3 was not upregulated. PNPLA3 expression has been shown to be induced by glucose and insulin (Rae-Whitcombe et al., 2010), with the effect of insulin mediated by SREBP1c (Qiao et al., 2011). In immortalised human hepatocytes, silencing ChREBP abolishes the upregulating effect of high glucose (11mM) on PNPLA3, suggesting that ChREBP is a mediator of the effects of carbohydrates on PNPLA3 regulation (Perttila et al., 2012). In contrast, our RT-qPCR data in Chapter 4 (section 4.3.1.4) did not show an effect of glucose or fructose on PNPLA3 expression in HepG2 cells; there was only a reduction in expression with fatty acid treatment. In PHH there were no significant effects of treatment on PNPLA3 mRNA, but a slight trend towards an effect of glucose ($P=0.154$) would be worth further investigation with more replicates. In HepG2 cells PNPLA3 expression was correlated to SREBP1c expression ($P<0.001$) but not in PHH, and there was no correlation with ChREBP in either cell type (Table 4.18).

One study found that 50 μ M fatty acid treatment upregulated PNPLA3 mRNA expression in HepG2 cells overexpressing either the wild-type or polymorphic variant, although this did not translate to the protein level (Liu et al., 2016b). This is in contrast to the mRNA decrease that we found with endogenous HepG2 PNPLA3; we found a down-regulation of both PNPLA3 and SREBP1c in HepG2 cells. This could be due to the composition of the

fatty acids used. We used a mix of fatty acids which included PUFA (linoleic acid) whereas Liu et al. (2016b) only used oleic and palmitic acids. PUFA selectively suppress SREBP1 expression and also suppress proteolytic processing of the SREBP1 protein, resulting in an auto-loop regulatory circuit (Takeuchi et al., 2010). This in turn could influence PNPLA3 expression. It would be useful to have a universally agreed mix and concentration of fatty acids used for NAFLD research to prevent discrepancies in results from this source. Also, a lot of conclusions are drawn from *in vitro* experiments using only oleic and palmitic acids but it is unphysiological to have a PUFA-free environment, as discussed in section 3.4.2. Further investigation is needed into the nutritional regulation of PNPLA3 and whether this translates between cell lines and PHH.

5.4.6 Concluding remarks

The PNPLA3 genotypes of HepG2 and Huh7 cells were confirmed to be GG as previously described, and all livers used for PHH preparation were genotyped. Although not enough livers were used to statistically determine effect of genotype, it was interesting that a heterozygous liver had the greatest effect of fructose on lipid accumulation by magnitude. Human PNPLA3 cDNA was successfully cloned into a lentiviral vector and mutagenesis used to create both WT and MUT viruses. Unfortunately, we were unable to successfully transfect and detect the PNPLA3 protein in HepG2 cells or PHH. However, once optimised, the system could be valuable for studying the PNPLA3 genotype and how it interacts with nutritional stimuli to induce lipid accumulation. Special consideration will need to be given to how to transduce, induce, treat and harvest/assay PHH before they lose viability. The function and regulation of PNPLA3 is still a developing area; more work is required to progress *in vitro* technologies that will help

identify its role in NAFLD development, and move beyond associations to causal mechanisms which can be targeted in the treatment of NAFLD.

Chapter 6: General discussion

The first conclusion of this work is that hepatoma cell lines and primary human hepatocytes do not behave the same in response to nutritional stimuli. This was shown by treating HepG2, Huh7, McA-RH7777, and PHH with glucose, fructose, and fatty acids and observing that whilst they all accumulated lipid in response to fatty acid treatment, the responses to monosaccharides were dependent on cell type (Table 6.1). We hypothesised that the hepatoma cell lines would not accumulate lipid in response to glucose or fructose, but while this was true for HepG2 and Huh7 cells, McA-RH7777 cells did accumulate lipid with 11mM glucose treatment when 200 μ M fatty acids were present. We demonstrated that HepG2 and Huh7 cells responded in a similar manner to each other and evidence is presented that both cell lines are insulin resistant. The microarray analysis showed that there are fundamental differences in gene expression between HepG2 cells and PHH even before treatment with nutritional stimuli, for example the upregulation of cytochrome P450 pathways in PHH and the upregulation of the cell cycle pathway in HepG2 cells demonstrating the proliferative versus differentiated phenotypes we expected to see. The RT-qPCR data showed that genes do not respond to nutrients in the same way across the two cell types; the unexpected downregulation of SREBP1a and SREBP1c by fructose in PHH but not HepG2 cells warrants further investigation. Overall, there was more response to fatty acid treatment in HepG2 cells, specifically downregulation of lipogenic genes. Table 6.1 summarises the main findings.

Another hypothesis was the PNPLA3 genotype would determine lipid content, with the polymorphic variant resulting in higher lipid accumulation. There was not enough data to statistically determine if genotype affected lipid content, but imaging of the cell lines suggested that McA-RH7777 cells had the lowest baseline lipid content, and these cells

have been shown by others to be homozygous wild type (Pirazzi et al., 2012). We also found that the liver with the highest fold change in lipid content was heterozygous which supports the original hypothesis. Developing an appropriate method for studying and manipulating the PNPLA3 genotype in cell lines and primary cells will be key to taking this work further.

		Primary Human Hepatocytes	HepG2	Huh7	McA-RH7777
Increase in lipid accumulation over 48 hours in response to:	Fatty acids (0 μ M vs 200 μ M)	Yes	Yes	Yes	Yes
	Glucose (5mM vs 11mM)	With fatty acids present (but dependent upon individual liver)	No	No	With fatty acids present
	Fructose (0mM vs 2mM vs 8mM)	Yes (but dependent upon individual liver)	No	No	No
	Insulin (0nM vs 5nM vs 10nM)	Yes (but dependent upon individual liver)	Yes	Not measured	Not measured
Insulin sensitive (measured by pAKT/total AKT)		Not measured	No	No	Yes
PNPLA3 genotype		Dependent upon individual liver	GG	GG	(CC)
Gene expression points from RT-qPCR data		<ul style="list-style-type: none"> Lipogenic genes not downregulated with fatty acid treatment except SREBP1a SREBP1a and SREBP1c downregulated by fructose Express SREBP1a more highly than SREBP1c 	<ul style="list-style-type: none"> Lipogenic genes downregulated with fatty acid treatment No effects of glucose or fructose on any genes measured except ApoB Express SREBP1a more highly than SREBP1c 	Not measured	Not measured
Gene expression points from microarrays		<ul style="list-style-type: none"> Reduction in CYP1A2 and increase in PCK1 with high glucose treatment Increase in PLIN2 with fatty acid treatment 	<ul style="list-style-type: none"> Cytochrome P450 pathways downregulated compared to PHH 	Not measured	Not measured

One limitation of this work is that the lipid accumulation of the four cell types could not be compared to each other using statistical tests. Combining the hepatoma cell lines and primary cells into one analysis would mean that different experiments with the primary cells represent biological replication whereas different experiments with the cell lines only represent technical replication. Also, fold change values were used for the ANOVA analysis meaning that the values cannot be compared to a control from another cell type. To make this type of analysis possible, absolute measurements of lipid content would need to be taken to remove effects of different baseline levels of lipid in both cell lines and primary cells. These measurements would be valuable additions to future work. However, it is that clear there were differences in the way that the four cell types responded to nutritional stimuli. For example, only certain livers showed statistically significant lipid accumulation with fructose (Figure 3.12), whereas there was no sign of fructose effects in any of the cell lines (Figure 3.10). There was also variability in lipid accumulation between PHH isolated from different livers, particularly in their response to glucose and fructose (Figure 3.12). Additionally, the maximum fold change value ranged between 1.403 and 4.822. This demonstrates the importance of using human based models for NAFLD research, as genetically identical cell lines or animal models would not highlight these important differences. Nutrigenomics and personalised nutrition is an important developing area (Isaak and Siow, 2013), and this work shows that inter-individual differences should be taken into account. The differences could be due to biological factors such as age, gender, ethnicity, and the metabolic health of the donor. It would be useful for more information about tissue donors to be provided to researchers so that these factors can be taken into account. Repeating the gene expression analysis with PHH from more livers would indicate whether gene regulation by nutrients is as variable across individuals as the lipid accumulation, as this was not possible due to limited supply.

There are many factors that make comparisons across different *in vitro* experiments in different publications difficult. For example, the concentrations and types of fatty acids used, the base media used (with or without serum), the concentrations of insulin and/or other hormones, and the conditions used as a control. Going forward, particular effort should be made to make the extracellular environment resemble the *in vivo* liver as closely as possible; for example, aiming to replicate a fatty acid profile found in human plasma and aiming to replicate portal blood concentrations of hormones and nutrients rather than circulatory concentrations. This will ensure a higher level of physiological relevance. Further measurements of portal blood concentrations, particularly of fructose, would be useful to more accurately describe the target *in vivo* environment. In addition, future research using human derived cells should include PNPLA3 genotyping as standard to help build up data about how this gene could interact with nutrients. Gene editing technologies will be key to investigating this genotype further, but these will need to be combined with techniques to maintain PHH phenotype and viability in culture for longer periods of time.

A current limitation to *in vitro* research is that the lipid accumulation induced is typically microvesicular, with lipid droplets less than 1 μ m in diameter, which affects about 10% of NAFLD patients and is linked to more severe disease progression (Green et al., 2018, Tandra et al., 2011). In mice, feeding 30% ((w/v)) fructose solution in their drinking water induced both macro- and microvesicular steatosis, but glucose feeding in the same way (30% (w/v) in drinking water) induced only macrovesicular steatosis (Softic et al., 2017). To better represent the *in vivo* liver and more accurately observe the effects of fructose, further research should aim to develop a way to induce macrovesicular lipid accumulation *in vitro*, particularly as this could interact with the PNPLA3 genotype; the amount of available surface area of the lipid droplets could influence the impact of PNPLA3 accumulation.

We did not measure lipoprotein secretion in this work as the majority of experiments were carried out in 96-well plates and the volume of media was too small for this type of analysis. However, future work should be expanded to include extracellular measurements, particularly as the main cause of death in NAFLD patients is CVD (Adams et al., 2017) which is influenced by plasma lipoproteins. As the different cell types have different VLDL secretion capacity, this could also be a factor impacting lipid accumulation.

Going forward, there are emerging technologies which may represent better models of the human liver. For example, stem cell derived hepatocytes could provide an unlimited supply of cells. Hepatocyte-like cells differentiated from both embryonic and induced pluripotent stem cells are able to accumulate lipid droplets with oleic acid treatment and show gene expression changes similar to those seen in liver biopsies upon induction of steatosis, all while maintaining liver-specific function such as cytochrome P450 enzyme activity (Graffmann et al., 2016). These cells, perhaps incorporated into a 3D co-culture model with hepatic stellate cells, offer a promising line of further research. They may also represent a better option for studies using lentiviruses due to the short lifespan of PHH.

In conclusion, hepatoma cell lines should be used with extreme caution to model NAFLD. There needs to be a shift towards better human based models which are physiologically relevant, and can take into account variability within the population.

Bibliography

- ACKERMAN, Z., ORON-HERMAN, M., GROZOVSKI, M., ROSENTHAL, T., PAPPO, O., LINK, G. & SELA, B. A. 2005. Fructose-induced fatty liver disease: hepatic effects of blood pressure and plasma triglyceride reduction. *Hypertension*, 45, 1012-8.
- ADAMEK, A. & KASPRZAK, A. 2018. Insulin-Like Growth Factor (IGF) System in Liver Diseases. *Int J Mol Sci*, 19, 1308.
- ADAMS, L. A., ANSTEE, Q. M., TILG, H. & TARGHER, G. 2017. Non-alcoholic fatty liver disease and its relationship with cardiovascular disease and other extrahepatic diseases. *Gut*, 66, 1138-1153.
- ALKHATATBEH, M. J., LINCZ, L. F. & THORNE, R. F. 2016. Low simvastatin concentrations reduce oleic acid-induced steatosis in HepG2 cells: An in vitro model of non-alcoholic fatty liver disease. *Exp Ther Med*, 11, 1487-1492.
- BASURAY, S., SMAGRIS, E., COHEN, J. C. & HOBBS, H. H. 2017. The PNPLA3 variant associated with fatty liver disease (I148M) accumulates on lipid droplets by evading ubiquitylation. *Hepatology*, 66, 1111-1124.
- BASURAY, S., WANG, Y., SMAGRIS, E., COHEN, J. C. & HOBBS, H. H. 2019. Accumulation of PNPLA3 on lipid droplets is the basis of associated hepatic steatosis. *Proc Natl Acad Sci U S A*, 116, 9521-9526.
- BECHMANN, L. P., HANNIVOORT, R. A., GERKEN, G., HOTAMISLIGIL, G. S., TRAUNER, M. & CANBAY, A. 2012. The interaction of hepatic lipid and glucose metabolism in liver diseases. *J Hepatol*, 56, 952-64.
- BEDOGNI, G., BELLENTANI, S., MIGLIOLI, L., MASUTTI, F., PASSALACQUA, M., CASTIGLIONE, A. & TIRIBELLI, C. 2006. The Fatty Liver Index: a simple and accurate predictor of hepatic steatosis in the general population. *BMC Gastroenterol*, 6, 33.
- BITTER, A., NUSSLER, A. K., THASLER, W. E., KLEIN, K., ZANGER, U. M., SCHWAB, M. & BURK, O. 2015. Human sterol regulatory element-binding protein 1a contributes significantly to hepatic lipogenic gene expression. *Cell Physiol Biochem*, 35, 803-15.
- BOECKMANS, J., NATALE, A., BUYL, K., ROGIERS, V., DE KOCK, J., VANHAECKE, T. & RODRIGUES, R. M. 2018. Human-based systems: Mechanistic NASH modelling just around the corner? *Pharmacol Res*, 134, 257-267.
- BOREN, J., RUSTAEUS, S. & OLOFSSON, S. O. 1994. Studies on the assembly of apolipoprotein B-100- and B-48-containing very low density lipoproteins in McA-RH7777 cells. *J Biol Chem*, 269, 25879-88.
- BRAVO, S., LOWNDES, J., SINNETT, S., YU, Z. & RIPPE, J. 2013. Consumption of sucrose and high-fructose corn syrup does not increase liver fat or ectopic fat deposition in muscles. *Appl Physiol Nutr Metab*, 38, 681-8.
- BREHER-ESCH, S., SAHINI, N., TRINCONE, A., WALLSTAB, C. & BORLAK, J. 2018. Genomics of lipid-laden human hepatocyte cultures enables drug target screening for the treatment of non-alcoholic fatty liver disease. *BMC Med Genomics*, 11, 111.
- BUZZETTI, E., PINZANI, M. & TSOCHATZIS, E. A. 2016. The multiple-hit pathogenesis of non-alcoholic fatty liver disease (NAFLD). *Metabolism*, 65, 1038-48.
- CALZADILLA BERTOT, L. & ADAMS, L. A. 2016. The Natural Course of Non-Alcoholic Fatty Liver Disease. *Int J Mol Sci*, 17, 774.
- CHALASANI, N., YOUNOSSI, Z., LAVINE, J. E., DIEHL, A. M., BRUNT, E. M., CUSI, K., CHARLTON, M., SANYAL, A. J., AMERICAN GASTROENTEROLOGICAL, A., AMERICAN ASSOCIATION FOR THE STUDY OF LIVER, D. & AMERICAN COLLEGE OF, G. 2012. The diagnosis and management of non-alcoholic fatty liver disease: practice guideline by the American Gastroenterological Association, American

- Association for the Study of Liver Diseases, and American College of Gastroenterology. *Gastroenterology*, 142, 1592-609.
- CHIU, S., SIEVENPIPER, J. L., DE SOUZA, R. J., COZMA, A. I., MIRRAHIMI, A., CARLETON, A. J., HA, V., DI BUONO, M., JENKINS, A. L., LEITER, L. A., WOLEVER, T. M., DON-WAUCHOPE, A. C., BEYENE, J., KENDALL, C. W. & JENKINS, D. J. 2014. Effect of fructose on markers of non-alcoholic fatty liver disease (NAFLD): a systematic review and meta-analysis of controlled feeding trials. *Eur J Clin Nutr*, 68, 416-23.
- CHOI, S. H. & GINSBERG, H. N. 2011. Increased very low density lipoprotein (VLDL) secretion, hepatic steatosis, and insulin resistance. *Trends Endocrinol Metab*, 22, 353-63.
- COHEN, J. C., HORTON, J. D. & HOBBS, H. H. 2011. Human Fatty Liver Disease: Old Questions and New Insights. *Science*, 332, 1519.
- COX, L. A., OLIVIER, M., SPRADLING-REEVES, K., KARERE, G. M., COMUZZIE, A. G. & VANDEBERG, J. L. 2017. Nonhuman Primates and Translational Research-Cardiovascular Disease. *ILAR J*, 58, 235-250.
- DAI, G., LIU, P., LI, X., ZHOU, X. & HE, S. 2019. Association between PNPLA3 rs738409 polymorphism and nonalcoholic fatty liver disease (NAFLD) susceptibility and severity: A meta-analysis. *Medicine (Baltimore)*, 98, e14324.
- DAVIS, J. N., LE, K. A., WALKER, R. W., VIKMAN, S., SPRUIJT-METZ, D., WEIGENBERG, M. J., ALLAYEE, H. & GORAN, M. I. 2010. Increased hepatic fat in overweight Hispanic youth influenced by interaction between genetic variation in PNPLA3 and high dietary carbohydrate and sugar consumption. *Am J Clin Nutr*, 92, 1522-7.
- DENTIN, R., GIRARD, J. & POSTIC, C. 2005. Carbohydrate responsive element binding protein (ChREBP) and sterol regulatory element binding protein-1c (SREBP-1c): two key regulators of glucose metabolism and lipid synthesis in liver. *Biochimie*, 87, 81-6.
- DONATO, M. T., LAHOZ, A., JIMENEZ, N., PEREZ, G., SERRALTA, A., MIR, J., CASTELL, J. V. & GOMEZ-LECHON, M. J. 2006. Potential impact of steatosis on cytochrome P450 enzymes of human hepatocytes isolated from fatty liver grafts. *Drug Metab Dispos*, 34, 1556-62.
- DONNELLY, K. L., SMITH, C. I., SCHWARZENBERG, S. J., JESSURUN, J., BOLDT, M. D. & PARKS, E. J. 2005. Sources of fatty acids stored in liver and secreted via lipoproteins in patients with nonalcoholic fatty liver disease. *J Clin Invest*, 115, 1343-51.
- DUBUQUOY, C., ROBICHON, C., LASNIER, F., LANGLOIS, C., DUGAIL, I., FOUFELLE, F., GIRARD, J., BURNOL, A. F., POSTIC, C. & MOLDES, M. 2011. Distinct regulation of adiponutrin/PNPLA3 gene expression by the transcription factors ChREBP and SREBP1c in mouse and human hepatocytes. *J Hepatol*, 55, 145-53.
- DUTTA, A. K. 2015. Adiponutrin (PNPLA3) in liver fibrogenesis: Is unaltered HepG2 cell line a better model system compared to murine models? *Med Hypotheses*, 85, 736-9.
- EASL-EASD-EASO 2016. EASL-EASD-EASO Clinical Practice Guidelines for the management of non-alcoholic fatty liver disease. *J Hepatol*, 64, 1388-402.
- FANG, Y. L., CHEN, H., WANG, C. L. & LIANG, L. 2018. Pathogenesis of non-alcoholic fatty liver disease in children and adolescence: From "two hit theory" to "multiple hit model". *World J Gastroenterol*, 24, 2974-2983.
- FELDER, T. K., KLEIN, K., PATSCH, W. & OBERKOFER, H. 2005. A novel SREBP-1 splice variant: tissue abundance and transactivation potency. *Biochim Biophys Acta*, 1731, 41-7.
- FISHER, C. D., LICKTEIG, A. J., AUGUSTINE, L. M., RANGER-MOORE, J., JACKSON, J. P., FERGUSON, S. S. & CHERRINGTON, N. J. 2009. Hepatic cytochrome P450 enzyme

- alterations in humans with progressive stages of nonalcoholic fatty liver disease. *Drug Metab Dispos*, 37, 2087-94.
- FRANCQUE, S. M., VAN DER GRAAFF, D. & KWANTEN, W. J. 2016. Non-alcoholic fatty liver disease and cardiovascular risk: Pathophysiological mechanisms and implications. *J Hepatol*, 65, 425-43.
- GEIDL-FLUECK, B. & GERBER, P. A. 2017. Insights into the Hexose Liver Metabolism- Glucose versus Fructose. *Nutrients*, 9, E1026.
- GEORGIADI, A. & KERSTEN, S. 2012. Mechanisms of gene regulation by fatty acids. *Adv Nutr*, 3, 127-34.
- GIBBONS, G. F., KHURANA, R., ODWELL, A. & SEELAENDER, M. C. 1994. Lipid balance in HepG2 cells: active synthesis and impaired mobilization. *J Lipid Res*, 35, 1801-8.
- GLEN, J., FLOROS, L., DAY, C., PRYKE, R. & GUIDELINE DEVELOPMENT, G. 2016. Non-alcoholic fatty liver disease (NAFLD): summary of NICE guidance. *BMJ*, 354, i4428.
- GOMEZ-LECHON, M. J., DONATO, M. T., MARTINEZ-ROMERO, A., JIMENEZ, N., CASTELL, J. V. & O'CONNOR, J. E. 2007. A human hepatocellular in vitro model to investigate steatosis. *Chem Biol Interact*, 165, 106-16.
- GRAFFMANN, N., RING, S., KAWALA, M. A., WRUCK, W., NCUBE, A., TROMPETER, H. I. & ADJAYE, J. 2016. Modeling Nonalcoholic Fatty Liver Disease with Human Pluripotent Stem Cell-Derived Immature Hepatocyte-Like Cells Reveals Activation of PLIN2 and Confirms Regulatory Functions of Peroxisome Proliferator-Activated Receptor Alpha. *Stem Cells Dev*, 25, 1119-33.
- GREEN, C. J., JOHNSON, D., AMIN, H. D., SIVATHONDAN, P., SILVA, M. A., WANG, L. M., STEVANATO, L., MCNEIL, C. A., MILJAN, E. A., SINDEN, J. D., MORTEN, K. J. & HODSON, L. 2015a. Characterization of lipid metabolism in a novel immortalized human hepatocyte cell line. *Am J Physiol Endocrinol Metab*, 309, E511-22.
- GREEN, C. J., PARRY, S. A., GUNN, P. J., CERESA, C. D. L., ROSQVIST, F., PICHE, M. E. & HODSON, L. 2018. Studying non-alcoholic fatty liver disease: the ins and outs of in vivo, ex vivo and in vitro human models. *Horm Mol Biol Clin Investig*, [Epub ahead of print].
- GREEN, C. J., PRAMFALK, C., MORTEN, K. J. & HODSON, L. 2015b. From whole body to cellular models of hepatic triglyceride metabolism: man has got to know his limitations. *Am J Physiol Endocrinol Metab*, 308, E1-20.
- GREENSPAN, P., MAYER, E. P. & FOWLER, S. D. 1985. Nile red: a selective fluorescent stain for intracellular lipid droplets. *J Cell Biol*, 100, 965-73.
- GROSS, D. N., VAN DEN HEUVEL, A. P. & BIRNBAUM, M. J. 2008. The role of FoxO in the regulation of metabolism. *Oncogene*, 27, 2320-36.
- GUNN, P. J., GREEN, C. J., PRAMFALK, C. & HODSON, L. 2017. In vitro cellular models of human hepatic fatty acid metabolism: differences between Huh7 and HepG2 cell lines in human and fetal bovine culturing serum. *Physiol Rep*, 5, E13532.
- HANNAH, V. C., OU, J., LUONG, A., GOLDSTEIN, J. L. & BROWN, M. S. 2001. Unsaturated fatty acids down-regulate srebp isoforms 1a and 1c by two mechanisms in HEK-293 cells. *J Biol Chem*, 276, 4365-72.
- HANNAH, W. N., JR. & HARRISON, S. A. 2016. Lifestyle and Dietary Interventions in the Management of Nonalcoholic Fatty Liver Disease. *Dig Dis Sci*, 61, 1365-74.
- HANSSON, P. K., ASZTELY, A. K., CLAPHAM, J. C. & SCHREYER, S. A. 2004. Glucose and fatty acid metabolism in McA-RH7777 hepatoma cells vs. rat primary hepatocytes: responsiveness to nutrient availability. *Biochim Biophys Acta*, 1684, 54-62.
- HAO, L., ITO, K., HUANG, K. H., SAE-TAN, S., LAMBERT, J. D. & ROSS, A. C. 2014. Shifts in dietary carbohydrate-lipid exposure regulate expression of the non-alcoholic

- fatty liver disease-associated gene PNPLA3/adiponutrin in mouse liver and HepG2 human liver cells. *Metabolism*, 63, 1352-62.
- HE, S., MCPHAUL, C., LI, J. Z., GARUTI, R., KINCH, L., GRISHIN, N. V., COHEN, J. C. & HOBBS, H. H. 2010. A sequence variation (I148M) in PNPLA3 associated with nonalcoholic fatty liver disease disrupts triglyceride hydrolysis. *J Biol Chem*, 285, 6706-15.
- HIMPE, E. & KOOIJMAN, R. 2009. Insulin-like growth factor-I receptor signal transduction and the Janus Kinase/Signal Transducer and Activator of Transcription (JAK-STAT) pathway. *Biofactors*, 35, 76-81.
- HIRAHATAKE, K. M., MEISSEN, J. K., FIEHN, O. & ADAMS, S. H. 2011. Comparative effects of fructose and glucose on lipogenic gene expression and intermediary metabolism in HepG2 liver cells. *PLoS One*, 6, e26583.
- HOANG, N. A., RICHTER, F., SCHUBERT, M., LORKOWSKI, S., KLOTZ, L. O. & STEINBRENNER, H. 2019. Differential capability of metabolic substrates to promote hepatocellular lipid accumulation. *Eur J Nutr*, 58, 3023-3034.
- HODSON, L. 2019. Hepatic fatty acid synthesis and partitioning: the effect of metabolic and nutritional state. *Proc Nutr Soc*, 78, 126-134.
- HODSON, L., ROSQVIST, F. & PARRY, S. A. 2019. The influence of dietary fatty acids on liver fat content and metabolism. *Proc Nutr Soc*, 1-12.
- HODSON, L., SKEAFF, C. M. & FIELDING, B. A. 2008. Fatty acid composition of adipose tissue and blood in humans and its use as a biomarker of dietary intake. *Prog Lipid Res*, 47, 348-80.
- HORWITZ, D. L., STARR, J. I., MAKO, M. E., BLACKARD, W. G. & RUBENSTEIN, A. H. 1975. Proinsulin, insulin, and C-peptide concentrations in human portal and peripheral blood. *J Clin Invest*, 55, 1278-83.
- HRIBAL, M. L., PROCOPIO, T., PETTA, S., SCIACQUA, A., GRIMAUDO, S., PIPITONE, R. M., PERTICONE, F. & SESTI, G. 2013. Insulin-like growth factor-I, inflammatory proteins, and fibrosis in subjects with nonalcoholic fatty liver disease. *J Clin Endocrinol Metab*, 98, E304-8.
- HUANG, Y., COHEN, J. C. & HOBBS, H. H. 2011. Expression and characterization of a PNPLA3 protein isoform (I148M) associated with nonalcoholic fatty liver disease. *J Biol Chem*, 286, 37085-93.
- HUI, H., HUANG, D., MCARTHUR, D., NISSEN, N., BOROS, L. G. & HEANEY, A. P. 2009. Direct spectrophotometric determination of serum fructose in pancreatic cancer patients. *Pancreas*, 38, 706-12.
- ISAAK, C. K. & SIOW, Y. L. 2013. The evolution of nutrition research. *Can J Physiol Pharmacol*, 91, 257-67.
- JANG, C., HUI, S., LU, W., COWAN, A. J., MORSCHER, R. J., LEE, G., LIU, W., TESZ, G. J., BIRNBAUM, M. J. & RABINOWITZ, J. D. 2018. The Small Intestine Converts Dietary Fructose into Glucose and Organic Acids. *Cell metabolism*, 27, 351-361.e3.
- JIN, R., WELSH, J. A., LE, N. A., HOLZBERG, J., SHARMA, P., MARTIN, D. R. & VOS, M. B. 2014. Dietary fructose reduction improves markers of cardiovascular disease risk in Hispanic-American adolescents with NAFLD. *Nutrients*, 6, 3187-201.
- JOHNSTON, R. D., STEPHENSON, M. C., CROSSLAND, H., CORDON, S. M., PALCIDI, E., COX, E. F., TAYLOR, M. A., AITHAL, G. P. & MACDONALD, I. A. 2013. No difference between high-fructose and high-glucose diets on liver triacylglycerol or biochemistry in healthy overweight men. *Gastroenterology*, 145, 1016-1025 e2.
- KANURI, G. & BERGHEIM, I. 2013. In vitro and in vivo models of non-alcoholic fatty liver disease (NAFLD). *Int J Mol Sci*, 14, 11963-80.

- KARPE, F., DICKMANN, J. R. & FRAYN, K. N. 2011. Fatty acids, obesity, and insulin resistance: time for a reevaluation. *Diabetes*, 60, 2441-9.
- KAYANO, T., BURANT, C. F., FUKUMOTO, H., GOULD, G. W., FAN, Y. S., EDDY, R. L., BYERS, M. G., SHOWS, T. B., SEINO, S. & BELL, G. I. 1990. Human facilitative glucose transporters. Isolation, functional characterization, and gene localization of cDNAs encoding an isoform (GLUT5) expressed in small intestine, kidney, muscle, and adipose tissue and an unusual glucose transporter pseudogene-like sequence (GLUT6). *J Biol Chem*, 265, 13276-82.
- KOPPENOL, W. H., BOUNDS, P. L. & DANG, C. V. 2011. Otto Warburg's contributions to current concepts of cancer metabolism. *Nat Rev Cancer*, 11, 325-37.
- KOSTRZEWSKI, T., CORNFORTH, T., SNOW, S. A., OURO-GNAO, L., ROWE, C., LARGE, E. M. & HUGHES, D. J. 2017. Three-dimensional perfused human in vitro model of non-alcoholic fatty liver disease. *World J Gastroenterol*, 23, 204-215.
- KOZLITINA, J., SMAGRIS, E., STENDER, S., NORDESTGAARD, B. G., ZHOU, H. H., TYBJAERG-HANSEN, A., VOGT, T. F., HOBBS, H. H. & COHEN, J. C. 2014. Exome-wide association study identifies a TM6SF2 variant that confers susceptibility to nonalcoholic fatty liver disease. *Nat Genet*, 46, 352-6.
- LABARCA, C. & PAIGEN, K. 1980. A simple, rapid, and sensitive DNA assay procedure. *Anal Biochem*, 102, 344-52.
- LEAMY, A. K., EGNATCHIK, R. A. & YOUNG, J. D. 2013. Molecular mechanisms and the role of saturated fatty acids in the progression of non-alcoholic fatty liver disease. *Prog Lipid Res*, 52, 165-74.
- LEAVENS, K. F. & BIRNBAUM, M. J. 2011. Insulin signaling to hepatic lipid metabolism in health and disease. *Crit Rev Biochem Mol Biol*, 46, 200-15.
- LEE, L., ALLOOSH, M., SAXENA, R., VAN ALSTINE, W., WATKINS, B. A., KLAUNIG, J. E., STUREK, M. & CHALASANI, N. 2009. Nutritional model of steatohepatitis and metabolic syndrome in the Ossabaw miniature swine. *Hepatology*, 50, 56-67.
- LI, P., HE, K., LI, J., LIU, Z. & GONG, J. 2017. The role of Kupffer cells in hepatic diseases. *Mol Immunol*, 85, 222-229.
- LIN, J., HANDSCHIN, C. & SPIEGELMAN, B. M. 2005a. Metabolic control through the PGC-1 family of transcription coactivators. *Cell Metab*, 1, 361-70.
- LIN, J., YANG, R., TARR, P. T., WU, P. H., HANDSCHIN, C., LI, S., YANG, W., PEI, L., ULDRY, M., TONTONOZ, P., NEWGARD, C. B. & SPIEGELMAN, B. M. 2005b. Hyperlipidemic effects of dietary saturated fats mediated through PGC-1beta coactivation of SREBP. *Cell*, 120, 261-73.
- LING, J., LEWIS, J., DOUGLAS, D., KNETEMAN, N. M. & VANCE, D. E. 2013. Characterization of lipid and lipoprotein metabolism in primary human hepatocytes. *Biochim Biophys Acta*, 1831, 387-97.
- LISTENBERGER, L. L., OSTERMEYER-FAY, A. G., GOLDBERG, E. B., BROWN, W. J. & BROWN, D. A. 2007. Adipocyte differentiation-related protein reduces the lipid droplet association of adipose triglyceride lipase and slows triacylglycerol turnover. *J Lipid Res*, 48, 2751-61.
- LIU, W., BAKER, R. D., BHATIA, T., ZHU, L. & BAKER, S. S. 2016a. Pathogenesis of nonalcoholic steatohepatitis. *Cell Mol Life Sci*, 73, 1969-87.
- LIU, Z. T., CHEN, T. C., LU, X. X., XIE, H. Y., ZHOU, L. & ZHENG, S. S. 2016b. Overexpression of variant PNPLA3 gene at I148M position causes malignant transformation of hepatocytes via IL-6-JAK2/STAT3 pathway in low dose free fatty acid exposure: a laboratory investigation in vitro and in vivo. *American Journal of Translational Research*, 8, 1319-U41.
- LONARDO, A., NASCIMBENI, F., MANTOVANI, A. & TARGHER, G. 2018. Hypertension, diabetes, atherosclerosis and NASH: Cause or consequence? *J Hepatol*, 68, 335-352.

- LUUKKONEN, P. K., SADEVIRTA, S., ZHOU, Y., KAYSER, B., ALI, A., AHONEN, L., LALLUKKA, S., PELLOUX, V., GAGGINI, M., JIAN, C., HAKKARAINEN, A., LUNDBOM, N., GYLLING, H., SALONEN, A., ORESIC, M., HYOTYLAINEN, T., ORHO-MELANDER, M., RISSANEN, A., GASTALDELLI, A., CLEMENT, K., HODSON, L. & YKI-JARVINEN, H. 2018. Saturated Fat Is More Metabolically Harmful for the Human Liver Than Unsaturated Fat or Simple Sugars. *Diabetes Care*, 41, 1732-1739.
- LUUKKONEN, P. K., ZHOU, Y., NIDHINA HARIDAS, P. A., DWIVEDI, O. P., HYOTYLAINEN, T., ALI, A., JUUTI, A., LEIVONEN, M., TUKIAINEN, T., AHONEN, L., SCOTT, E., PALMER, J. M., AROLA, J., ORHO-MELANDER, M., VIKMAN, P., ANSTEE, Q. M., OLKKONEN, V. M., ORESIC, M., GROOP, L. & YKI-JARVINEN, H. 2017. Impaired hepatic lipid synthesis from polyunsaturated fatty acids in TM6SF2 E167K variant carriers with NAFLD. *J Hepatol*, 67, 128-136.
- MAERSK, M., BELZA, A., STODKILDE-JORGENSEN, H., RINGGAARD, S., CHABANOVA, E., THOMSEN, H., PEDERSEN, S. B., ASTRUP, A. & RICHELSEN, B. 2012. Sucrose-sweetened beverages increase fat storage in the liver, muscle, and visceral fat depot: a 6-mo randomized intervention study. *Am J Clin Nutr*, 95, 283-9.
- MAIER, K., HOFMANN, U., REUSS, M. & MAUCH, K. 2010. Dynamics and control of the central carbon metabolism in hepatoma cells. *BMC Syst Biol*, 4, 54.
- MALDONADO, E. M., FISHER, C. P., MAZZATTI, D. J., BARBER, A. L., TINDALL, M. J., PLANT, N. J., KIERZEK, A. M. & MOORE, J. B. 2018. Multi-scale, whole-system models of liver metabolic adaptation to fat and sugar in non-alcoholic fatty liver disease. *NPJ Syst Biol Appl*, 4, 33.
- MANCINA, R. M., DONGIOVANNI, P., PETTA, S., PINGITORE, P., MERONI, M., RAMETTA, R., BOREN, J., MONTALCINI, T., PUJIA, A., WIKLUND, O., HINDY, G., SPAGNUOLO, R., MOTTA, B. M., PIPITONE, R. M., CRAXI, A., FARGION, S., NOBILI, V., KAKELA, P., KARJA, V., MANNISTO, V., PIHLAJAMAKI, J., REILLY, D. F., CASTRO-PEREZ, J., KOZLITINA, J., VALENTI, L. & ROMEO, S. 2016. The MBOAT7-TMC4 Variant rs641738 Increases Risk of Nonalcoholic Fatty Liver Disease in Individuals of European Descent. *Gastroenterology*, 150, 1219-1230 e6.
- MARCHISELLO, S., DI PINO, A., SCICALI, R., URBANO, F., PIRO, S., PURRELLO, F. & RABUAZZO, A. M. 2019. Pathophysiological, Molecular and Therapeutic Issues of Nonalcoholic Fatty Liver Disease: An Overview. *Int J Mol Sci*, 20, E1948.
- MCGEOCH, L. J., PATEL, P. R. & MANN, J. P. 2018. PNPLA3: A Determinant of Response to Low-Fructose Diet in Nonalcoholic Fatty Liver Disease. *Gastroenterology*, 154, 1207-1208.
- MEERBREY, K. L., HU, G., KESSLER, J. D., ROARTY, K., LI, M. Z., FANG, J. E., HERSCHKOWITZ, J. I., BURROWS, A. E., CICCIA, A., SUN, T., SCHMITT, E. M., BERNARDI, R. J., FU, X., BLAND, C. S., COOPER, T. A., SCHIFF, R., ROSEN, J. M., WESTBROOK, T. F. & ELLEDGE, S. J. 2011. The pINDUCER lentiviral toolkit for inducible RNA interference in vitro and in vivo. *Proc Natl Acad Sci U S A*, 108, 3665-70.
- MEISSEN, J. K., HIRAHATAKE, K. M., ADAMS, S. H. & FIEHN, O. 2015. Temporal metabolomic responses of cultured HepG2 liver cells to high fructose and high glucose exposures. *Metabolomics*, 11, 707-721.
- MIN, H. K., SOOKOIAN, S., PIROLA, C. J., CHENG, J., MIRSHAHI, F. & SANYAL, A. J. 2014. Metabolic profiling reveals that PNPLA3 induces widespread effects on metabolism beyond triacylglycerol remodeling in Huh-7 hepatoma cells. *Am J Physiol Gastrointest Liver Physiol*, 307, G66-76.
- MONDUL, A., MANCINA, R. M., MERLO, A., DONGIOVANNI, P., RAMETTA, R., MONTALCINI, T., VALENTI, L., ALBANES, D. & ROMEO, S. 2015. PNPLA3 I148M Variant Influences Circulating Retinol in Adults with Nonalcoholic Fatty Liver Disease or Obesity. *J Nutr*, 145, 1687-91.

- MOORE, J. B., GUNN, P. J. & FIELDING, B. A. 2014. The role of dietary sugars and de novo lipogenesis in non-alcoholic fatty liver disease. *Nutrients*, 6, 5679-703.
- NEHLIG, A. 2018. Interindividual Differences in Caffeine Metabolism and Factors Driving Caffeine Consumption. *Pharmacol Rev*, 70, 384-411.
- NIKOLAOU, N., GREEN, C. J., GUNN, P. J., HODSON, L. & TOMLINSON, J. W. 2016. Optimizing human hepatocyte models for metabolic phenotype and function: effects of treatment with dimethyl sulfoxide (DMSO). *Physiol Rep*, 4, E12944.
- NOBILI, V., BEDOGNI, G., DONATI, B., ALISI, A. & VALENTI, L. 2013. The I148M variant of PNPLA3 reduces the response to docosahexaenoic acid in children with non-alcoholic fatty liver disease. *J Med Food*, 16, 957-60.
- NWOSU, Z. C., BATTELLO, N., ROTHLEY, M., PIORONSKA, W., SITEK, B., EBERT, M. P., HOFMANN, U., SLEEMAN, J., WOLFL, S., MEYER, C., MEGGER, D. A. & DOOLEY, S. 2018. Liver cancer cell lines distinctly mimic the metabolic gene expression pattern of the corresponding human tumours. *J Exp Clin Cancer Res*, 37, 211.
- OLSAVSKY, K. M., PAGE, J. L., JOHNSON, M. C., ZARBL, H., STROM, S. C. & OMIECINSKI, C. J. 2007. Gene expression profiling and differentiation assessment in primary human hepatocyte cultures, established hepatoma cell lines, and human liver tissues. *Toxicol Appl Pharmacol*, 222, 42-56.
- OTA, T., GAYET, C. & GINSBERG, H. N. 2008. Inhibition of apolipoprotein B100 secretion by lipid-induced hepatic endoplasmic reticulum stress in rodents. *J Clin Invest*, 118, 316-32.
- OU, J., TU, H., SHAN, B., LUK, A., DEBOSE-BOYD, R. A., BASHMAKOV, Y., GOLDSTEIN, J. L. & BROWN, M. S. 2001. Unsaturated fatty acids inhibit transcription of the sterol regulatory element-binding protein-1c (SREBP-1c) gene by antagonizing ligand-dependent activation of the LXR. *Proc Natl Acad Sci U S A*, 98, 6027-32.
- PANASEVICH, M. R., MEERS, G. M., LINDEN, M. A., BOOTH, F. W., PERFIELD, J. W., 2ND, FRITSCH, K. L., WANKHADE, U. D., CHINTAPALLI, S. V., SHANKAR, K., IBDAH, J. A. & RECTOR, R. S. 2018. High-fat, high-fructose, high-cholesterol feeding causes severe NASH and cecal microbiota dysbiosis in juvenile Ossabaw swine. *Am J Physiol Endocrinol Metab*, 314, E78-E92.
- PARRY, S. A. & HODSON, L. 2017. Influence of dietary macronutrients on liver fat accumulation and metabolism. *J Invest Med*, 65, 1102-1115.
- PERTTILA, J., HUAMAN-SAMANEZ, C., CARON, S., TANHUANPAA, K., STAELS, B., YKI-JARVINEN, H. & OLKKONEN, V. M. 2012. PNPLA3 is regulated by glucose in human hepatocytes, and its I148M mutant slows down triglyceride hydrolysis. *Am J Physiol Endocrinol Metab*, 302, E1063-9.
- PETERSEN, M. C. & SHULMAN, G. I. 2017. Roles of Diacylglycerols and Ceramides in Hepatic Insulin Resistance. *Trends Pharmacol Sci*, 38, 649-665.
- PINGITORE, P., PIRAZZI, C., MANCINA, R. M., MOTTA, B. M., INDIVERI, C., PUJIA, A., MONTALCINI, T., HEDFALK, K. & ROMEO, S. 2014. Recombinant PNPLA3 protein shows triglyceride hydrolase activity and its I148M mutation results in loss of function. *Biochim Biophys Acta*, 1841, 574-80.
- PINGITORE, P. & ROMEO, S. 2019. The role of PNPLA3 in health and disease. *Biochim Biophys Acta Mol Cell Biol Lipids*, 1864, 900-906.
- PINGITORE, P., SASIDHARAN, K., EKSTRAND, M., PRILL, S., LINDEN, D. & ROMEO, S. 2019. Human Multilineage 3D Spheroids as a Model of Liver Steatosis and Fibrosis. *Int J Mol Sci*, 20, E1629.
- PIRAZZI, C., ADIELS, M., BURZA, M. A., MANCINA, R. M., LEVIN, M., STAHLMAN, M., TASKINEN, M. R., ORHO-MELANDER, M., PERMAN, J., PUJIA, A., ANDERSSON, L., MAGLIO, C., MONTALCINI, T., WIKLUND, O., BOREN, J. & ROMEO, S. 2012. Patatin-like phospholipase domain-containing 3 (PNPLA3) I148M (rs738409) affects hepatic VLDL secretion in humans and in vitro. *J Hepatol*, 57, 1276-82.

- PIRAZZI, C., VALENTI, L., MOTTA, B. M., PINGITORE, P., HEDFALK, K., MANCINA, R. M., BURZA, M. A., INDIVERI, C., FERRO, Y., MONTALCINI, T., MAGLIO, C., DONGIOVANNI, P., FARGION, S., RAMETTA, R., PUJIA, A., ANDERSSON, L., GHOSAL, S., LEVIN, M., WIKLUND, O., IACOVINO, M., BOREN, J. & ROMEO, S. 2014. PNPLA3 has retinyl-palmitate lipase activity in human hepatic stellate cells. *Hum Mol Genet*, 23, 4077-85.
- QIAO, A., LIANG, J., KE, Y., LI, C., CUI, Y., SHEN, L., ZHANG, H., CUI, A., LIU, X., LIU, C., CHEN, Y., ZHU, Y., GUAN, Y., FANG, F. & CHANG, Y. 2011. Mouse patatin-like phospholipase domain-containing 3 influences systemic lipid and glucose homeostasis. *Hepatology*, 54, 509-21.
- QIN, L. & CRAWFORD, J. M. 2018. 1 - Anatomy and Cellular Functions of the Liver. In: SANYAL, A. J., BOYER, T. D., LINDOR, K. D. & TERRAULT, N. A. (eds.) *Zakim and Boyer's Hepatology (Seventh Edition)*. Philadelphia: Elsevier.
- RAE-WHITCOMBE, S. M., KENNEDY, D., VOYLES, M. & THOMPSON, M. P. 2010. Regulation of the promoter region of the human adiponutrin/PNPLA3 gene by glucose and insulin. *Biochem Biophys Res Commun*, 402, 767-72.
- RAYCHAUDHURI, S., STUART, J. M. & ALTMAN, R. B. 2000. Principal components analysis to summarize microarray experiments: application to sporulation time series. *Pacific Symposium on Biocomputing. Pacific Symposium on Biocomputing*, 455-466.
- RICCHI, M., ODOARDI, M. R., CARULLI, L., ANZIVINO, C., BALLESTRI, S., PINETTI, A., FANTONI, L. I., MARRA, F., BERTOLOTTI, M., BANNI, S., LONARDO, A., CARULLI, N. & LORIA, P. 2009. Differential effect of oleic and palmitic acid on lipid accumulation and apoptosis in cultured hepatocytes. *J Gastroenterol Hepatol*, 24, 830-40.
- RINELLA, M. E. 2015. Nonalcoholic fatty liver disease: a systematic review. *JAMA*, 313, 2263-73.
- RINGNER, M. 2008. What is principal component analysis? *Nat Biotechnol*, 26, 303-4.
- RIORDAN, J. D. & NADEAU, J. H. 2014. Modeling progressive non-alcoholic fatty liver disease in the laboratory mouse. *Mamm Genome*, 25, 473-86.
- ROMEO, S., KOZLITINA, J., XING, C., PERTSEMLIDIS, A., COX, D., PENNACCHIO, L. A., BOERWINKLE, E., COHEN, J. C. & HOBBS, H. H. 2008. Genetic variation in PNPLA3 confers susceptibility to nonalcoholic fatty liver disease. *Nat Genet*, 40, 1461-5.
- ROMEO, S., SENTINELLI, F., DASH, S., YEO, G. S., SAVAGE, D. B., LEONETTI, F., CAPOCCIA, D., INCANI, M., MAGLIO, C., IACOVINO, M., O'RAHILLY, S. & BARONI, M. G. 2010. Morbid obesity exposes the association between PNPLA3 I148M (rs738409) and indices of hepatic injury in individuals of European descent. *Int J Obes (Lond)*, 34, 190-4.
- ROSQVIST, F., KULLBERG, J., STAHLMAN, M., CEDERNAES, J., HEURLING, K., JOHANSSON, H. E., IGGMAN, D., WILKING, H., LARSSON, A., ERIKSSON, O., JOHANSSON, L., STRANIERO, S., RUDLING, M., ANTONI, G., LUBBERINK, M., ORHO-MELANDER, M., BOREN, J., AHLSTROM, H. & RISERUS, U. 2019. Overeating Saturated Fat Promotes Fatty Liver and Ceramides Compared With Polyunsaturated Fat: A Randomized Trial. *J Clin Endocrinol Metab*, 104, 6207-6219.
- ROWE, C., GERRARD, D. T., JENKINS, R., BERRY, A., DURKIN, K., SUNDSTROM, L., GOLDRING, C. E., PARK, B. K., KITTINGHAM, N. R., HANLEY, K. P. & HANLEY, N. A. 2013. Proteome-wide analyses of human hepatocytes during differentiation and dedifferentiation. *Hepatology*, 58, 799-809.
- RUHANEN, H., PERTTILA, J., HOLTTA-VUORI, M., ZHOU, Y., YKI-JARVINEN, H., IKONEN, E., KAKELA, R. & OLKKONEN, V. M. 2014. PNPLA3 mediates hepatocyte triacylglycerol remodeling. *J Lipid Res*, 55, 739-46.
- RUI, L. 2014. Energy metabolism in the liver. *Compr Physiol*, 4, 177-97.

- SALTER, A. M., WIGGINS, D., SESSIONS, V. A. & GIBBONS, G. F. 1998. The intracellular triacylglycerol/fatty acid cycle : a comparison of its activity in hepatocytes which secrete exclusively apolipoprotein (apo) B100 very low-density lipoprotein (VLDL) and in those which secrete predominantly apoB48 VLDL. *Biochem J*, 332, 667-72.
- SANDERS, F. W. & GRIFFIN, J. L. 2016. De novo lipogenesis in the liver in health and disease: more than just a shunting yard for glucose. *Biol Rev Camb Philos Soc*, 91, 452-68.
- SANTORO, N., SAVOYE, M., KIM, G., MAROTTO, K., SHAW, M. M., PIERPONT, B. & CAPRIO, S. 2012. Hepatic fat accumulation is modulated by the interaction between the rs738409 variant in the PNPLA3 gene and the dietary omega6/omega3 PUFA intake. *PLoS One*, 7, e37827.
- SCHWARZ, J. M., NOWOROLSKI, S. M., WEN, M. J., DYACHENKO, A., PRIOR, J. L., WEINBERG, M. E., HERRAIZ, L. A., TAI, V. W., BERGERON, N., BERSOT, T. P., RAO, M. N., SCHAMBELAN, M. & MULLIGAN, K. 2015. Effect of a High-Fructose Weight-Maintaining Diet on Lipogenesis and Liver Fat. *J Clin Endocrinol Metab*, 100, 2434-42.
- SEWTER, C., BERGER, D., CONSIDINE, R. V., MEDINA, G., ROCHFORD, J., CIARALDI, T., HENRY, R., DOHM, L., FLIER, J. S., O'RAHILLY, S. & VIDAL-PUIG, A. J. 2002. Human obesity and type 2 diabetes are associated with alterations in SREBP1 isoform expression that are reproduced ex vivo by tumor necrosis factor-alpha. *Diabetes*, 51, 1035-41.
- SHARP, K. P. H., SCHULTZ, M. & COPPELL, K. J. 2018. Is non-alcoholic fatty liver disease a reflection of what we eat or simply how much we eat? *JGH Open*, 2, 59-74.
- SHIMOMURA, I., SHIMANO, H., HORTON, J. D., GOLDSTEIN, J. L. & BROWN, M. S. 1997. Differential expression of exons 1a and 1c in mRNAs for sterol regulatory element binding protein-1 in human and mouse organs and cultured cells. *J Clin Invest*, 99, 838-45.
- SMAGRIS, E., GILYARD, S., BASURAY, S., COHEN, J. C. & HOBBS, H. H. 2016. Inactivation of Tm6sf2, a Gene Defective in Fatty Liver Disease, Impairs Lipidation but Not Secretion of Very Low Density Lipoproteins. *J Biol Chem*, 291, 10659-76.
- SOFTIC, S., COHEN, D. E. & KAHN, C. R. 2016. Role of Dietary Fructose and Hepatic De Novo Lipogenesis in Fatty Liver Disease. *Dig Dis Sci*, 61, 1282-93.
- SOFTIC, S., GUPTA, M. K., WANG, G. X., FUJISAKA, S., O'NEILL, B. T., RAO, T. N., WILLOUGHBY, J., HARBISON, C., FITZGERALD, K., ILKAYEVA, O., NEWGARD, C. B., COHEN, D. E. & KAHN, C. R. 2017. Divergent effects of glucose and fructose on hepatic lipogenesis and insulin signaling. *J Clin Invest*, 127, 4059-4074.
- SOOKOIAN, S. & PIROLA, C. J. 2011. Meta-analysis of the influence of I148M variant of patatin-like phospholipase domain containing 3 gene (PNPLA3) on the susceptibility and histological severity of nonalcoholic fatty liver disease. *Hepatology*, 53, 1883-94.
- SORENSEN, K. K., SIMON-SANTAMARIA, J., MCCUSKEY, R. S. & SMEDSRD, B. 2015. Liver Sinusoidal Endothelial Cells. *Compr Physiol*, 5, 1751-74.
- SPEICHER, T., FOEHRENBACHER, A., POCHIC, I., WEILAND, T. & WENDEL, A. 2010. Malignant but not naive hepatocytes of human and rodent origin are killed by TNF after metabolic depletion of ATP by fructose. *J Hepatol*, 53, 896-902.
- STANHOPE, K. L., SCHWARZ, J. M., KEIM, N. L., GRIFFEN, S. C., BREMER, A. A., GRAHAM, J. L., HATCHER, B., COX, C. L., DYACHENKO, A., ZHANG, W., MCGAHAN, J. P., SEIBERT, A., KRAUSS, R. M., CHIU, S., SCHAEFER, E. J., AI, M., OTOKOZAWA, S., NAKAJIMA, K., NAKANO, T., BEYSEN, C., HELLERSTEIN, M. K., BERGLUND, L. & HAVEL, P. J. 2009. Consuming fructose-sweetened, not glucose-sweetened,

- beverages increases visceral adiposity and lipids and decreases insulin sensitivity in overweight/obese humans. *J Clin Invest*, 119, 1322-34.
- SUGIMOTO, K., HOSOTANI, T., KAWASAKI, T., NAKAGAWA, K., HAYASHI, S., NAKANO, Y., INUI, H. & YAMANOUCHI, T. 2010. Eucalyptus leaf extract suppresses the postprandial elevation of portal, cardiac and peripheral fructose concentrations after sucrose ingestion in rats. *J Clin Biochem Nutr*, 46, 205-11.
- SUNNY, N. E., PARKS, E. J., BROWNING, J. D. & BURGESS, S. C. 2011. Excessive hepatic mitochondrial TCA cycle and gluconeogenesis in humans with nonalcoholic fatty liver disease. *Cell Metab*, 14, 804-10.
- TAKANAGA, H., CHAUDHURI, B. & FROMMER, W. B. 2008. GLUT1 and GLUT9 as major contributors to glucose influx in HepG2 cells identified by a high sensitivity intramolecular FRET glucose sensor. *Biochim Biophys Acta*, 1778, 1091-9.
- TAKEUCHI, Y., YAHAGI, N., IZUMIDA, Y., NISHI, M., KUBOTA, M., TERAOKA, Y., YAMAMOTO, T., MATSUZAKA, T., NAKAGAWA, Y., SEKIYA, M., IIZUKA, Y., OHASHI, K., OSUGA, J., GOTODA, T., ISHIBASHI, S., ITAKA, K., KATAOKA, K., NAGAI, R., YAMADA, N., KADOWAKI, T. & SHIMANO, H. 2010. Polyunsaturated fatty acids selectively suppress sterol regulatory element-binding protein-1 through proteolytic processing and autoloop regulatory circuit. *J Biol Chem*, 285, 11681-91.
- TALIENTO, A. E., DALLIO, M., FEDERICO, A., PRATI, D. & VALENTI, L. 2019. Novel Insights into the Genetic Landscape of Nonalcoholic Fatty Liver Disease. *Int J Environ Res Public Health*, 16, E2755.
- TANDRA, S., YE, M. M., BRUNT, E. M., VUPPALANCHI, R., CUMMINGS, O. W., UNALP-ARIDA, A., WILSON, L. A. & CHALASANI, N. 2011. Presence and significance of microvesicular steatosis in nonalcoholic fatty liver disease. *J Hepatol*, 55, 654-659.
- TARGHER, G., BYRNE, C. D., LONARDO, A., ZOPPINI, G. & BARBUI, C. 2016. Non-alcoholic fatty liver disease and risk of incident cardiovascular disease: A meta-analysis. *J Hepatol*, 65, 589-600.
- TEFF, K. L., GRUDZIAK, J., TOWNSEND, R. R., DUNN, T. N., GRANT, R. W., ADAMS, S. H., KEIM, N. L., CUMMINGS, B. P., STANHOPE, K. L. & HAVEL, P. J. 2009. Endocrine and metabolic effects of consuming fructose- and glucose-sweetened beverages with meals in obese men and women: influence of insulin resistance on plasma triglyceride responses. *J Clin Endocrinol Metab*, 94, 1562-9.
- TER HORST, K. W. & SERLIE, M. J. 2017. Fructose Consumption, Lipogenesis, and Non-Alcoholic Fatty Liver Disease. *Nutrients*, 9, E981.
- THEYTAZ, F., DE GIORGI, S., HODSON, L., STEFANONI, N., REY, V., SCHNEITER, P., GIUSTI, V. & TAPPY, L. 2014. Metabolic fate of fructose ingested with and without glucose in a mixed meal. *Nutrients*, 6, 2632-49.
- THRIFT, R. N., FORTE, T. M., CAHOON, B. E. & SHORE, V. G. 1986. Characterization of lipoproteins produced by the human liver cell line, Hep G2, under defined conditions. *J Lipid Res*, 27, 236-50.
- TIWARI, S. & SIDDIQI, S. A. 2012. Intracellular trafficking and secretion of VLDL. *Arterioscler Thromb Vasc Biol*, 32, 1079-86.
- TOWBIN, H., STAHELIN, T. & GORDON, J. 1979. Electrophoretic transfer of proteins from polyacrylamide gels to nitrocellulose sheets: procedure and some applications. *Proceedings of the National Academy of Sciences of the United States of America*, 76, 4350-4354.
- VANDER HEIDEN, M. G., CANTLEY, L. C. & THOMPSON, C. B. 2009. Understanding the Warburg effect: the metabolic requirements of cell proliferation. *Science*, 324, 1029-33.

- WANG, Y., VISCARRA, J., KIM, S. J. & SUL, H. S. 2015. Transcriptional regulation of hepatic lipogenesis. *Nat Rev Mol Cell Biol*, 16, 678-89.
- WARBURG, O. 1925. Über den Stoffwechsel der Carcinomzelle. *Klin. Wochenschr.*, 4, 534-536.
- WILKENING, S., STAHL, F. & BADER, A. 2003. Comparison of primary human hepatocytes and hepatoma cell line Hepg2 with regard to their biotransformation properties. *Drug Metab Dispos*, 31, 1035-42.
- WINDEMULLER, F., XU, J., RABINOWITZ, S. S., HUSSAIN, M. M. & SCHWARZ, S. M. 2016. Lipogenesis in Huh7 cells is promoted by increasing the fructose: Glucose molar ratio. *World J Hepatol*, 8, 838-43.
- WISNIEWSKI, J. R., VILDHEDE, A., NOREN, A. & ARTURSSON, P. 2016. In-depth quantitative analysis and comparison of the human hepatocyte and hepatoma cell line HepG2 proteomes. *J Proteomics*, 136, 234-47.
- XU, S., ZHANG, X. & LIU, P. 2018. Lipid droplet proteins and metabolic diseases. *Biochim Biophys Acta Mol Basis Dis*, 1864, 1968-1983.
- YAMAGUCHI, K., YANG, L., MCCALL, S., HUANG, J., YU, X. X., PANDEY, S. K., BHANOT, S., MONIA, B. P., LI, Y. X. & DIEHL, A. M. 2007. Inhibiting triglyceride synthesis improves hepatic steatosis but exacerbates liver damage and fibrosis in obese mice with nonalcoholic steatohepatitis. *Hepatology*, 45, 1366-74.
- YONEDA, M., HOTTA, K., NOZAKI, Y., ENDO, H., UCHIYAMA, T., MAWATARI, H., IIDA, H., KATO, S., HOSONO, K., FUJITA, K., YONEDA, K., TAKAHASHI, H., KIRIKOSHI, H., KOBAYASHI, N., INAMORI, M., ABE, Y., KUBOTA, K., SAITO, S., MAEYAMA, S., WADA, K. & NAKAJIMA, A. 2008. Association between PPARGC1A polymorphisms and the occurrence of nonalcoholic fatty liver disease (NAFLD). *BMC Gastroenterol*, 8, 27.
- YOUNOSSI, Z. M., BLISSETT, D., BLISSETT, R., HENRY, L., STEPANOVA, M., YOUNOSSI, Y., RACILA, A., HUNT, S. & BECKERMAN, R. 2016a. The economic and clinical burden of nonalcoholic fatty liver disease in the United States and Europe. *Hepatology*, 64, 1577-1586.
- YOUNOSSI, Z. M., KOENIG, A. B., ABDELATIF, D., FAZEL, Y., HENRY, L. & WYMER, M. 2016b. Global epidemiology of nonalcoholic fatty liver disease-Meta-analytic assessment of prevalence, incidence, and outcomes. *Hepatology*, 64, 73-84.
- YU, K., KE, M. Y., LI, W. H., ZHANG, S. Q. & FANG, X. C. 2014. The impact of soluble dietary fibre on gastric emptying, postprandial blood glucose and insulin in patients with type 2 diabetes. *Asia Pac J Clin Nutr*, 23, 210-8.
- ZAMULE, S. M., STROM, S. C. & OMIECINSKI, C. J. 2008. Preservation of hepatic phenotype in lentiviral-transduced primary human hepatocytes. *Chem Biol Interact*, 173, 179-86.
- ZEILINGER, K., FREYER, N., DAMM, G., SEEHOFER, D. & KNOSPEL, F. 2016. Cell sources for in vitro human liver cell culture models. *Exp Biol Med (Maywood)*, 241, 1684-98.
- ZHAO, L., GUO, X., WANG, O., ZHANG, H., WANG, Y., ZHOU, F., LIU, J. & JI, B. 2016. Fructose and glucose combined with free fatty acids induce metabolic disorders in HepG2 cell: A new model to study the impacts of high-fructose/sucrose and high-fat diets in vitro. *Mol Nutr Food Res*, 60, 909-21.
- ZHENG, J. 2012. Energy metabolism of cancer: Glycolysis versus oxidative phosphorylation (Review). *Oncol Lett*, 4, 1151-1157.
- ZHENG, J., ZHOU, Y., ZHANG, K., QI, Y., AN, S., WANG, S., ZHAO, X. & TANG, Y. D. 2018. Association between nonalcoholic fatty liver disease and subclinical atherosclerosis: a cross-sectional study on population over 40 years old. *BMC Cardiovasc Disord*, 18, 147.
- ZHOU, H. & LIU, R. 2014. ER stress and hepatic lipid metabolism. *Frontiers in genetics*, 5, 112-112.

Appendix – Supplementary Tables

Table S1: Effects of fatty acids, glucose and fructose on lipid accumulation in HepG2 cells. Data was measured as Nile Red fluorescence per μg DNA then converted to fold change relative to $0\mu\text{M}$ fatty acid + 5mM glucose + 0mM fructose. Values are expressed as mean \pm SEM. Data analysed by three-way ANOVA with blocking for plate. $n=5$ wells per treatment per plate. FA: fatty acid, G: glucose, F: fructose. $\dagger P<0.1$, $*P<0.05$, $P<0.01$, $***P<0.001$**

HepG2	5mM G, 0 μM FA			11mM G, 0 μM FA			5mM G, 200 μM FA			11mM G, 200 μM FA			P-values from three-way ANOVA						
F (mM)	0	2	8	0	2	8	0	2	8	0	2	8	FA	G	F	FA \times G	FA \times F	G \times F	FA \times G \times F
Exp 1 ($n=10$)	1.000 ± 0.100	1.039 ± 0.053	0.980 ± 0.104	1.134 ± 0.066	1.200 ± 0.100	1.232 ± 0.092	5.098 ± 0.277	5.896 ± 0.173	6.213 ± 0.329	5.247 ± 0.205	5.446 ± 0.311	5.093 ± 0.201	***		\dagger	**		\dagger	*
Exp 2 ($n=10$)	1.000 ± 0.103	1.073 ± 0.132	0.891 ± 0.083	1.020 ± 0.064	1.046 ± 0.066	1.122 ± 0.066	4.051 ± 0.371	3.781 ± 0.267	3.519 ± 0.223	4.372 ± 0.280	4.117 ± 0.311	4.632 ± 0.558	***	*		\dagger			
Exp 3 ($n=10$)	1.000 ± 0.052	0.986 ± 0.045	1.058 ± 0.032	1.039 ± 0.067	0.941 ± 0.088	0.944 ± 0.075	4.587 ± 0.235	4.475 ± 0.215	4.370 ± 0.282	3.958 ± 0.348	4.341 ± 0.335	4.051 ± 0.182	***	*					
Overall ($n=30$)	1.000 ± 0.049	1.032 ± 0.049	0.976 ± 0.046	1.064 ± 0.038	1.062 ± 0.052	1.081 ± 0.053	4.579 ± 0.185	4.717 ± 0.205	4.701 ± 0.261	4.495 ± 0.187	4.615 ± 0.212	4.570 ± 0.219	***						

Table S2: Effects of fatty acids, glucose and fructose on lipid accumulation in Huh7 cells. Data was measured as Nile Red fluorescence per μg DNA then converted to fold change relative to $0\mu\text{M}$ fatty acid + 5mM glucose + 0mM fructose. Values are expressed as mean \pm SEM. Data analysed by three-way ANOVA with blocking for plate. $n=5$ wells per treatment per plate. FA: fatty acid, G: glucose, F: fructose. $1P<0.1$, $*P<0.05$, $P<0.01$, $***P<0.001$**

Huh7	5mM G, 0 μM FA			11mM G, 0 μM FA			5mM G, 200 μM FA			11mM G, 200 μM FA			P-values from three-way ANOVA							
F (mM)	0	2	8	0	2	8	0	2	8	0	2	8	FA	G	F	FA \times G	FA \times F	G \times F	FA \times G \times F	
Exp 1 ($n=5$)	1.000 ± 0.042	1.005 ± 0.036	1.051 ± 0.060	1.196 ± 0.064	1.089 ± 0.064	1.025 ± 0.045	6.032 ± 0.311	6.354 ± 0.227	6.282 ± 0.059	5.990 ± 0.431	5.873 ± 0.163	5.702 ± 0.203	***			*				
Exp 2 ($n=10$)	1.000 ± 0.045	0.955 ± 0.026	1.008 ± 0.019	1.024 ± 0.017	0.909 ± 0.035	0.912 ± 0.038	3.701 ± 0.079	3.604 ± 0.119	3.445 ± 0.128	3.322 ± 0.148	3.490 ± 0.117	3.406 ± 0.131	***							
Exp 3 ($n=15$)	1.000 ± 0.019	0.956 ± 0.031	0.982 ± 0.025	1.058 ± 0.079	0.930 ± 0.028	0.945 ± 0.029	4.643 ± 0.190	4.555 ± 0.217	4.442 ± 0.216	4.521 ± 0.239	4.542 ± 0.216	4.557 ± 0.162	***							
Overall ($n=30$)	1.000 ± 0.018	0.964 ± 0.019	1.002 ± 0.017	1.070 ± 0.042	0.949 ± 0.023	0.947 ± 0.021	4.560 ± 0.181	4.538 ± 0.207	4.416 ± 0.210	4.366 ± 0.220	4.413 ± 0.189	4.364 ± 0.175	***							

Table S3: Effects of fatty acids, glucose and fructose on lipid accumulation in McA-RH7777 cells. Data was measured as Nile Red fluorescence per μg DNA then converted to fold change relative to $0\mu\text{M}$ fatty acid + 5mM glucose + 0mM fructose. Values are expressed as mean \pm SEM. Data analysed by three-way ANOVA with blocking for plate. $n=5$ wells per treatment per plate. FA: fatty acid, G: glucose, F: fructose. $!P<0.1$, $*P<0.05$, $P<0.01$, $***P<0.001$**

McA-RH7777	5mM G, 0 μM FA			11mM G, 0 μM FA			5mM G, 200 μM FA			11mM G, 200 μM FA			P-values from three-way ANOVA							
	F (mM)	0	2	8	0	2	8	0	2	8	0	2	8	FA	G	F	FA \times G	FA \times F	G \times F	FA \times G \times F
Exp 1 ($n=10$)	1.000 ± 0.046	0.989 ± 0.020	1.083 ± 0.026	0.913 ± 0.064	0.826 ± 0.077	0.863 ± 0.064	6.250 ± 0.216	6.582 ± 0.334	6.241 ± 0.423	6.285 ± 0.641	6.990 ± 0.597	6.710 ± 0.491	***							
Exp 2 ($n=10$)	1.000 ± 0.060	0.854 ± 0.058	0.911 ± 0.040	0.891 ± 0.068	0.787 ± 0.058	0.842 ± 0.068	6.545 ± 0.652	6.294 ± 0.515	6.247 ± 0.644	7.487 ± 0.523	7.582 ± 0.375	7.292 ± 0.348	***	*		**				
Exp 3 ($n=10$)	1.000 ± 0.029	0.896 ± 0.033	1.008 ± 0.028	1.004 ± 0.048	0.862 ± 0.055	0.948 ± 0.059	8.136 ± 0.579	7.996 ± 0.767	7.985 ± 0.497	8.381 ± 0.549	8.548 ± 0.454	8.840 ± 0.517	***							
Overall ($n=30$)	1.000 ± 0.026	0.913 ± 0.025	1.001 ± 0.022	0.936 ± 0.035	0.825 ± 0.036	0.884 ± 0.037	6.977 ± 0.327	6.957 ± 0.345	6.824 ± 0.332	7.385 ± 0.357	7.707 ± 0.295	7.614 ± 0.305	***	*		**				

Table S4: Effects of fatty acids, glucose and fructose on lipid accumulation in primary human hepatocytes. Data was measured as Nile Red fluorescence per μg DNA then converted to fold change relative to $0\mu\text{M}$ fatty acid + 5mM glucose + 0mM fructose. Values are expressed as mean \pm SEM. Data analysed by three-way ANOVA with blocking for plate. $n=5$ wells per treatment per plate. FA: fatty acid, G: glucose, F: fructose. $\dagger P<0.1$, * $P<0.05$, ** $P<0.01$, * $P<0.001$**

F (mM)	5mM G, 0 μM FA			11mM G, 0 μM FA			5mM G, 200 μM FA			11mM G, 200 μM FA			P-values from three-way ANOVA						
	0	2	8	0	2	8	0	2	8	0	2	8	FA	G	F	FA \times G	FA \times F	G \times F	FA \times G \times F
L312 ($n=10$)	1.000 ± 0.127	0.954 ± 0.081	1.036 ± 0.084	0.888 ± 0.082	0.981 ± 0.074	1.275 ± 0.097	2.771 ± 0.117	3.150 ± 0.288	4.025 ± 0.178	3.247 ± 0.296	4.348 ± 0.487	4.822 ± 0.594	***	**	***	*	**		
L317 ($n=10$)	1.000 ± 0.019	1.265 ± 0.028	1.529 ± 0.063	0.948 ± 0.042	1.160 ± 0.055	1.428 ± 0.066	2.340 ± 0.060	3.035 ± 0.087	3.062 ± 0.182	2.317 ± 0.091	2.697 ± 0.108	3.278 ± 0.091	***		***		**	*	†
L321 ($n=10$)	1.000 ± 0.056	0.984 ± 0.044	0.937 ± 0.049	0.797 ± 0.031	0.828 ± 0.024	0.888 ± 0.050	1.145 ± 0.042	1.229 ± 0.042	1.192 ± 0.056	1.285 ± 0.075	1.403 ± 0.091	1.379 ± 0.101	***			***			
L326 ($n=10$)	1.000 ± 0.039	1.079 ± 0.057	1.117 ± 0.084	1.055 ± 0.062	1.056 ± 0.105	1.090 ± 0.048	1.647 ± 0.132	1.776 ± 0.150	1.660 ± 0.141	1.901 ± 0.117	1.916 ± 0.083	1.905 ± 0.089	***	*		*			
L329 ($n=10$)	1.000 ± 0.055	1.068 ± 0.056	1.199 ± 0.083	1.018 ± 0.043	1.150 ± 0.048	1.248 ± 0.062	2.275 ± 0.131	2.451 ± 0.165	2.350 ± 0.097	2.715 ± 0.223	2.672 ± 0.128	2.321 ± 0.154	***	†			*		
Overall ($n=50$)	1.000 ± 0.030	1.070 ± 0.029	1.164 ± 0.043	0.941 ± 0.027	1.035 ± 0.034	1.186 ± 0.039	2.036 ± 0.093	2.328 ± 0.127	2.458 ± 0.156	2.293 ± 0.124	2.607 ± 0.175	2.741 ± 0.212	***	*	***	**			

Table S5: L312 fatty acid × glucose interaction: Bonferroni multiple comparisons				
Fatty acid (μM)	Glucose (mM)	Mean	Bonferroni	s.e.d
0	5	0.997	a	0.2156
0	11	1.048	a	
200	5	3.315	b	
200	11	4.139	c	

Table S6: L326 fatty acid × glucose interaction: Bonferroni multiple comparisons				
Fatty acid (μM)	Glucose (mM)	Mean	Bonferroni	s.e.d
0	5	1.065	a	0.0682
0	11	1.067	a	
200	5	1.695	b	
200	11	1.907	c	

Table S7: L321 fatty acid × glucose interaction: Bonferroni multiple comparisons				
Fatty acid (μM)	Glucose (mM)	Mean	Bonferroni	s.e.d
0	5	0.973	a	0.0484
0	11	0.838	b	
200	5	1.189	c	
200	11	1.356	d	

Table S8: L312 fatty acid × fructose interaction: Bonferroni multiple comparisons				
Fatty acid (μM)	Fructose (mM)	Mean	Bonferroni	s.e.d
0	0	0.944	a	0.2641
0	2	0.968	a	
0	8	1.156	a	
200	0	3.009	b	
200	2	3.749	bc	
200	8	4.423	c	

Fatty acid (μM)	Fructose (mM)	Mean	Bonferroni	s.e.d
0	0	0.974	a	0.0794
0	2	1.213	b	
0	8	1.478	c	
200	0	2.328	d	
200	2	2.866	e	
200	8	3.170	f	

Fatty acid (μM)	Fructose (mM)	Mean	Bonferroni	s.e.d
0	0	1.009	a	0.1176
0	2	1.109	a	
0	8	1.224	a	
200	0	2.495	b	
200	2	2.562	b	
200	8	2.336	b	

Glucose (mM)	Fructose (mM)	Mean	Bonferroni	s.e.d
5	0	1.670	a	0.0794
5	2	2.150	bc	
5	8	2.295	c	
11	0	1.632	a	
11	2	1.928	b	
11	8	2.353	c	

Table S12: Effects of fatty acids, glucose and insulin on lipid accumulation in HepG2 cells. Data was measured as Nile Red fluorescence per μg DNA then converted to fold change relative to $0\mu\text{M}$ fatty acid + 5mM glucose + 0nM insulin. Values are expressed as mean \pm SEM. Data analysed by three-way ANOVA with blocking for plate. $n=5$ wells per treatment per plate. FA: fatty acid, G: glucose, I: insulin. $\dagger P<0.1$, $*P<0.05$, $P<0.01$, $***P<0.001$**

I (nM)	5mM G, 0 μM FA			11mM G, 0 μM FA			5mM G, 200 μM FA			11mM G, 200 μM FA			P-values from three-way ANOVA							
	0	5	10	0	5	10	0	5	10	0	5	10	FA	G	I	FA \times G	FA \times I	G \times I	FA \times G \times I	
Exp 1 ($n=10$)	1.000 ± 0.075	0.988 ± 0.101	1.033 ± 0.119	0.934 ± 0.042	0.942 ± 0.075	0.938 ± 0.076	3.434 ± 0.180	3.814 ± 0.154	4.076 ± 0.259	3.226 ± 0.304	3.657 ± 0.254	3.453 ± 0.337	***							
Exp 2 ($n=10$)	1.000 ± 0.099	1.031 ± 0.036	1.018 ± 0.056	0.788 ± 0.050	0.839 ± 0.063	0.941 ± 0.044	3.266 ± 0.254	3.480 ± 0.185	3.219 ± 0.280	2.974 ± 0.476	3.662 ± 0.292	3.691 ± 0.358	***	*	\dagger					
Overall ($n=20$)	1.000 ± 0.061	1.010 ± 0.052	1.026 ± 0.064	0.861 ± 0.036	0.891 ± 0.049	0.939 ± 0.043	3.350 ± 0.153	3.647 ± 0.123	3.647 ± 0.210	3.100 ± 0.276	3.659 ± 0.188	3.572 ± 0.241	***		*					

Table S13: Effects of fatty acids, glucose and insulin on lipid accumulation in primary human hepatocytes. Data was measured as Nile Red fluorescence per μg DNA then converted to fold change relative to $0\mu\text{M}$ fatty acid + 5mM glucose + 0nM insulin. Values are expressed as mean \pm SEM. Data analysed by three-way ANOVA with blocking for plate. $n=5$ wells per treatment per plate. FA: fatty acid, G: glucose, I: insulin. $\dagger P<0.1$, $*P<0.05$, $P<0.01$, $***P<0.001$**

I (nM)	5mM G, 0 μM FA			11mM G, 0 μM FA			5mM G, 200 μM FA			11mM G, 200 μM FA			P-values from three-way ANOVA						
	0	5	10	0	5	10	0	5	10	0	5	10	FA	G	I	FA \times G	FA \times I	G \times I	FA \times G \times I
L317 ($n=10$)	1.000 ± 0.043	1.018 ± 0.035	1.024 ± 0.073	1.075 ± 0.068	1.101 ± 0.078	1.068 ± 0.051	2.091 ± 0.178	2.584 ± 0.206	2.927 ± 0.227	2.066 ± 0.072	2.227 ± 0.044	2.234 ± 0.078	***	**	**	***	**	\dagger	\dagger
L319 ($n=10$)	1.000 ± 0.048	1.065 ± 0.058	1.048 ± 0.070	0.909 ± 0.062	0.966 ± 0.071	1.063 ± 0.065	1.690 ± 0.157	1.666 ± 0.125	1.673 ± 0.143	2.019 ± 0.135	2.232 ± 0.132	2.118 ± 0.110	***	***		***			
L321 ($n=10$)	1.000 ± 0.014	1.106 ± 0.030	1.054 ± 0.038	0.808 ± 0.021	0.909 ± 0.036	0.958 ± 0.043	1.264 ± 0.063	1.316 ± 0.045	1.268 ± 0.039	1.281 ± 0.057	1.469 ± 0.064	1.515 ± 0.050	***		***	***		*	
Overall ($n=30$)	1.000 ± 0.021	1.063 ± 0.025	1.042 ± 0.035	0.930 ± 0.037	0.992 ± 0.039	1.029 ± 0.031	1.682 ± 0.101	1.855 ± 0.127	1.956 ± 0.158	1.789 ± 0.085	1.976 ± 0.083	1.956 ± 0.075	***		**	\dagger			

Table S14: L317 fatty acid × glucose interaction: Bonferroni multiple comparisons				
Fatty acid (μM)	Glucose (mM)	Mean	Bonferroni	s.e.d
0	5	1.014	a	0.0824
0	11	1.081	a	
200	5	2.534	b	
200	11	2.176	c	

Table S15: L317 fatty acid × insulin interaction: Bonferroni multiple comparisons				
Fatty acid (μM)	Insulin (nM)	Mean	Bonferroni	s.e.d
0	0	1.037	a	0.1010
0	5	1.059	a	
0	10	1.046	a	
200	0	2.079	b	
200	5	2.405	c	
200	10	2.581	c	

Table S16: L319 fatty acid × glucose interaction: Bonferroni multiple comparisons				
Fatty acid (μM)	Glucose (mM)	Mean	Bonferroni	s.e.d
0	5	1.038	a	0.0756
0	11	0.979	a	
200	5	1.676	b	
200	11	2.123	c	

Table S17: L321 fatty acid × glucose interaction: Bonferroni multiple comparisons				
Fatty acid (μM)	Glucose (mM)	Mean	Bonferroni	s.e.d
0	5	1.054	a	0.0360
0	11	0.891	b	
200	5	1.283	c	
200	11	1.422	d	

Table S18: L321 fatty acid × insulin interaction: Bonferroni multiple comparisons				
Glucose (mM)	Insulin (nM)	Mean	Bonferroni	s.e.d
5	0	1.132	ab	0.0440
5	5	1.211	b	
5	10	1.161	ab	
11	0	1.045	a	
11	5	1.189	b	
11	10	1.236	b	

Table S19: Fatty acid × fructose interaction effect on fatty acid synthase (FASN) mRNA expression in primary human hepatocytes: Bonferroni multiple comparisons				
Fatty acid (μM)	Fructose (mM)	Mean	Bonferroni	s.e.d
0	0	0.5583	ab	0.1154
0	2	0.6494	ab	
0	8	0.9085	b	
200	0	0.6300	ab	
200	2	0.6077	ab	
200	8	0.4919	a	

Table S20: Glucose × fructose interaction effect on fatty acid synthase (FASN) mRNA expression in primary human hepatocytes: Bonferroni multiple comparisons				
Glucose (mM)	Fructose (mM)	Mean	Bonferroni	s.e.d
5	0	0.5895	a	0.1154
5	2	0.6126	a	
5	8	0.8769	a	
11	0	0.5987	a	
11	2	0.6445	a	
11	8	0.5235	a	

Table S21: Glucose × fructose interaction effect on stearoyl-coA desaturase (SCD) mRNA expression in primary human hepatocytes: Bonferroni multiple comparisons

Glucose (mM)	Fructose (mM)	Mean	Bonferroni	s.e.d
5	0	1.0111	a	0.1415
5	2	0.8703	a	
5	8	1.1089	a	
11	0	0.9132	a	
11	2	1.1472	a	
11	8	0.8426	a	

Table S22: Glucose × fructose interaction effect on ApoB mRNA expression in HepG2 cells: Bonferroni multiple comparisons

Glucose (mM)	Fructose (mM)	Mean	Bonferroni	s.e.d
5	0	1.169	a	0.1384
5	2	1.342	a	
5	8	1.452	a	
11	0	1.486	a	
11	2	1.328	a	
11	8	1.250	a	

Table S23: Glucose × fructose interaction effect on ApoB mRNA expression in primary human hepatocytes: Bonferroni multiple comparisons

Glucose (mM)	Fructose (mM)	Mean	Bonferroni	s.e.d
5	0	1.490	a	0.1860
5	2	1.253	a	
5	8	1.441	a	
11	0	1.230	a	
11	2	1.499	a	
11	8	0.969	a	

Table S24: Glucose × fructose interaction effect on ChREBP mRNA expression in primary human hepatocytes: Bonferroni multiple comparisons

Glucose (mM)	Fructose (mM)	Mean	Bonferroni	s.e.d
5	0	1.462	a	0.2708
5	2	1.531	ab	
5	8	2.355	b	
11	0	1.583	ab	
11	2	2.044	ab	
11	8	1.679	ab	

Table S25: Fructose effect on LPK mRNA expression in primary human hepatocytes: Bonferroni multiple comparisons

Fructose (mM)	Mean	Bonferroni	s.e.d
0	1.486	ab	0.1448
2	1.657	b	
8	1.263	a	

Table S26: Fructose effect on GLUT2 mRNA expression in primary human hepatocytes: Bonferroni multiple comparisons

Fructose (mM)	Mean	Bonferroni	s.e.d
0	0.8812	b	0.1157
2	0.6851	ab	
8	0.4879	a	